HHS Public Access

Author manuscript

Adv Drug Deliv Rev. Author manuscript; available in PMC 2022 March 01.

Published in final edited form as:

Adv Drug Deliv Rev. 2021 March ; 170: 142–199. doi:10.1016/j.addr.2021.01.005.

Recent Advances in Nanomaterials for Therapy and Diagnosis for Atherosclerosis

Jun Chen[a], **Xixi Zhang**[a], **Reid Millican**[a], **Jennifer Sherwood**[a], **Sean Martin**[a], **Hanjoong Jo**[c,d], **Young-sup Yoon**[d,e], **Brigitta C Brott**[b], **Ho-Wook Jun**[a]

[a]Department of Biomedical Engineering, The University of Alabama at Birmingham, Birmingham, Alabama, United States

[b]Division of Cardiovascular Disease, Department of Medicine, The University of Alabama at Birmingham, Birmingham, Alabama, United States

[c]Wallace H. Coulter Department of Biomedical Engineering, Georgia Institute of Technology and Emory University, Atlanta, Georgia, United States

[d]Division of Cardiology, Department of Medicine, Emory University, Atlanta, Georgia, United States

[e]Severance Biomedical Science Institute, Yonsei University College of Medicine, Seoul, South Korea

Abstract

Atherosclerosis is a chronic inflammatory disease driven by lipid accumulation in arteries, leading to narrowing and thrombosis. It affects the heart, brain, and peripheral vessels and is the leading cause of mortality in the United States. Researchers have strived to design nanomaterials of various functions, ranging from non-invasive imaging contrast agents, targeted therapeutic delivery systems to multifunctional nanoagents able to target, diagnose, and treat atherosclerosis. Therefore, this review aims to summarize recent progress (2017-now) in the development of nanomaterials and their applications to improve atherosclerosis diagnosis and therapy during the preclinical and clinical stages of the disease.

Graphic abstract

Declaration of Competing Interest

The authors declare no conflict of interest in the publication of this work.

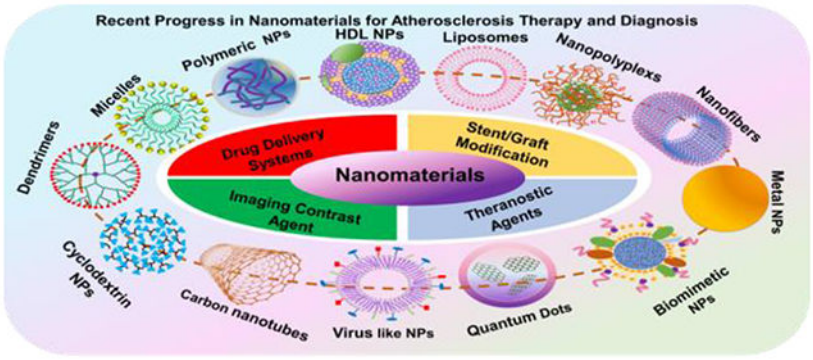

Keywords

Atherosclerosis; Nanomaterials; Therapeutic delivery system; Imaging Contrast Agents; Theranostic Agents; Clinical Use

1. Introduction

Cardiovascular diseases (CVDs) are the primary cause of mortality and morbidity globally. It is reported that 17.9 million deaths were associated with CVDs in 2016, representing 31% of all global deaths [1]. The primary cause of CVDs is atherosclerosis, a condition where the arteries become narrower and harden due to the accumulation of plaque within the coronary arterial walls [2]. Atherosclerotic plaques are detrimental to human physiology. They severely limit the flow of oxygen-rich blood to the heart, brain, and other organs, leading to severe problems, such as stroke, myocardial infarction, peripheral vascular disease, or death [3].

Currently, clinical strategies for addressing atherosclerosis have mainly focused on relieving symptoms of CVDs and preventing future cardiac events. Up to now, the most common strategy is pharmacologic treatment with medications. The extensively used statin therapy, for instance, is used to frequently prevent atherosclerosis or reduce its progression by inhibiting cholesterol synthesis [4]. Despite the significant therapeutic benefits from drug therapy, oral or intravenous administration of drugs may be accompanied with side effects as the drugs can also target normal and healthy tissues. In addition to drugs, another widely used strategy to combat atherosclerosis is through stent-assisted therapies, where stents are employed during late atherosclerosis when medications fail to provide proper treatment. Despite low complication rates, stent therapy is still associated with issues such as restenosis, inflammation, and thrombosis in patients [5]. Besides stent-based therapies, alternative therapy for treating atherosclerosis is coronary artery bypass surgery. While it is clear that surgical interventions made significant contributions to reducing cardiovascular mortality and symptoms, it should also be noted that they also lead to a risk of complications, and recovery can take a longer time. Similar to strategies for atherosclerosis treatments, the currently available clinical screening methods for atherosclerosis diagnosis sometimes have led to disappointment by their inability to diagnose the disease before its first clinical manifestation. Particularly, atherosclerosis sometimes cannot be detected until a

narrowed lumen (stenosis) of the artery is observed or myocardial infarction, sometimes even a fatal event, has occurred in patients [6]. In addition, the commonly used imaging modalities such as magnetic resonance imaging (MRI), computed tomography (CT), and ultrasonography (US) only provide information at the anatomical and physiological levels. Thus, considerable efforts are made to explore new approaches to detect early-stage abnormalities and vulnerable plaques, as well as to improve the efficacy of therapeutics for atherosclerosis.

Recent advances in nanotechnology have given rise to nanomedicine, which focuses on designing, fabricating, and characterizing nanomaterials for delivering cargoes to prevent, diagnose, and treat a wide variety of diseases [7]. Nanomaterials are materials with size in the nanoscale (10^{-9} meters), which are generally divided into zero-dimensional (e.g., nanoparticles (NPs)) [8], one dimensional (e.g., nanofibers, nanowires, nanorods, and nanotubes [8, 9], two dimensional (e.g., nanofilms) [8, 10], and three dimensional (bulk materials) nanomaterials [8, 11, 12]. Over the last decade, nanomaterials were thoroughly investigated as platforms to deliver either therapeutic or imaging contrast agents for producing breakthroughs in cancer therapy and diagnosis [13, 14]. Numerous studies have reported that nanomaterial mediated therapeutic delivery and imaging can outperform traditional systematic free drug and contrast agent delivery by providing several advantages. Particularly, nanomaterials of size ranging from 6 nm to 100 nm can avoid kidney clearance because they can be blocked by the kidney glomerular basement membrane of pore size around 2-8 nm [15]. Also, nanomaterials size less than 200 nm can passively target and penetrate tumors and be internalized by endocytic vesicles [13, 14]. Moreover, drug and contrast agent loaded nanomaterials demonstrate relatively long circulation time, show a good distribution in tumors, exhibit controllable drug pharmacokinetics, and allow for active cancer-targeting [13, 14]. These are in great contrast to traditional systematic drug delivery associated with limitations such as fast clearance, solubility issues, and undesirable accumulation of drugs in healthy tissues. Additionally, the characteristics of nanomaterials are highly controllable as their physical properties, and chemical compositions can be easily tuned for achieving specific functions. In addition, for cancer imaging, improved contrast intensity has been observed by taking advantage of using nanomaterials [14]. Notably, early-stage cancer imaging diagnosis and therapy monitoring are feasible via nanomaterial mediated imaging [14].

Given the aforementioned progress that nanomaterials have brought to cancer therapy and diagnosis, nanomaterials are expected to present great opportunities for advancing atherosclerosis diagnosis and treatment. Indeed, in the past several years, a multitude of nanomaterials have been designed into a variety of nanoplatforms with specific desirable functionalities, such as therapeutic delivery systems, imaging contrast agents, and theranostic agents for diagnosis and therapy [16, 17]. Therefore, this review provides a comprehensive, up-to-date overview focusing on the recent advances (2017-2020) of the state-of-the-art nanomaterials for atherosclerosis therapy and diagnosis spanning over several essential aspects (Fig.1). Some crucial studies prior to 2017 are also included in this review. Particularly, following the introduction section, we discuss recent progress in preclinical studies of nanomaterials for atherosclerosis therapy and diagnosis. Next, we summarize the advancement of nanomaterials in atherosclerosis diagnosis and therapy in

clinical care. Lastly, we provide a summary of the review and outline of critical perspectives for future directions. Although several reviews have discussed NPs for atherosclerosis applications, many investigate either atherosclerosis therapy or diagnosis alone, and if both are presented, they only remain in the context of the preclinical phase [18–22]. In other words, a comprehensive review involving nanomaterials in both preclinical and clinical stages for atherosclerosis therapy and diagnosis has not been reported. Moreover, this review also includes the recent advances in nanomaterials for stent and vascular graft functionalization for improving atherosclerosis therapy, which is not discussed in these recent reviews (Fig.1). Thus, this review is expected to provide complete and useful information for researchers working in this field to explore better approaches for atherosclerosis therapy and diagnosis.

2. Preclinical Studies of Nanomaterials for Atherosclerosis Therapy and Diagnosis

Over the past several decades, nanomaterials have arisen as delivery systems and imaging contrast agents that aim to improve the efficiency and efficacy for diagnosing and treating various diseases. In this section, we mainly focus on the recent advances of nanomaterials as therapeutic delivery systems and imaging contrast agents for improving diagnosis and treatment of atherosclerosis in preclinical stages. Moreover, nanomaterials used for stent functionalization and vascular graft fabrication for atherosclerosis therapy are also discussed. As it follows, numerous types of nanomaterials such as polymeric nanoparticles (NPs), inorganic NPs, lipid-based NPs (high-density lipoprotein NPs, solid lipid NPs, and liposomes), dendrimers, micelles, nanofibers, carbon-based nanomaterials, and biomimetic NPs are also discussed (Fig.1).

2.1. Nanomaterials for Atherosclerosis Therapy

2.1.1. Nanomaterials as Therapeutic Delivery Systems for Atherosclerosis Therapy

2.1.1.1. Polymeric NPs: Polymeric NPs are colloidal particles that are usually fabricated using biocompatible and biodegradable polymers. Due to their easy modification for encapsulating therapeutics, their ability to target desired sites, and their potential to release cargos upon specific biological or external stimuli, polymeric NPs have attracted considerable attention for biomedical applications. To date, among polymeric NPs, the most studied polymer NPs for atherosclerosis therapy are hyaluronic acid (HA) and poly (lactic-co-glycolic acid) (PLGA)-based NPs, in addition to the polymeric micelles and dendrimers that are discussed in other sections.

2.1.1.1.1. Hyaluronic NPs: HA is a linear biopolymer - a polysaccharide and hydrated polyanionic macromolecule composed of alternating units of N-acetylglucosamine and β-glucuronic acid. HA is also a vital component of the extracellular matrix (ECM) [23, 24]. Due to its excellent biodegradability, non-toxicity, non-immunogenicity, non-inflammatory response, and specific binding ability to stabilin-2 and cluster of differentiation 44 (CD44) on cancer cells, NPs composed of HA were studied intensively for the targeted delivery of drugs for cancer therapy [25–27]. Until 2015, Kim and coworkers investigated the capability

of HA NPs to actively target atherosclerotic lesions as stabilin-2 and CD44 are also highly expressed in activated macrophages, smooth muscle cells (SMCs), and endothelial cells (ECs) of atherosclerotic plaques. As expected, the authors found that the amount of HA NPs accumulated in the atherosclerotic plaque of apolipoprotein E deficient ($ApoE^{-/-}$) mice was much higher than that of hydrophobically modified glycol chitosan NPs, showing the targeting ability of HA NPs to the plaque after systemic administration [28]. This study was the first demonstration that showed HA NPs could selectively and actively target and accumulate in the plaque via binding to stabilin-2 and CD44. Later, Kluza and coworkers advanced the concept by showing that HA NPs targeted macrophages in the atherosclerotic plaque and improved plaque stability. Notably, it was first evidenced that the interaction between macrophages and HA NPs was strongly associated with the disease stage [29]. Specifically, in the study, the authors first showed that the amount of HA NPs taken up by the macrophages in the plaque was 6- and 40-fold higher than those taken up by the macrophages in the spleen and the bone marrow of $ApoE^{-/-}$ mice, respectively (Fig.2a). Moreover, fewer macrophages accumulated, and more collagen formed in the plaque of mice treated with HA NPs than that of mice treated with free HA (Fig 2b–c), indicating the anti-inflammatory and plaque stabilization effects of HA NPs. Interestingly, significantly more HA NPs were observed to be taken up by the macrophages in early lesions than those located in advanced lesions. One possible speculation for this observation, according to the authors, was that the macrophages in early atherosclerotic lesions had great phagocytic activity; in contrast, macrophages in advanced lesions had been fed with lipids and underwent cell apoptosis and necrosis, thereby rendering it difficult to internalize HA NPs [29]. In a subsequent study, the true underlying mechanism driving the striking differences in HA NP amount taken up by macrophages resided in plaque at different stages was unveiled by the same group. Rather than macrophage activity, the authors found that endothelial barrier changes upon atherosclerosis progression, indicated by the changes in vascular endothelial cell (VEC) junction space and continuity, was an important factor contributing to the discrepancy of HA NP accumulation between early and advanced plaque. Particularly, the authors found that the VEC in advanced plaque demonstrated better continuity and endothelial normalization than that in early plaque (Fig.2d–f). In addition, a significantly greater amount of collagen and SMCs were observed in the advanced atherosclerotic plaque, which most likely provided better stabilization of the endothelium, thus delaying the extravasation of HA NPs. Furthermore, the trafficking of HA NPs was also investigated. Intriguingly, the authors demonstrated that most of the HA NPs entered the plaque via endothelial junctions, followed by a distribution in endothelium extracellular matrix, and finally engulfed by macrophages (Fig.2g). These observations explained the earlier findings on why less HA NPs were taken up in the advanced atherosclerotic plaque than that of early lesions [30]. Besides the targeting ability of HA NPs to plaque and associated underlying mechanisms, HA NPs were investigated in a more recent study by Huang and coworkers as drug delivery systems for the first time to deliver high quantities of atorvastatin (AT) for atherosclerosis treatment. In particular, HA NPs were conjugated with atorvastatin (AT) (HA-AT NPs) for targeted delivery of the AT to the plaque. The authors showed that a one-week treatment of HA-AT NPs presented a significantly better anti-inflammatory effect than free AT on macrophages both *in vitro* and *in vivo*. It is worth noting that another critical finding of this study was that a one-week treatment of HA-AT

NPs at a dose of 17 mg HA/kg demonstrated equivalent anti-inflammatory effect as a 3-month administration of HA-NPs at a dose of 50 mg HA/kg [31].

Despite significant progress shown here, the current utility of HA NPs as therapeutic delivery systems for atherosclerosis treatment is still at its nascent stage. However, as it is known, macrophage polarization plays a vital role in both atherosclerosis progression and regression; therefore, researchers have conducted numerous studies centering on exploring the effects of HA NPs loaded with various cargoes on reprogramming macrophage polarization. These HA NPs also hold great potentials for being investigated as alternatives to HA-AT NPs for atherosclerosis treatment in the future. For instance, in 2018, Santos and coworkers explored the possibility of HA NPs loaded with interleukin 4 (HA-IL-4) for inducing macrophage repolarization *in vitro* [32]. The authors showed the ability of the HA-IL-4 for repolarization increased with an increased molecular weight of HA used for the fabrication of these HA NPs. Furthermore, HA NPs with IL-4 showed a more excellent capability of repolarizing classically activated macrophages (M1 macrophages) into alternatively activated macrophages (M2 macrophages) compared to the free HA NPs [32]. Similar studies were also conducted by several other groups who demonstrated that HA-PLA NPs with curcumin (Cur) [33], HA-Polyethylenimine (PEI)-NPs with microRNA-233 (miR-233) [34], and HA-PEI with plasmid DNA [35] could also modulate the polarity of macrophages; note, from pro-inflammatory M1 to anti-inflammatory M2 phenotype.

2.1.1.1.2. PLGA NPs: PLGA is an FDA-approved biodegradable and biocompatible copolymer consisting of lactic acid and glycolic acid. Due to its excellent biocompatibility and biodegradability, PLGA has been used to prepare NPs for delivering a wide variety of drugs for treating cancers extensively [36–38]. Furthermore, the surface of PLGA NPs can be modified with ligands to achieve targeted delivery of drugs to a specific disease site. In some studies, researchers mainly focused on using PLGA NPs to deliver a range of therapeutics, primarily conventional drugs and pro-resolving mediators, for treating atherosclerosis at the molecular level. For instance, Egashira and coworkers showed that PLGA NPs with pitavastatin (PT), a clinical drug that lowers low-density lipoprotein (LDL), could suppress the destabilization and rupture of plaque by interfering with the monocyte chemoattractant protein-1 (MCP-1)/chemokine receptor type 2 (CCR2) signaling pathway associated with monocyte migration in $ApoE^{-/-}$ mice [16]. Other relevant studies also showed that PLGA NPs with PT could attenuate atherosclerosis development and more effectively alleviate atherosclerosis than free PT in $ApoE^{-/-}$ mice, while PLGA NPs with AT demonstrated similar effects to free AT [39, 40]. In addition to statins, Fisher and coworkers developed NPs assembled with PLGA-b-Polyethylene glycol (PEG) to deliver GW3965, a liver X receptor (LXR) agonist, to inhibit the development of atherosclerosis [41]. The authors demonstrated that after two weeks of intravenous injections of PLGA-b-PEG NPs with GW3965 (NP-LXR) in a low-density lipoprotein receptor-deficient ($Ldlr^{-/-}$) mouse, the quantity of CD68 positive macrophages in plaque was reduced by 50%. More importantly, in contrast to free LXR associated with adverse effects on the liver, the liver lipogenic gene causing hepatic steatosis was not stimulated in mice treated with those NP-LXR. This further indicated the significance of PLGA NPs in minimizing the side effects of LXR [41]. Meanwhile, another study reported by Egashira and coworkers demonstrated that PLGA

NPs loaded with pioglitazone (PIO), an agonist for peroxisome proliferator-activated receptor-γ (PPAR-γ), could influence macrophage polarization into the M2 phenotype, inhibit plaque destabilization and rupture, and exhibit more effective therapeutic efficacy than free PIO in ApoE$^{-/-}$ mice. The therapeutic efficacy of PIO-PLGA NPs was attributed to the capability of these NPs to regulate inflammatory cytokines, reduce the number of pro-inflammatory monocytes, and decrease the production of ECM metalloproteinases, all of which significantly contribute to plaque rupture [42]. Besides, stabilin-2 targeting (S2P) peptide conjugated PLGA NPs were also developed for delivering imatinib for atherosclerosis targeting and therapy. Imatinib is an inhibitor for platelet-derived growth factor receptor, which plays a crucial role in atherosclerosis progression. However, this study mainly discussed the development of PLGA NPs with imatinib and no *in vitro* and *in vivo* studies regarding the therapeutic efficacy of these NPs were included [43]. As chronic inflammation plays crucial role in the development of advanced atherosclerotic plaque, Tabas and coworkers applied collagen targeting PLGA-b-PEG NPs to deliver an amino-terminal peptide encompassing amino acids 2–26 (Ac2-26) that mimics annexin A1 to resolve local inflammation in advanced plaque. With this approach, the Ldlr$^{-/-}$ mice with existing plaque exhibited suppressed necrosis and oxidative stress and increased number of collagen layers of the plaque [44]. Similar to Ac2-26 loaded PLGA NPs, an unprecedented study conducted by the same group demonstrated that PLGA NPs encapsulated with potent anti-inflammatory cytokine, IL-10, could inhibit monocyte recruitment, negatively regulates pro-inflammatory cytokines, decrease oxidative stress, stimulate fibrous cap formation, and decrease the necrotic core number in Ldlr$^{-/-}$ mice fed with a high fat diet(HFD). Remarkably, the NPs presented better efficacy for treating inflammation than native IL-10 [45]. These studies demonstrated that PLGA NP mediated delivery of anti-inflammatory cytokines holds great promise for treating atherosclerosis.

With the emergence of genetic engineering, nucleic acid therapy has provided an alternative to chemical drugs, showing potential for treating diseases ranging from cancer to cardiovascular diseases [46–48]. However, as nucleic acids have notable inherent limitations such as high instability, adverse effect if off target, low efficiency through intravenous injection, and fast clearance [49]. Thus, several recent studies have emphasized applying PLGA NPs to deliver nucleic acids systemically to overcome the challenges and combat atherosclerosis. For gene therapy, small interfering RNA (siRNA) delivery has been regarded as a robust approach to inhibit specific gene expression for therapeutic purposes. Therefore, in 2018, advanced PLGA NPs were employed by Liu and coworkers to silence lectin-like ox-LDL receptor-1 (LOX-1) on macrophages using siRNA [50]. The rationale to select LOX-1 as a target is that it has long been regarded as associated with atherosclerosis initiation and pathogenesis due to its capability to mediate the uptake of ox-LDL into macrophages. To fabricate the PLGA NPs targeting LOX-1, the PLGA NPs were first condensed with siRNA specific for LOX-1, then modified with a cell-penetrating peptide, and finally coated with HA of various molecular weights including 8 kDa (NPs-1), 20 kDa (NPs-2), or 200 kDa (NPs-3) to target the plaque. All NPs demonstrated better cellular accumulation and gene efficacy for preventing foam cell formation than free LOX-1 siRNA. More interestingly, NPs-3 showed the best atheroprotective efficacy in ApoE$^{-/-}$ mice as NPs-3 treated mice showed the smallest lesion size and the least lipid accumulation and

macrophage infiltration in the plaque compared to the controls, NPs-1, and NPs-2. These results not only revealed the significant role of HA molecular weight in regulating PLGA NP's targeting ability but also substantiated the great atheroprotective efficacy of such prospective systems combining PLGA NPs and siRNA for atherosclerosis therapy [50]. Such advances in NP mediated siRNA delivery have motivated the use of siRNA to inhibit Ca^{2+}/calmodulin-dependent protein kinase (CaMKIIγ) in lesional macrophages. Lesional macrophages have been reported to promote the transformation of stable fibrous plaques into vulnerable plaques that may lead to thrombosis. In a recent study, similar to Liu's strategy, Shi and coworkers constructed lipid-PLGA NPs to encapsulate siRNA that specifically targets the Camk2g gene to silence macrophage CaMKIIγ and promote efferocytosis and plaque stability. To improve NP accumulation in the plaque, S2P was conjugated on the PLGA NPs to target stabilin-2 overexpressed in the plaque. By utilizing S2P-siCamk2g PLGA NPs, the expression of CaMKIIγ was reduced by 60%, leading to increased Mer proto-oncogene tyrosine kinase expression and enhanced efferocytosis in macrophages *in vitro*. It is worth noting that the S2P-siCamk2g PLGA NPs also displayed excellent therapeutic efficacy for atherosclerosis *in vivo*, as the plaque in $Ldlr^{-/-}$ mice after treated with these NPs showed decreased necrotic cores, as well as thickened fibrous cap, suggesting a more stable plaque formation upon S2P-siCamk2g PLGA NPs treatment. Furthermore, an increased ratio of macrophage-associated apoptotic cells to free apoptotic cells was observed in mice treated with S2P-siCamk2g NPs compared to the control, indicating the excellent ability of these NPs to promote efferocytosis [51]. Taken together, the siRNA PLGA NPs demonstrated a novel type of approach to suppress atherosclerosis progression and prevent acute atherothrombosis development, which shed light on exploring new types of NPs containing other kinds of RNA therapeutics, such as miR or messenger RNA (mRNA), for the treatment of atherosclerosis. Despite the effectiveness of siRNA PLGA NPs, the translation of these NPs into the clinical setting might still be challenging. This is mostly because the current evaluation was limited to the use of $Ldlr^{-/-}$ mice and large animals such as atherosclerotic pig models are needed to validate the efficacy of such an approach in the future. Moreover, whether the current formulation is robust and sufficient for achieving large scale manufacture remains to be addressed.

In addition to RNA, Yang and coworkers explored the potential of delivering vascular endothelial growth factor (VEGF) plasmid in the combination of paclitaxel (PTX) via PLGA NPs to prevent restenosis. Specifically, the NPs consisted of a PLGA core for the encapsulation of PTX and a VEGF plasmid as the outer layer. The authors reported that the local administration of VEGF-PTX-PLGA NPs promoted re-endothelialization and inhibited SMC growth sequentially in the atherosclerotic plaque *in vivo* [52]. The VEGF-PTX-PLGA NPs provided a prospective approach for treating lesions located in branched sites or small arteries where stents cannot be employed. In addition, this study introduced that dual-therapeutic delivery therapy may be a better strategy to improve the therapeutic efficacy of treating atherosclerosis

2.1.1.1.3. Other Polymeric NPs: Besides PLGA and HA NPs, there have been prominent recent progress in the development of polymeric NPs composed of other types of polymers for atherosclerosis therapy. For example, one study demonstrated that polymeric NPs

assembled with CS and polyaspartic acid (PAA) enabled the delivery of epigallocatechin gallate (EGCG) to decrease the area of rabbit aorta occupied with lipid deposits [53]. Another study reported that polymeric NPs comprised of PEG and sebacic acid were used to carry D-Threo-1-phenyl-2-decanoylamino-3-morpholino-1-propanol (D-PDMP), an inhibitor for glycosphingolipid synthesis, thereby improving the delivery of D-PDMP, reducing the aortic intima thickness, and altering the genes involved in atherosclerosis pathology for cholesterol biosynthesis *in vivo* [54]. Moreover, Moghe and coworkers designed anti-oxidative polymeric NPs to regulate macrophage lipogenesis and reactive oxygen species (ROS) generation in atherosclerotic plaque [55]. The NPs were composed of a polyester core comprised of ferulic acid-based poly(anhydride-ester) and a shell modified with amphiphilic molecules for targeting scavenger receptors. Ferulic acid is a natural antioxidant and has been reported to reduce macrophage lipogenesis; thus, these ferulic acid NPs were found to reduce the CD36 and LOX-1 scavenger receptor expression by macrophages and inhibit oxidized low-density lipoprotein (ox-LDL) uptake by macrophages [55]. Moreover, in another study, Zhang and coworkers investigated the effect of Cur loaded polymeric NPs, made of linear-dendrimer methoxy-poly (ethylene glycol)-b-poly(ε-caprolactone), on the stabilization of vulnerable plaques. The authors showed that the Cur-loaded NPs dramatically decreased the size of atherosclerotic lesions and improved the efficacy for stabilizing vulnerable plaques than free Cur. The improved anti-atherosclerotic effectiveness was because the Cur-loaded NPs possessed an enhanced ability to suppress matrix metalloproteinase (MMP) activity and inflammation and regulate lipoprotein cholesterol metabolism [56]. In a more recent study, Scott and coworkers compared the mononuclear phagocyte uptake of PEG-b-poly(propylene sulfide) NPs with different morphologies. Intriguingly, the authors discovered that tissue selectivity of polymeric NPs could be engineered by their morphologies. For instance, spherical micelles were shown to be associated with liver macrophages, filomicelles were mainly found in blood-resident phagocyte, and polymersomes specifically targeted splenic dendritic cells. Moreover, by conjugating polymersomes with peptide targeting dendritic cells (P-D2-NPs), the NPs were found to only accumulated in dendritic cells in atherosclerotic lesions in $ApoE^{-/-}$ mice. More importantly, 1,25-dihydroxy vitamin D3 (aVD) loaded P-D2-NPs significantly inhibited atherosclerosis progression in $ApoE^{-/-}$ mice, possibly due to the suppression of pro-inflammatory T cells by aVD treated dendritic cells [57].

2.1.1.2. Lipid-Based NPs

2.1.1.2.1. Liposomes: Liposomes have been developed for more than 40 years and have evolved into therapeutic delivery systems for treating cancers [58]. Specifically, liposomes are self-assembled spherical shaped amphiphilic vesicles comprised of a hollow core and lipid bilayer shell composed of various phospholipids. By taking advantage of the core cavity, researchers have loaded various therapeutics inside the liposomes [59]. Furthermore, the lipid shell can be modified with ligands to target desired disease sites specifically [59]. Therefore, liposomes have been explored to deliver therapeutics to treat atherosclerosis.

Dysfunctional endothelium has been long regarded as a key factor contributing to early atherosclerosis. In the field of liposome-mediated atherosclerosis treatment, several studies have reported the delivery of liposomal therapeutics to dysfunctional endothelium as anti-

atherosclerosis therapy to suppress monocyte adhesion, macrophage differentiation, and foam cell formation. For instance, in 2015, Jo and coworkers developed liposomes to deliver a prototypic compound, anti-miR-712, to suppress the expression of pro-atherogenic microRNA 712 (miR-712) in dysfunctional endothelium. To target the dysfunctional endothelium, the liposome shell was modified with peptide ligand (VHPK). Promisingly, after the ApoE$^{-/-}$ mice were treated with VHPK-anti-miR-712 liposomes, a decrease in expressions of miR-712, tissue inhibitor of metalloproteinase-3, and reversion-inducing cysteine-rich protein with Kazal motifs were observed, thereby significantly inhibiting the metalloproteinase activity in the plaque. In addition, a stronger anti-atherosclerotic strength of VHPK-anti-miR-712 liposomes was found compared to that of naked anti-miR-712, indicating the potential use of liposomes to enhance the efficacy of miR for atherosclerosis treatment [60]. Another type of endothelium targeting liposome was developed by Simionescu and coworkers to deliver Teijin, an antagonist of CCR2, to suppress atherosclerosis. The Teijin-liposomes were modified with peptide ligand (VHPKQHRGGSKG) to target vascular cell adhesion protein 1 (VCAM-1) expressing dysfunctional endothelium. The *in vivo* study demonstrated that Teijin-liposomes induced a significantly better reduction of monocyte infiltration and adhesion in the plaque than liposomes without peptide ligands [61]. Likewise, in 2018, the Albeda group loaded fumagillin, a mycotoxin, into liposomes and investigated whether fumagillin-loaded liposomes could inhibit the early-stage of atherosclerosis progression and prevent atheroma formation. Promisingly, the plaque growth in ApoE$^{-/-}$ mice was decreased by 23.7%. The therapeutic function of fumagillin-loaded liposomes might result from the inhibition of EC migration and proliferation induced by the anti-angiogenic fumagillin [62]. This study postulated that the utility of an anti-atherogenic agent could be an effective method to treat early atherosclerosis. In addition, a recent study from Desikan and coworkers reported on the development of anti-inflammatory liposomal formulations for treating myeloperoxidase-mediated atherosclerosis [63]. Myeloperoxidase is a key player for initiating atherosclerosis by inducing EC dysfunction and generating highly atherogenic LDL [64]. In particular, the authors encapsulated anti-inflammatory thioctic acid conjugates into liposomes and found that those liposomes demonstrated effective inhibition of myeloperoxidase *in vitro* [63]. These approaches indicated the feasibility of treating atherosclerosis by targeting the chemokine receptors and enzymes associated with dysfunctional endothelium. Inspired by the idea that Cur could reduce statin-associated symptoms, in a study in 2019, Cheng and coworkers leveraged liposomes to targeted co-delivery of atorvastatin (AT) and Cur to inflamed/dysfunctional endothelium for synergistically treating atherosclerosis and reducing deleterious side effects of AT. The authors observed that the liposomes loaded with both AT and Cur (AC-Lipo) significantly suppressed ICAM-1 and E-selectin expression as well as induced anti-oxidative function, more than liposomes loaded with either AT or Cur. The *in vivo* study also showed that the AC-Lipo induced the largest atherosclerotic plaque reduction (76.58%), significantly more than either AT (51.59%) or Cur loaded liposomes (32.43%), due to the ability of AC-Lipos to reduce lipid content and inflammatory cytokines synergistically [65]. This study demonstrated the importance of combination therapy with dual therapeutics for enhancing therapeutic efficacy while minimizing side effects. More efforts can be devoted to continuing to drive the field of combination therapy forward in the future.

Throughout the recent studies, apart from dysfunctional ECs, macrophages have also become a key focus for developing liposome-mediated approaches to treat atherosclerosis because of their essential role in promoting plaque inflammation. In earlier studies, researchers have attempted to deliver therapeutics to macrophages using liposomes for combating atherosclerosis. For instance, in 2014, Tacke and coworkers loaded dexamethasone (Dex) into liposomes (Dex-Lipo) and demonstrated that the Dex-Lipo decreased the production of TNF-α and IL-6 in activated macrophages and inhibited macrophage and monocyte migration *in vitro* [66]. Likewise, ST loaded liposomes showed effects on suppressing macrophage proliferation and uptake of ox-LDL by macrophages [67]. Despite great progress in the inhibition of macrophage activity by ST and Dex-Lipo, liposomes loaded with prednisolone phosphate (PLP-Lipo), a synthetic glucocorticoid, developed by Stroes and coworkers to reduce macrophage amount and suppress plaque development, paradoxically increased monocyte influx and the number of macrophages in the plaque as well as aggravated plaque formation in $Ldlr^{-/-}$ mice [68]. Surprisingly, this result contradicted their early study where PLP-Lipo were found to accumulate in rabbit lesions and suppressed plaque inflammation [69]. The possible speculation for the discrepant results in mouse and rabbit models may be due to the differences in dose, treatment time duration, and induced plaque composition between mouse and rabbit studies. Particularly, the rabbit model was induced by balloon injury and represented the traditional balloon injury inflammation without a lipid environment, which is different from the lipid-driven inflammation induced in $Ldlr^{-/-}$ mice by an HFD [68]. Moreover, a relevant study reported by the same group also showed comparable results, further substantiating that PLP-Lipo may promote rather than suppress atherosclerosis development. Specifically, the study demonstrated that $Ldlr^{-/-}$ mice infused with PLP-Lipo for six weeks were found to have more advanced plaques with a greater number of inflammatory cells compared to the $LDLr^{-/-}$ mice treated with PLP-Lipo for 2 weeks [70]. These studies pointed out one of the main challenges in the current process of therapeutic or nanomaterial-mediated therapeutic development – merely using mice or rabbit models might result in an unreliable prediction of the outcome in patients, thus potentially promoting ineffective approaches into clinical trials

Despite the negative results observed in some earlier liposome studies, several recent studies demonstrated the great potential of using liposomal therapeutics to target macrophages for treating atherosclerosis. This is because more advanced liposomal therapeutics with excellent functionality and targeting ability to macrophages have been developed. For instance, in 2018, one study reported by Song and coworkers enquired into the possibility of applying folate modified liposomes loaded with telmisartan (TE-FA-Lipo) to treat atherosclerosis. Promisingly, the $ApoE^{-/-}$ mice with atherosclerotic plaque treated with TE-FA-Lipo for 12 weeks demonstrated features of regression of atherosclerosis, such as reduced macrophage content and necrosis, enhanced cholesterol efflux of macrophages, and increased collagen content [71]. In addition, Slutter and coworkers encapsulated the LXR agonist, GW3965, in liposomes functionalized with the cyclic peptide Lyp-1 (CGNKRTRGC) that binds to the p32 receptor expressed on foam cells. GW3965-containing Lyp-1 liposomes were shown to be taken up by foam cells *in vitro* and accumulate in atherosclerotic plaques in $Ldlr^{-/-}$ mice compared to non-targeted liposomes.

Moreover, these liposomes exhibited increased retention in the macrophages in the plaque compared to controls and reduced plaque macrophage content by 50% without inducing any side effects [72]. Similar to PLGA NPs, the anti-inflammatory cytokine, IL-10, was also loaded inside cRGD conjugated liposomes to target macrophages, mitigate inflammatory cytokine production, and resolve inflammation in the plaque [73].

Meanwhile, Zhang and coworkers created apoptotic body mimicking liposomes (AP-Lipo) that could target and emit an “eat-me” signal to macrophages to increase delivery efficiency. In particular, the AP-Lipo were prepared by first decorating liposomes with phosphatidylserine (PtdSer) to emit a phagocytic signal and initiate macrophage endocytosis of apoptotic cells, thus avoiding necrosis. Then, pioglitazone (PIO) was loaded in the PtdSer liposomes (PtdSer-Lipo) to increase the ratio of M2 macrophages, thereby suppressing the inflammation in the plaque. After that, the PIO loaded PtdSer-Lipo were further modified with cyclic peptide bearing a sequence of RGDfk (cRGDfK), a ligand targeting the integrin $\alpha v\beta 3$ in the plaque to construct the AP-Lipo (Fig.3a).

The TEM image showed that the AP-Lipo maintained a good spherical shape (Fig.3b). It was also demonstrated the AP-Lipo manifested a sustained release of PIO in phosphate-buffered saline (PBS, 10%) and serum (50%) within 72h (Fig.3c). Compared with PIO loaded unmodified liposome (Lipo) and PtdSer-Lipo, liposomes only modified with cRGDfK (cRGDfK-Lipo), and AP-Lipo demonstrated better cellular uptake in activated human umbilical vein endothelial cells (HUVECs) (Fig.3d). Nevertheless, the AP-Lipo were internalized more by M1 macrophages compared to cRGDfK-Lipo. Furthermore, a stronger green fluorescence from the antibody binding to CD206 was observed from the plaque of $ApoE^{-/-}$ mice treated with AP-Lipo compared to those treated with controls, indicating an excellent ability of AP-Lipo to increase the number and polarization of M2 macrophages (Fig.3e). The M2 polarization induced by AP-Lipo was also supported by the increase of mRNA expression of M2 macrophage markers (IL-4 and IL-10) and the decrease of M1 macrophage markers (IL-1β) in the plaque of AP-Lipo treated $ApoE^{-/-}$ mice (Fig.3f–h). More interestingly, Apo-Lipo induced a more remarkable increase in the collagen content of the plaque than the other groups(Fig. 3i,k), although there were no differences in the plaque area size between AP-Lipo and control-treated mice (Fig. 3j) [74]. This study was the first to use liposomes to fabricate advanced biomimetic NPs and demonstrated the advantages of using such an unprecedented biomimetic approach to improve the efficacy of atherosclerosis therapy. Besides apoptotic body mimicking liposomes, Kopaczynska and coworkers created photoactive liposomes to decrease macrophage amount in atherosclerotic plaque via photodynamic treatment. In this study, the liposomes were conjugated with Chlorin e6, a photosensitizer. The authors showed that the Chlorie e6-loaded liposomes accumulated in macrophages and induced macrophage phototoxicity *in vitro* [75]. Although photoactive liposomes have been studied for inducing apoptosis of cancers, it was the first time to apply them for atherosclerosis associated application. Despite the decreased number of macrophages upon the light-induced cytotoxicity from photosensitizer, this study did not provide any *in vivo* data. Thus, questions remain open whether the death of macrophages induced by light would promote or suppress atherosclerosis *in vivo*.

Along with macrophages and endothelial cells, immune cells, such as B and T lymphocytes, were investigated as targets for preventing or mitigating atherosclerosis through immunotherapy. It was reported that the naive T cells could develop into effector T cells upon the stimulation of antigens such as LDL, ApoB100, and ApoB100-derived peptide [76]. There are three types of well-known effector T cells. One type is T helper (T_H1) cells that have been found in atherosclerotic plaque and lead to atherosclerosis formation by activating macrophages and producing pro-inflammatory cytokines [76]. In contrast, another type of effector T cell is regulatory T (Treg) cells, which can release anti-inflammatory cytokines and suppress lesion growth. The third type of effector T cells is known as follicular helper T (T_{FH}) cells, which can help activated B cells to produce antibodies, such as an antibody against LDL (anti-LDL) for removing LDL and alleviating inflammation [76]. Thus, the successful development of an anti-atherosclerotic vaccine strongly depends on whether a specific antigen can induce the mobilization of Treg, T_{FH}, or B cell response. Liposomes have been investigated as vaccine adjuvant-delivery systems as their physicochemical properties can be modified easily. Numerous liposomal vaccines have reached markets for cancers, influenza virus, and fungal infections [77]. Although liposomal vaccines for atherosclerosis are still in preclinical development, significant advances in this field are encouraging. It was reported that the administration of apoptotic cells stimulates autoimmune and leads to the production of IL-10 by B cells. In 2015, Kyaw and coworkers investigated whether the administration of apoptotic cells or apoptotic cell mimicking liposomes comprised of PtdSer could regulate B cells and attenuate atherosclerosis formation in $ApoE^{-/-}$ mice. The *in vitro* and *in vivo* studies substantiated that both were able to diminish atherosclerosis development and suppress local inflammation by stimulating B1a cell proliferation, enhancing the secretion of polyreactive Immunoglobulin M (IgM) antibody (e.g., IgM antibody against Ox-LDL and leucocytes), and increasing production of anti-inflammatory cytokines [78]. Later in 2018, Slütter and coworkers compared the efficacy of 1,2-distearoyl-sn-glycero-3-phospho-rac-glycerol (DSPG), 1,2-dipalmitoyl-sn-glycero-3-phosphoserine, and 1,2-dipalmitoyl-3-trimethylammonium-propane liposomes with Ovalbumin 323 (OVA323) for inducing Treg safely. The *in vivo* study showed that all the three OVA323 loaded liposomes induced significant T cell proliferation in the $ApoE^{-/-}$ mice blood, which was in contrast to the free OVA323 that failed to induce any T cell production. Moreover, among those liposomes, the DSPG-liposomes were found to induce the largest Treg population and reduced 50% of atherosclerotic plaque formation in mice. Their findings demonstrated the potential for using DSPG-liposomes as vaccines to prevent atherosclerosis [79]. Additionally, in 2019, Sahebkar and coworkers evaluated the therapeutic effect of a liposome vaccine ($L\text{-}IFPTA^+$) to inhibit the proprotein convertase subtilisin/kexin 9 (PCSK9), which plays an essential role in regulating Ldlr and controlling low-density lipoprotein cholesterol amount. The $L\text{-}IFPTA^+$ was fabricated by first conjugating the liposomes with immunogenic fused PCSK9-tetanus (IFPT) composed of PCSK9 and tetanus peptides, followed by formulating the liposomes with alum vaccine adjuvant (A^+). $L\text{-}IFPTA^+$ was found to induce the greatest antibody immune response against PCSK9 peptide compared to the controls such as L-IFPT, $IFPTA^+$ and IFPT in the plasma of BALB/c albino mice fed with a standard diet. More importantly, this vaccine increased the population of anti-inflammatory T helper 2 cells but did not affect pro-inflammatory T_H1 cell amount [80]. Likewise, in other studies, the same group evaluated the

function of L-IFPTA$^+$ against the PCSK9 in hypercholesterolemic C57BL/6 mice. A similar immune response triggered by L-IFPTA$^+$ was also observed here. The vaccine could also decrease the size and severity of the lesion as well as reduce the total plasma cholesterol, very low-density lipoprotein cholesterol (VLDL), and LDL levels. Moreover, after vaccination, a decreased amount of IFN-γ secreting cells while an increased amount of IL-10 producing cells were observed in the splenocytes from the vaccinated mice[81, 82]. Due to the inadequate immune response observed after free cholesterol ester transfer protein (CETP) vaccine administration in clinical trials, a liposomal vaccine (Lipo-CETP) targeting the cholesterol ester transfer protein (CETP) was developed to improve the effect of free CETP vaccine. The Lipo-CETP was fabricated by encapsulating tetanus toxoid (TT)-CETP into liposomes. It was demonstrated that Lipo-CETP vaccinated rabbits showed fewer foam cells and less severe EC dysfunction compared to the controls, indicating the atheroprotective effect of Lipo-CETP. However, the underlying mechanisms have not been explored; thus, further studies are needed, as the efficacy of Lipo-CETP did not result from improving the lipoprotein levels in plasma or increasing the antibodies against TT-CETP [83]. These studies substantiate the potential for using liposomes loaded with proper antigen as a vaccine to prevent atherosclerosis.

2.1.1.2.2. High-Density Lipoprotein (HDL) NPs: The majority of native HDLs are composed of phospholipids and apolipoprotein A1 (apoA-1), with diameters ranging between 7 and 13 nm [84]. Numerous studies reported that native HDLs are anti-inflammatory, anti-oxidative, and anti-atherosclerotic, as they can remove cholesterol from foam cells in plaque by reverse cholesterol transport [85, 86]. Our recent review has provided a thorough summary of the progress on the development of HDL NPs for atherosclerosis treatment and diagnosis; thus, we only provide a brief highlight of some important recent studies [87]. Previous studies primarily focused on developing reconstituted HDL (rHDL) NPs and evaluating their efficacy for atherosclerosis treatment. However, the emphasis has recently shifted to the design of rHDL-based systems as therapeutic delivery carriers for targeted delivery of clinical medicines, antagonists, or genes to treat atherosclerotic plaques (Table 1). rHDL NPs are mainly fabricated by mixing apoA-1 from human plasma with phospholipid films [87].

In addition to the utility of rHDL NPs for atherosclerosis therapy, HDL mimetic NPs that are not fabricated with natural apoA-I are also being investigated to treat atherosclerosis. HDL mimetic NPs are commonly created by assembling phospholipids with either apoA-I mimetics, constructs of multivalent apoA-I mimetics, or apoA-I generated by bacteria (Table 2). The primary advantage of using apoA-I mimetics is that the cost and time for fabricating HDL mimetic NPs are dramatically reduced compared to those of rHDL fabrication due to the time-consuming process for extracting apoA-I from human plasma.

Overall, recent studies have focused on the development of more advanced rHDL NPs to improve the efficacy of rHDL NPs for atherosclerosis treatment. These advanced rHDL NPs were made by modifying them with plaque targeting ligands and loaded with various therapeutics ranging from clinical statins to RNAs to inhibitors for specific pathways associated with atherosclerosis. Moreover, co-delivery of dual therapeutics using rHDL NPs was investigated. These advanced rHDL NPs demonstrated exceptional ability to suppress

atherosclerosis development. Some of them even demonstrated efficacy for regression of atherosclerosis. However, the major issue of rHDL NP synthesis is that it requires apoA-I extraction, which may be challenging. As more understanding of rHDL NPs, to address the issue, HDL mimetic NPs were developed by using structure synthetic peptide instead of apoA-I. The use of synthetic peptides can be particularly useful for future large-scale production of therapeutics for atherosclerosis treatment in the clinical stage.

Aside from the HDL mimetic NPs, several studies have reported the development of novel anti-atherosclerotic peptides (Table 3). Table 3 summarizes these novel peptides that have been reported to show anti-atherosclerotic or anti-inflammatory function as well as the corresponding main functional component. The peptides listed hopefully inspire new research opportunities for the fabrication of novel HDL mimetic NPs or other types of anti-atherosclerotic pharmaceutical formulations.

2.1.1.2.3. Other Types of Lipid NPs: Several studies have highlighted the use of lipidic emulsion (LDE) that mimics the structure of protein-free low-density lipoprotein to deliver anti-cancer drugs for atherosclerosis treatment. This approach can suppress macrophage proliferation and migration, thereby alleviating atherosclerosis. For example, as early as 2007, Pereira and coworkers investigated the anti-atherosclerotic efficacy of PTX-LDE in rabbits. The authors observed that the LDE-PTX reduced the atherosclerotic lesion area by 60%, decreased the intima-media ratio by 4 -fold, and significantly suppressed SMC proliferation and macrophage migration. Later in 2011, Maranhao and coworkers showed that etoposide-loaded LDE (EPEG-LDE) provided an anti-atherosclerotic effect, as demonstrated by the fact that etoposide-LDE reduced the rabbit lesion and intima by 85% and 50% [117]. Similarly, in 2016, the same group conducted another study where carmustine (CAR), another anti-cancer drug, was loaded into LDE, and then the anti-atherosclerotic efficacy of CAR loaded LDE (CAR-LDE) was investigated in rabbits. The authors found that CAR-LDE reduced 90% of plaque formation and decreased the intima-media ratio by 8-fold in rabbits fed with high cholesterol diet. Moreover, macrophage content and inflammatory cytokines were significantly decreased by CAR-LDE compared to controls. However, T lymphocytes and collagen amounts remained unchanged upon CAR-LDE treatment [118]. Later in 2019, Maranhao and colleagues evaluated the anti-atherosclerotic efficacy of another type of LDEs, docetaxel (DTX) loaded LDE (DTX-LDE), in rabbits with atherosclerosis. Compared with controls, the atheroma area of rabbits was reduced by 80%, as well as MCP-1 and CD68 expression were decreased by 80% and 60%, respectively, via DTX-LDE treatment. The expression of pro-apoptotic factors (e.g., caspase 3 and caspase 9) and pro-inflammatory markers (e.g., TNF-α and IL-1β) were also reduced by the treatment [119].

To enhance therapeutic efficacy for treating atherosclerosis, several groups have co-delivered LDE loaded with different drugs and investigated the synergistic effect of these LDEs on atherosclerosis. As an example, in 2018, Tavares and coworkers delivered the combination of PTX and methotrexate (MTX) loaded LDE to treat atherosclerosis. They found less of a reduction in plaque area (49%) in rabbits treated with PTX-LDE alone compared to the ones treated with the combination of PTX-LDE and MTX-LDE (59%). Interestingly, intima reduction was only observed in rabbits treated with a combination of both LDEs. A greater

reduction in MMP-9 production, TNF expression, and macrophage quantity were also observed in PTX-LDE and MTX-LDE co-treated rabbits compared to those treated with either PTX or MTX-LDE alone [120]. Similarly, in another study, Maranhao and coworkers also evaluated the therapeutic efficacy of the combined treatment of LDE-MTX and EPEG-LDE in rabbits. A 95% reduction of lesion area was observed in rabbits treated with both LDEs, significantly more reduction than the rabbits treated with only LDE-MTX or EPEG-LDE [121]. These studies indicated a synergistically therapeutic effect by combining the delivery of different anti-cancer drugs

2.1.1.3. Micelles: Micelles are self-assembled nanostructures with a hydrophobic core and hydrophilic corona, commonly fabricated with amphiphilic molecules [122]. The amphiphilic molecules can range from peptide amphiphile (PA) to block copolymers. Micelles as drug delivery platforms have had a significant impact on cancer therapy [123]. A recent investigation targeting atherosclerosis has taken advantage of micelles' properties developed for cancer treatment, such as targeting the disease sites, improving the drug's hydrophilicity, and stabilizing the drug molecule.

PEG-based micelles are being widely investigated for atherosclerosis treatment due to their simple structures with easily manipulated lipid tails. One early example reported by the Moghe group in 2015 demonstrated that sugar-PEG micelles could effectively block lipid uptake through targeting the scavenger receptor (SR) and reduce lesion size in mice. In particular, to develop the most effective micelle system, the authors first created a library containing micelle systems composed of a mucic acid-based hydrophobic core (M12) but with various charges, stereochemistry, and hydrophobicity. Then, after screening these micelles' bioactivity, the authors discovered that the micelles with chiral symmetry provided better binding to the SR domain, suppressed the SR expression, and reduced lipid uptake in human monocyte-derived macrophages *in vitro*. In addition, among these micelles, it was found that only M12PEG micelles showed binding ability to CD36. Furthermore, compared with the untreated control, M12PEG micelles treatment resulted in a significant reduction of lipid uptake, neointimal hyperplasia, and inflammation, which led to a 37% reduction in the vascular occlusion *in vivo* [124]. Later in 2016, Uhrich and coworkers investigated the structure-activity relationship of PEG-based micelles. Particularly, the authors studied the effect of the hydrophobic tail of PEG amphiphilic polymers on micellar stability and anti-atherogenic activity. Compared with ester tails, micelles containing ether tails demonstrated higher storage and degradation stability in the presence of serum and lipases with more anti-atherogenic bioactivity. These improved properties were due to their enhanced alignment within the hydrophobic domain. In addition, the authors also discovered that increased hydrophobicity of PEG-amphiphilic polymers led to micelles with greater atheroprotective effects. The speculation for this finding was that micelles assembled by PEG-amphiphilic polymers with stronger hydrophobicity presented enhanced interactions in the micelle core, thereby preventing the micelles from disassembly [125]. These studies highlighted the importance of micelle structure and its effect on anti-atherosclerotic activity.

Inflammation cascade and oxidative stress contribute significantly to atherosclerosis formation and progression. Therefore, PEG-based micelles have been investigated to deliver anti-inflammatory agents to resolve local inflammation and decrease oxidative stress in

atherosclerotic plaques. One typical example is the ROS-responsive PEG micelles that release encapsulated drugs when interacting with excess levels of ROS in atherosclerotic plaques. The ROS responsiveness of the micelles is strongly dependent on the polymeric structures and components of the micelles. We do not intend to discuss how to design ROS-responsive micelles in this review. To treat atherosclerosis, Shuai and coworkers developed PEG-block-poly(propylene sulfide) (PEG-b-PPS) micelles, which were responsive to the oxidative microenvironment, to deliver andrographolide (Andro). Andro is a labdane diterpenoid and demonstrated anti-inflammatory effects; however, due to the low solubility of Andro in aqueous solution, its clinical application has been impaired. Because of the intrinsic ROS-responsive nature of PEG-b-PPS micelles, Andro loaded PEG-b-PPS micelles were able to release a large quantity of anti-inflammatory Andro to suppress the inflammatory response and alleviate oxidative stress in plaques *in vivo* [126]. This study provided proof of concept of using ROS responsive micelles to release anti-inflammatory agents in the plaque to combat atherosclerosis. Similarly, in the same year, Scott and coworkers applied ROS responsive PEG-b-PSS micelles to deliver celastrol, a hydrophobic inhibitor capable of downregulating receptors that activate the NF-κB pathway, which plays a crucial role in atherosclerosis. Notably, the PEG-b-PSS micelles showed high loading efficacy for celastrol, leading to a significant decrease in the effective concentration (4.2 pg/mL) required to inhibit NF-κB signaling in RAW 264.7 cells compared to free celastrol (0.2 μg/mL). Moreover, the *in vivo* study demonstrated a significantly smaller plaque in the $Ldlr^{-/-}$ mice treated with a low dose of celastrol loaded micelles compared with the mice treated with blank micelles and free celastrol at the same dose. Furthermore, the population of inflammatory immune cells, such as neutrophils and monocytes, were reduced by the celastrol loaded micelles [127]. Taken together, the above findings demonstrated that PEG-b-PSS micelles could improve the therapeutic efficacy of hydrophobic therapeutics significantly, which hold great promise for facilitating the resolution of local inflammation in atherosclerotic plaque in the future. Besides PEG-b-PSS micelles, micelles fabricated with other components have been developed to alleviate inflammation to treat atherosclerosis. For example, the Jiang group in the same year demonstrated that d-α-tocopherol PEG succinate based micelles loaded with berberine, a botanical medicine, could suppress inflammation in $ApoE^{-/-}$ mice fed with HFD by interrupting the crosstalk between macrophages and adipocytes and downregulating critical gene expression associated with inflammation such as NF-κB [128]. In a different approach, Nostrum and coworkers encapsulated a light-responsive photosensitizer, meta-tetra (hydroxyphenyl) chlorin, in PEG-lipid micelles to target the macrophages in plaques for potentially resolving the inflammation and suppressing plaque rupture. The *in vitro* study demonstrated the PEG-lipid micelles showed a selectivity of macrophages over vascular ECs, most likely due to the higher lipase activity in macrophages than that of ECs. However, *in vivo* studies failed to demonstrate such selectivity due to instability of the micelles *in vivo* [129]. The selective targeting of macrophages may reduce inflammation and avoid atherosclerotic plaque rupture resulting from photocytotoxicity to ECs caused by the photosensitizers.

Instead of directly targeting inflammation, some studies using PEG-based micelles focus on dendritic cells, Treg cells, or SMCs as targets for alleviating atherosclerosis. Dendritic cells play a crucial role in regulating atherosclerosis inflammation. One representative study

demonstrated that by adjusting the PEG and PSS block ratio, PEG-b-PSS micelles could be turned into polymersomes to selectively deliver anti-inflammatory aVD to dendritic cells, resulting in an increase in the number of Treg cells as well as an inhibition of atherosclerosis in ApoE$^{-/-}$ mice.[130]. Later in 2020, a follow-up study regarding the use of novel PEG-b-PSS cylindrical filomicelles was conducted to increase Tregs for improving atherosclerosis therapy. The uniqueness of PEG-b-PSS filomicelles was that they could form injectable filamentous hydrogels that can deliver monodisperse micelles with aVD to antigen-presenting cells. More importantly, these hydrogels were found to provide sustained release of aVD for over 2 months, which significantly enhanced the proliferation and homing of Tregs in ApoE$^{-/-}$ atherosclerotic mice [131]. An early study showed that PIO-PLGA NPs demonstrated excellent anti-atherosclerotic effect due to PIO's ability to bind to PPAR-γ, thus leading to macrophage repolarization [42]. Here, the Lv group used a similar strategy, where VCAM-1 targeting PEG micelles were assembled to deliver a PPAR-δ agonist, GW0742. However, in this study, instead of macrophages, the authors focused on SMCs and demonstrated that the VCAM-1 GW072-loaded micelles could target ox-LDL-treated SMCs and inhibit their migration and apoptosis [132]. These studies substantiated suppressing PPAR might be an effective approach to treat atherosclerosis. Peptide-based micelles have also been studied to improve the treatment of atherosclerosis. Typically, to construct functional spherical or cylindrical peptide-based micelles (nanofibers) for atherosclerosis treatment, several types of peptide amphiphile (PA) with specific functions were synthesized. In this respect, Tirrell and coworkers synthesized PA containing a hydrophilic part, VCAM-1-binding peptide (CVHPKQHR), and a hydrophobic lipid part, 1,2-distearoyl-sn-glycero-3-phosphoethanolamine-N-[maleimide(polyethylene glycol)-2000. Due to the PA's amphiphilic nature, it can self-assemble into spherical micelles and targeted the inflamed ECs *in vitro*. The *in vivo* studies demonstrated that significantly more PA micelles than the PEG micelles without targeting peptides accumulated in mice's plaque [133]. In a similar approach, Fang and coworkers developed plaque targeting PA micelles to deliver inhibitors to suppress miR-33 and miR-92a expression in the plaque. To target VCAM-1 and fibrin in the plaque, two peptides with sequences of VHPKQHR and REKA were conjugated to hydrophobic part for forming PA micelles, respectively. The authors demonstrated that the successful delivery of these micelles resulted in a decrease in targeted miR expression, leading to activation in macrophage cholesterol efflux and an increased expression of genes regulating the restoration of vascular function [134]. Later in 2017, Yoon and coworkers constructed nanosized hydrogel assembled with ECM-mimicking PA nanofibers (cylindrical micelles) containing a cell-adhesive ligand (RGDS) and an MMP-2 degradable peptide (GTAGLIGQ) to encapsulate human pluripotent stem cell (hPSC) induced ECs. The authors demonstrated that the nanomatrix PA gel improved the long-term survival and neovascularization effect of the encapsulated hPSC derived endothelial cells, indicating its promising clinical utility [135]. In 2018, Kibbe and coworkers reported the development of PA nanofibers for the targeted delivery of LXR to induce plaque regression. In particular, the ApoA1 mimetic peptide, 4F (DWFKAF-YDKVAEKFKEAF-NH2), was conjugated to palmitic acid to form the PA-4F nanofibers. The *in vivo* study demonstrated that high concentrations of PA-4F remained in atherosclerotic plaque for 2 days and were gradually cleared out after 14 days. Moreover, intravenous injection of PA-4F-LXR in Ldlr$^{-/-}$ mice led to much greater plaque reduction than scrambled PA, whereas slightly better plaque

reduction was observed in PA-4F-LXR treated Ldlr$^{-/-}$ mice compared with PA-4F treated ones. More importantly, neither PA-4F-LXR nor PA-4F resulted in increased aspartate aminotransferase levels, which were observed in LXR and scrambled PA treated mice, indicating both PA-4F-LXR and PA-4F did not induce liver toxicity as LXR and scrambled PA did. The advantage of using PA nanofibers compared to spherical NPs for drug delivery is that PA nanofibers showed better interaction with the vessel wall as drug delivery systems due to their increased surface area [136, 137].

Recent advances in immunotherapy have leveraged the progress in developing effective atherosclerosis vaccine and nanomaterial mediated vaccines [138]. It has also become evident in the field of micelles. For instance, in 2019, Mas-Oliva and coworkers reported that the *in vivo* evaluation of a lipid micelle intranasal vaccine, HB-ATV-8, was expected to prevent atherogenesis and non-alcohol fatty liver disease by generating antibodies against the CETP. The *in vivo* results showed that the HFD group treated with HB-ATV-8 vaccine exhibited a higher concentration of immunoglobulin G (IgG) against CETP than the untreated groups, without affecting body weight gain. After 7-month HB-ATV-8 treatment, the reduction of triglycerides concentration caused by the vaccine was also significant. Moreover, the collagen fiber of the aorta of the vaccine treated HFD group was better ordered, more tightly arranged, and close to that of the normal pig group, which was in great contrast to the disordered and loosely arrayed collagen fiber in the untreated HFD group. At a molecular level, the expression of atherosclerosis-related genes in the HB-ATV-8 vaccine treated HFD group tended to return to normal levels as measured in the control group. Furthermore, the fat accumulation and inflammation of hepatocytes in the vaccine-treated HFD group were comparable to the normal level [139]. This HB-ATV-8 vaccine provides a novel preventative means with great potentials for suppressing atherogenesis.

As mentioned earlier, HA NPs are biocompatible and can target plaque; several groups have designed atherosclerosis approaches by taking advantage of HA and micelles. In this study, the Li group reported an interesting study regarding the utility of copolymer micelles to load ST and cross-link HA hydrogel for treating atherosclerosis. The most interesting finding of this study is that the copolymer micelles cross-linked HA hydrogel was mechanically sensitive. The drug release rate increased as the mechanical stress stimulus from vascular occlusion increased. Particularly, the drug release rate increased from 58% to 74% when the stenosis increased from 55% to 75% occlusion. Moreover, the *in vivo* study showed that ApoE$^{-/-}$ mice treated with ST-loaded micelle cross-linked HA hydrogel showed only a small area of stenosis, which was in contrast to the rabbits treated with ST alone, showing relatively large occlusions in their carotid arteries [140]. In another study, Chen and coworkers developed ROS responsive micelles self-assembled by amphiphilic oligomeric HA to deliver Cur. These Cur-loaded micelles were sensitive to ROS due to the oligosaccharide. They could also target CD44 through HA, which led to a 47% reduction of plaque in mice compared with the controls without treatment.

2.1.1.4. Dendrimers: Dendrimers are synthetically produced polymeric nanostructures characterized by highly branched structures, named from the Greek word “dendron” to describe the polymeric structure. Dendrimers are typically composed of three major parts from the core to the exterior layer: 1) the central core molecule; 2) the repeating units that

could be several layers, with each layer termed as a “generation”; and 3) the external functional groups. The unique structure of dendrimers makes them promising drug carriers because of the cavity between the repeating units, providing space to encapsulate therapeutics. The functional groups of the external layer also possess high flexibility for modification to control properties, such as hydrophobicity and conjugation with agents. Additionally, the advantages of using dendrimers include high purity, uniformity, and stability. As drug carriers, dendrimers can also stabilize the drug molecule, enhance solubility, and achieve sustained release [141]. For atherosclerosis treatment, dendrimers have been utilized to deliver therapeutic agents with lesion targeting and controlled release. Among the various types of dendrimers, polyamidoamine (PAMAM) was widely studied for dendrimer assembly because of its simple synthesis and modification; other dendrimer types are also described.

Polyamidoamine (PAMAM) dendrimers, which are composed of repetitive subunits of amide and amine, are biocompatible and non-immunogenic with high water solubility [142]. It can either encapsulate or attach molecules in the nonpolar interior cavity or dendrimer surface, respectively. Moreover, PAMAM can induce multivalent effects to prevent drug aggregation. Therefore, PAMAM dendrimers have been extensively studied in the field of treating atherosclerosis. As early as 2013, Santos and coworkers aimed to create a novel dendrimer that could effectively prevent thrombosis. Particularly, they synthesized several PAMAM dendrimer derivatives and investigated their hemocompatibility, the effect on red blood cells’ viability, and antithrombotic effects *in vitro*. The authors showed that one of the dendrimer derivatives, PAMAM G4 (generation 4)-Arginine-Tos derivative, demonstrated the best hemocompatibility and antiplatelet/antithrombotic effect, as it increased the concentration of platelet response inhibitor cyclic adenosine monophosphate [143]. Later, in 2015, Qi and coworkers developed a liposome-G5 PEGylated PAMAM dendrimer complex as a carrier for the lipid-lowering oral drug, probucol (PB), to enhance water solubility, transepithelial transport, and oral absorption of PB. It was demonstrated that the lipid-lowering effect and plasma drug concentration were both significantly higher in PB-liposome/G5-PEG PAMAM-treated $Ldlr^{-/-}$ hyperlipidemia mice compared with those treated with PB alone [144]. Soon after, for optimization, the same group modified their G5-PEG PAMAM dendrimers into PB-liposome/G7 PEG-PAMAM dendrimers. Moreover, the authors showed that both PB-liposomes/PEG-PAMAM dendrimers (G5 and G7) achieved better stability and sustained PB release as well as displayed higher amounts of PB release compared to PB-liposomes. Additionally, there were no differences between G5 and G7 PB-liposome/PEG-PAMAM dendrimers in size, encapsulation efficiency, and PB release; however, G7 PB-liposome/PEG-PAMAM dendrimers had higher water solubility but lower cellular uptake compared to G5 PB-liposome/PEG-PAMAM [145]. Soon after, Cefalas and coworkers reported another example of using PAMAM dendrimers combining with photosensitizer for atherosclerosis. In this study, the authors utilized zero generation PAMAM dendrimer (G0) as a carrier for the photosensitizer zinc phthalocyanine (ZnPc) (G0/ZnPc) and discovered that, compared to the unloaded drug carrier (G0), G0/ZnPc had greater accumulation in the atheromatous plaque. Therefore, the PAMAM dendrimer with photodynamic therapy (PDT) shows promise in treating atherosclerosis [146]. In 2018, Christensen and coworkers complexed the cyclooxygenase-2 drug, a nonsteroidal anti-

inflammatory drug, with three different generations of 4-carbomethoxypyrrolidone surface-modified PAMAM dendrimers to mitigate severe side effects caused by free cyclooxygenase-2 delivery. The drug-PAMAM complex demonstrated a temperature-dependent drug-release profile, reduced toxicity, and significantly higher anti-inflammatory activity than free cyclooxygenase-2 [147].

Apart from enhancing drug stability and solubility and reducing cytotoxicity, the external layer of dendrimer could be easily modified to achieve targeting delivery. Several studies developed ligand-functionalized PAMAM dendrimers for the targeted delivery of therapeutics to improve the therapeutic efficacy for atherosclerosis. In one study, Low and coworkers created PEG-coated, acetic anhydride-capped, folate-targeted PAMAM dendrimers and investigated their application for inflammatory disease treatment [148]. The *in vitro* studies demonstrated a great binding of dendrimers to folate receptor-positive macrophages, and the *in vivo* studies exhibited selective accumulation of the dendrimers at the inflammation site [148]. Likewise, Ghosh and colleagues developed galactose-functionalized PAMAM G5 dendrimers (Gal-G5) to targeted deliver cholesteryl ester hydrolase (CEH) gene expression vectors to hepatocytes for removing blood cholesterol. The targeting ability of Gal-G5 dendrimers to hepatocytes was due to the strong affinity of GAL to asialoglycoprotein receptors expressed by hepatocytes. The great targeting ability of the Gal-G5 was demonstrated by a significantly higher accumulation of Gal-G5 observed in the liver compared to other organs in C57BL/6 mice. In contrast, a similar observation was not evident in the mice group treated with G5. It is worth mentioning that the mice treated with Gal-G5/CEH showed a 3 -fold higher CEH expression in the liver than that observed in G5/CEH treated mice. More importantly, the authors also explored the underlying mechanism for eliminating cholesterol by Gal-G5/CEH; they found that-Gal-G5/CEH could hydrolyze HDL-cholesteryl ester into free cholesterol and then convert the free cholesterol into fecal bile acids that can be cleared from the body [149]. Similar to galactose, mannose was also used to decorate PAMAM dendrimers for targeted delivery of therapeutics to atherosclerotic plaque. For example, in 2018, Ghosh and coworkers developed a mannose functionalized PAMAM dendrimer to selectively deliver ligands for LXR, an anti-inflammatory agent, to macrophages by targeting their mannose receptors. They discovered that the presence of these dendrimers enabled drug uptake by macrophages and circumvented hepatic degradation. Additionally, significant accumulation of the dendrimer-conjugated drug and atherosclerosis regression were observed in mice [150]. In a recent study in 2020, the same group applied their mannose functionalized PAMAM dendrimers to deliver therapeutics to regress atherosclerosis through a two-pronged approach. In particular, the authors hypothesized that the efficacy of regressing atherosclerosis would be enhanced if the macrophage cholesterol efflux and influx were increased and decreased at the same time, respectively. To test their hypothesis, the PAMAM dendrimers were loaded with LXR ligand and siRNA which were expected to increase macrophage cholesterol efflux and knockdown scavenger receptor class A (SR-A) for decreasing cholesterol influx, respectively. As expected, the two-pronged dendrimers showed better effect on lowing cellular cholesterol than SR-A siRNA and LXR ligand. This was supported by the finding that significantly more reduction of cholesterol in macrophages was seen in the two-pronged dendrimers treated macrophages than those treated with either SR-A siRNA or LXR ligand alone. To

assess the two-pronged dendrimer effect on atherosclerosis regression, $Ldlr^{-/-}$ mice were injected with two-pronged dendrimers weekly for 20 weeks. Promisingly, after 20 weeks, it was found that the mice treated with those dendrimers showed a regression of plaque where more than 20% decrease of total lesion and 40% reduction of plaque were observed compared to control mice [151]. As described above, lesion-specific targeting has gained immense attention and is the focus of atherosclerosis therapies via PAMAM-based dendrimers.

Aside from PAMAM-based dendrimers, other types of dendrimers have also demonstrated anti-CVD potential. For example, in 2019, the Turrini group developed gallic acid (GA)-enriched polyester-based G5 dendrimer (GAD) to enhance the therapeutic effect. The authors also compared the efficiency of GAD with free GA, *in vitro*, for inhibiting platelet aggregation. GA is a naturally occurring compound existing in many herbal plants and fruits, reported having antithrombotic, anti-ROS, and antibacterial activity. The authors found that, for the inhibition of platelet aggregation induced by collagen and thrombin, GAD exhibited 7.3- and 7.1- times higher potency, respectively, compared to free GA. Meanwhile, the GAD achieved 8.1- and 6.9- times stronger inhibition for ROS production by platelets, respectively [152]. In the same year, the Ornelas group reported enhancing the anti-inflammatory effect of bile acid via conjugation of the bile acid to polyamide dendrimers. The *in vitro* studies displayed little or no cytotoxicity and great anti-inflammatory effects of bile acid conjugated dendrimers, indicating that these bile acid-conjugated dendrimers could potentially treat chronic inflammatory diseases, such as atherosclerosis [153]. In 2020, the same group successfully synthesized a novel polyamide dendrimer, Dendri-$(ONO_2)_{18}$, with eighteen NO-releasing termini, aimed to achieve a long-term controlled NO release to treat inflammation. It was observed that Dendri-$(ONO_2)_{18}$ could achieve slow NO release after reacting with cysteine at pH 7.4 at room temperature and under anaerobic conditions. The authors estimated that the dendrimers could release NO for up to 4 months if that rate was maintained. Notably, the dendrimers also exhibited anti-inflammatory properties, with 27.9% of IL-8 inhibition from activated THP-1 cells at 4.17×10^3 nM (7.50×10^4 nM of NO moiety). Compared with the NO-releasing precursors, the dendrimer obtained slow NO release in a controlled fashion, thus showing a negligible pro-inflammatory property. Therefore, the Dendri-$(ONO2)_{18}$ are promising anti-inflammatory NPs that could release NO slowly with low cytotoxicity [154].

2.1.1.5. Cyclodextrin Based Nanomaterials: Cyclodextrins (CD) are cyclic oligosaccharides that exhibit biocompatibility, biodegradability, and low immunogenicity. CDs are mainly divided into three classifications, including α, β, γ-CDs. Earlier studies have demonstrated that CDs were also able to bind with lipids, regulate cholesterol metabolism, dissolve both extracellular and intracellular cholesterol crystals, deplete LDL, more importantly, and prevent LDL from being oxidized. For atherosclerosis treatment, beta-cyclodextrin (β-CD) and its derivatives are the most commonly used cyclodextrins due to their low cost, ease of accessibility and ability to form a stable inclusion complex with cholesterol. It is also reported that 2-hydroxypropyl-β-CD administration reduced plaque sizes in $ApoE^{-/-}$ mice on high cholesterol diet and NZW rabbits on HFD as well as decreased inflammation cytokines but increase HDL levels in these NZW [155, 156]. More

importantly, β-CD has been reported to form stimuli-responsive NPs that respond to internal or microenvironmental stimulus, such as pH, oxidative stress, enzyme, and light, which is beneficial for drug delivery applications [157, 158]. These promising studies led to a hypothesis that β-CD NPs might demonstrate extraordinary anti-atherosclerotic effects and deliver therapeutics in a controlled release manner. In fact, one of the limitations of treatment of atherosclerosis by free CD is that a high dose of CD is required, which may result in side effects. Therefore, researchers have been working towards the development of CD NPs. In the following section, we only review the recent advances in β-CD NPs for atherosclerosis treatment. We do not intend to discuss how to design the stimulus-responsive β-CD NPs via tuning the chemistry structure of β-CD, as a recent review has included a thorough discussion about this topic [157, 158].

Since there are high ROS levels and low pH levels during atherosclerosis progression, one impressive advance in CD NPs is the design of pH-responsive, redox-responsive, or dual-responsive β-CD NPs for delivering various therapeutics for treating atherosclerosis. For instance, in 2016, Zhang and coworkers synthesized acetalated β-CD (Ac-β-CD) NPs to deliver rapamycin (RAP) for preventing atherosclerosis progression. The unique property of Ac-β-CD NPs was that they exhibited a pH-dependent degradation profile, where under acidic pH, accelerated degradation of these NPs occurred. Moreover, the authors demonstrated that the kinetic release of RAP/Ac-β-CD NPs was strongly dependent on the structure of Ac-β-CD. An increased number of cyclic acetal units of Ac-β-CD resulted in a more sustained release of RAP in Ac-βCD NPs. The mice treated with RAP/Ac-β-CD NPs showed reduced plaque area, necrotic core area, inflammatory cytokine secretion, and macrophage number compared to the free RAP-treated mice. The great therapeutic function of RAP/Ac-β-CD NPs was due to the attenuation of mammalian target of rapamycin complex 1 (mTORC1) and mammalian target of rapamycin complex 2 (mTORC2) signaling pathways induced by these NPs [159]. In a subsequent study, the same team also developed advanced H_2O_2-eliminating and ROS-responsive β-CD NPs with great anti-oxidative and anti-inflammatory properties. Particularly, the H_2O_2-NPs were assembled using a series of oxidative β-CD (Ox-β-CD) synthesized by conjugating β-CD with phenylboronic acid pinacol with different types of linkers. The authors demonstrated that all Ox-β-CD NPs were able to eliminate H_2O_2, thereby inhibiting the apoptosis of macrophages caused by inflammation and oxidative stress resulting from H_2O_2. Moreover, the Ox-β-CD NPs also exhibited a synergistically therapeutic effect with zymosan for resolving inflammation in mice [160]. Soon after, a follow-up study was conducted by the same group where Zhang and coworkers applied the ROS-responsive NPs (Ox-β-CD NPs) to deliver RAP for treating atherosclerosis. The authors showed that Ox-β-CD NPs loaded with RAP inhibited macrophage proliferation and foam cell formation. More importantly, the atherosclerotic plaque was reduced to 4.5% after administration of RAP loaded Ox-β-CD NPs in $ApoE^{-/-}$ mice. This observation was remarkably better than the efficacy of RAP loaded PLGA NPs, which only decreased atherosclerotic plaque area to 19.8%. In addition, the authors also compared the therapeutic efficacy between RAP loaded Ac-β-CD NPs and PLGA NPs against atherosclerosis. It was found that the pH-sensitive RAP loaded Ac-β-CD NPs also possessed a superior anti-atherosclerotic effect over the RAP loaded PLGA NPs [161]. Later in 2018, Zhang and coworkers developed another type of ROS-eliminating β-CD NPs,

abbreviated as TPCD NPs, which consisted of β-CD linked with a free radical scavenger (Tempol), phenylboronic acid pinacol ester, and DSPE-PEG. The *in vitro* studies showed that the TPCD NPs significantly suppressed foam cell formation from RAW264.7 and mouse VSMCs, whereas free Tempol did not exhibit any inhibitory effect on these cells. More significantly, the anti-atherosclerotic efficacy of the TPCD NPs was significantly better than that of free Tempol. It was demonstrated that high and low-dose of TPCD NPs decreased the plaque area in ApoE$^{-/-}$ mice to 9.7±1.0% and 6.3±0.9%, respectively, which was much smaller than the plaque size of free Tempol treated mice (~22.5±1.5%). In addition, the TPCD NPs significantly reduced necrotic core size, the number of macrophages, as well as suppressed the expression of MMP in the lesions. The anti-atherosclerotic efficacy of TPCD NPs may result from their ability to inhibit the proliferation of inflammatory monocytes and suppress monocyte recruitment to the plaque [162]. In a more recent study, Zhang and coworkers conjugated their β-CD NPs with luminol (LCD NPs) for treating acute and chronic inflammatory diseases. The *in vitro* studies showed that the LCD NPs efficaciously suppressed inflammatory cytokines and ROS produced by neutrophils and macrophages, as well as inhibited cell migration. Moreover, compared to controls, a much smaller plaque containing fewer macrophages and neutrophils, but more collagen was observed in the ApoE$^{-/-}$ mice treated with LCD NPs [163]. Meanwhile, Hu and coworkers developed advanced pH and ROS dual responsive β-CD NPs to deliver RAP. The dual responsive NPs (RAP-AOCD NPs) were fabricated using pH-responsive material (ACD) and oxidation-responsive material (OCD) derived from β-CD. The pH and oxidation responsiveness were modulated by the ratio of ACD and OCD. Notably, the authors demonstrated the RAP-AOCD NPs possessed significantly greater capability of preventing SMC proliferation and migration, *in vitro*, compared to both free RAP and NPs that were either not responsive or single responsive. More promisingly, the RAP loaded NPs demonstrated potent efficacy for suppressing neointimal formation *in vivo* [164]. Besides being used as RAP delivery systems, in a study in 2020, pH-responsive CD NPs conjugated with an integrin targeting ligand were applied to deliver antisense oligonucleotide against microRNA-33 (anti-miR-33) for treating atherosclerosis. miR-33 has been reported to play a crucial role in regulating atherogenesis and regressing the expressions of several important adenosine triphosphate binding transporters that can reduce cholesterol efflux. In addition, long-term use of clinically used cholesterol-lowering drugs induce adverse effects such as myopathy and liver injury. Thus, the approach combining CD NPs and anti-miR-33 might be a potential alternative strategy to treat atherosclerosis. Indeed, the integrin targeted anti-miR-33 CD NPs showed excellent therapeutic efficacy, which was demonstrated by that the mice treated with 2 mg kg^{-1} NPs showed lower plaque area, smaller necrotic cores, reduced macrophage content, and MMP9 expression than the control without treatment or NPs without targeting ligand. These results indicated that these NPs suppressed plaque progression and increased plaque stability. Moreover, in addition to transporter regulation and cholesterol efflux promotion, the therapeutic efficacy of these NPs was also attributed to their ability to switch M1 macrophages to M2 macrophages and promote Treg cell differentiation [165]. The work discussed here strongly highlighted the tremendous therapeutic benefits from the CD NP-mediated approach; with the assistance of CD NPs, the therapeutic's efficacy can be enhanced to facilitate atherosclerosis therapy.

The studies mentioned above mainly focused on developing CD NPs targeting ROS and pH in the plaque. In a more recent study, Park and coworkers, rather than designing NPs with pH sensitivity and ROS responsiveness, developed novel cargo switching nanoparticles (CSNPs) to remove cholesterol and foamy macrophages from the plaque. The CSNP possessed a core-shell structure composed of a CD/statin core and a phospholipid shell (Fig.4a). CSNPs were expected to scavenge cholesterol in an atherosclerotic environment and release statin by cargo-switching to significantly enhance anti-atherosclerotic function (Fig.4a). Indeed, the CSNPs displayed an excellent ability to dissolve cholesterol, which was demonstrated by the fact that 6.5 mg CSNPs could effectively dissolve 0.2 mg of cholesterol in a buffer solution. Additionally, the CSNPs were shown to reduce the cholesterol in macrophages and plaque cholesterol significantly. More importantly, the *in vivo* studies demonstrated that the CSNPs could prevent plaque growth and lesion formation as well as suppress macrophage accumulation in ApoE$^{-/-}$ mice; this was in great contrast to free ST, free CD, and liposomal statin (LPST), which did not induce remarkable plaque, lesion and macrophage area reduction (Fig.4b–d). Unlike most nanomaterials discussed above, which only prevented atherogenesis, the CSNPs also exhibited the capability of regressing existing plaque in ApoE$^{-/-}$ mice fed with HFD or normal diet (NCD). Particularly, significant smaller lesion areas were observed in the aortic root, aortic arch, and thoracic aorta in the mice treated with CSNPs compared to that of untreated mice (Fig.4g–i); however, CSNPs did not affect the plasma cholesterol level notably (Fig.4f) [166]. Thus, it is anticipated that the effective elimination of cholesterol and foam cells via CD NPs could be a powerful intervention to resolve inflammation in the plaque.

Besides being used as the primary material for the fabrication of anti-atherosclerotic NPs, CD could also be utilized to functionalize other types of NPs and synthesize polymers for atherosclerosis treatment. For instance, human ferritins were found in plaque and could be taken up by macrophages. Therefore, CD-ferritin nanocages were expected to target foam cells and reduce their number by inducing cholesterol efflux. Thus, in 2018, the Lim group chemically conjugated CD on either the internal or external surface of ferritin nanocages and compared the nanocage's ability to reduce cholesterol levels in foam cells. Consistent with the expectation, both types of CD-ferritin nanocages decreased intracellular cholesterol levels while the type with a modified external surface-induced more reduction. More interestingly, the accumulation of CD-ferritin nanocages in foam cells was 3 times higher than that in macrophages due to the endocytosis mediated by transferrin receptors on foam cells [167]. Later, the Park group focused on developing nanosized cyclodextrin polymer (CDP) for atherosclerosis therapy. The CDP was synthesized by covalently crosslinking CD with epichlorohydrin. CDP showed a much longer half-life (~26.8 h) than monomeric CD (~5 h). In addition, significantly more CDP accumulated in the plaque of ApoE$^{-/-}$ mice than that of CD, which induced cholesterol efflux, reduced lesions in the aortic arch, and increased collagen content effectively, thereby stabilizing the plaque [167]. Additionally, in one study, Daunert and coworkers showed that a complex composed of β-CD and alpha-tocopheryl phosphate could decrease lipid accumulation by affecting both the signaling pathway mediated by CD36 and the expression of genes related to lipid hemostasis and inflammation. The authors demonstrated that the depletion of lipids and the reprogramming macrophages' polarity in the plaques were induced by β-CD released from the NPs [168].

Taken together, these studies discussed here demonstrated that CD-based nanomaterials hold a great promise as therapeutic delivery systems for treating atherosclerosis effectively.

2.1.1.6. Carbon-Based Nanomaterials: Carbon-based nanomaterials have obtained increasing attention for atherosclerosis treatment because of their unique properties after modification. Recently, carbon nanotubes, graphene, and fullerene are the most well-studied carbon-based nanomaterials, which have shown therapeutic effects for atherosclerosis after functionalization or when combined with other agents/materials.

Carbon nanotubes (CNTs) are nanosized tubular structures composed of carbon atoms. CNTs are mainly classified into single-wall carbon nanotubes (SWNTs) and multi-carbon nanotubes (MWNTs). CNTs were not as widely investigated as other types of nanomaterials for atherosclerosis treatment in the past. This was because several earlier studies reported that CNTs would injure the endothelium and promote monocyte adhesion and calcification, advancing atherosclerosis development [169, 170]. However, some recent studies have brought excitement to researchers working in this field by demonstrating the great potential for using modified CNTs to treat atherosclerosis. For instance, in the view of the strong optical absorbance of SWNT upon NIRF, as early as 2012, McConnell and coworkers showed successful photothermal ablation of macrophages in plaque via SWNTs *in vitro* and *in vivo*. [171]. Later in 2016, to further improve the photothermal ablation process of macrophages via SWNTs, the Kim group functionalized the SWNTs with phenoxylated-dextran (pD-SWNT). It was hypothesized that the modification would improve the solubility of SWNTs and allow for macrophage targeting, thereby alleviating the aggregation of SWNTs and enhancing the anti-inflammatory efficacy of SWNTs. The *in vitro* study met the authors' expectations, as demonstrated by apoptosis of a large quantity of RAW264.7 cells after pD-SWNTs treatment and laser irradiation. The authors also demonstrated that unmodified SWNTs had low efficiency in converting photon energy to thermal energy and presented limitations such as high cytotoxicity, aggregation issues, and lack of targeting ability [172].

Likewise, the Leeper group reported a fascinating study in 2020 that significantly advance the field. They developed a novel type of macrophage-specific targeting pro-efferocytic SWNTs, showing tremendous potential for the use of modified SWNT for atherosclerotic treatment. Particularly, given the important role of CD47 signaling in promoting atherosclerosis, an innovative type of SWNTs, SWNTs-SHP1i, was developed by first modifying the SWNTs with PEG, followed by loading pro-efferocytic inhibitors (SHP1i) in the SWNTs. The SWNTs-SHP1i were expected to inhibit the signaling pathway for CD47 and signal regulatory protein-α (SIRPα) in the monocytes and macrophages. The inhibition of CD47 binding to SIRPα served to prevent the activation of Src homology 2 domain-containing phosphatase-1 (SHP1), thereby suppressing plaque expansion. For investigating the uptake of SWNTs-SHP1i by macrophages, SHP1i-free SWNTs were further modified with Cy5.5 (SWNT-Cy5.5). *In vivo* biodistribution of those SWNTs-Cy5.5 substantiated the targeting ability of those SWNTs to the lesional macrophages and monocytes. This was demonstrated by SWNT-Cy5.5 accumulation in 70% and 60% of monocytes and macrophages in plaque, respectively. In contrast, negligible amounts of the SWNTs were taken up by ECs and SMCs (Fig. 1a). The selective targeting to lesional macrophages may

be explained by two possible mechanisms: first, the SWNTs did not target the lesional macrophages directly but were first taken up by circulating monocytes and subsequently traveled to the plaque during atherogenesis; second, due to the nanoscale size of SWNTs, macrophages in the lesions were targeted passively via extravasation. Of note, the ApoE$^{-/-}$ mice with inflammation showed less plaque area after being treated with SWNTs-SHP1i than the controls treated with SWNTs-Cy5.5 (Fig. 5b–c). This finding occurred because the SWNT-SHP1i interrupted the CD47-SIRP± signaling, supported by a decrease in intraplaque SHP-1 phosphorylation activity caused by SWNT-SHP1i compared to the control (Fig. 5d–e). In addition, an enhancement of efferocytosis activity by SWNT-SHP1i treatment was also demonstrated by a lower ratio of free apoptotic cells to apoptotic cells associated with macrophages in the lesion of SWNT-SHP1i-treated mice than the controls (Fig. 5f). Therefore, compared to the controls, a smaller necrotic core, less apoptotic cells, and reduced inflammation were observed in the lesion of SWNT-SHP1i treated mice (Fig. 5g–h). Moreover, single-cell RNA sequencing of macrophages isolated from SWNT-SHP1i and SWNT-Cy5.5-treated mice aortas revealed that SWNTs-SHP1i induced the downregulation of pro-inflammatory genes but upregulation of genes associated with anti-inflammation of macrophages. Also, the SWNT-SHP1i treated macrophages were enriched in genes associated with processes, such as phagocytosis and antigen presentation, upregulating necrotic cell clearance. The pathway analyses also demonstrated that SWNTs-SHP1i downregulated genes relevant to chemokine mediated signaling, cellular response to pro-inflammatory cytokines, and monocyte chemotaxis (Fig. 5i–j) [173].

Graphene is another type of carbon-based nanomaterial, composed of a single layer of carbon atoms in the form of a honeycomb lattice. Graphene-based nanomaterials have not been widely investigated for atherosclerosis treatment. Many studies instead focused on graphene derivatives as a biochemical sensor for atherosclerosis-related pathological processes [174–176]. Graphene oxide (GO), deriving from graphene, were explored as potential anti-inflammatory therapeutics and found to attenuate gastrointestinal tract and colitis *in vivo* [177, 178]. However, until recently, researchers have not investigated the therapeutic effect of graphene nanomaterials for atherosclerosis using *in vitro* or *in vivo* atherosclerosis models; only a few studies investigated the GO'S effect on cells associated with atherosclerosis such as macrophages, ECs, and SMCs. For instance, the Lee group in 2015 demonstrated targeted photothermal ablation of macrophages using mannosylated-reduced graphene oxide (Man-rGO), *in vitro*. The Man-rGO showed great targeting affinity to mannose receptors on macrophages; therefore, the combination of NIR and Man-rGO induced 30% macrophage apoptosis, showing a great promise for atherosclerosis treatment [179]. In another study, Keyoumu and coworkers synthesized polyphenol-gold co-loaded graphene (poly-Au-GO) nanocomposite and studied their effects on rat vascular smooth muscle cell (VSMC) proliferation, cell cycle proteins, and downregulation of messenger RNA. A notable therapeutic component used in fabricating poly-Au-GO nanocomposite was polyphenol. Polyphenol was reported to prevent oxidation of LDL and inhibit EC/SMC proliferation. Experimental data showed that poly-Au-GO nanocomposite at 0.5 μg/mL significantly inhibited VSMC proliferation by 30% compared with the control (fetal bovine serum) at 24 h up to 72 h, where VSMC DNA synthesis was found to be also inhibited. Also, real-time PCR analysis revealed that the nanocomposite arrested the VSMC cell cycle

in the G1 phase by downregulating cyclin D1 and E genes, thereby suppressing VSMC proliferation. More importantly, poly-Au-GO nanocomposite also reduced TNF-α-induced inflammation as shown by the decrease in expression of cytokines (e.g., IL-1β, IL-6), adhesion molecules (e.g., ICAM-1 and VCAM1), and chemokines (e.g., MCP-1) [164]. In a more recent study, Kim and coworkers demonstrated that the macrophage targeting GO complexes (MGCs) reduced ROS and inflammation in M1 macrophages. Moreover, IL-4 pDNA-loaded MCGs were shown to polarize M1 macrophages into M2 macrophages both *in vitro and in vivo* [180]. Despite slow progress in this field, graphene was also studied as a component of vascular stent coating for treating atherosclerosis as well as avoiding severe complications resulting from stent deployment, which is described in the stent section below.

In addition, fullerene and its derivatives were also studied to treat atherosclerosis. Fullerene possesses a hollow spherical structure composed of sp^2 hybridized carbons of different sizes [181, 182]. Like other nanomaterials, fullerene has also been investigated as delivery systems for various pharmaceutical applications due to its ability to down-regulate ROS or generate oxygen species by light exposure [181–183]. However, the use of fullerene for atherosclerosis treatment was not as promising as it was expected. It was reported that fullerene with PDT treatment did not suppress but promoted atherosclerosis development in the atherosclerotic rabbit model [184]. Thus, most studies have shifted their center and focused on developing modified fullerene or its derivatives for applications associated with atherosclerosis therapy. One representative example was reported by Kepley and workers in 2017. In this study, the authors tested the anti-inflammatory efficacy of thirty fullerene derivatives for inhibiting foam cell formation *in vitro*. Among the tested fullerene derivatives, the authors found that the fullerene derivatives, tris-malonate fullerene and amphiphilic liposomal malonylfullerene showed competitive efficacy for inhibiting foam cell formation via reducing TNF receptor-associated factor 2 and NF-KB expression. Moreover, the mice treated with either of the derivatives showed inhibition of plaque growth [185]. Similarly, in the same year, Li and coworkers also demonstrated that trimetallic nitride endohedral fullerenes with carboxyl suppressed TNF-α expression in macrophages and showed robust ROS scavenging ability [186]. Likewise, in a more recent study, Wei and colleagues synthesized carnosine-modified fullerene NPs to scavenge ROS. The NPs were found to be highly biocompatible and water-soluble. More importantly, these NPs exhibited excellent ROS scavenging capability for hydroxyl radical, indicating the great potential for using NPs to treat atherosclerosis strongly associated with oxidative stress [187]. Therefore, fullerene modification for atherosclerosis treatment deserves further exploration in future studies.

2.1.1.7. Inorganic Nanomaterials: Inorganic nanomaterials, as discussed in recent atherosclerosis therapy studies, are mainly metallic NPs and hybrid nanomaterials (e.g., metallic oxide nanomaterials, quantum dots, and metallic sulfide nanomaterials). Taking metallic NPs for instance, in 2016, Jo and coworkers investigated the use of VCAM-1 binding peptide modified gold (Au) nanospheres for the targeted delivery of therapeutic against miR-712 (anti-miR-712) to inflamed ECs for atherosclerosis treatment. By using the Au spheres, enhanced uptake of anti-miR-712 by ECs was observed [188]. Later, in 2017, Dou and coworkers encapsulated photosensitizer Ce6 into silica NPs to form upconversion

NP Ce6 complex for PDT. The authors found that the complex-mediated PDT could effectively promote the cholesterol efflux of foam cells by enhancing ROS generation to induce foam cell autophagy [189].

Metal oxide NPs, particularly iron oxide NPs, are well-studied for atherosclerosis treatment. For example, in 2018, Choi and coworkers investigated whether DNA coating could enhance the targeted accumulation of superparamagnetic iron oxide NPs (SPIONs) in atherosclerotic plaque. The authors hypothesized that DNA coating could promote the accumulation of SPIONs in the atherosclerotic plaque, as the negatively charged DNA coating would allow the NPs to be easily taken up by macrophages. Indeed, the *in vitro* results supported their hypothesis, where the amount of DNA-coated superparamagnetic iron oxide NPs (DNA-SPIONs) taken up by RAW264.7 cells was 5- fold higher than PEG-modified SPIONs without DNA coating. Consistent with *in vitro* study results, the *in vivo* study demonstrated that DNA-SPIONs accumulated significantly more in mice aorta than PEG-SPIONs [190]. In addition to DNA coating to enhance the local accumulation of iron oxide NPs, in another study, Tae and colleagues explored another approach using peptide ligands. In particular, the authors modified pluronic F127 nanocarriers (NCs) containing iron oxide with two different peptide ligands, cRGD peptide ligand and collagen IV peptide ligand (KLWVLPKGGGC). The authors compared their targeting efficacy to the plaque and found that the cRGD modified NCs showed better efficiency for targeting the early atherosclerotic plaque *in vivo* compared with collagen IV peptide. Therefore, in the following study in 2020, the same group applied the cRGD modified pluronic NCs with iron oxide to deliver IL-10 for treating atherosclerosis. The NC extended the release of IL-10 up to 2 weeks, which was in great contrast to the free IL-10 that diffused out within 24 h *in vitro*. Furthermore, the *in vivo* study showed that IL-10-NC with iron oxide NPs demonstrated a prolonged elimination half-life (~8 h) and improved the accumulation of IL-10 in the mice plaque compared to free IL-10 (~0.6 h half-life), which led to a 30% decrease of plaque area in $ApoE^{-/-}$ mice [191].

In addition to iron oxide NPs, other transitional metals are also being investigated for atherosclerosis therapy because of their advantages such as low cost and toxicity, high stability, and excellent photothermal conversion efficiency. For example, in 2019, the Parkin group reported using molybdenum dioxide (MoO_2) nanoclusters to treat atherosclerosis via photothermal ablation. The authors showed that the MoO_2 mediated photothermal ablation demonstrated a significant effect on eliminating macrophages with minimal damage to ECs, thereby reducing the inflammation *in vitro*. Moreover, when combined with photothermal ablation, MoO_2 prevented the thickening of the vessel wall and eliminated macrophages in mice [163]. In the same year, the Lu group explored the possibility of using $CuCO_2S_4$ nanocrystals for treating arterial inflammation via photothermal ablation. It was found that the $ApoE^{-/-}$ mice treated with $CuCO_2S_4$ nanocrystals and NIR irradiation demonstrated much less macrophage infiltration than the controls treated with PBS [192]. Other than photothermal ablation, metal-based nanomaterials were also utilized in gene therapy. Tang and coworkers developed cerium oxide nanowire (CeO_2 NW) to deliver antisense oligonucleotides (ASOs) to silence the mTOR, thereby activating the autophagy process and suppressing foam cell formation. Although RAP inhibitors can activate autophagy, it is challenging to apply them clinically due to their low solubility and bioavailability. Thus, to address these issues, the authors developed CeO_2 NWs with a high aspect ratio for

endosome escape; in addition, the CeO_2were also modified with PEG for extended circulation and functionalized with an S2P specific peptide ligand for plaque targeting. Thus, the S2P-CeO_2-ASOs were found to have a better ability to knock down mTOR, thereby preventing atherosclerosis progression more effectively than free CeO_2-ASOs, free ASOs, and free RAP [193].

Quantum dots (QD), a type of semiconducting NPs with unique optoelectronic properties, have also recently been investigated for atherosclerosis therapy. Specifically, in one study, Berestein-Lopez and coworkers inquired into whether liposome QD can be used to deliver siRNA that targets the fatty acid binding protein 4 (FABP4) gene of macrophages. FABP4 has been reported to be associated with CVD; it has also been used as a circulating biomarker to predict CVD risk due to its ability to transport lipids into cells. Their studies showed that siRNA-loaded liposome QDs could attenuate apoptosis of macrophages by blocking the apoptotic pathway. Additionally, these NPs were also found to suppress autophagy, therefore enhancing the plaque stability. However, there was no *in vivo* evaluation of the anti-atherosclerotic efficacy of these NPs in the current study [194]. In another study, Yang and coworkers demonstrated that amorphous nano-selenium quantum dots (SeQDs) could prevent endothelium dysfunction and reduce atherosclerosis formation in mice. The anti-atherosclerotic effect of SeQDs resulted from their ability to inhibit Na^+/H^+ exchanger 1 [163]. In a recent study, graphene quantum dots were used to fabricate advanced NPs, monocyte GQDs-miR-223 complexes, taking advantage of inorganic and organic nanomaterials as well as biologic components, to deliver miR-223 for regulating the immune system and inflammation in the plaque. To construct the monocyte GQDs-miR-223 complexes, miR-233 was first attached to the GQDs through disulfide linkage, followed by grafting the GODs-miR-223 onto the monocyte membrane using a C18 peptide with an MMP-9 degradable sequence (GVFHQTVSR). Due to the unique components of the complex, the complexes were expected to first target the plaque by the monocyte, then release GQD-miR-223 by C18p digestion via MMP-9, and finally deliver the miR-223 to the macrophages via intracellular cleavage of disulfide linkage via lysosomes, thus regulating the inflammatory response caused by atherosclerosis. Therapeutically, the authors showed that the $ApoE^{-/-}$ mice treated with monocyte GQDs miR-223 complex exhibited 84.34% unobstructed area and 45.82% reduction in plaque size compared to mice without any treatment [195].

2.1.1.8. Biomimetic NPs: Biomimetic NPs are an innovative type of NPs that combine favorable characteristics of synthetic materials and natural materials. They provide advantages for drug delivery, such as extended circulation time, better targeting ability, and more efficient immune escape when compared with traditional nanomaterials [196]. Such advantages have driven the employment of these NPs to deliver therapeutics to improve the efficacy of atherosclerosis therapy [196]. Biomimetic NPs can be divided broadly into whole cells, NPs coated with cell membranes, and cells modified with targeting ligand mimicking cell surface proteins. However, the most interesting biomimetic NPs developed in recent studies for improving atherosclerosis therapy are mainly cell membrane coated NPs; thus, we will mainly discuss them in this section. NPs with biomimicking targeting ligands are summarized in other sections based on the main component of the NPs.

By taking advantage of PLGA NPs as drug delivery systems, in a recent study, Ge and coworkers developed biomimetic platelet-mimicking NPs (PNPs) by coating the platelet membrane around PLGA NPs (PNPs) [197]. The authors also loaded RAP in the PNPs and investigated the anti-atherosclerotic effects of RAP loaded PNPs (RAP-PNPs). Due to the platelets' high affinity to atherosclerotic plaque, the PNPs exhibited a great binding affinity to collagen and fibrin, allowing for selective plaque targeting, which was demonstrated by the observation of preferential accumulation of PNPs in the atherosclerotic plaque. For therapeutic function, RAP-PNPs attenuated atherosclerosis progression, as demonstrated by a 14% decrease of lesion and plaque area but an increase in lumen area, collagen content, and smooth muscle cell amount in the plaque of mice [197].

In addition to platelet membranes, another example of designing biomimetic NPs were conducted by Wang and coworkers; they developed biomimetic NPs (RBC/RAP@PLGA) by coating red blood cell (RBC) membranes on PLGA NPs loaded with RAP. The authors showed that the RBC/RAP@PLGA demonstrated excellent immune-evasive properties due to the natural properties of RBCs. This was evidenced by the fact that these NPs were observed to avoid macrophage-mediated phagocytosis *in vitro* and *in vivo*. Additionally, compared to the uncoated NPs in the aortas of $ApoE^{-/-}$ mice, an improved accumulation of RBC coated PLGA NPs was observed. The mice treated with RBC/RAP@PLGA showed the lowest ratio of the plaque to the whole aorta as well as the smallest plaque size among all the experimental groups, indicating a better anti-atherosclerotic efficacy of RBC/RAP@PLGA than that of free drug or uncoated NPs. Moreover, a decrease in macrophage, SMC, and MMP amount were observed in the plaque of mice treated with RBC/RAP@PLGA, suggesting the RBC/RAP@PLGA could stabilize the plaque stabilization [198].In addition to platelet and RBC biomimetic NPs, in one interesting study, Tasciotti and coworkers designed leukosome biomimetic NPs to deliver RAP to treat vascular inflammation. The leukosome biomimetic NPs were fabricated by integrating leukocyte-derived membrane proteins on to lipid NPs. The authors demonstrated that RAP encapsulated leukosome biomimetic NPs (Leuko-RAP) significantly decreased the macrophage population and pro-inflammatory cytokine secretion associated with macrophages and granulocytes in mice compared to the untreated groups. Moreover, the plaque percentage was reduced from 73% to 65% when the mice were treated with Leuko-RAP [199].

Also, for the treatment of atherosclerosis, Tang and coworkers developed another type of biomimetic NPs. The biomimetic NPs were fabricated by coating EC membranes on bovine serum albumin manganese oxide NPs (EC-BSA-MnO_2). Due to the EC membrane coating, the EC-BSA-MnO_2 were expected to escape from phagocytosis and accumulate in the plaque by targeting the homotypic ECs. MnO_2 NPs were chosen to fabricate the biomimetic NPs because they can be decomposed easily into Mn^{2+} by abundant hydrogen peroxide in atherosclerotic plaques. The Mn^{2+} from the EC-BSA- MnO_2 can function as integrin activators to suppress the inflammation signal coupled by integrin, reducing macrophage accumulation and suppressing plaque formation. The *in vivo* study supported this expectation, as it was found that the EC-BSA-MnO_2 could target the plaque of $ApoE^{-/-}$ mice and suppress the expression of Yes-associated protein phosphorylation and nuclear exportation resulted from integrin activation. More importantly, more reduced lesion size

was observed in the ApoE$^{-/-}$ mice treated with EC-BSA-MnO_2 (73.9%) compared with that treated with the control, manganese(II) chloride (53.2%) [200]. Besides, Wang and coworkers recently developed ROS responsive macrophage biomimetic NPs (MM-NPs) by self-assembling oxidation-sensitive amphiphilic chitosan oligosaccharide followed by coating the NPs with macrophage cell membrane via extrusion (Fig.6a–b). Moreover, to treat atherosclerosis, the authors encapsulated AT into the MM-NPs to construct MM-AT-NPs with a diameter of 220 nm (Fig.6d–e). Because cells are also suitable drug carriers, the authors encapsulated the ROS responsive NPs into macrophages to construct AT-NPs/MAs for being compared with the MM-AT-NPs (Fig.6c). Better targeting ability of MM-NPs for inflammation was demonstrated by a significantly stronger fluorescence in the aorta of mice treated with Cy7.5-MM-NPs compared to that in mice aortas treated with Cy7.5-NPs without macrophage membrane coating (Cy7.5-NPs) and free Cy7.5 (Fig.6f). However, the mice treated with Cy7.5-NPs/MAs demonstrated slightly higher fluorescence intensity in the aorta than the mice treated with Cy7.5-MM-NPs, possibly due to the macrophage recruitment during atherogenesis. Regarding therapeutic function, when used to prevent plaque formation in mice, MM-AT-NPs showed the best efficacy compared with the controls as they induced the smallest lesion and plaque and macrophage accumulation areas (Fig.6g–i). In addition, MM-AT-NPs treatment also led to smaller necrotic cores in the mice compared with other groups such as free AT, AT-NPs, and AT-NPs/MAs. Meanwhile, a thicker fibrous cap, less MMP expression (Fig. 6j), and more SMCs were observed in the mice treated with MM-AT-NPs compared with other groups, indicating the excellent ability of MM-AT-NPs to stabilize plaques. Of note, MM-AT-NPs were found not only to prevent atherogenesis but also to sequester pro-inflammatory cytokines (TNF-α, ILI-β, and MCP-1) by binding to these cytokines through the antigen of the macrophage membrane coated on the NPs (Fig. 6k–m). This study strongly demonstrated the advantages of using ROS responsive biomimetic NPs for treating atherosclerosis [201].

Overall, several types of biomimetic NPs were synthesized by coating cell membranes from platelets, RBCs, macrophages, and ECs on synthetic nanomaterials, such as polymeric NPs or inorganic NPs. Using these biomimetic NPs for the targeted delivery of drugs, atherosclerosis progression has been significantly reduced *in vivo*. More remarkably, some biomimetic NPs loaded with drugs even demonstrated better therapeutic efficacy than their counterparts. It is also worth mentioning that besides the biomimetic NPs mentioned here, apoptotic mimicking NPs and HDL mimic NPs discussed in the earlier sections are also representative examples of the biomimetic NPs exhibiting excellent anti-atherosclerotic effects.

2.1.1.9. Other Nanomaterials: Besides the aforementioned nanomaterials used in delivering therapeutics for atherosclerosis treatment, other nanomaterials such as nanopolyplexes and nanofibers were also investigated. For instance, in 2017, the Kim group reported the development of DNA nanopolyplexes for treating atherosclerosis. The nanopolyplexes were fabricated by condensing eNOS plasmids with either redox-sensitive poly(oligo-L-arginine) (rsPOLA) or redox-sensitive poly(oligo-D-arginine) (rsPODA, control). L-arginine was selected as intracellular L-arginine was reported to be associated with endothelial nitric oxide synthase (eNOS)-mediated production of NO. The *in vitro*

study showed that rsPOLA induced higher nitrate levels in TNF-α activated ECs than rsPODA. A better efficacy for decreasing anti-inflammatory cytokines in activated ECs was also observed in rsPOLA compared with rsPODA. Moreover, *in vitro* data was found to agree well with the *in vivo* study where a greater reduction in inflammatory cytokine expression and higher nitrite levels were observed in $Ldlr^{-/-}$ mice treated with rsPOLA compared with that were treated with rsPODA [202]. Similarly, in 2019, Shuai and coworkers also demonstrated the use of CD36 targeting nanopolyplexes (TNPP) as gene vectors to deliver anti-PAK1 siRNA to macrophages for alleviating atherosclerosis. Serine/threonine-protein kinase (PAK1) is expressed by macrophages and associated with atherosclerosis development. Thus, TNPP was expected to suppress atherosclerosis progression by downregulating the expression of PAK1, RAW264.7 cells treated with TNPP demonstrated 65% less production of PAK1 protein, much lower ox-LDL uptake, and less expression of IL-6 and MCP-1 compared with controls. The anti-atherosclerotic effect of TNPP was also demonstrated by the decreased lesion size (63%) in mice treated with TNPP compared with the untreated groups. Significantly lower production of MCP-1 and IL-6 by foam cells were also observed in TNPP-treated mice [203].

In another study, the Wickline group formulated NPs by using peptide against JNK (anti-JNK2 peptide) and p5RHH-siRNA and evaluated the NPs' anti-atherosclerotic efficacy *in vitro* and *in vivo*. Anti-JNK2 peptide and p5RHH-siRNA were utilized to target the JNK protein, which is known to regulate foam cell formation. The $ApoE^{-/-}$ mice fed with a Western diet showed decreased JNK mRNA and the corresponding protein, as well as the number of macrophages in the plaques after being treated with p5RHH-siRNA-anti-JNK NPs. More importantly, the endothelium barrier's integrity was recovered, and the likelihood of thrombosis was also reduced [204]. Likewise, in the same year, nanosuspensions (NS) were used to deliver Cur via ultrasound by the Lian group. Their study demonstrated that Cur-NS was more easily phagocytosed by macrophages than free Cur. Additionally, the phagocytosis of Cur-NS was further enhanced by ultrasound. The synergistic effect between ultrasound and Cur-NS was clearly substantiated by the fact that the highest ROS production by macrophages and MMP-2 reduction was induced by Cur-NS combining ultrasound irradiation compared with Cur and Cur-NS. It was also interesting to observe that more portions of M2 macrophages than that of M1 macrophages were found in mice plaque treated with Cur-NS. This finding indicated that the combination of Cur-NS and ultrasound might reprogram the macrophage subtypes [187].

2.1.2. Nanomaterials for Stent Functionalization and Vascular Graft Fabrication for Atherosclerosis Therapy

2.1.2.1. Nanomaterials for Stent Functionalization: In advanced lesions, different stent types have been developed to maintain luminal integrity but are still faced with respective weaknesses. Bare metal stents (BMS) are limited by restenosis [205]; drug-eluting stents (DES) reduce restenosis, but the non-specific anti-proliferative agents induce delayed endothelialization, late stent thrombosis, and the polymeric drug carrier causes inflammation [206]; and bioresorbable vascular scaffolds (BVS) have been withdrawn from the market due to a high risk of thrombosis and target lesion failure [206]. Therefore, nanotechnology-based approaches, such as NP conjugation and surface nano-scale coating, are used to

assemble novel designs for nanomaterials to improve biocompatibility, achieve targeted drug delivery, and improve stent safety and efficacy. So far, the nanomaterials that have been widely studied in stent applications for coating include inorganic nanomaterials, polymeric nanomaterials, carbon-based nanomaterials, and hybrid nanomaterials.

Taking inorganic nanomaterials for example, as early as 2015, Ding and coworkers attempted to solve the rapid degradation issue of Mg stents. They reported a simple method to prepare a nanoscale magnesium fluoride (MgF_2) film coating with a 200 nm flake-like feature and a thickness of 0.8 μm on Mg alloy stents to reduce corrosion and improve stent efficacy *in vitro* and *in vivo*. Coating characterization and *in vitro* studies showed that the MgF_2 nanofilm-coated stent reduced corrosion and increased EC viability and adhesion. *In vivo* studies in the abdominal aorta of NZW rabbits exhibited that MgF_2 nanofilm-coated stents attenuated inflammatory cell adhesion and achieved complete and well-aligned endothelialization [207]. Another example of using inorganic nanomaterials for stent coating was demonstrated by the Desai group in 2017, where a titanium dioxide (TiO_2) nanotube (NT) array with a mean diameter of 90±5 nm and a length of 1800±300 nm was used to modify the stent surface. The authors showed that the TiO_2 coating could suppress in-stent restenosis with negligible side effects. *In vivo* evaluation in the over-inflation rabbit iliofemoral artery model, compared with bare-metal stainless steel stents (SS) and bare metal titanium stents (Ti), NT-covered titanium stents (TiNT) could reduce neointima with the lowest stenosis rates and obtain a strong interaction between newly formed tissue and the NT array [208]. The Webster group reported a similar study where a nano-film of TiO_2 was coated on the stent to stimulate EC adhesion and proliferation [209].

Like inorganic nanomaterials, polymers were also modified with nanotechnology to improve biocompatibility and therapeutic efficacy. For instance, in 2018, the Virmani group developed a drug-free COBRA-PzF coronary stent system (COBRA-PzF™, CeloNova BioSciences, Inc., TX, USA) by depositing Polyzene-F (PzF) nanocoating on BMS (≤0.050 μm thickness) aimed to suppress thrombus formation and improve biocompatibility. PzF is an inorganic nano-thin polymer made of repeatable phosphazene units. Compared with commercially available BMS, the COBRA-PzF stented arteries demonstrated a larger lumen area, less neointimal thickness, and lower injury score at days 28 and 90 in porcine normal coronary arteries. However, there were no clear differences in re-endothelialization and inflammation among all experimental groups on day 90, indicating the recovery of all stented arteries. Of note, nano-coating significantly reduced monocyte/macrophage adhesion, inflammatory cytokine secretion, and thrombus formation compared with BMS and COBRA stents without nanocoating. Moreover, ongoing clinical trials have shown very low rates of thrombosis. Consequently, this novel COBRA-PzF coronary stent system has great potential of being used in patients with high bleeding rate [210]. Another related study was reported by Belle and workers in 2020. In this study, the authors evaluated the early re-endothelization of COBRA-PzF stent in rabbit iliac arteries and demonstrated that complete reendothelization was observed 7 days after stent implantation [211].

Besides PzF, polydopamine (PDA) was also investigated for stent coating because PDA has been shown to promote EC but inhibit SMC attachment as well as it is easy to be modified. For instance, in 2019, Kwon and colleagues developed a novel 3D printed heparin-loaded,

PLA-based biodegradable stents with excellent hemocompatibility and an ability to inhibit restenosis and thrombosis. The heparin-loaded, nanocoated (~328.13 nm) PLA stent was prepared by coating PDA, PEI, and heparin on the 3D printed PLA stent. *In vitro* fibrinogen and platelet adhesion tests displayed minimal protein attachment/activation and low hemolysis on the coated surface, indicating great thrombo-resistance and hemocompatibility of the developed coating materials. These attributes were also confirmed in the *ex vivo* porcine arteriovenous shunt model. More interestingly, it was found that heparin-loaded stents suppressed SMC proliferation while improving EC proliferation. For *in vivo* evaluation in the porcine restenosis model, nanocoating reduced the fibrin score and the restenosis rate at 28 days. Hence, the 3D printed biodegradable stent may be another candidate for the new generation of coronary artery stents [212]. Likewise, Liu and coworkers prepared fibronectin-loaded heparin/poly-l-lysine NPs and immobilized these NPs on the stents with PDA coating. The *in vitro* study showed that the coated stents effectively suppressed platelet adhesion and activation and demonstrated improved biocompatibility and faster endothelization than uncoated ones [213]. Additionally, in one study, Wang and coworkers synthesized PDA NPs modified with EC targeting peptide (REDV) to improve endothelization on stent-grafts. Synergetic improvement of EC proliferation and reduction of platelet attachment by the PDA NPs and REDV was observed [214]. In another study, an antithrombotic drug, EP224283, was immobilized on PDA coated stents by the Blanchemain group to address thrombosis. It was shown that the coated stents exhibited anticoagulation activity for 7 days [215]. In addition, PDA was also used along with HA to coat stents by Guan and coworkers to promote endothelization. The authors investigated the effect of HA molecular weight on the stent function. They found that coating composed of PDA and HA of 1×10^5 Da showed the best ability to promote endothelization and resist alloy degradation *in vivo* [216]. Meanwhile, Xu and coworkers developed a reduction-responsive branched vector (SKP) with disulfide bonds, which could form complexes with VEGF plasmids. The authors coated the SKP/VEGF plasmid complexes on the stents pretreated with PDA and demonstrated that such coating resulted in an improvement of endothelization on the stent via local upregulation of VEGF production in rabbits [217].

In addition to PDA, PLGA based nanomaterials were also explored for stent coating for single or dual drug-releasing and miR delivery. For instance, in 2019, the Liu group evaluated the in situ delivery of vildagliptin from PLGA nanofibrous stent coating for single drug release. Vildagliptin, a dipeptidyl peptidase-4 enzyme inhibitor, was shown to improve endothelialization and suppress SMC proliferation when administered as oral medicine, which might also be effective when delivered with stents. Drug release curves showed the drug's initial burst release, followed by a controlled release for up to 28 days. Moreover, the authors discovered that higher drug dosing could lead to larger nanofiber diameter and pore size, as well as increased promotion of EC migration *in vitro*. This was confirmed by the *in vivo* evaluation in rabbit abdominal aorta, where the rabbits treated stents with -high drug dose for 8 weeks exhibited the least neointimal thickness. As a result, the vildagliptin-releasing stent has the potential to treat atherosclerosis lesions and improve the recovery of injured stented arteries [198]. Due to the limitations of sirolimus-eluting stents, such as delayed re-endothelialization and late stent thrombosis, in the same year, the Wen group

displayed their stent with a novel single drug coating composed of ticagrelor-releasing biodegradable PLGA nanofibers. Ticagrelor was reported to inhibit SMC proliferation. *In vitro* evaluations exhibited that the stent coated with ticagrelor-releasing nanofibers (152.1 ± 53.4 nm diameter) improved cell attachment to the stent surface, achieved continuous drug release for up to 28 days, and reduced platelet adhesion. In addition, after 4 weeks of implantation in the rabbit descending abdominal aorta, the ticagrelor-eluting stent showed significantly higher endothelialization, less SMC proliferation marker expression, and upregulated protective superoxide dismutase 1 expression when compared with the sirolimus-eluting stent [218]. For dual-drug release to obtain multifunctional efficacy, in 2018, the Wang group reported a novel metallic stent coating that could release dual drugs to suppress both restenosis and thrombosis. The coating is composed of core/shell NPs that can load anti-proliferative DTX in their PLGA cores and platelet GP IIb/IIIa monoclonal antibody (SZ-21) in their CS shell. The core/shell structure of the NPs achieved different release kinetic profiles of DTX and SZ-21 from the NPs; there was a faster release of SZ-21 from NP shell and slower release of DTX from NP core observed for up to 28 days. Moreover, compared to blank NP coated stents and stainless-steel stents, the stents coated by NPs loaded with SZ-21 and DTX demonstrated significantly better hemocompatibility *in vitro*, shown as reduced platelet adhesion and activation. Consistent with *in vitro* results showing the promotion of endothelialization and inhibition of SMC proliferation and migration, the *in vivo* evaluation in pig coronary arteries indicated that the dual drug-loaded NP coating obtained the least restenosis compared to controls after 1, 3, and 6 months [219]. Similarly, the Hung group, in 2018, reported a novel dual drug-loaded biodegradable stent (DLBS) for lesions located at the bifurcation to achieve suppression of thrombosis and restenosis. The DLBS surface was electrospun with PLGA/rosuvastatin and PLGA/PTX as the nanofibers' inner and outer portions, respectively, with average diameters of about 600 nm. Release kinetics tests displayed the controlled release of rosuvastatin and PTX for up to 27 and 70 days, respectively. Then, the inhibition of platelet aggregation and SMC viability was significantly greater than the metallic stent control. Therefore, this DLBS might have unique advantages for treating atherosclerosis, especially for bifurcation lesions [220]. In addition, PLGA was also used for gene therapy to deliver microRNA effectively. Ono and coworkers conjugated miR-126 to cholesterol and utilized PLGA NPs for site-specific induction. In the rabbit model, the miR-126 NP-conjugated stent suppressed neointimal hyperplasia, indicating its potential to prevent restenosis.

Besides PLGA based nanomaterials, other novel polymers were also used for stent surface modification. The Logothetidis group, in 2017, reported their dual-drug (rosuvastatin and heparin) stent nanocoating composed of cellulose acetate nanofibers with a diameter of 200-800 nm and a pore diameter of 6-16 μm to improve biocompatibility and suppress both restenosis and thrombosis. Drug release study demonstrated that both rosuvastatin and heparin had initial burst release caused by the drug on the fiber surface and later, sustained release for up to 4 weeks caused by fiber degradation. [221]. In another study in 2019, Borros and coworkers tried to achieve gene therapy using stents by coating BMS with a thin layer of pentafluorophenyl methacrylate covalently bonded with poly (β-amino ester) NP-loaded with green fluorescence plasmid. The authors endeavored to ensure the controlled release of green fluorescent protein plasmid from the NPs and successful transfection of

targeting cells. By incubating with COS-7 cells, transfected cells with green fluorescence were observed, indicating the successful delivery of plasmid from the NP-loaded polymer coating and its potential for delivering therapeutic plasmids [222]. In addition, in 2020, Martel and coworkers reported stent coating developed by electrospinning containing nanofibers made of CS and poly-cyclodextrin. The coating was shown to release the statin about 3μg/mm^2 within 6h, leading to a great potential to prevent restenosis later.[223] Moreover, Mao and co-workers designed poly(2-dimethylamino ethyl methacrylate-co-ethylene glycol diacrylate) nanocoating used a novel vapor based approach to release sirolimus and atorvastatin from the stents. Strikingly, by controlling the coating's thickness, the zero-order sustained release of sirolimus and atorvastatin from the coated stents for 30 days was achieved. Moreover, the suppression of SMC proliferation was induced at a low dose of atorvastatin of 5 ug/cm^2[224]. In another study, Kim and coworkers created an elastic interpenetrated hydrogel network with improved mechanical property and enhanced hemocompatibility, consisted of methyl methacrylate terpolymer incorporated with polyurethane [225]. In addition, polymer coating generated from poly(R, S)-3,3-dimethylmalic acid) [226], phosphorylcholine [227] and zwitterionic poly(ester sulfobetaine)urethane ureas [228] were also investigated for employing for stent coating recently.

Similarly, carbon-based nanomaterials were also studied for functional stent coating. Although carbon-based nanomaterials were not studied for stent application as widely as polymer nanomaterials, it has the unique feature to repel ox-LDL after modification. For example, the Garcia group, in 2017, reported a novel method to functionalize CNT easily and quickly with α-bromoacid and the organic compound 2-(methacryloyloxy) ethyl phosphorylcholine for stent coating. The wettability analysis of the CNT and functionalized CNT (F-CNT) demonstrated that the functionalization could induce a better repellent behavior of F-CNT to ox-LDL compared with CNT. Moreover, the authors also showed that both CNT and F-CNT had no distinct cytotoxicity to HepG2 cells *in vitro*. Thus, the F-CNT has great potential to be used on stent surfaces to reduce ox-LDL adhesion and neoatherosclerosis initiation effectively [221]. In 2019, the same group reported another study about *in situ* nitrogen doping method and reduction of graphene oxide (N-rGO) as nanomaterials for stent coating. Wettability tests demonstrated that the N-rGO were able to repulse ox-LDL and did not affect the cell viability of HUVECs for up to 100 μg/mL. Thus, N-rGO may serve as an effective and protective stent coating in the future [229].

Likewise, hybrid nanomaterials fabricated with organic and inorganic materials were also investigated to treat atherosclerosis. For instance, in 2017, our lab developed a multifunctional NO-releasing PA nanofiber-coated stent to improve reendothelialization while suppressing restenosis, thrombosis, and inflammation.NO was conjugated to PA so the resulting PA-NO could form nanofibers and achieve sustained NO release to suppress SMC proliferation and inflammation while improving re-endothelialization. The *in vitro* study demonstrated that, under physiological flow, the NO-releasing nanomatrix coating successfully inhibited SMC migration, monocyte adhesion, and platelet adhesion while improving endothelialization, compared with commercially available BMS and DES [230]. Besides, the Jung group, in 2019, developed a nanoscale CS-silica xerogel hybrid coating to incorporate sirolimus for improving hemocompatibility and endothelialization of stents. The

authors showed that the addition of silica could improve the adhesion between the coating and substrate, significantly increasing the hydrophilicity to enhance initial cell attachment and prolong the release of sirolimus. Specifically, the CS-30 wt% silica coating showed better HUVEC adhesion and spreading and more prohibited platelet attachment/activation, indicating the enhancement of endothelialization and suppression of thrombosis from the hybrid coating. Therefore, the CS-silica xerogel hybrid coating shows great promise in promoting vascular recovery after stenting [231]. Another study conducted by the Yang group in 2019 developed a novel stent copper-based organic metal framework (Cu-MOF) coating immobilized by PDA to promote desirable vascular healing by simultaneously inhibiting platelet activation, enhancing endothelialization, and suppressing hyperplasia (Fig. 7a). Particularly, TEM images demonstrated Cu-MOF nanocrystals ranging in size from tens to hundreds of nanometers that were uniformly distributed in the PDA coating. In addition, chemiluminescence analysis indicated that Cu-MOF coating catalyzed NO release from the wide-spread NO donor, S-nitrosoglutathione., As the authors expected, *in vitro* and *ex vivo* evaluations confirmed that Cu-MOF coating reduced platelet adhesion and activation, reduced SMC proliferation, and improved endothelialization, especially after the addition of NO donor, compared with controls (Fig. 7b–d). Moreover, the extracorporeal blood circulation study demonstrated that the surfaces coated with titanium (Ti) and PDA showed thrombosis with severe occlusion, which was in great contrast to MOF coated surface where almost no occlusion or thrombosis was observed (Fig. 7e–f). Similarly, the *in vivo* evaluations in rabbits also demonstrated that the MOF coating significantly decreased the neointimal thickness and restenosis compared with the control stent without coating (Fig. 7g–i). Additionally, immunostaining of CD31 of MOF coated and uncoated Ti wires implanted in the rabbits indicated that a promoted endothelialization was induced by MOF coating compared with bare Ti wires. Less neointima thickness was also observed in the MOF coated Ti. Meanwhile, by immunostaining α-SMA (contractile SMC marker) and OPN (synthetic SMC marker), the authors also found that the MOF-coated Ti wire showed a more nearly complete contractile SMC circle compared with Ti wire that was surrounded by a large quantity of synthetic SMCs and demonstrated a discontinuous contractile SMC layer (Fig.7j). The mechanism for a better inhibition of neointimal hyperplasia by MOF coating was that the coating could suppress the NO-cyclic guanosine monophosphate pathway, induce faster reendothelialization, and reduce inflammation produced by macrophages that led to SMC migration and proliferation [232]. One example regarding hybrid materials was reported by Wang and workers, where a stent coating consisted of GO-loaded with DTX and chitosan-loaded with heparin were developed to suppress thrombosis and restenosis. The authors showed that the coating inhibited platelet adhesion and activation, SMC migration, and proliferation [233]. In addition, the stent coating composed of GO, polystyrene sulfonate, heparin, and poly(3,4-ethylene dioxythiophene) demonstrated excellent anti-fouling and anti-clotting properties, demonstrated by Hsu and coworkers lately [234]. In another example, instead of using GO, the graphene sheet was decorated with TiO_2 NPs by the Talaat group to coat stents. The coated stents showed better mechanical and hematological properties than the uncoated ones [235]. Also utilizing graphene, the Pan group created a novel 3D printed patient-specific dual-drug releasing biodegradable stent system composed of nanocomposites made with PCL nanofiber and graphene. Interestingly, the authors demonstrated the customization of their stents based on the 3D CT imaging of

the patients' lesions. *In vitro* evaluations showed no harmful effects on HUVECs from the stent. Moreover, the anti-coagulative inositol phosphate (IP6) and anti-proliferative niclosamide were incorporated in the nanocomposites coated on the stent. *Ex vivo* evaluations in swine coronary arteries exhibited a great antithrombotic function of the PCL-GR-Nic-IP6 stents [236]. Besides, in a recent study, Han and coworkers demonstrated that hybrid stent coating composed of an abluminal layer, PLGA, magnesium hydroxide, and sirolimus were also shown to exhibit enhanced re-endothelialization and great anti-inflammatory function resulted from Mg^{2+} and OH^{-} ions released from the coating. Meanwhile, the authors also showed that the magnesium hydroxide could neutralize the acidic compounds degraded from PLGA to suppress side effects [237]. Furthermore, the Huang group fabricated another type of hybrid stent coating using biodegradable poly(1,3-trimethylene carbonate) and Ti-O film with and without drugs. The inner layer Ti-O film coating was shown to enhance re-endothelialization, whereas the outer layer Ti-O film was demonstrated to suppress platelet adhesion and activation as well as SMC growth [238]. Similarly, in 2020, Monjo and coworkers described their unique stent coating composed of a Ti nanonet nanostructure functionalized with quercitrin (NNQR). It was found that the NNQR-coated surface demonstrated significantly higher roughness and hydrophilicity than non-nanostructured Ti and quercitrin only coated surface. Reduced adhesion of platelets and bacterials, lowered NO production, and increased HUVEC metabolism were observed in NNQR coated surface compared with non-nanostructured Ti and quercitrin only coated surface. The NNQR coating also showed great hemocompatibility. [239]. Therefore, hybrid stent coating could take advantage of features from different material with relatively simple fabrication and promoted safety and efficacy.

Several innovative biomimetic designs could effectively promote stent efficacy. Interestingly, mussel's adhesive property inspired several studies to utilize the mussel adhesive protein to further functionalize stent surface, improve re-endothelialization and antiplatelet effects, and suppress SMC proliferation. For instance, Wang and coworkers applied mussel adhesive protein on the stent, followed by immobilization of VEGF or CD34 to create a biofunctional coating for stents. As shown, EC proliferation and spreading were enhanced by VEGF-coated stents, while CD34-coated stents could capture $CD34^{+}$ cells [240]. In one study, Pan and coworkers designed a biomimetic stent coating composed of mussel inspired peptide, EC-specific moieties, NO-generating organoselenium, and EPC targeting peptide. For coating, the mussel inspired peptide could bind to the surface of stents via metalcatechol coordination, thereby allowing the further modification of stents with EC specific ligand on stents. The dual functional material coated stents exhibited excellent EPC capture ability *in vivo*; 2 h after implantation in rabbits, the stents were covered with EPCs. More importantly, an intact EC layer consisted of elongated ECs was observed after 12 weeks of coated stent implantation with decreased neointimal hyperplasia, while the uncoated stents were covered by ECs with abnormal morphology [241]. In addition to direct use of mussel associated peptide for coating, NO-releasing coatings inspired by mussels were also generated in other studies reported by Yang and coworkers. These coatings consisted of dopamine (DA) with selenocystamine or copper ion, serving as catalysts to generate NO locally by converting endogenous NO donors, S-nitrosothiols in blood, to NO instead of directly delivering short half-life NO. According to the studies, both coatings could generate abundant NO for more

than 30 days, which suppressed SMC growth and migration while promoting EC growth and reducing restenosis. However, it is interesting to find that the coating composed of DA and copper ion generated NO in flux more comparable to the physiological value than the one consisted of DA and selenocystamine. In addition, DA and copper ion coated stents also inhibited platelet activation and aggregation [242, 243]. Similarly, stent coating was also designed by the same group by a metalcatechol-amine surface engineering strategy in a more recent study, where hexamethylenediamine (HD) grated with a high amount of heparin (1 ug/cm^2), Cu^{II} for local production NO, and catechol DA to produce a nano-thin layer of adhesive PDA were used to form a Cu^{II}-DA/HD network to provide a prohealing microenvironment for stents. Remarkably, after the coating, stable NO generation for 60 days with a rate around 2.2×10^{-10} mol/cm^2/min from the coated stents was observed. It is of more importance to note that the authors also demonstrated that the Cu ion concentration affected the cell behaviors on stents; when the concentration ranges between 12.5 μg/mL and 50 μg/mL, the coating could effectively inhibit SMC proliferation and migration without compromising its ability to stimulate EC proliferation. Moreover, due to the high density of heparin grafted on the coating, the *ex vivo* anti-thrombogenic test demonstrated that the coated stents significantly could reduce occlusive thrombosis, which was in great contrast to the uncoated ones on which severe thrombus formed [244]. In addition to NO, this year, VEGF was used along with Cu^{II}-DA to coat stents for improving re-endothelialization at the early stage. *In vivo* studies showed that the Cu^{II}-DA and VEGF coated stents achieved compact endothelization with a neointimal area of 2.3 ± 0.48 mm^2 in 1 month, while the uncoated stents did not show complete coverage of ECs and demonstrated significantly larger neointimal area [245]. Besides the use of mussel mimicking materials, in another study, an “endothelium mimicking strategy” was brought up by Yang and coworkers, where a stent coating was developed to mimic the two key physiological functions of endothelium utilizing selenocystamine (as NO donor) and heparin aimed to improve the re-endothelization and the stents’ antiplatelet activity [246]. Additionally, the pro-healing multifunctional endothelium-mimicking nanomatrix stent coating developed in our lab also utilized the “endothelium mimicking strategy,” which is described in the earlier peptide amphiphile part.

In sum, it is clear that nanomaterial-based approaches ranging from NP modification to nanocoating hold great potentials for improving re-endothelialization and promoting the recovery of a stented artery with healthy functions while suppressing restenosis, thrombosis, and inflammation and minimizing negligible side effects. Encouraged by the promising results, substantial efforts should be devoted to the realm of designing nanomaterials for future stent applications.

2.1.2.2. Nanomaterials for Vascular Graft Fabrication: Vascular grafts are used in the surgical process via coronary artery bypass grafting for treating occluded vessels caused by atherosclerosis. However, current vascular grafts are sometimes associated with limitations such as delayed endothelialization, thrombus formation, and occlusion [247], neointimal hyperplasia [248], and low mechanical strength [249].To solve these issues, several studies focused on applying nanomaterials to surface modifications to improve the performance of vascular grafts.

For instance, in 2017, the Heath group developed a nano-scale clustering surface, composed of ligands that can bind to integrin using RGD-functionalized copolymers, for potential vascular graft modifications. The authors demonstrated that the nano-scale clustering surface showed much less fibrinogen adsorption compared with a polystyrene surface. Interestingly, the nano-scale clustering surface was also found to enhance endothelialization [250]. A similar study in 2019 reported by the Jang group showed that the nano-thick tantalum layer could enhance the growth and adherence of ECs to vascular grafts made by expanded polytetrafluoroethylene (ePTFE). Additionally, the tantalum-modified ePTFE vascular grafts also demonstrated a great ability to suppress platelet adhesion and activation [251]. Simultaneously, the Turng and Li groups deposited nano-scale multilayer coating composed of VEGF and Hep on electrospun PCL vascular grafts through the layer-by-layer assembly. The authors showed that the multilayered grafts released VEGF and Hep through MMP-2 degradation, promoting the angiogenesis of ECs and exhibiting anti-thrombogenic properties [252]. Similarly, the Rouxel group used piezoelectric polymers, poly(vinylidene fluoride-trifluoroethylene) P(VDF-TrFE), to fabricate vascular grafts. In addition, they incorporated zinc oxide (ZnO) NPs into the scaffold; they found that 1-2% ZnO did not enhance the attachment of ECs and human mesenchymal stem cells and decreased the chances of failure after implantation. Interestingly, after implanting the P(VDF-TrFE) and P(VDF-TrFE/ZnO) scaffolds, the authors illustrated that ZnO NP-modified scaffolds induced a high degree of vessel formation in contrast to unmodified scaffolds, in which only a few vessels formed [253]. Additionally, the Roicotti group doped barium titanate NPs, a type of elastomeric material, into polyurethane and polydimethylsiloxane vascular grafts. The doped grafts demonstrated 1100 kPa burst strength, which was similar to that of a native artery and higher than un-doped grafts, possessing a burst strength at 800 kPa. In addition, the doped grafts displayed high stability and good biocompatibility. This enhancement may have resulted from the ability of ZnO NPs to induce ROS production, enhancing cell proliferation, and improving angiogenesis [254].

Recently, many studies emphasize the use of nanofibers to address the limitations of current vascular grafts by either promoting endothelialization, better mimicking native artery structures, or enhancing the mechanical properties of the vascular grafts. Great progress has been made in this area (Table 4).

Despite NPs being used for decorating vascular grafts, the primary nanomaterials studied for improving the vascular graft property were nanofibers. Nanofibers were employed to strengthen mechanical properties and deliver therapeutics in a controlled manner, thereby improving EC proliferation, decreasing inflammation and hyperplasia, and enhancing the ability to regulate cell phenotype and prevent platelet attachment compared with vascular grafts without drugs and lower mechanical properties. The improvement resulting from the nanofibers described above demonstrates that nanofiber-incorporated vascular grafts show great promises, and future work in this field might assist in facilitating the development of new approaches for treating atherosclerotic vessels.

2.2. Nanomaterials as Contrast Agents for Atherosclerosis Imaging and Diagnosis

Nanomaterials, especially NPs, have shown great potential for improving atherosclerosis imaging for diagnosis. Engineered nanomaterials combined with numerous contrast agents (iron oxide and gold, for example) provide higher specificity and selectivity compared to contrast agents themselves. In this section, we discuss recent nanomaterial developments and advancements in improved evaluation and quantification of atherosclerosis across the current imaging modalities.

2.2.1. Molecular Imaging and Molecular Imaging Modalities—Molecular imaging is the process of visualizing, characterizing, and quantifying biological processes at the molecular and cellular levels within living things, including patients for disease diagnosis [264, 265]. Computed tomography (CT), magnetic resonance imaging (MRI), positron emission tomography (PET), and ultrasound are four of the most common molecular imaging modalities in the medical industry for identification and diagnosis of plaque development in arterial systems [266]. Briefly, CT scans use X-ray measurements at different angles and any tissue penetration to create cross-sectional, tomographic “slices” of a particular area of interest with high spatial resolution. In imaging plaque lesions, calcium is the most readily identified. However, due to the heterogeneous nature of plaques, signal attenuation is observed, and imaging specificity is impacted [267]. In contrast to CT, MRI does not use X-rays. In our bodies, naturally abundant protons in hydrogen atoms can align in the direction of a strong magnetic field and then emit a detectable signal after being subjected to a short radiofrequency pulse, as the protons realign with the magnetic field. The contrast between tissues can be observed and imaged dependent on the number of protons, resulting in different MR signal intensity. The contrast imaging can be obtained by using paramagnetic species. MRI offers advantages such as high spatial resolution, excellent tissue penetration; however, it can only detect the disease, not elucidate the pathology. Also, metal implants pose a dangerous risk when imaging with MRI considering the magnetic field. The low sensitivity, high cost, and long operation time are also limitations of MRI. In addition to MRI, PET is also a commonly used imaging technique based on γ -ray irradiation. PEI scanning requires intravenous administration of a radioisotope labeled ligand or tracer for specific tissue imaging, or in the most common atherosclerosis cases – blood flow. Despite the high sensitivity and good tissue penetration ability of PET, the resolution of the anatomy imaged by PET is poor and requires confirmation via CT or MRI. Ultrasound provides a fast and low-cost imaging approach in real-time; however, the resolution of ultrasound imaging is low, and the imaging is limited to specific organs or bones. Another imaging technique, photoacoustic imaging (PAI), has also been applied; however, it has not been widely used as other mentioned imaging approaches for cardiovascular disease due to its limitations such as low sensitivity and tissue penetration.

Therefore, these limitations of these common imaging modalities present a need for further refining them with the use of nanomaterials [268, 269]. The nanomaterial assisted molecular imaging approach is a method that images the site of interest during atherosclerosis development and progression using exogenous contrast agents which can target molecular components critical for atherosclerosis pathogenesis. These potential targets can be ECs, SMCs, macrophages, platelets, ECM, and cell adhesive proteins. So far, many groups have

investigated the potential ability of nanomaterials for imaging atherosclerotic plaques, and good summaries of these studies were discussed in previous reviews [270–274]. Here, we are only discussing the recent advancements of nanomaterials, including iron oxide-based NPs, gold NPs, polymeric NPs, liposomes, and micelles for atherosclerosis imaging.

2.2.2. Inorganic NPs—Inorganic NPs are colloidal metal-based nanoparticles and are the most widely investigated nanomaterials as contrast agents for diagnosing and imaging atherosclerosis. Among the inorganic NPs, iron oxide and gold-based NPs are the most widely studied NPs for atherosclerotic plaque imaging. Thus, in this section, we are primarily focusing on iron oxide and gold NPs.

2.2.2.1. Iron-Based NPs

2.2.2.1.1. Iron Oxide NPs: MRI contrast agents are commonly divided into T1 and T2 contrast agents. T1 contrast agents include manganese and gadolinium (Gd), whereas T2 includes iron oxide and iron platinum. Particularly, T1 contrast agents generate imaging with high tissue resolution, while T2 contrast agents provide a feasible approach to detect lesions [275]. These contrast agents shorten the relaxation time for both T1 and T2-weighted imaging, increasing signal intensity on T1-weighted images, and reducing signal intensity on T2-weighted imaging [276]. Iron oxide NPs are metallic, crystalline NPs that consist of maghemite (Fe_2O_3) and magnetite (Fe_3O_4) with intrinsic magnetic property, typically ranging from 1100 nm in size [277]. The shapes of iron oxide NP shapes can be carefully controlled during synthesis for different applications, ranging from spherical, cubic, wire, and cluster to worm shaped. Besides the unique magnetic properties, great biocompatibility, favorable degradation mechanism, and the facile surface modification [277] of iron oxide NPs to specifically target and accumulate in regions of atherosclerosis render them excellent MRI contrast agents for atherosclerosis imaging to improve diagnosis of both early-stage atherosclerosis as well as vulnerable plaque.

Particularly, iron oxide NPs have been widely investigated as T2 contrast agents. For instance, an interesting study reported by Huang and coworkers in 2018 developed HA conjugated iron oxide nanoworms for imaging atherosclerotic plaques by targeting CD44 in ECs. The nanoworms demonstrated high magnetic T2 relaxivity. Compared to previously reported HA conjugated spherical iron oxide NPs, the worm shaped HA-iron oxide nanoworms showed higher binding efficiency to CD44 in vulnerable plaque lesions and induced less inflammation [278]. This study indicated the importance of the nanoworm shape and its interactions with cells. In another study in 2019, Chen and coworkers developed a mesoporous silica NP containing iron oxide NPs capable of delivering drugs and showing T2 contrast for MRI. For improving the targeting and accumulation of the NPs in early-stage atherosclerosis, silica iron oxide NPs ($Fe_3O_4@SiO_2$) were functionalized with the peptide with a sequence of VHPKQHR for targeting late antigen-4, a known ligand of VCAM-1 in injured ECs MRI showed that the $Fe_3O_4@SiO_2$ NPs had significantly higher intensity in T2-weighted imaging compared to control groups [279]. Very recently, in 2019, Hu and colleagues conjugated green fluorescent protein (EGFP) with epidermal growth factor domain (EGF-1) to superparamagnetic iron oxide nanoparticles (SPIONs). These SPIONs were specifically developed to enhance the specificity for imaging high-risk

vulnerable plaques. Specifically, EGF-1 is a cell-adhesive ligand that has been demonstrated to target tissue factor (TF), which is strongly associated with atherosclerosis progression and the plaque's stability. Thus, by tagging the EGF-1 with EGFP and conjugating it to SPIONs, the SPIONs were expected to function as a TF-targeting nanoprobe that could image the atherosclerotic plaque via MRI. Consistent with the expectation, after injecting EGFP-EGF1-SPIONs and imaging ApoE$^{-/-}$ mice via MRI, the authors showed that the EGFP-EGF1-SPIONs demonstrated higher MRI contrast in mice with vulnerable plaques. This finding was further confirmed by immunohistochemical analysis, which indicated that indeed more of the EGFP-EGF1-SPIONs accumulated in the TF-rich vulnerable plaque. This result also demonstrated increased specificity for imaging vulnerable plaques using targeting SPIONs [280]. Moreover, this year, Li and colleagues also developed IL-6 targeting ultra-small superparamagnetic iron oxide (USPIO) nanoparticles to image vulnerable atherosclerotic plaques. The NPs were modified with an antibody that can specifically bind to IL-6 (antibody-IL6) overexpressed macrophages. Using antibody-IL-6 USPIOs, they were able to target foamy macrophages of progressive atherosclerosis and vulnerable plaques. After injection into the ear vein of HFD mice, significant T2-weighted signal loss was detected in plaque lesions at 24 h. This outcome demonstrated effective and specific targeting of lesions via IL-6 and foamy macrophages [227]. In addition to showing iron oxide NPs as T2 contrast agents, these studies also demonstrated the importance of surface functionalization and shape for targeting and accumulation in atherosclerotic plaque for imaging.

Dual T1/T2 imaging contrast agents have emerged as promising candidates for atherosclerosis diagnosis and imaging, as they take advantage of T1 contrast agents for high tissue resolution and T2 contrast agents for feasible lesion detection. Thus, in addition to MRI contrast agents with T2 contrast intensity, iron oxide NPs have also been used to develop dual contrast agents with T1 and T2 contrasts to improve the imaging of atherosclerosis and associated thrombosis. For instance, in 2017, Whittaker and coworkers developed iron oxide NPs that could be utilized as a dual T1/T2 MRI contrast agent (DCIONs) for the noninvasive detection of atherosclerosis associated thrombosis. DCIONs were functionalized with scFv for targeting activated platelets in the plaque and were fluorescently labeled for optical imaging. *In vitro*, the activated platelet targeting DCIONs bound significantly to thrombi and were observed using both T1 and T2-weighted MRI. For *in vivo* studies, the targeted DCIONs were also injected into mice with thrombi and imaged using T1 and T2-weighted MRI. The targeted DCIONs showed a signal enhancement in T1-weighted MRI, but a signal decrease in T2-weighted MRI. Non-targeted DCIONs did not show any significant change in MRI contrast for T1 or T2-weighted MRI images [281]. This data suggested that DCIONs could be modified to specifically target activated platelets for early detection of thrombosis using noninvasive MRI imaging. Likewise, for imaging atherosclerosis using both T1 and T2-weighted MRIs, in 2018, Xu and coworkers developed a dual-imaging contrast agent, polyacrylic acid-coated iron oxide nanoclusters (IONCs) for T2, with an outer layer of Gd for T1 MRI contrast intensity. In the presence of thrombin, Gd could be cleaved from the IONCs surfaces to exhibit T1 MRI positive contrast to detect thrombus and provide details on its age. In the absence of thrombin, the Gd remained linked to the IONCs and then functioned as a T2 MRI contrast agent, maintaining dark signals and

indicating late-stage thrombus. To assess the T1/T2 nanosensors' ability to distinguish between fresh and old thrombi, the IONCs were incubated *in vitro* with fresh and aged thrombi. *In vitro* MRI imaging of the thrombi showed T1 contrast in fresh thrombi and T2 contrast in aged thrombi, indicating the successful use of the nanosensor to detect disease progression [282]. The use of the dual T1/T2 nanosensors to noninvasively detect and determine disease progression of atherosclerosis could greatly improve diagnosis and treatment. Importantly, this study provided substantial proof of concept for utilizing dual T1/T2 activatable nanosensors for more specifically indicating the progression of atherosclerosis.

Combined imaging modalities may provide improved imaging and specificity, thereby improving the diagnosis of atherosclerosis. The following studies were significant for understanding and developing iron oxide-based NPs as contrast agents for dual imaging using a combination of imaging techniques such as MRI, PET, CT, ultrasound, and near-infrared fluorescence (NIRF) for the diagnosis of atherosclerosis plaques. For example, endothelial dysfunction plays an integral role as an early indicator in the development of atherosclerosis. In a couple of interesting studies, Cao and coworkers designed iron oxide NPs for dual imaging modalities specifically to identify vulnerable atherosclerotic plaques. For instance, in 2017, this group developed iron oxide nanoparticles that targeted osteopontin (OPN) in macrophages of atherosclerotic plaque. The iron oxide NPs were conjugated with Cy5.5-labeled OPN antibody to function as a dual MRI/optical imaging probe to assess plaque vulnerability via foam macrophage proliferation [283]. In another study, Cao and coworkers developed paramagnetic iron oxide NPs conjugated with a PET Gallium-68 (Ga) chelator for MR and PET imaging to assess atherosclerosis progression. Since angiogenesis occurs during atherosclerosis progression, to target and image angiogenesis in atherosclerotic plaque, the NPs (Ga-NGD-MNPs) were further modified with a GEBP11 peptide for targeting plaque microvessels. To assess the targeting ability of the Ga-NGD-MNPs, *in vivo*, rabbit atherosclerosis models were injected with Ga-NGD-MNPs and imaged using MRI/PET. Significantly higher uptake of the targeted NPs was observed in the plaque vasculature compared to the control MNPs. Additionally, these microvessels' density could be measured and assessed for the severity of atherosclerosis, providing an early-stage diagnosis. The use of these GEBP11 targeting MNPs as dual MRI/PET contrast agents may provide a useful tool for imaging and diagnosing progressive plaque angiogenesis [284]. In a similar study focusing on imaging vulnerable plaques, the Clofent-Sanchez group reported ultra-superparamagnetic iron oxide NPs (VUSPIO) that functioned as dual imaging MRI/near-infrared fluorescence probes. In this study, to target platelets in vulnerable plaques, the VUSPIO NPs were conjugated with an scFv platelet reactive TEG4 antibody. Additionally, the multivalent property of the scFv improved the retention time, as the authors demonstrated that plaque detection was achieved in $ApoE^{-/-}$ mice for up to 24 h after injection [285]. In addition to identifying and diagnosis plaque vulnerability, dual imaging was also used for early-stage atherosclerosis diagnosis. In one study, Jaffer and colleagues developed USPIO NPs conjugated with a near-infrared fluorescent tag, CyAm7. Using CyAm7-USPIOs, they identified that USPIOs localized in the atheroma intima and neovascularization areas with NIRF and ultrasound imaging. Therefore, these results provided a mechanism for early atherosclerosis imaging and

detection [286]. In another study, the Jiang group in 2019 reported rhodamine-labeled USPIO NPs that could detect early atherosclerosis lesions using MRI and fluorescence imaging by showing uptake of NPs in macrophages during luminal narrowing, an indicator of early-stage pathophysiology of atherosclerosis. The USPIO NPs were synthesized by reacting N-hydroxysuccinimide-rhodamine with the amino-terminal PEG-coated iron oxide NPs. The USPIO NPs presented a dual-modality function because USPIO could induce strong T2 shortening effects during MRI, *in vivo*, while the rhodamine assisted with *ex vivo* fluorescence observation. After inducing atherosclerotic aortic lesions in ApoE$^{-/-}$ mice under HFD, the authors successfully demonstrated the *in vivo* T2 signal loss under MRI. The *ex vivo* red fluorescent rhodamine signal from macrophages also showed higher intensity in atherosclerotic plaques compared to the cell wall. Thus, USPIO NPs have great potential as dual-modality imaging NPs to detect atherosclerotic lesions with better precision [287].

The studies mentioned above mainly discuss the development of single or dual-imaging contrast agents. However, dual imaging has also been developed to detect different stages of atherosclerosis maturity, utilizing probes that can switch contrast effects under specific stimuli. For example, an interesting study reported in 2019 by Makowski and coworkers developed a novel type of iron oxide NP as a dual-specific targeting probe for simultaneous detection of pathological ECM and inflammation progression in early-stage atherosclerotic lesions. This dual-targeting probe was developed to target two key molecules in the plaque [288]. The dual-probe was composed of an elastin-specific Gd-based probe (T1-weighted MR imaging) and a macrophage-specific iron oxide probe (both T1- and T2-weighted imaging) for ECM (assessment of plaque vulnerability) and inflammation detection (early atherosclerosis imaging), respectively. In the atherosclerotic lesions of ApoE$^{-/-}$ mice under HFD, the authors displayed that the *in vivo* detection of the two probes agreed with the *ex vivo* histopathological analysis. It was also shown that the two probes did not affect the visualization of each other. More interestingly, the accumulation of probes in the plaque was different; the elastin-specific probe showed the highest accumulation in advanced atherosclerotic plaque, whereas the iron oxide-based probe displayed the highest accumulation in early plaque [288]. If further developed, these dual-imaging probes provide opportunities to use non-invasive imaging techniques to more specifically target, diagnose atherosclerosis progression, and identify atherosclerosis risk factors, all of which can lead to better treatment plans and options for patients.

2.2.2.1.2. Ferritin Nanocages: Iron-based NPs have also been developed for imaging and diagnosing atherosclerosis using other imaging modalities such as CT and PET. ^{18}F-fluorodeoxyglucose (^{18}F-FDG) is regarded as a gold standard for vulnerable plaque identification via CT and PET scans. However, due to the high metabolic uptake of ^{18}F-FDG and the limited resolution and specificity of PET imaging, it requires extremely high amounts of localized accumulation of ^{18}F-FDG to achieve efficacious imaging [266–268, 289]. Thus, in 2018, Yan and coworkers explored the use of inorganic H-ferritin (HFn) nanocages radiolabeled with technetium-99m (^{99m}Tc-HFn) for quantitative imaging of vulnerable atherosclerotic plaques via singlephoton emission computed tomography. In particular, ^{99m}Tc-HFn showed colocalization fluorescence with areas of atherosclerotic

plaques 2 h after administering the NPs in the aorta of atherosclerotic ApoE$^{-/-}$ mice. The fluorescent signal intensified up to 33 weeks (Fig.8a). Moreover, NP uptake increased as atherosclerosis progressed, which was also well correlated with the plaque areas (Fig.8b–c). This data strongly indicated the feasibility of using these NPs for imaging atherosclerotic plaque. Moreover, intense macrophage infiltration was observed in the plaque region where the ^{99m}Tc-HFn accumulated (Fig.8d). Further immunofluorescent staining also confirmed the colocalization of ^{99m}Tc-HFn signal with macrophages within plaques via Mac-3 staining, and the macrophage infiltration degree correlated well with the ^{99m}Tc-HFn taken up in the macrophage (Fig 8e). This finding indicated that the NPs were able to target macrophages in the plaque specifically, and the signal from ^{99m}Tc-HFn would provide important information regarding therapeutic efficacy for inflammation. Indeed, the authors assessed the inflammation change induced by statin treatment by using ^{99m}Tc-HFn NPs. The ^{99m}Tc-HFn signal observed in the mice treated with statins at early atherosclerosis indicated statin significantly inhibited the atherosclerosis progression, whereas a high fluorescent signal from ^{99m}Tc-HF was observed in mice treated with statins in the advanced atherosclerosis stage, suggesting a less prevalent anti-atherosclerotic efficacy of statin for treating late atherosclerosis (Fig.8f–g). The inflammation prediction using ^{99m}Tc-HF strongly correlated with the plaque area characterized by Oil red O staining (Fig.8h) [290]. Significantly, this study showed that not only can nanoparticles be utilized to indicate atherosclerosis progression but also utilizing nanoparticles as imaging contrast agents may provide important information on the efficacy of atherosclerosis treatment at different stages of progression. To further increase the specificity of infiltrating macrophages, in the same year, the same group further expanded upon the use of HFn NPs to develop M-HFn NPs by functionalizing the HFn NPs with magnetoferritin nanozymes. Compared to other traditional methods, the M-HFn NP-based method is relatively cheap and fast. The M-HFn NPs also demonstrated specific peroxidase enzymatic activity that can recognize and bind to plaque-infiltrating macrophages. Their results showed that M-HFn NPs were able to specifically stain ruptured plaques, not stable plaques. A strong correlation between M-HFn NPs and plaque vulnerability shows great potential for using M-HFn NPs as an index to identify plaque vulnerability clinically [291].

Many of the above-discussed studies have improved iron oxide NPs with increased specificity and localization for atherosclerosis imaging and diagnosis. These avenues of detection have further improved the detection of early stable lesions and plaque progression and the risk factors for vulnerable plaques. These recent advancements can improve the clinical outcomes of CVD and atherosclerosis with earlier detection, prognosis, and evaluation of risk factors for plaques. These methods also contribute many approaches available for diagnosing different severity levels of atherosclerosis to provide clinicians with improved data for diagnosis and treatment.

2.2.2.2. Gold NPs: As discussed above, the development of NPs with iron oxide cores has been studied to increase the specificity and sensitivity of current imaging modalities [227, 242, 281, 287, 292–297]. Along with the use of iron oxide NPs, gold (Au) NPs have also been explored for improving the atherosclerosis diagnosis process. Gold NPs provide stability and versatility and are easily functionalized. Certain ligands or antibodies can be

conjugated to the gold surface to interact with numerous cell types *in vitro* and *in vivo*. A study done by Cormode and colleagues in 2016 reported the use of gold NPs capped with 11- mercaptoundecanoic acid ligand to target monocytes specifically. They hypothesized these NPs could track monocyte infiltration into vulnerable atherosclerotic plaques. After intravenous injection of these NPs in ApoE$^{-/-}$ mice and 5 days of imaging, their results showed a significant increase in signal compared to the initial time point and the control group (non-labeled monocytes) over 5 days. These results demonstrated the ability to track monocytes to the atherosclerotic plaque and serve as a high efficacy cell-labeling imaging modality for atherosclerosis detection [298].

Like iron oxide NPs, Au NPs have also been applied for imaging under dual-imaging models. For instance, in 2018, Ahn and colleagues developed a novel thrombus-specific fluorescence/micro-CT dual-imaging contrast agent to monitor thrombin activity in blood for early detection of vulnerable plaques and thrombosis. For optical imaging of thrombosis, the fluorescent probe Cy5.5 was conjugated to a thrombin cleavable peptide to create activatable fluorescent peptide molecules, called TAP, for NIRF imaging. In the presence of thrombin, quenched TAP molecules were cleaved from the peptide sequence resulting in a fluorescent signal for NIRF imaging. The TAP molecules were further conjugated to silica gold nanoparticles (SiO_2@AuNPs) to create dual-imaging NIRF/micro-CT probes. To assess the dual-imaging functionality of TAP-SiO_2@AuNPs, NIRF, and micro-CT imaging techniques were used in atherosclerotic mouse models, *in situ*. Strong NIRF signals were observed in atherosclerotic lesions, indicating successful accumulation of the TAP-SiO_2@AuNPs and subsequent cleavage of TAP molecules in the presence of thrombosis. Additionally, the accumulation of the NPs in atherosclerotic lesions was further verified using micro-CT. Successful detection of the TAP-SiO_2@AuNPs in atherosclerotic lesions using dual NIRF/micro-CT imaging indicated the potential use of this probe to detect thrombi [299]. This study demonstrated rapid accumulation of TAP-SiO_2@AuNPs in thrombus *in situ*, with accurate dual-imaging specificity for thrombotic lesions compared to surrounding tissues, providing a fast and accurate method for atherosclerosis imaging. More recently, in 2019, Zhang and colleagues developed Gd-based Au NPs targeting scavenger receptor type I (SR-AI) overexpression on lesion macrophages of advanced plaques using peptide called PP1 (LSLERFLRCWSDAPAK) as a selective SR-AI homing device. They developed the NPs by using glutathione as a template containing Gd and Au conjugated with the PP1 peptide. After injection into ApoE$^{-/-}$ mice with PP1-gold-Gd NPs, a significant signal increase in the carotid atherosclerotic lesion was visible at 4 h and 12 h. This demonstrated increased penetration and retention compared to untargeted gold-Gd NPs [300]. Furthermore, as most NP imaging studies emphasize dual imaging of atherosclerotic lesions specifically, this study demonstrated selective targeting of foam macrophages as an approach for measuring plaque vulnerability and atherosclerosis risk factors. In 2019, the same group expanded upon the use of PP1 peptide for SR-AI specific targeting for atherosclerosis imaging. Instead of using gold NPs, gold nanoclusters were used to further increase the T1-weighted MR imaging of infiltrative macrophages localized in vulnerable atherosclerotic plaques [301]. Results showed increased circulation, deeper penetration of the NPs into foam macrophages, with no visible toxic effects to surrounding tissues. These MRI data were further confirmed by *ex vivo* fluorescent imaging. Fluorescent intensity was

significantly higher in areas of atherosclerotic lesions, consistent with T1-weighted MR imaging.

In summary, we discussed the easy functionality of Au NPs for targeting atherosclerosis. Specifically, the studies included the direct targeting the infiltrating macrophages by Cormode and colleagues using 11- mercaptoundecanoic acid. After the functionality of Au NPs was further explored, Ahn and colleagues engineered Au NPs to effectively measure plaque vulnerability by targeting thrombin. The Zhang group further explored the incorporation of gadolinium to Au NPs and further expanded by the following study to improve circulation and NPs specificity for atherosclerotic lesions. Increasing circulation time, specificity, and MRI intensity, as well as detecting risk factors for atherosclerosis, will continue to be an area for future development with Au NPs. Additionally, the conjugation with additional contrasting agents is a possible future avenue for Au NPs to improve atherosclerosis imaging and diagnosis.

2.2.3. Polymeric NPs, Liposomes, and Micelles.—Polymeric NPs are not only used as delivery cargos for treating atherosclerosis but also show great potential for assisting in imaging atherosclerotic plaque. Wei and coworkers, in 2017, developed polymeric nanocapsules with dual-imaging capabilities (MRI and ultrasonography) to specifically target neoangiogenic, advanced, and vulnerable atherosclerotic plaques [302]. Particularly, the nanocapsules were fabricated using PLGA and perfluorooctyl bromide, which is an ultrasound contrasting agent. SPIO NPs were also embedded for MRI imaging. Moreover, anti-VEGFR-2 antibodies were attached to the nanocapsule surface to target VEGF receptor 2 (VEGFR-2), which is highly expressed on the ECs within plaques. *In vivo* gray scale intensity (GSI), the measurement for ultrasonography, of the atherosclerotic targeting VEGFR-2-targeted nanocapsules (VTNCs) showed a marked increase of the mean and peak GSI in the targeted group compared to the control group. Post-injection means and peak GSI measurements were 65.09±6.21 and 69.44±4.45 compared to 46.66±4.01 and 45.24±1.92, respectively, for the non-targeted nanocapsules. In MRI, contrast-to-noise ratio (CNR) mean and peak signals were significantly higher in targeted VTNCs (mean: 74.02±11.46, peak: 87.51±6.63) versus non-targeted nanocapsules (mean: 48.86±4.07, peak: 49.22±3.19). This result demonstrated a more specific, dual probe targeting mechanism for imaging plaques than regular MRI and ultrasonography. Later, in 2019, Woodard and coworkers synthesized polymeric comb NPs, ^{64}Cu-CANF-comb NPs. In this study, C-atrial natriuretic factor (CANF), a peptide cell-adhesive ligand, was used to target the natriuretic peptide clearance receptors on the ECs in atherosclerotic plaques for enhancing imaging specificity. Moreover, CANF-comb NPs were radiolabeled with ^{64}Cu to trace the accumulation of the ^{64}Cu-CANF-comb NPs upon their binding to natriuretic peptide clearance receptors in atherosclerotic plaques in ApoE$^{-/-}$ mice. PET scanning showed that the number of ^{64}Cu-CANF-comb NPs taken up by injured arteries was 2.5- times higher than that by healthy arteries. The ability of ^{64}Cu-CANF-comb NPs to specifically target natriuretic peptide clearance receptor (NPRC) via improved binding efficiency of the Cu-CANF-comb to the NPRC, rapid internalization, improving the clinician's ability to detect atherosclerotic buildup far earlier than conventional contrast agents [303]. Another interesting example was demonstrated recently by Gu and colleagues in 2020. In this study, the authors developed

beta-galactosidase (β-Gal)-activatable NIR fluorescent nanoprobes to target the senescent SMCs and ECs in the plaque for atherosclerosis imaging. To fabricate the nanoprobe, PLGA NPs were modified with boron dipyrromethene fluorophore linked with β-galactose residues to target β-Gal that were highly expressed in senescent cells in the plaque. The nanoprobes' fluorescence was found to be switched on *in vitro* only once they came in contact with β-Gal. Moreover, the ability to detect senescent SMCs *in vitro* and *in vivo* were also demonstrated. Specifically, strong fluorescence was observed in angiotensin II treated SMCs. Moreover, a significant difference was observed between the fluorescent signal in atherosclerotic and senescent mice and control mice treated with the nanoprobes. More interestingly, the regions showed a strong fluorescent signal in the aortic arch of atherosclerotic mice, which was in good accordance with the regions that demonstrated positive Oil red O staining, which indicated the excellent potential of using such nanoprobes to visualize atherosclerotic senescent vasculature [304]. This study showed a novel method to detect early aging-related atherosclerosis via senescent cells in the vasculature.

Liposomes provide a promising alternative approach to iron oxide and gold-based NPs for atherosclerosis imaging. With excellent biocompatibility, liposomes are engineered to target specific areas of atherosclerosis for assessment of plaque ruptures and vulnerability. For example, targeting inflammation is a route for detecting and evaluating the severity of atherosclerosis. By targeting immune cells for imaging, plaques can be visualized to assess severity. Thus, in 2018, Annapragada and colleagues developed a liposomal MRI Gd contrast agent that targeted integrin α4β1, an integrin expressed on immune cells in the plaque for early atherosclerosis detection. Particularly, to target integrin α4β1, the liposomal NPs were modified with THI0567, a cell-adhesive ligand, specifically binding to integrin α4β1. Gd was also conjugated to the liposomal NPs to trace atherosclerotic formation in mouse models using MRI. THI0567-conjugated liposomal-Gd was found to accumulate in the plaque where THP-1 cells were located and demonstrated an excellent capability to detect atherosclerosis formation in the early stage [305]. The results of this study showed the THI0567 conjugated liposomal NPs localized within CD11b and F4/80 monocyte markers in the subendothelial regions instead of endothelial regions of plaque accumulation resulting in remarkable specificity for imaging of vulnerable plaques, compared to standard PET imaging, which isn't able to obtain that degree of specificity. Similarly, in 2019, Ogawa and colleagues developed macrophage targeting liposomes for imaging atherosclerosis. However, at this time, instead of early plaques, the detection of vulnerable plaques using liposomes was investigated by NIRF imaging. The liposomes, labeled as P-ICG2-PtdSer-Lip (or PS Lip), contained phosphatidylserine (PtdSer) for macrophage targeting and encapsulated with a NIRF probe, a novel activatable peptide (KGGGFLGK) conjugated with two molecules of indocyanine green fluorescent dye (ICG2). The fluorescence of peptide-ICG2 would be switched on after the peptide was cleaved by the lysosomal enzyme (cathepsin B) that is highly expressed in the lysosomes of macrophages in the plaque (Fig.9a). In particular, the P-ICG2-PtdSer-Lip are round, unilamellar vesicles with an average size of 200 nm. It did not show any fluorescence when the peptide was conjugated to the ICG2 (Fig.9b–c). The quenching and activation of the fluorescence by cathepsin B of the P-ICG2-PtdSer-Lip were successfully demonstrated *in vitro* (Fig.9d). Moreover, P-ICG2-PtdSer-Lip were found to target macrophages *in vitro* as demonstrated by that much

higher PtdSer-Lip (PS liposomes) were taken up by the macrophages than PC liposome. In addition, more NPs were taken up by the macrophages as time progressed (Fig.9e). Furthermore, intracellular activation of P-ICG2-PtdSer-Lip was also demonstrated by that a strong fluorescence was observed after the NPs were incubated with macrophages for 6 h (Fig.9f). More importantly, the *in vivo* study demonstrated that P-ICG2-PtdSer-Lip showed increased fluorescence in atherosclerosis areas (Fig.9g). Moreover, the liposome can detect infiltrative macrophages and provide data on the severity of atherosclerosis. Imaging results displayed a strong fluorescence in both the aorta and the lipid-rich blood vessel walls of $ApoE^{-/-}$ mice, indicating the liposomes' specificity to plaque regions [306]. This study is significant because of the ability of P-ICG2-PtdSer-Lip NPs to specifically target macrophages via phosphatidylserine combined with the unique fluorescent activation via cathepsin B in plaque macrophages, providing plaque rupture risk assessment with deeper tissue signaling.

Besides targeting immune cells, in a recent study in 2020, Mulder and colleagues also imaged vulnerable atherosclerotic plaques by targeting dysfunctional endothelium using PEGylated liposomes containing a PLP (an anti-inflammatory steroid) hydrophilic core, radiolabeled with zirconium-89 (^{89}Zr). PLP has been previously encapsulated and used for the anti-inflammatory treatment of atherosclerosis by the same group. After injection with ^{89}Zr-labeled liposomes, radioactivity was detected in the arterial walls of atherosclerotic New Zealand white rabbits using a balloon injury atherosclerosis model. The authors showed that these liposomes accumulated in the endothelium of an HFD rabbit's vessel wall by multi-modal imaging with ^{89}Zr (PET/MRI, PET/CT) both *in vivo* at 5 days and *ex vivo* at 15 days, displaying the degree of vascular permeability between control and diseased vessels. Signal was significantly increased in the vessels with increased permeability in diseased models compared to little uptake in the less permeable control models. More interestingly, by using these liposomes, the authors found that vessel permeability was correlated with the number of liposomes taken up by the vessel. This finding indicated the potential use of these liposomes to measure the severity of endothelial dysfunction, which leads to plaque inflammation and rupture [307]. These results provided data on atherosclerosis severity and biodistribution, allowing for an avenue of personalized care with anti-atherosclerosis nanotherapy. In another study in 2020, platelets were used as targets by Li and colleagues. The authors developed a PEGylated liposome modified with RGD targeting moiety for integrin GP IIb/IIIa on activated platelets on vulnerable thrombolytic plaques. This liposome construct was loaded with either Gd or SPIO. Results showed the RGD PEGylated liposome had a strong affinity for activated platelets, as shown by increased dual-mode MRI T1 and T2 level intensity compared to control. Additionally, the signal was considerably stronger in arterial blood clots, suggesting the potential for dual-mode imaging of thrombosis [308]. Most importantly, the liposomal Gd-DTPA when PEGylated had increased circulation time, providing avenues for possible antithrombotic therapies due to its rapid uptake in platelet-rich and rupture-prone areas of atherosclerotic plaques.

Similar to liposomes, micelles were also applied for imaging atherosclerosis. For instance, in 2017, Chung and colleagues investigated the potential of using PAMs to specifically target macrophages for imaging vulnerable plaques. The targeting ability of the PAMs resulted from MCP-1 that was conjugated to the PEG component of the micelles and can bind to the

C-C chemokine receptor on monocytes in plaque. *In vitro* studies demonstrated that the MCP-1 PAMs were able to specifically bind to monocytes. Moreover, the amount of PAMs binding to the monocytes was shown to be directly proportional to plaque progression [309]. This study is significant because PAMs can be used to monitor plaque progression (by specific binding to monocytes), with the additional incorporation of targeting moieties, therapeutics, and nucleic acids for further specificity of target atherosclerotic tissue, as evidenced in the following study. Later in 2018, instead of targeting macrophages, the same group modified PAMs with the peptide with a sequence of CREKA to target fibrin, a molecule found on the necrotic cores of intermediate plaques. By targeting fibrin, PAMs can bind directly to the entire plaque surface and localize at the shoulder where the plaque is the most vulnerable to rupture and where microthrombi are located. In addition, PAMs contained two different metal oxide cores, manganese oxide core and iron oxide core, which can produce strong MRI contrast. The authors showed that PAMs with manganese oxide core and iron oxide core demonstrated 4.7- and 2.7-fold higher binding to fibrin than that of control micelles without CREKA, *in vitro*, respectively. Furthermore, the *in vivo* study demonstrated that the CREKA PAMs could modify and increase the signal intensity of MRI (62% for manganese oxide core and 65% for iron oxide core) and provided clot specificity enhancement 3- to 5- times higher than non-targeted micelle controls. This result demonstrated a novel, plaque-specific imaging approach using MRI. In another study conducted by the same group, the authors investigated the use of PAMs to detect thrombosis by targeting the vascular calcification correlated with atherosclerosis. Here, the PAMs were modified with hydroxyapatite (HAP-binding peptides that can target calcifications in atherosclerotic plaque. For imaging, the HAP PAMs were further modified with the additional incorporation of fluorophores, Cy7. After the *in vivo* injection of Cy7 containing HAP PAMs (and controls) in $ApoE^{-/-}$ mice, HAP PAMs were found to co-localize in calcified regions of plaque [310]. Their results demonstrated a novel detection tool for identifying calcification and subsequent thrombosis. These three studies demonstrated the ability of PAMs to incorporate various targeting peptides to measure the severity of the disease, as well as possible avenues for theranostics.

In summary, polymeric, liposome, and micelle NPs can be incorporated with various peptides, targeting sequences, and enzymes for targeting atherosclerosis at different stages. This allows atherosclerosis severity and plaque vulnerability to be assessed. These NPs, as shown in the data and studies above, can be uniquely modified to increase circulation time, specificity to target tissues, deeper tissue penetration for higher intensity imaging.

2.2.4. Other Types of Nanomaterials—One challenge to *in vivo* molecular imaging is the opacity of tissues, and to address this issue, inorganic nanomaterial composites were explored for dual imaging applications. For example, Gao and colleagues, in 2017, developed macrophage-specific molecular upconversion NPs (UCNP-anti-OPN) for imaging both stable and vulnerable atherosclerotic plaque under dual optical/MRI. The UCNPs were composed of core@shell structure ($NaGdF_4$: Yb, Er@$NaGdF_4$) and conjugated with macrophage-specific antibodies binding to OPN (UCNP-anti-OPN). The ytterbium (Yb) and erbium (Er) molecules of the UCNPs upconvert the photoluminescence, increasing the NIRF's signal intensity and brightness. Optical imaging 6h post-injection of UCNP-anti-

OPN NPs showed distinctive signals for vulnerable and stable plaques in mice. However, 24h post-injection, signals were maintained only in the portion of the artery containing vulnerable atherosclerotic plaques. Additionally, MRI showed higher T1 signals in the low shear stress (vulnerable plaque) portion of the artery, further indicating enhanced accumulation of the UCNP-anti-OPN NPs in vulnerable plaques. Results indicated that UCNP-anti-OPN NPs could provide a dual optical/MRI imaging method to diagnose both stable and vulnerable atherosclerotic plaques by detecting the foamy macrophage expression of OPN [311]. Later in 2019, the same group further modified their novel UCNPs by conjugating the NPs with a macrophage receptor with collagenous structure (MARCO) surface receptors. These NPs were designed to specifically target infiltrative M1 macrophages with MARCO antibodies (anti-MARCO), which are known to be upregulated on M1 macrophages in ruptured plaque sections for imaging vulnerable plaques. After intravenous administration of the anti-MARCO-NPs, high T1-weighted signal intensity via Gd was demonstrated in mice's carotid artery wall at 24 h. This finding demonstrated high specificity for atherosclerosis plaques for the anti-MARCO probe [312].

In addition to UCNPs, protein and virus-based NPs have been explored for atherosclerosis and atherothrombosis imaging. Specifically, inorganic based nanoparticles were encapsulated into protein and virus-based nanomaterials to improve accumulation in atherosclerotic plaque. Particularly, Cui and coworkers in 2016 developed a trifunctional Simian virus 40 (SV40) NPs to encapsulate near-infrared quantum dots for enhancing the imaging of early atherosclerosis in a non-invasive ma6nner. SV40 NPs had core-shell structures, which possessed an F6 quantum dot core and a shell composed of 12 VPI viral capsid protein pentamers. To target the plaque, SV40 NPs were conjugated with CGNKRTRGC peptide to bind to the plaque macrophages. The near-infrared quantum dots in NPs provide brightness and quality imaging for early atherosclerosis imaging and diagnosis. The assembled virus-based NP contained a peptide sequence for targeting macrophages (CGNKRTRGC) and a Hirulog peptide (a thrombin inhibitor). This virus-based NP, MH-QD (MH for macrophage hirulog), could be seen approximately 3.4- fold more than their non-targeted, wild-type virus-like particle quantum dots (VLP-QDs). MH-QD could be seen 8.8- fold more than plain QDs. The MH-QDs also showed localized fluorescence in the aortic tree of $ApoE^{-/-}$ mice compared to a weak fluorescent signal for non-targeted VLP-NPs [313]. Similarly, in 2018, Francis and colleagues developed NPs made of bacteriophage MS2 viral capsids conjugated with antibodies specific to target active ECs and macrophages to image early plaques. MS2 is a viral capsid of the bacteriophage family and provides many advantages for cargo protection and delivery to target tissues. After intravenous injection of the MS2 capsids, the descending aortas were excised and imaged. The study showed that 24 h after intravenous injection of AlexaFluor680 labeled MS2 viral NPs in $ApoE^{-/-}$ mice, a colocalized fluorescent signal was observed at the early plaque located in the aorta. The MS2 viral NPs that targeted ECs exhibited a 3- fold increase in localization signals in atherosclerotic plaques compared to non-targeted MS2 viral capsids. This finding indicated the potential use of these NPs for detecting early atherosclerotic plaques [314]. Similarly, in the same year, Hagemeyer and coworkers designed NPs for detecting vulnerable plaque. The NPs were composed of low-fouling PEG, a hydrophilic recombinant protein (PASKE), as well as antibodies binding to GPIIb-III and

scFV that targeted inflamed endothelium and activated platelets in vulnerable plaques, respectively. The use of PASKE and PEG limits the opsonization of the NPs to increase the circulation time of the NPs to 24 h for imaging purposes. Specifically, these NPs are around ~730 nm in diameter and highly biocompatible. For detecting plaque formation using infrared imaging, the PASKE-anti-GPIIb/IIIa-scFv was further conjugated with Cy7, a near-infrared fluorescent dye. The authors demonstrated that PASKE-anti-GPIIb/IIIa-scFv-Cy7 NPs enhanced the fluorescent imaging of atherothrombosis *in vitro* and *in vivo* compared to its untargeted control. Moreover, PASKE-anti-GPIIb/IIIa-scFv-Cy7 NPs showed fewer side effects and cytotoxicity than PEG NPs [315]. As well, an exciting approach developed by Tang and colleagues in 2019 was to assess plaque vulnerability and inflammation based on redox homeostasis of plaques using novel fluorescent bovine serum albumin (BSA) NPs as nanoprobes under photoacoustic imaging. By tagging the NPs with small molecule dyes, they can be detected via photoacoustic imaging. After pulsed laser irradiation of these dyes, the dyes gave off ultrasonic waves at 765 and 680 nm that can be detected without the need for ionizing radiation. Furthermore, increased oxidative stress can weaken the fibrous cap of atherosclerotic plaques by releasing metalloproteases and inflammatory cytokines. This oxidative stress can be detected to measure the degree of vulnerability of the plaque to rupture. The nanoprobes were composed of self-assembled BSA and two fluorescent NIR probes, Cy3-NO_2 and Mito-NIRHP, which target the glutathione and hydrogen peroxide, respectively. These pathways are essential for the redox homeostasis of plaques. After intravenous injection of the redox state-targeting tagged BSA NPs in plaque bearing ApoE $^{-/-}$ mice, a pronounced enhancement of photoacoustic signal intensity was observed in the aortic region compared to the rest of the body of the mouse [316]. This observation indicated increased levels of oxidative stress and inflammation in plaques infiltrated with macrophages. These results provided a novel mechanism for the detection of rupture-prone plaques in the early stages.

Other than traditional imaging contrast agents and imaging modalities, in a unique study in 2020, the Kim group developed a novel type of CNTs for detection of the lipid-rich region of foam cells in atherosclerotic lesions using capacitance imaging that measures the dielectric constant (ε). The authors discovered that lipids have a specific dielectric constant and could be used to detect lipid-filled foam cells in atherosclerotic lesions via capacitance and the relationship $C = \varepsilon A/d$, where A is the electrode area and d is the distance between the two electrodes. Thus, the foam cells could be targeted by their specific dielectric constant by creating an electrode array using a capacitance imaging technique. Specifically, the CNTs were coated with polypyrrole arranged in a multi-electrode array to detect the dielectric constant of the foam cells. Upon measurement using the CNTs, the lipid-rich regions of the atherosclerotic plaques showed high capacitance values than the lipid-poor regions of the surrounding aorta ex *vivo* using the multi-electrode array. Even though this was not done *in vivo*, this demonstrated differences between lipid-rich and lipid-free regions for specific targeting of atherosclerosis and risk assessment for future clinical application [317].

In addition to imaging and diagnosis applications, inorganic nanomaterials have also been recently focused on developing nanomaterials for targeting atherosclerosis only. Notably, in 2018, Yu and colleagues conjugated a novel type of peptide

(YNFTNRKISVQRLASYRRITSSK) derived from chemokine receptor CCR2 to iron oxide NPs to target MCP-1 of monocytes. This technique could be used to assess the risk of plaque rupture in vulnerable plaques. It was observed that the peptide-modified iron oxide NPs could be located within the monocytes after the monocytes were treated with the NPs. A similar result was found, *in vivo*, that the MCP-1-motif NPs accumulated in the atherosclerotic aorta of ApoE$^{-/-}$ mice [295]. Later in 2019, the Steinmetz group evaluated the targeting ability of peptide modified tobacco mosaic virus NPs (TMV) to the SA-100A9 of vulnerable atherosclerotic plaques. SA-100A9 was commonly secreted by immune cells such as neutrophils and monocytes and was strongly associated with vulnerable plaques. The targeting ligands for SA-100A9 were G3 and H6. The authors demonstrated that the G3-TMV and H6-TMV showed similar but higher binding affinities to SA-100A9 than PEG and scrambled peptide conjugated TMV. Similarly, the *in vivo* study demonstrated that fluorescent-labeled G3-TMV and H6-TMV exhibited greater targeting ability compared to controls; 40- and 14- fold higher fluorescent intensity was found in the aorta G3-TMV and H6-TMV, respectively, in the ApoE$^{-/-}$ mice than that of controls [318].

In another study in the same year, Zhang and coworkers explored neutrophils (NE) as cellular vesicles to actively target atherosclerosis and assess the risk of thrombosis in atherosclerotic plaques. Specifically, the authors loaded coumarin 6 cationic liposomes (C6-CL) into the NEs and labeled the NEs with Dil (a cell membrane dye) for tracking. The *in vitro* study demonstrated that the C6-CL/Dil-NEs were recruited by foam cells because TNF-α secreted by foam cells can stimulate NE migration. Active targeting of a plaque was also observed *in vivo*, which was shown by the strong fluorescence from Dil observed in the plaque of ApoE$^{-/-}$ mice [319]. In another study, the Wang group developed a fusion protein, EGFP-EGF1, which could target TF highly expressed by the macrophages and VSMCs in the plaque. Furthermore, they conjugated EGFP-EGF1 to the PLGA NPs and showed these NPs could be taken up by macrophages *in vitro* efficiently and accumulated in the aorta of mice fed with HFD [320]. Lately, the Couvreur group showed that NPs made of rhodamine squalene, a metabolic precursor of cholesterol, were able to target atherosclerotic plaque. Interestingly, unlike other studies, receptors on macrophages and ECs were chosen as targets for plaque targeting; in this study, squalene NPs were shown to efficiently target the LDL in the macrophages in the plaque [321]. In the same year, Venkatranman and coworkers explored the effect of PEG-to-folate ligand ratio on liposome targeting ability. The authors demonstrated that targeting ability decreased as the PEG-to-ligand ratio increased [322]. The development of these nanomaterials for targeting atherosclerosis holds great potential for being applied as templates for the development of nanomaterials for imaging or delivery of therapeutic agents in the future.

2.3. Nanomaterials as Theranostic Agents for Atherosclerosis Imaging and Therapy

In recent years, there has been a growing interest in developing theranostic agents that can exhibit therapeutic function and diagnosis capability in one unit due to the emerging concept that theranostic strategy might improve the efficacy of therapy and diagnosis simultaneously while reducing side effects. In order to design theranostic agents, several important factors need to be considered. Firstly, the nanomaterials used to fabricate the theranostic agents should be biocompatible. Secondly, for therapeutic effect, proper therapeutics effective for

atherosclerosis should be chosen and incorporated in the nanomaterials. The therapeutics vary from traditional chemical drugs to newly emerged therapeutics such as photosensitizers, proteins, and nucleic acids. As it is known, atherosclerosis development is a complicated process that involves multiple stages; thus, targets for treatment in different stages may be varied. Therefore, choosing the right therapeutics is particularly important for successfully developing theranostic agents. Thirdly, for diagnosis, the agents should be modified with appropriate imaging moieties that show prominent imaging enhancement under imaging modality discussed in the earlier imaging contrast section for atherosclerosis imaging. Sometimes, to improve the imaging process and achieve specific experiment aims, taking advantage of multimodal imaging via modification of the agents with multiple imaging moieties should also be considered. A fourth consideration is that using targeting ligands are needed to achieve active targeting and selective accumulation of the agents in plaque. Moreover, a stimuli-driven turn on and release strategy, by which the agents fabricated do not exhibit imaging contrast and release the payloads until their contrast signal and release are turned on upon specific stimuli in the disease sites, needs to be considered [323]. The stimuli can be but are not limited to light, pH, oxidative stress, and temperature [323]. Last but not least, it is of importance to note that, on one hand, the theranostic agents can be designed using separate therapeutics and imaging moieties. On the other hand, the theranostic agents can be developed using a single theranostic molecule that simultaneously shows the therapeutic function and diagnosis capability.

Despite great progress observed in the development of cancer theranostics, studies in this field of simultaneously diagnosing and treating atherosclerosis are not as prevalent as those reported in therapy or imaging for atherosclerosis. This dilemma is mainly due to the complexity of designing theranostic agents. Regardless, we still discuss the up-to-date studies that have been conducted for the design of theranostic agents, such as polymeric NPs, lipid-based NPs, micelles, inorganic NPs, and biomimetic NPs. In some studies, these NPs are involved in photothermal and photodynamic therapies that converted light energy into thermal or chemical energy to kill cells that promoted atherosclerosis development. However, we do not anticipate discussing the basic principles for each therapy, as earlier comprehensive reviews have described them thoroughly [324–327].

2.3.1. Polymeric NPs—Without modification, polymer NPs cannot emit contrast intensity for imaging purposes. Thus, according to recent studies, polymeric NPs developed as theranostics were mainly fabricated by combining photosensitizers or fluorescent chemical drugs for both therapy and diagnosis. In this regard, in 2014, Choi and coworkers developed a novel type of ROS-responsive macrophage-targeting theranostic NPs (MacTNPs) that can induce phototoxicity to macrophages and also be dequenched to express fluorescence via photosensitizers (Ce6). MacTNPs were synthesized by inducing self-assembly of ROS-responsive amphiphilic molecules, HA-Ce6. Fluorescence switch-on and macrophage death were observed when the HA-Ce6 NPs were applied to activate RAW264.7 cells along with 670 nm light *in vitro* [328]. This study is a representative example demonstrating photosensitizers as a theranostic agent for the photodynamic treatment of atherosclerosis. Besides the use of photosensitizers, in the same year, the same group developed another type of theranostic NP, doxorubicin (DOX)-loaded HA-polypyrrole

NPs (DOX-HA-PPy NPs) to detect and kill the activated macrophages. However, in this study, DOX served as a molecule with a theranostic function. In particular, these DOX-HA-PPyNPs were composed of a polypyrrole (PPy) core conjugated with HA and DOX. When DOX was attached to the PPyNPs surface, its fluorescence was quenched because of the energy transfer from DOX to the PPyNPs. However, after the macrophages took up the DOX-HA-PPy NPs in the atherosclerotic plaque, DOX was released from the NPs, resulting in fluorescence recovery of DOX for detecting the macrophages. The *in vitro* results demonstrated that 3 h after RAW264.7 cells were treated with DOX-HA-PPyNPs, the cells became fluorescent. Moreover, 60% of RAW264.7 cells were dead after being treated with DOX-HA-PPyNPs for 48 h, whereas 90% of vascular cells were viable after the same treatment. The significant discrepancy observed here may be due to the specific targeting ability of DOX-HA-PPyNPs to the activated macrophages via HA [329]. These two studies are also illustrative examples of developing polymeric theranostic agents using fluorophores that can be activated after interaction with macrophages, which hold great potential for macrophage targeted atherosclerosis therapy.

Moreover, later in 2020, an interesting study reported by the Harth group developed a collagentargeting fluorescent polymeric nanosponge for targeted delivery of therapeutics for preventing vulnerable plaque formation, which holds potentials as theranostic delivery systems in the future. The nanosponge was composed of poly(δ-valerolactone-co-α-allylvalerolac-tone) as the main component, encapsulated with MMP-14 inhibitor (naphthofluorescein) for inhibiting MMP activity. It was also further modified with a collagen-homing T-peptide (TLTYTWS), a cell penetrating peptide (ACPP), and Cy3 for targeting plaque enhancing naphthofluorescein penetration Cy3 for enhancing naphthofluorescein penetration fluorescent imaging. With the fluorescent tag, the internalization of nanosponges by MMP-2 enriched HT1080 cells was observed. Additionally, the authors also showed that nanosponges could evade lysosomal phagocytosis due to the ACPP peptide and were taken up by RAW264.7 cells, *in vitro* [330]. However, the evaluation of the therapeutic efficacy was not discussed in detail here.

Besides, polymeric theranostic agents showing contrast intensity under dual imaging modality were also developed. One interesting study was reported by the Decuzzi group, where theranostic polymeric platforms, fluorescent-labeled lipid-PLGA spherical NPs loaded with MTX and radiolabeled with ^{64}Cu (MTX-SNPs), were developed for combined fluorescent and optical imaging and atherosclerosis inhibition. The MTX-SNP with 0.06 g ml^{-1} of MTX showed great anti-inflammatory efficacy for activated macrophages and no cytotoxicity. Specific targeting of lesions was observed via nuclear and optical imaging after the MTX-SNPs were injected in ApoE$^{-/-}$ mice fed with HFD. Additionally, after 4 weeks of MTX-SNP administration, a 50% decrease of plaque area in ApoE$^{-/-}$ mice was observed compared with the control group [331]. However, the developed theranostic agents were not stimuli-driven turn on theranostics.

2.3.2. Lipid-Based NPs—Similar to polymeric NPs, lipid-based NPs were fabricated in the realms of atherosclerosis therapy and diagnosis for achieving theranostic function. Lipid-based NPs are commonly loaded with various therapeutics and modified with numerous imaging moieties that show contrast intensity under MRI, NIRF imaging, or both.

Taking liposomes, for example, the Nahrendof group investigated the delivery of siRNA to mice for suppressing inflammation by using CCR2-targeting theranostic liposomes as gene vectors. To construct the liposomal theranostic agents, the siRNA against CCR2 was encapsulated inside the liposomes and labeled with near-infrared fluorochrome for *in vivo* tracking. Three weeks post-injection of siRNA-encapsulated liposomes, the number of monocytes/macrophages in the atherosclerosis plaque was reduced to 18%, and the plaque's size was decreased by 38% [332]. In another study, Mulder and coworkers demonstrated an example of liposomal theranostic agents that exhibited dual imaging contrast and anti-inflammatory effects. Therapeutically, the liposomes were loaded with glucocorticoids (PLP), a powerful drug used to treat atherosclerotic plaques. For imaging, liposomes were labeled with Gd and Cy5 for MRI and NIRF imaging of intact aortas to explore the location of the liposomal theranostics. The *in vivo* MRI demonstrated considerable liposome accumulation within the lesion in rabbits 2 days post-administration, whereas the NIRF imaging demonstrated that the liposomes were distributed across the entire rabbit aortic lesion. Furthermore, the anti-inflammatory effects of the liposomal theranostic agents in the rabbits were also demonstrated by the observation that the aorta's inflammation decreased by 40% after treatment of the liposomal theranostics, which was a great improvement compared with free PLP [333]. Despite the promising result observed here, targeting moieties were not used in the current study to further improve the accumulation of these agents.

Besides liposomes, hybrid lipid NPs were also developed as theranostic agents for atherosclerosis. For example, in an early study, dual imaging theranostic lipid-latex (LiLa) hybrid NPs (LiLa NPs) were fabricated via hydration of a lipid film containing phosphatidylserine, phosphatidylethanolamine-PEG2000, Rosiglitazone (Rosi), Gd, DTPAbis(stearylamide) and fluorescent tag (FITC). On the one hand, for imaging, the r1 relaxivity of Gd-FITC-LiLa NPs (8.3 mM^{-1} s^{-1}) was 2- fold higher than clinically approved Magnevist Gd-DTPA (4.0 mM^{-1} s^{-1}) NPs. On the other hand, for therapy, the authors demonstrated the anti-inflammatory activity of Rosi-LiLa NPs by showing a significant decrease in the production of TNF-α and IL-6 in M1 macrophages treated with Rosi-LiLa NPs. Selective accumulation of Gd-LiLa NPs, *in vitro*, was observed in T1 macrophages and can, therefore, be used for MRI and NIRF imaging in the detection of macrophages. However, there was no *in vivo* evaluation of Rosi-LiLa NPs [334]. The Maiseyeu group developed self-assembled PEG-lipid NPs, nano-antagonists (CCTV), for treating and imaging atherosclerosis. To guarantee effective therapeutic function, the lipid NPs were conjugated with therapeutic 4-mer peptide ligand, which granted the NPs with antagonistic properties, including suppressing the chemotactic migration of monocytes and secondary inflammatory response as well as inhibiting actin polymerization, deactivating inflammasome and downregulation of the NLR family pyrin domain containing 3. Moreover, for tracking NPs *in vivo* via MRI and fluorescent imaging, the authors conjugated europium (Eu) cryptate or Gd to the CCTV NPs. The authors demonstrated more accumulation of CCTV-Eu in atherosclerotic aorta than control (VTCC-Eu), primarily located in the liver and lung. MRI imaging revealed that even 24h after injection, the CCTV NPs still targeted and were retained in the plaque [335]. In another study, peptide-lipid-polymer hybrid NPs with peptide ligands were investigated as theranostic agents for treating

and imaging atherosclerotic plaque. The polymer-lipid hybrid theranostic NPs, UP-NP-C11, were composed of PLGA, lipid, USPIO for imaging plaque, conjugated with C11 polypeptide for targeting lesions via its binding affinity to collagen V and loaded with PTX for treating atherosclerosis. The NPs demonstrated a sustained release of PTX and showed good MRI contrast. In addition, UP-NP-C11 showed much better accumulation in macrophages *in vitro* compared with control NPs without C11 polypeptide (UP-NP). Furthermore, the macrophage inhibition resulted from UP-NP-C11 was shown to be better than that of UP-NP. Using rabbit atherosclerosis models, the authors also demonstrated that the UP-NP-C11 accumulated in plaque was significantly more than that of UP-NPs with excellent MRI ability for imaging atherosclerotic plaque [336].

2.3.3 Micelles—The development of micellar theranostic agents is similar to that of liposomal ones, requiring therapeutic encapsulation and imaging functionality incorporation. The Wang group demonstrated one recent prominent example regarding micelles as theranostic agents for atherosclerosis therapy and detection under multimodal imaging. In this study, the most important and fascinating part is that to achieve both diagnosis and therapeutic functions, novel theranostic compounds, named TPP, were first fabricated by bridging prednisolone (Pred) to a two-photofluorophore (TP) and then loaded into ROS-responsive micelles made by self-assembled amphipathic polymers, PMEMA–PMPC (PMM) (Fig.10a). This strategy is distinguished from the approaches used in most previous studies, where the imaging capability and therapeutic function were obtained by co-encapsulation of separate drugs and imaging contrast agents into nanomaterials. It was expected that once the TPP loaded micelles (TPP@PMM) were delivered to the plaque, the oxidative stress in the plaque would trigger the micelle to degrade and release TPP (Fig.10a). In particular, the ROS-responsiveness of the TPP@PMM was demonstrated by the release of 89% of Pred from the micelles in 48 h under H_2O_2 stimuli. Furthermore, foam cell formation was significantly reduced when the RAW264.7 cells fed with Ox-LDL were co-cultured with TPP@PMM. The theranostic ability of TPP@PMM was also demonstrated *in vivo*; TPP@PMM was first found to accumulate in ApoE$^{-/-}$ mice aorta 6 h post-injection and continuously accumulated in the aorta 18 h post-injection (Fig.10b). Furthermore, due to the fluorescence of TPP@PMM, the location of the plaque was detected by two-photon imaging, indicating TPP mediated a great way to imaging atherosclerosis (Fig.10c–d). Moreover, significant inhibition of plaque formation was observed in mice treated with TPP@PMM, whereas the mice treated with free Pred and saline did not experience the same anti-atherosclerotic effects as TPP@PMM (Fig.10e). The therapeutic effect of TPP@PMM was also demonstrated by the *in vivo* result that the mice treated with TPP@PMM showed less necrotic cores, fewer macrophage activation, and reduced inflammatory cytokine expression than mice treated with their counterparts (Fig.10f–h) [337].

Other representative micellar theranostic agents were developed by the Chung group in 2020. In this study, to achieve theranostic function, peptide amphiphile micelles (MCG PAMs) were incorporated with MCP-1 peptide (NFTNRKISVQR-LASYRRITSS), Gd and Cy7, and collagenase-cleaving peptide (VPMS-MRGG) to target, image, and stabilize unstable atherosclerotic plaque, respectively. It was observed that the relaxivity of MCG PAMs ($4.14 \pm 0.46\ mM^{-1}s^{-1}$) was similar to that of the commercially available Gd- dTPA

contrast agent, indicating MCG PAMs could serve as great contrast agents as well. The imaging and targeting ability of MCG PAMs were evaluated under MRI and NIRF imaging using ApoE$^{-/-}$ mice treated with HFD and angiotensin II for late-stage atherosclerotic plaque formation. Interestingly, the enhancement of the MR signal was observed right after the injection. Moreover, the signal-to-noise ratio (SNR) from mice aorta treated with MCG PAMs was significantly higher than those of mice aorta treated with PBS and PAMs incorporated with scramble peptides and Gd (SCG PAMs). Moreover, by quantifying the Cy7 fluorescence signal, significantly more MCG PAMs were found to accumulate in the mice's atherosclerotic lesions than SCG PAMs. These results indicate an excellent targeting and imaging capability of MCG PAMs to atherosclerotic plaques. More importantly, for diagnosis, compared to other imaging contrast agents, iron oxide or Gd, which showed the strongest contrast enhancement 24 h post-injection, the MCG PAMs offered a fast imaging approach with great plaque selectivity by which prominent SNR was observed 1 h after injection. The greater therapeutic efficacy of MCG PAMs was demonstrated by showing that MCG PAM-treated mice had thicker fibrous caps (68 ± 29 μm) in the lesions than that of mice treated with SCG PAMs (42 ± 12 μm) and PBS (32 ± 16 μm). However, MCG-PAM-treated mice also displayed the least collagenase activity in each plaque. [338]. Overall, this study presented novel multimodal micellar theranostic agents that could target and identify plaque as well as inhibit collagenase allowing for thickening fibrous cap and preventing thrombosis, thereby providing a novel way to diagnose and treat atherosclerosis.

2.3.4. Inorganic NPs—Unlike organic nanomaterials ranging from polymeric NPs to lipid-based NPs discussed above, many inorganic NPs exhibit prominent contrast intensity under a particular imaging modality, making them excellent candidates for generating theranostic agents. Here, we discuss the current recent advance in inorganic NPs as theranostic agents, such as Au NPs and iron oxide NPs.

2.3.4.1. Gold NPs: Gold (Au) NPs have been widely studied for bioimaging and phototherapy. Besides the excellent properties of Au nanostructures such as facile synthesis, great biocompatibility, and easy surface modification with functional ligands, Au NPs also possessed other distinguishing features, making them good candidates for being developed into theragnostic agents. Firstly, AuNPs showed localized surface plasmon resonance absorption or scattering, leading them to be applied in imaging modalities such as darkfield microscopy, optical coherence tomography, and photoacoustic tomography. Secondly, Au NPs can also be imaged by photoluminescence imaging because of their luminescence property. Thirdly, the high electron density in AuNPs allows them to be used in X-ray and CT imaging. Lastly, another important feature of AuNPs is that they can absorb light energy and then convert it into thermal energy to kill the cells for a therapeutic purpose. This feature was widely applied in PTT therapy.

The most familiar Au NPs are Au nanospheres, Au nanorods, Au nanocages, and Au nanoshells. Nevertheless, among these Au nanostructures, Au nanorods and Au spheres have been investigated as theranostic platforms for atherosclerosis. For instance, one interesting study in the field was reported by Lu and coworkers, where gold nanorods were synthesized as a diagnostic tool and therapeutic agent for imaging macrophages via NIR and CT and

photothermal ablating inflammatory macrophages, respectively. Their results demonstrated that even low concentrations of gold nanorods exhibited efficacy for killing macrophages *in vitro* under low power. The gold nanorods also showed great effectiveness for imaging and induced macrophage death in the femoral artery with restenosis *in vivo* [339].

Another emerging strategy to develop gold theranostic agents for atherosclerosis is modifying nanorods with photosensitizers or other types of inorganic components. For instance, in one study, the Courrol group advanced Au nanospheres into aminolevulinic acid (ALA)- Au nanospheres as a photo and sonosensitizer agent for photodynamic and sonodynamic therapy. In addition, as reported, external delivery of ALA can lead to accumulatio of fluorescent protoporphyrin IX (PpIX) in the macrophages, which can be used as an indicator of macrophage content in plaque. Indeed, the authors observed an increase in PpIX fluorescence in THP-1 macrophages after the cells were incubated with ALA-Au nanospheres. The Courrol group advanced Au nanospheres into aminolevulinic acid (ALA)-Au nanospheres as photo and sonosensitizer agents for photodynamic and sonodynamic therapy. In addition, as reported, external delivery of ALA can lead to the accumulation of fluorescent protoporphyrin IX (PpIX) in the macrophages, which can be used as an indicator of macrophage content in plaque. Indeed, the authors observed an increase in PpIX fluorescence in THP-1 macrophages after the cells were incubated with ALA-Au nanospheres. Besides, the ALA-Au nanospheres demonstrated efficacy for eliminating macrophages after they were exposed to light or treated with ultrasound. However, the effectiveness of ALA-Au nanospheres using SDT is better than that of ALA alone or ALA-Au nanospheres using PDT due to a greater ROS generated by ultrasound activated PpIX leading to macrophage damage. Since Au nanospheres can be used for atherosclerosis imaging under multimodalities, MALA-Au nanospheres and ALA-Au nanospheres exhibit great potential as theranostic agents for atherosclerosis imaging and therapy [340]. In another study, Emelianov and coworkers developed silica-coated gold nanorod (SiO_2AuNR) for imaging plaque via a dual-imaging modality combining intravascular ultrasound (IVUS) and photoacoustic imaging (IVPA), allowing for visualization of atherosclerotic plaque morphology via investigation of the cellular components in plaque by IVUS and IVPA, respectively. The most interesting part of this study is that the IVPA signal intensity from the NPs demonstrated a linear relationship with temperature when the laser was applied; in other words, the IVPA signals can be used as sensitive thermal sensors to monitor the local temperature. Besides, the IVUS signal can be utilized to monitor the heat accumulated resulting from laser irradiation. Although the authors did not show any data about the *in vitro* or *in vivo* photothermal ablation of macrophages using SiO_2AuNR, the IVUS/IVPA combined SiO_2AuNR holds promise for theranostic platforms by first detecting the location of SiO_2AuNR, followed by photothermal heating via catheter [341].

In summary, Au nanospheres and nanorods were demonstrated as promising candidates for developing theranostic platforms. Despite that, no studies have reported the design of nanocage and nanoshell-based theranostic agents for atherosclerosis. Thus, the integration of these nanostructures with therapeutics should be explored in the future. In addition, the shape, size, and aspect ratio of Au nanostructures have an important effect on localized surface plasmon resonance abortion or scattering in light that is strongly associated with their imaging contrast and photothermal ability; thus, designing Au nanostructures with

favorable properties is key to the successful development of Au-based theranostic agents with high efficacy.

2.3.4.2. Iron Oxide NPs: As described earlier, iron oxide NPs were employed for diagnosing atherosclerosis via MRI as they show T1 or T2 contrast due to their superparamagnetic property. Therefore, iron oxide NPs show great promise in this matter as theranostic agents if therapeutic molecules are conjugated to iron oxide NP surfaces. This idea was demonstrated in early 2006 by Weissleder and coworkers, who designed dextran-coated magnetofluorescent iron oxide NPs (MFNPs) conjugated with-(4-carboxyphenyl)-10,15,20-triphenyl-2,3-dihydroxychlorin (TPC), a photosensitizer, which can induce phototoxicity and show fluorescence in the presence of light. TPC-MFNPs can be detected by MR and NIRF imaging and were shown to kill murine and human macrophages *in vitro*. However, TPC-MFNPs suffer from inherent instability [342]. Later in 2010, to improve stability and therapeutic efficacy of their NPs, the same group developed a second generation of magnetofluorescent dextran-coated iron oxide (CLIO) NPs by modifying CLIO with Alexa Fluor 750 for NIRF imaging and conjugated with a new phototoxic therapeutic moiety, meso-tetraphenylchlorin derivative (THPC), for ablating macrophages. The loading capacity of THPC is 3- times higher than that of TPC reported earlier. For diagnosis, strong fluorescence was observed 24 h after CLIO-THPCs were injected in ApoE $^{-/-}$ mice, indicating the capability of these NPs to localize and accumulate in atherosclerotic plaques. Therapeutically, more than 50% of macrophage death was observed when the mice were treated with CLIO-THPCs and laser light, in contrast to mice treated with control NPs where more than 99% of macrophages were alive in plaque after the light was applied [343]. Later, Zhou and coworkers designed another type of theranostic iron oxide NP that can treat and image atherosclerosis by MR imaging and releasing the drug, RAP. The theranostic NPs, referred to as RAP@PFN1-CD-MNs, were composed of iron oxide NPs for MRI imaging intensity, pH-sensitive cyclo-dextrin for drug release, and profilin-1 antibody for targeting SMCs in the plaque. The RAP@PFN1-CD-MNs were shown to induce a more drastic decrease in the T2 signal in the plaque compared with the control NPs without any targeting ligand. Moreover, the atherosclerotic plaque size of ApoE$^{-/-}$ mice was reduced and delayed by these NP [344]. In addition to drugs and photosensitizers, the antibody that suppresses specific factors crucial for atherosclerosis progression is also conjugated to the iron oxide NPs for obtaining effective therapy and diagnosis function. This finding was demonstrated in a recent study reported by the Liu group. In this study, ultrasmall superparamagnetic iron oxides (USPIOs) were applied to deliver an antibody suppressing connective tissue growth factors (anti-CTGF) to treat atherosclerotic plaque in ApoE$^{-/-}$ mice under MRI. The connective tissue growth factor (CTGF) is highly expressed in atherosclerotic plaque and associated with fibrosis, postulating its key role in atherosclerosis development. For imaging, *In vitro* MRI showed that macrophages treated with anti-CTGF-USPIO NPs demonstrated remarkably shorter T2 relaxations compared with macrophages treated with PEG-coated USPIO NPs. A reduced contrast-to-noise ratio was also observed in anti-CTGF-USPIO NPs treated mice. Furthermore, macrophage number, as well as MMP-2 and CTGF expression, were significantly decreased upon the CTGF-USPIO NP treatment in mice [345].

Apart from modifying the iron oxide NPs with therapeutics mentioned above, they have also been used to enable theranostic functions. For example, in an early study in 2009, multifunctional nanorose (nanocluster)-iron oxide NPs were coated with 2.5 nm thin gold shell by Johnston and workers for dual imaging and ablating macrophages. As a result of the presence of ~70 iron particles and the gold shell in the nanoclusters, the nanoclusters showed strong NIR absorbance (700-850 nm), r_2 magnetic relaxivity (>200 Mm^{-1}), and optical contrast for imaging. The authors also demonstrated that nanoroses were taken up by macrophages after incubation for 24 h. Moreover, by only 50s laser irradiation, the nanoclusters in the macrophages absorbed a great amount of energy, which led to a positive terminal deoxynucleotidyl transferase dUTP nick end labeling (TUNEL) in the macrophages, indicating the ability of nanoroses to induce apoptosis of macrophages [346]. Likewise, in another study, the Ta group developed theranostic nanocomposites that targeted ROS using Fe_3O_4 NPs. The theranostic agents were composed of layered double hydroxide (LDH) coated with CeO_2 and Fe_3O_4 NPs. The authors demonstrated the CeO_2-Fe_3O_4-LDH showed a great antioxidant effect on macrophages and MRI contrast intensity *in vitro*, of which CeO_2 and Fe_3O_4 served as therapeutic agents for ROS scavenging and contrast agents for monitoring the NPs under MRI [287].

Additionally, an innovative strategy, the integration of fluorocarbon, PLGA, and iron oxide for the fabrication of advanced theranostic agents, was reported by Guo and coworkers in 2019. Using this approach, a new type of phase-transition theranostic iron oxide (Fe_3O_4) NPs, abbreviated as Fe-PFH-PLGA/CS-DXS NPs, were developed for ultrasound and MRI guided atherosclerosis imaging and treatment. The NPs were composed of PLGA, whose shells were embedded with iron oxide for MRI, and cores were loaded with perfluorohexane (PFH), which can perform phase transition for treating plaque under ultrasound irradiation. The surfaces of the NPs were also modified with dextran sulfate (DXS) using chitosan (CS) for targeting SR-A, overexpressed in activated macrophages in atherosclerotic plaque. More importantly, the NPs demonstrated ultrasound contrast at both B and contrast modes and reduced the T2 signal for MRI. The *in vitro* study demonstrated that the Fe-PFH-PLGA/CS-DXS NPs (67.76%) were taken up by the activated macrophages 2 h after incubation, while other groups demonstrated much less uptake (4.65%). Moreover, significant macrophage apoptosis was observed *in vivo* after the NPs were administered in $ApoE^{-/-}$ mice for 2 h after 10 min low intensity focused ultrasound (LIFU) irradiation. The apoptosis of macrophages caused by Fe-PFH-PLGA/ CS-DXS NPs was due to the acoustic droplet/ vaporization (ADV) effect inside macrophages, due to the phase transition of PFH stimulated by LIFU. The ADV effect also enhanced the stability of vulnerable plaque. However, the limitation of this study is that, as described by the authors, the improper use of LIFU may result in plaque damage and, ultimately, plaque rupture. Additionally, the investigation of NP biodistribution and PFH safety have not been explored in the current study [347].

2.3.4.3. Other Types of Inorganic NPs.: In addition to iron oxide NPs, metal sulfate was also developed as theranostic agents. For instance, although photothermal therapy has been reported effective for ablating various cells for treating diseases, its therapeutic efficacy is limited by several issues associated with the laser used. Specifically, the laser cannot

penetrate deep tissues and is easy to be absorbed by surrounding tissues. To address these issues and improve the therapeutic efficacy, in 2020, the Lu group reported the development of Fe_3S_4 NPs that was expected to show both photothermal and magnetic hyperthermia properties and be used to eliminate inflammatory macrophages for atherosclerosis treatment. As expected, Fe_3S_4 NPs were able to convert both light and magnetic energy into heat to kill inflammatory macrophages, thereby suppressing the progression of atherosclerosis in ApoE $^{-/-}$ mice [348]. In addition, these NPs also showed T2 MRI intensity (52.8 Mm^{-1}) *in vitro*. This was the first study to design NPs combining photothermal and magnetic hyperthermia therapies.

Besides Fe_3S_4, copper sulfide NPs (CuS NPs) were investigated as theranostic platforms for atherosclerosis in a recent study by the Tang group. In this study, TRPV1 was selected as the target to alleviate atherosclerosis because it is a well-known thermosensitive cation channel that can be activated by capsaicin, thus inducing autophagy in ox-LDL loaded SMCs and preventing foam cell formation. In the view of the role of TRPV1 signaling for atherosclerosis development, copper sulfide NPs were developed to photothermally switch TRPV1 signaling in SMCs for treating atherosclerosis [349]. The authors expected that the local temperature in plaque to increase upon NIR irradiation, leading to the activation of the TRPV1 channel and the initiation of Ca^{2+} influx, thereby activating autophagy, enabling upregulation of ABCA1, decreasing lipid accumulation, and reducing foam cell formation derived from SMCs (Fig. 11a). Moreover, because of the inherent property of CuS NPs, TRPV1-CuS NPs were also expected to be used as platforms to image the vascular structure via PA imaging, which provides an excellent opportunity to control the TRPV1 signaling *in vivo* [349]. As expected, the *in vitro* study showed that the CuS-TRPV1 NPs with a diameter of 1057 nm could bind to the SMC surface 2h after incubation with SMCs. Furthermore, the TRPV1 was activated when the local temperature of CuS and SMC coculture increased from 37°C to 42°C, resulting from NIR irradiation in an on-and-off mode for 30 times. The opening of TRPV1 was confirmed by observing an increase of adenosine monophosphate-activated protein kinase associated phosphorylation and the double membrane structure. The autophagy resulting from ox-LDL was significantly suppressed by CuS-TRPV1, as demonstrated by the downregulation of microtubule-associated proteins 1A/1B light chain 3B (LC3)-II and the upregulation of LC3-II. Furthermore, the CuS-TRPVI NPs showed strong photoacoustic contrasts 2 h post-injection, while the control (CuS NPs) only showed weak photoacoustic signals (Fig.11b). More importantly, the immunofluorescence images indicated a significant accumulation of CuS-TRPV1 NPs (green fluorescence) in atherosclerotic aortas. The authors also showed that CuS-TRPV1 NPs were mostly located at the intimal and medial layers, as the red immunostaining of α-SMA overlapped with the green fluorescence. In contrast, the NPs without TRPV1 did not show any specific accumulation in the plaque (Fig.11c). Therapeutically, the *in vivo* study demonstrated that CuS-TRPV1 NPs and laser treatment induced 54.2% and 72.3% reduction in aortic root lesion areas and aortic arch lesion areas compared with the control, respectively (Fig.11d–i) [349].

Selenium (Se), an essential trace element, has been reported to act as a key regulator for inducing the expression of inflammatory genes and associated pathways in macrophages, thereby having a crucial effect on immunity and inflammation. In addition, NPs containing

Se were demonstrated to show various therapeutic functions beneficial for treating atherosclerosis, such as antioxidant and anti-inflammatory properties, demonstrated by their ability to scavenge ROS and inhibit inflammatory cytokine production, respectively [350]. Therefore, inspired by Se's property, in 2017, Mi and coworkers developed H_2O_2-depleting and (O_2-generating photodynamic selenium NPs (CAT/1st-SeNPs) to clearing activated macrophages and limit their proliferation for combating inflammation. In particular, CAT/1st-SeNPs were composed of Se NPs conjugated with a fluorescent photosensitizer (rose bengal) and a thiolated CS loaded with catalase (CAT) for converting H_2O_2 into O_2. To increase the local accumulation of these NPs, The CAT/1st-SeNPs were then coated with HA conjugated with folate acid to form dual targeting H_2O_2-depleting and (O_2-gegenerating photodynamic selenium NPs, CAT/2nd-SeNPs, which can target CD44 and folate receptor-β receptor in the plaque. The authors showed that CAT/2nd-SeNPs demonstrated better cellular internalization than CAT/1st-SeNPs and could generate high levels of O_2 to enhance the efficacy of eliminating activated macrophages by releasing catalase and photoirradiation, *in vitro*. Though these newly developed NPs are attractive, future *in vivo* evaluation is needed [351].

2.3.5. Other Types of Theranostic Nanomaterials—Recently, several studies reported the development of protein and biomolecule related theragnostic agents. One typical study was shown by Cao and coworker in 2018, where novel theranostic nanomaterials for inhibiting the progression of vulnerable plaque by suppressing SMC phenotype change during atherogenesis were developed. Specifically, the theranostic nanomaterials, abbreviated as ICG/SRT@HSA-pept, consisted of human serum albumin conjugated with peptide ligand (HAS-pep) for OPN targeting in the plaque, fluorescent indocyanine green (ICG) for NIRF imaging, and the sirtuin 1 (Sirt1) activator (SRT1720) for the therapeutic effect. The *in vitro* study showed that the ICG/SRT@HSA-pept were taken up by ox-LDL-stimulated synthetic VSMCs. Promisingly, ICG/SRT@HSA-pept increased the expression of Sirt1 and inhibited the transition of ox-LDL stimulated VSMCs from contractile to synthetic phenotypes. Particularly, an increase in contractile marker protein (e.g., α-actin and calponin) expression and a decrease in synthetic marker (e.g., vimentin and OPN) expression were observed in the VSMCs treated with ICG/SRT@HSA-pept. Besides, ICG/SRT@HSA-pept exhibited strong ICG fluorescence in the plaque of mice carotid artery as observed in the *ex vivo* NIRF imaging, which is in great contrast to the ICG/SRT@HSA and PBS-treated mice whose carotid artery barely showed any fluorescence by NIRF imaging. More importantly, compared with free SRT1720 and free vesicles, the ICG/SRT@HSA-pept showed significantly better anti-atherosclerotic effects, as substantiated by smaller but more stable plaque area with higher collagen content in the mice treated with ICG/SRT@HSA-pept than the mice treated with free SRT1720 or vesicles [352]. The ICG/SRT@HSA-pept provided an approach that holds prospects for improving atherosclerosis therapy by combining precise diagnosis and targeted atherosclerosis treatment. In addition, many previous studies primarily focused on treating atherosclerosis by developing nanotherapeutics to alleviate inflammation, suppress EC dysfunction and foam cell formation, or eliminate activated macrophages; thus, this study is particularly fascinating because it substantiated that the therapeutic strategy of inducing SMC phenotype

change, was also effective and can be an alternative to existing strategies for exploring efficient treatments for atherosclerosis in the future.

As discussed earlier, biomimetic NPs are newly developed nanomaterials with numerous advantages as therapeutic delivery systems to improve atherosclerosis efficacy. Such type of NPs was also applied for diagnosing and treating atherosclerosis simultaneously. For instance, a recent study demonstrated the development of bioinspired magnetic nanoclusters (MNC@M-ST/AP) for targeted treating and diagnosing early atherosclerosis via targeting intimal macrophages under MRI. The MNC@M-ST/AP consisted of a Fe_3O_4 core (MNC), and leukocyte membranes (M), and apoA-I mimetic 4F peptide (AP) loaded with a potent anti-inflammatory drug, ST. The AP and leukocyte membranes served as targeting molecules to interact with macrophages, thereby allowing MNC@M-ST/AP to actively target the atherosclerotic plaque (Fig. 12a). This targeting approach via the leukocyte membrane was inspired by the leukocytes' capability to migrate from circulation to inflammatory states and interact with dysfunctional endothelial ECs. Indeed, the in vitro result showed that the MNC@M-AP could adhere and keep tethering and rolling on inflammatory HUVECs; conversely, the nanoclusters coated with red blood cell membranes demonstrated worse adhesion and finally detached from the ECs. In addition, the MNC@M-AP exhibited excellent transmigration ability due to the presence of receptors on the leukocyte membrane coating, such as CCR-2, CXCR-2, VLA-4, and LFA-1, which leads to 4 times higher internalization efficiency in foam cells than ECs. For imaging, due to the magnetic nature of the Fe_3O_4 core, MNC@M-ST/AP was also expected to possess MRI contrast for imaging atherosclerotic plaques. This finding was demonstrated in the study, as mice treated with MNC@M-ST/AP showed the most prominent T2-weighted signal-to-noise ratio compared with the mice groups treated with control, MNC, and MNC@M (Fig. 12b–c). Large quantities of MNC@M-ST/AP were observed to accumulate in the area of plaque with abundant macrophages. More importantly, a great anti-atherosclerotic effect was achieved via the synergistic therapeutic effect between AP and ST through anti-inflammatory action and cholesterol efflux promotion. The *in vivo* study showed that mice treated with MNC@M-ST/AP exhibited a 72.3% reduction of aorta lesion area compared with the mice treated with PBS (Fig. 12d). The proinflammatory cytokine production (e.g., MCP-1, IL-6, TNF-α, and MMP-10) and microcalcification formation decreased and were suppressed more by MNC@M-ST/AP than those of other groups, such as PBS, free ST, MNC@M-ST, free AP, and MNC@M-AP (Fig. 12e) [353]. Similarly, Tasciotti and coworkers developed novel biomimetic NPs called leukosomes for potential atherosclerosis imaging and treatment in 2018. In this study, macrophage-derived membrane proteins were integrated with phospholipid films to form the leukosomes. Then, the leukosomes were modified with Gd for imaging purposes with r_1 and r_2 values at 6 and 30 $mM^{-1}S^{-1}$, respectively. In addition, leukosomes demonstrated a sufficient targeting ability to the atherosclerotic plaque in $ApoE^{-/-}$ mice via similar mentioned earlier, recognizing and adhering to inflamed cells in the plaque. The therapeutic efficacy of leukosomes was not evaluated in the current study; still, they hold great potential for future use as theranostic agents, as leukosomes were reported to encapsulate various therapeutics [354]. The above two studies described here demonstrate the advantages of leukosome biomimetic NPs as

theranostic agents enable targeted delivery and imaging, making them promising candidates for clinical translation in the future.

In addition to cell membrane coated biomimetic NPs, exosomes, one type of extracellular vesicles secreted by a wide variety of cells, has emerged as attractive endogenous nanomaterials for drug delivery due to their excellent features, such as great biocompatibility, long blood circulation, reduced clearance possibility, and targeting ability. Besides these features, it is reported that exosomes possess the biological functions of the cells they are isolated from, making them good therapeutic candidates for treating different diseases. As it is known, M2 macrophages are anti-inflammatory by secreting multiple anti-inflammatory cytokines. Consequently, the M2 macrophage-derived exosomes are also expected to show potent anti-inflammatory effects. Encouraged by the features of exosomes, in a recent study, Xie and coworkers developed engineered M2 exosomes (HAL@M2 Exo) for atherosclerosis treatment and imaging via loading hexyl 5-aminolevulinate hydrochloride (HAL) into M2 macrophage-derived exosomes (Fig. 13a). The use of HAL is expected to initiate heme biosynthesis and metabolism to generate molecules with anti-inflammatory functions, such as carbon monoxide and bilirubin in cells, thereby synergistically enhancing the therapeutic efficacy with M2 exosomes (Fig. 13b–c). The authors found that the chemokine receptors (CD44), monocyte very late antigen-4 (VLA4), and monocyte lymphocyte function-associated antigen 1 (LFA1)) on the HAL@M2 Exo could improve the accumulation of Exo in activated HUVECs by recognizing and interacting with receptors such as E-selectin, VCAM1, and ICAM1 on HUVECs. Furthermore, the generation of ROS and pro-inflammatory cytokines (e.g., MMP-10, IL-6, TNF-α, and IL-1β) were reduced by HAL@M2 Exo treatment. The excellent anti-inflammatory capability of HAL@M2 Exo was exhibited when the 5-week administration of HAL@M2 Exo induced the smallest area of the lesion and necrotic cores, as well as the highest PpIX fluorescent signal in ApoE$^{-/-}$ mice with early atherosclerosis compared with other controls (Fig.13d–g). Moreover, greater upregulation of ABCA-1 and SR-BI receptors were observed in the aorta of mice treated with HAL@M2 Exo compared to the controls (Fig. 13h) [355].

3. Clinical Studies of Nanomaterials for Atherosclerosis Therapy and Diagnosis

Despite the great advancements of nanomaterials in preclinical studies for treating and diagnosing, nanomaterial mediated atherosclerosis treatment and diagnosis have not yet been widely investigated in the clinical setting. The challenges for conducting clinical studies may be due to various factors, such as significantly higher cost in clinical trials than *in vitro* or *in vivo* models, the length of time required to finish studies feasible results, and safety concerning patient morbidity and mortality. Although developing multimodal NPs for diagnostic and therapeutic uses at the clinical level proceeds at a relatively stagnant rate, up to now, some advances have also been achieved in the field. Thus, in this section, we summarize the nanomaterials that have been studied in clinical trials for atherosclerosis (Table 5).

3.1. Clinical Studies of Nanomaterials for Atherosclerosis Therapy

3.1.1. Lipid NPs

3.1.1.1. LN-PLP: One method in which drug delivery to atherosclerotic plaques can be potentially accomplished in clinical studies is via liposomal NPs encapsulating prednisolone phosphate (LN-PLPs). LN-PLP consists of a hydrophilic core encapsulating PLP, surrounded by a lipid bilayer of phospholipids and cholesterol, coated with PEG. LN-PLP was developed for targeted therapeutic delivery to atherosclerotic plaque macrophages in 2015 by Stroes and colleagues. The authors conducted a single-dose study in thirteen patients to assess the pharmacokinetics of LN-PLP via single intravenous administration of 0.375 mg/kg (n=3), 0.75 mg/kg (n=3), or 1.5 mg/kg (n=7) in a 2.5 h time frame. The prolonged circulation half-life of LN-PLPs were found to range from 45 to 63 h. They also evaluated the LN-PLP delivery to plaque macrophages through a randomized, placebo-controlled, double-blind trial in fourteen patients with iliofemoral atherosclerotic plaques. Patients either received 1.5 mg/kg LN-PLP (n=7) or saline (n=7) via an antecubital vein on days 0 and 7, followed by vascular surgery on day 10. The results indicated that 88% of DAPI positive cells isolated from plaques stained positive for the macrophage marker CD68 – 77% of which were also positive for liposomal PEG – suggesting a high co-localization between PEG and macrophages [364]. LN-PLP therapeutic efficacy was then assessed through a randomized, placebo-controlled, double-blind trial of thirty patients with a documented history of CVD. Patients received either LN-PLP 1.5 mg/kg (n=20) or saline (n=10) intravenously on days 0 and 7. On day 10, therapeutic efficacy was evaluated by dynamic contrast-enhanced (DCE)-MRI and fluorodeoxyglucose (FDG)-PET/CT imaging of both carotid arteries. The results of this study showed that LN-PLPs were shown to be present in 75% of macrophages isolated from atherosclerotic patients but did not reduce arterial wall permeability or inflammation in patients with atherosclerotic disease (n=30) [364]. This study demonstrated that the successful delivery of LN-PLPs to atherosclerotic plaque macrophages in clinical patients; nevertheless, the therapeutic efficacy of LN-PLPs for atherosclerosis in patients was not observed. However, later in another study, the same group demonstrated that LN-PLP showed anti-atherosclerotic effectiveness *in vitro* and *in vivo* [391].

3.1.1.2. LDE: As introduced earlier, LDEs are lipid structures that are shown to mimic protein-free LDL composition. To assess the effectiveness of PTX-LDE for human use, Maranhao and coworkers conducted a clinical study in patients with aortic atherosclerosis in 2016. Ten patients with aortic dilations and systemic arterial hypertension were administered via intravenous injection with 175 mg/m^2 PTX-LDE dissolved in a 0.9% saline solution. A control group of nine untreated patients with aortic atherosclerosis was also examined. MDCT angiography was conducted before treatment, as well as 1-2 months after treatment. The study showed that PTX-LDE treatment did not induce any clinical or laboratory toxicity. However, the difference between the pre-and post-treatment values was not statistically significant ($p = 0.348$). The mean plaque volume in the aortic artery wall presented mixed results, with reduced volume within 4 patients, constant volume in 3 patients, and increased volume in 1 patient [368]. Encouraged by the outcome of Maranhao's study, a randomized, double-blind, placebo-controlled study (NCT04148833) is

currently being conducted to evaluate the safety and efficacy of PTX-LDE in patients who have coronary disease. The recruited patients will be divided into two groups; one group will be treated with placebo-LDE, and another group will be treated with PTX-LDE at a dose of 175 mg/m^2 for 6 weeks.

Besides PTX-LDE, a clinical study of MTX-LDE is also being conducted by Marahao's group currently. This ongoing study (NCT04616872) is a prospective, randomized, double-blind, placebo-controlled study, where the safety and anti-inflammatory efficacy of the MTX-LDE will be evaluated in 40 patients with stable coronary disease. The patients will be divided into two groups randomly. One group will receive placebo-LDE, and the other group will receive MTX-LDE through IV injection for 12 weeks, 7 days per injection. Coronary and aortic CT angiography will be performed at three-time points.

3.1.2. HDL Mimetic NPs

3.1.2.1. CER-001: CER-001 are lipoprotein particles with negative charges. Similar to PTX-LDE, these NPs are also mimetic, but instead of LDLs, they mimic the natural pre-beta HDLs, consisting of recombinant human apoA-1 and two natural phospholipids-sphingomyelin and dipalmitoylphosphatidylglycerol with a respective ratio of 1:2.7. They can perform all the steps of reverse cholesterol transport, the only natural pathway responsible for lipid elimination, thereby delivering their payload into plaque macrophages.

For clinical applications, in 2014, the Waters group initiated an investigation on the effect of CER-001 on regressing atherosclerosis in randomized patients with acute coronary syndrome using intravascular ultrasonography (IVUS) and quantitative coronary angiography (CHI-SQUARE study). In particular, 507 patients with the acute coronary syndrome (ACS) were randomized to receive an infusion of placebo with CER-001 at dosages of 3 mg/kg, 6 mg/kg, and 12 mg/kg weekly for 6 weeks. IVUS examination was conducted before randomization (baseline) and three weeks after the last infusion of CER-001. Unfortunately, no significant differences in baseline changes to follow up in the total volume of atheroma, coronary artery score, and cumulative coronary stenosis score were observed among doses tested compared with the placebo [363]. These results indicated that the infusion of CER-001 at the tested dose range did not reduce atherosclerosis compared with placebo based on IVUS. However, whether other dosages work or what effect of the CER-001 on patients with different degree of atheroma volume is still unknown. Thus, in 2017, another similar CHI-SQUARE study was conducted by Nicholls and coworkers to investigate CER-001 in patients with coronary atherosclerosis. 369 patients with ACS were infused with CER-001 at dosages of 3 mg/kg, 6 mg/kg, and 12 mg/kg weekly or placebo for 6 weeks and checked with IVUS. Interestingly, unlike the previous study in 2015, the authors found that the patients with baseline percent atheroma volume (B-PAV) above 30% showed atheroma regression after infused with CER-001, while the patients with B-PAV below 30% did not obtain benefits from CER-001 infusion [377]. In addition, the optimal dose among the tested dose range was found to be 3 mg/kg for the patients with B-PAV above 30%; however, 6 mg/kg and 12 mg/kg infusions induced minor and no regression in the patients, respectively. As indicated by the authors, a high dosage of CER-001 infusion would downregulate ABCA1 expression, thereby diminishing the

therapeutic effect of CER-001. This study suggested that CER-001 infusion at a specific dosage would benefit the patients with higher plaque burden [377]. In the same year, Nicholls and coworkers conducted a clinical study (CARAT, phase 2) to explore CER-OOTs therapeutic efficacy on patients with ACS and with PAV above 30%. A total of 292 patients were randomly assigned to treat with 10 infusions of CER-001 at 3 mg/kg weekly. It should be noted that, unlike the patients in the previously mentioned trials, the patients eligible for this study were those who presented an ACS within 7 days before the study. As expected, CER-001 was found to regress the plaque in those patients with recent ACS [378]. In 2018, another study (CARAT trial) investigating the therapeutic efficacy of CER-001 on patients with ACS was also conducted by the Butters group. 272 patients were involved in this study, including 86 patients who had statin treatment. The patients were either infused with CER-001 at the dose of 3 mg/kg or placebo weekly for 10 weeks, followed by IVUS checking [382]. Interestingly, the authors found no benefits of CER-001 were received by the patients who had statin treatment.

Besides patients with ACS and different degrees of PAV, in 2017, Dasseux and colleagues gave a single intravenous dose of CER-001 to 32 healthy volunteers aged from 18 to 55 years old. The dose level ranged from 0.25 to 45 mg/kg of CER-001. The volunteers were required to stay in clinics for 72 h after the administration and followed up in the next 3 weeks. The results demonstrated that all doses were well-tolerated by clinical patients. No effect from the CER-001 treatment on the clinical chemistry, hematology, and electrocardiogram (ECG) in the subjects was observed. When the CER-001 dose level is smaller than 10 mg/kg, the level of apoA-I in plasma increased as the dose of CER-001 increased right after administration but decreased to the original level 24 h post-administration. When the dose level of CER-001 is above 10 mg/kg, CER-001 was able to circulate in the plasma for more than 72 h. More significantly, the administration of CER-001 increased reverse cholesterol transport, as demonstrated by increasing cholesterol and rapid mobilizing cholesterol in HDL fractions in the volunteers [379].

For assessing the targeting ability of CER-001 in humans, in 2016, Zheng and colleagues labeled the CER-001 with ^{89}Zr and conducted a single-center observational study in carotid plaques in patients. Eight patients with atherosclerotic carotid artery disease received a single infusion of unlabeled CER-001 (3 mg/kg body weight) with co-administration of ^{89}Zr-labeled CER-001 (18 mBq), followed by serial PET/CT imaging and CE-MRI. By radiolabeling CER-001 with ^{89}Zr, it can be used to readily access atherosclerotic plaques and achieve images with good spatial resolution. Through PET/CT imaging, arterial uptake of CER-001 was measured as target-to-background ratio (TBR_{max}) and was found to significantly increase 24 h after infusion (t=10 min: 0.98, t=24 h: 1.14 [p=0.001]). TBR_{max} was revealed to be higher in plaque compared with non-plaque segments (1.18 vs 1.05; $p < 0.001$) [370].

Recently in 2020, another clinical trial was conducted by Stroes and coworkers to investigate whether an infusion of CER-001 would improve patients with atherosclerosis with low HDL levels. In this study, 30 patients aged between 50 and 60 with HDL-cholesterol less than 0.9 mmol/L or apoA-I less than 1.1 g/L. The patients were then randomly divided into two groups for receiving CER-001 (8 mg/kg) and placebo, respectively. Three phases were

included in the study. In the first phase, the patients received CER-001 weekly for 8 weeks with a total of 9 doses; in the second phase, biweekly treatment was given to the patients for 16 weeks with a total of 8 doses; in the last phase, the patents also received CER-001 every two weeks for 24 weeks with the total of 12 doses. After 24 weeks, unfortunately, it was found that there were no significant differences in carotid arterial vessel dimension and inflammation between the groups based on MRI and FDG PET/CT scanning [388].

3.1.2.2. CSL112: CSL112 is another type of reconstituted HDL mimetic, composed of apoA-I and phosphatidylcholine and possesses a discoidal shape. As early as 2015, the Alexander group investigated the therapeutic effect of CSL112 in patients with stable atherosclerotic disease via intravenous infusion of a single ascending dose of CSL112. 45 patients were involved in this study, and CSL112 dosages of 1.7 g, 3.4 g, and 6.8 g were investigated. It was found that CSL112 infusion significantly increased the apoA-I and total serum cholesterol efflux capacity (CEC) in patients. However, the limitation of this study was that the sample size was too small [365]. Later in 2018, the pharmacokinetics and pharmacodynamics of CSL112 were evaluated by the Wright group. The studies were conducted in patients with stable atherosclerosis. Single and multiple ascending doses were studied. The changes of CEC induced by CSL112 were compared with the corresponding data obtained from healthy volunteers. The CEC baseline mediated by ABCA1 in patients was remarkably lower than that of healthy volunteers; however, their apoA-I levels were slightly higher than those of healthy subjects. Besides apoA-I, a higher level of triglycerides was also observed in patients with stable atherosclerosis. After CSL112 infusion, the elevation of cholesterol efflux was observed in the patients, similar to that of healthy individuals treated with CSL112 in prior studies. In addition, the infusion of CSL122 did not affect the apoA-I pharmacokinetics or pre-α1-HDL levels in patients [383]. However, this study's limitation was that the comparison was based on data generated in different studies. Besides the anti-atherosclerotic effect, in the same year, the anti-platelet capability of CSL112 was explored in patients with stable atherosclerosis and ongoing dual anti-platelet therapy (DAPT) by the Tricoci group. Single ascending doses of CSL112 at 1.7 g, 3.4 g, and 6.8 g were given randomly to patients after receiving DAPT. It was found that the administration of CSL122 at tested doses did not show marked effects on platelet aggregation, indicating that CSL112 administration may not change hemostasis in patients [384]. Currently, an ongoing CLS112 associated clinical study (NCT03473223) is at its recruiting stage. The goal of the phase 3 study is to evaluate the efficacy and safety of CSL112 on reducing major adverse cardiovascular events (MACE) risk. This study is a multicenter, double-blind, randomized, placebo-controlled, parallel-group research. 17400 patients are going to be recruited in this study.

3.1.2.3. ETC-216/MDCO-216: An alternative HDL mimetic to CER-001 and CSL112 studied in clinical trials is ETC-216. As early as 2003, a study showed that an HDL mimetic, ETC-216, composed of recombinant apoA-I Milano (AIM), a mutation of human apoA-I palmitoyl-oleoyl phosphatidylcholine showed the ability to regress atherosclerosis by decreasing atheroma volume in patients [357]. Due to the improvement of the manufacturing process of ETC-216, ETC-216 was later renamed MDCO-216. In 2013, the safety and efficacy of MDCO-216 were evaluated in cynomolgus monkeys by the Wijngaard group.

The study demonstrated that the ABCA1-dependent CEC and free cholesterol increased in the studied monkeys after the infusion [392]. Because of the promising results observed *in vivo*, the same group investigated the safety and efficacy of MDCO-216 in healthy individuals and patients with atherosclerosis in 2016 [372]. In this study, 24 patients and healthy volunteers received MDCO-216 at a single ascending dose in a randomized and placebo-controlled manner. The dose ranged from 5 to 40 mg/kg. Remarkably, MDCO-216 was found to modulate the apoA levels in both patients and healthy participants. Particularly, the apoA-I level of healthy individuals increased right after the infusion of 40 mg/kg MDCO-216 and dropped to baseline 48 h after the infusion. Similarly, an increase in apoA levels was observed in patients infused with 40 mg/kg MDCO-216. However, 2-h post-infusion, the apoA levels dropped below baseline 24 h later and did not return to the baseline until sometime after day 6, but before day 28. Furthermore, the infusion of MDCO-216 also increased pre-beta 1 HDL in both patients and healthy volunteers. Of note, the most encouraging finding in this study is that the infusion of MDCO-216 increased the ABCA1-mediated CEC to a maximum of 4- fold after the patients, and healthy individuals completed the 2-h infusion [372]. Then, the CEC decreased gradually and returned to the baseline on day 7. MDCO-216 also enhanced SR-BI-mediated CEC in both groups. Like ABCA1-mediated CEC, the maximum CEC was reached at the end of the infusion but dropped to baseline after 24 h. Also, an increase in TG after the infusion in the patients and healthy volunteers was observed. Lastly, the MDCO-216 infusion did not induce any significant safety issues and was well tolerated [372].

Though the infusion of MDCO-216 showed an impact on the TG, CEC, pre-beta 1 HDL, and the total plasma cholesterol levels of both populations remained unchanged after the infusion. Thus, in the same year, the same group conducted a continuous study to investigate the MDCO-216 effect on levels of free cholesterol (FC), esterified cholesterol (CE) in total plasma, and lipoproteins (e.g., HDL, LDL, and VLDL) in healthy volunteers and patients. The subjects were treated with MDCO-216 at the same dose used in the 2016 study. The subjects' blood was collected at 2, 4, and 8 h, as well as 1, 2, 7, and 30 days for analysis. The results showed that the FC peaked at 8-h and reached another peak 48-h after the infusion in patients at all doses. However, a significant increase was observed only in healthy volunteers receiving MDCO-216 at doses above 20 mg/kg. Upon infusion, the FC of HDL and VLDL were found to increase before that of LDL. In addition, CE in the plasma was slightly increased by the low-dose MDCO-216 infusion; decreased CE levels in LDL and HDL were observed right after the infusion, while increased CE levels in LDL and VLDL were seen 24-h after infusion [373]. Between 2 and 8-h after infusion, 10 mg/kg MDCO infusion induced an increase of HDL concentration in both studied groups. Overall, this study indicated that MDCO-216 could induce persistent changes in lipid level and protein composition. Besides LDL, HDL, and VLDL, the same group also reported that the infusion of MDCO-216 induced an increase in apoA-I in α-1 and α-2 HDL by eliminating small HDLs; however, a decrease in α-3 HDL was also observed upon infusion. The effect of the MDCO-216 on CEC may result from the formed α-1 and α-2 HDL, which were found to contain wild apoA-I and AIM. As mentioned earlier, the CER-001 did not affect patients who had ST treatment [374]. Therefore, in 2018, Nissen and coworkers investigated the effect of MDCO-2016 on the regression of atherosclerosis in ST-treated patients. 112

patients were infused with MDCO-2016 at a dose of 20 mg/kg for 6 wk. Similar to CER-001, the MDCO-216 also did not show any therapeutic effect on the improvement of plaque regression in ST-treated patients [382].

3.1.3. NANO—NANOs are silica-gold NPs of a core-shell nanostructure used along with plasmatic photothermal therapy (PPTT) via NIR laser treatment for atherosclerosis therapy. In 2012, NANOs were reported to induce 22.92% of total atheroma volume reduction in Yucatan miniature swine studies when combined with NIR irradiation. This finding was significantly higher than that of swine treated with ferromagnetic NPs delivered either by microbubbles or implanted with sirolimus-releasing stents [393].

Therefore, in 2015, the Ganbinsky group conducted the first-in-man trial (the NANOM-FIM trial: NCT01270139) for assessing the safety and feasibility of using silica-gold NPs for regressing total atheroma volume (TAV) using PPTT. This study is an observational three-arm study that involved 180 patients. Patients were divided into three groups, in which the first group was treated with NANO on artery patches, the second group was treated with stem cells along with silica-gold NPs of irons using microbubbles (Ferro), and the third group was only implanted with XIENCE V stents. After 12 months, the authors found that more than 92% of patients treated with NANO exhibited decreased TAV by 60.3 mm^3 (37.8% of the burden). More importantly, less risk for deaths and complications were observed in the groups treated with NPs compared with other methods [366]. In the same year, by using intravascular ultrasound, the authors also found that there was a Glagov window of enlargement of an external elastic membrane observed in patients ranging from 21% and 44% of percent atheroma volume (PAV), as well as a 30.7% reduction of PAV after the treatment [367].

Later in 2017, a continued study for assessing the safety and efficacy of the NPs long-term (5 years) was conducted by the same group. The patients were also divided equally into three groups and treated with NANO, Ferro, and XIENCE V stents. Similar to the 12-month study, the NANO treated group showed less mortality (6 vs. 9 vs. 10), complications (14.3 vs. 20.9 vs. 22.9%), and late thrombosis (2 vs. 4 vs. 6) when compared with the other two groups [380]. In addition, severe cytotoxicity was observed in the group treated with Ferro. Furthermore, in 2018, the same group reported that the patient-oriented composite endpoint and target vessel failure of the NANO group in the same trial were lower than those of the stenting and Ferro groups. Although promising clinical results regarding the use of NANO for atherosclerosis treatment were demonstrated, the author also found that this approach was associated with cytotoxicity and was not safe enough for real clinical practice, as an increase of defects in erythrocyte membranes was observed after the NANO was applied to patients [381]. Thus, in the future, more biocompatible NPs may be needed to replace the metal NPs.

In 2019, the lesion preparation effect on the 5-year clinical results of NANO combined with PPTT was studied. Three groups of patients participated in this study: 1) patients treated with stent first and then NANO; 2) patients treated with pre-dilution by drug-coated balloon; 3) patients without any lesion preparation. The results demonstrated that MACE-free survival was 65%, 53.3%, and 56.7% for groups 1, 2, and 3, respectively. The POCE of

group 1 (38.5%) is much lower than that of the group treated with conventional stenting (83.3%), pre-dilution (50%), and no preparation groups (77%). This data indicated that lesion preparation helps to achieve the maximal safety level in the long-term treatment of NANO [385].

3.1.4. COBRA PzF NanoCoated Stents—As mentioned earlier, COBRA PzF NanoCoated stents are cobalt-chromium alloy stents coated with PzF (≤ 0.05 μm) for reducing late stent thrombosis. As early as 2016, one successful case of using COBRA PzF NanoCoated stents was reported by Silber and coworkers [371]. Then, in the following year, the first clinical testing of COBRA PzF NanoCoated Stents was initiated conducted by Vochelet and coworkers [375]. In this study, 100 patients were recruited, and all were assigned to receive stent implantation. In total, 151 lesions were treated with 166 stents. In a one-year follow-up, among all the patients, 12% of patients showed targeted lesion failure (TVF), which included a 5%, 2%, and 5% for targeted lesion revascularization (TLR) rate, mortality rate, and elevation of isolated troponin at surgery, this outcome was better than these with BMS. The limitation of this study was that this research was a single-center study without proper control groups and randomization; therefore, the patients selected were suitable for these COBRA PzF NanoCoated stents. In addition, angiography was not used. In the same year, another clinical study associated with the COBRA PzF NanoCoated stents was conducted by Siber and coworkers. Different from the other previous study, angiography was applied in the follow-up in this study. Particularly, 296 patients with coronary artery lesions were enrolled, and the TVF was assessed 9 months after stent implantation. It was found that 11.5% of the patients showed TVF, of which cardiac death, myocardial infarctions (Ml), and TLR were 0.3%, 7%, and 5.9%, respectively. No stent thrombosis was observed. The limitation of this study was that patients with high risk were not recruited in the study. The sample size was limited and lacked randomization [376]. In 2019, the Tavildari group reported another 1-year clinical study regarding exploring the safety and efficacy of COBRA PzF NanoCoated stents in patients with high bleeding risk and the need for mono-anti-platelet therapy. Specifically, 77 patients were recruited, and a total of 120 lesions were treated. Two endpoints were set; the primary one was at one month for thrombosis, and then the second one was MACE at 12 months. The authors found no stent thrombosis occurred at the primary point, while the MACE at 12 months was 3.8%, including 3.8% TLR without cardiac death and MI [386]. Later, in 2020, an e-cobra study reported the evaluation of the COBRA PzF NanoCoated stents in patients in the routine practice who require short DAPT after percutaneous coronary intervention. The primary endpoint was MACE at one year. Particularly, in the study, 940 patients of high risk were enrolled with 1229 lesions treated with 1314 stents. Among those patients, 47% showed acute coronary syndromes, and 62% had a high risk of bleeding. Angiography was applied to all the patients. Promisingly, the MACE rate was 9% with 3.7%, 4.8%, and 4.3% for cardiac death, MI, and TLR, respectively. However, stent thrombosis occurred in 6 patients (0.7%). Though this study was a multi-center study, randomization and no control groups were also the main limitations [389]. Currently, a randomized trial (NCT02594501) of COBRA Pz-F NanoCoated stents is ongoing to study if the use of COBRA PzF NanoCoated stents and 14- day DAPT have higher safety than but similar to Food and Drug

Administration (FDA) approved DES with 3 or 6 DAPT. The study will recruit 996 participants. So far, COBRA PzF NanoCoated stents are the second FDA-approved stents.

3.2. Clinical Studies of Nanomaterials for Atherosclerosis Diagnosis

3.2.1. Ferumoxtran (Sinerem®)—Sinerem® consists of suspended colloids of ultra-small superparamagnetic iron oxide (USPIO) NPs coated with dextran, making it one of the first iron oxide NPs used as an imaging contrast agent in human AS patients. Initially, in 1992, Guerbet, LLC designed and used this agent to detect metastatic disease in lymph nodes, as it is taken up by macrophages present in lymph nodes. Upon MRI scanning, the particles showed increased signals due to their magnetic iron oxide core. Because of their small size and the dextran coating, Sinerem® uptake by macrophages in the liver and spleen were delayed, resulting in a long circulation time. Moreover, this agent was shown to have a blood half-life of around 3.3 h in humans, allowing for prolonged exposure to the vessel wall and increased accumulation in the macrophages of atherosclerotic plaques. In 2001, Hamm and colleagues explored the use of Sinerem® to image human atherosclerotic plaques by intravenously injecting 2.6 mg of Fe/kg of the USPIO NPs in twenty patients and MRI scanning using a T2*-weighted high-resolution gradient-echo sequence before and 24-36 h post-administration. Atherosclerotic vessel wall changes were analyzed by the examination of both common external and internal iliac aorta. The pronounced signal loss was observed in the aortic and pelvic arterial walls, postulating that Sinerem® could be administered via intravenous injection as a contrast agent in human atherosclerotic plaques [356]. The accumulation of this contrast agent in macrophages effectively reduced the signal intensity of normal functioning nodes attributable to the T2* and T2-shortening effects of the contrast agent. In another study in 2003, Engelshoven and colleagues reported Sinerem® to be present in 75% of the ruptured and rupture-prone lesions, but in only 7% of the stable lesions of eleven patients. These eleven patients showed symptoms of recurrent transient ischemic attacks (TIAs) and ultrasound-proven carotid stenosis. A 24% signal decrease in regions with changes in the T2*-weighted MR post-contrast images after 24 h indicated a concentrated, albeit in a lower-than-injected concentration, accumulation of Sinerem® in macrophages in predominantly ruptured and rupture-prone human atherosclerotic lesions [358].

In one study in 2008, Gillard and coworkers investigated the effect of Sinerem® administration using a cohort of 10 asymptomatic patients with carotid atheroma and 10 asymptomatic patients with carotid stenosis. The contrast agent caused a signal loss of 94% in the carotid stenosis group, compared with the 24% in carotid atheroma patients ($p < 0.001$). Carotid plaques from the carotid stenosis patients exhibited a mean signal intensity decrease of 16.4% after infusion, while otherwise undetected plaques showed a mean signal intensity increase of 8.4% after infusion. This finding indicated that USPIO uptake in the carotid artery is more likely to occur if another vascular territory is symptomatic [359]. In a different study in the same year, the same group found that the Spearman's rank correlation coefficient for USPIO-enhanced signal change and maximal biomechanical stress was −0.60 ($p=0.009$), indicating an association between USPIO enhanced signal change and maximal biomechanical stress [360]. By using ultrasmall superparamagnetic iron oxides (USPIOs), a better understanding of the complex interaction between the physiological processes and the

biomechanical mechanisms in carotid atheroma development can be achieved. In 2009, Gillard and colleagues evaluated the effects of low-dose (10 mg) and high-dose (80 mg) AT on carotid plaque inflammation as determined by USPIO-enhanced carotid MR imaging in forty patients with carotid stenosis. They observed a significant reduction from baseline in USPIO-defined inflammation in the high-dose group at both 6 and 12 weeks. The 80- mg statin dose was also found to significantly lower total cholesterol by 15% ($p = 0.0003$) and LDL cholesterol by 29% ($p = 0.0001$) at 12 weeks, demonstrating the usefulness of USPIO-enhanced MRI as an effective imaging contrast agent for atherosclerotic lesion detection [361]. In the same year, a follow-up study by the same group assessed the effectiveness of USPIO-enhanced MR imaging in both symptomatic and asymptomatic individuals. The authors wanted to explore the difference of USPIO utility with twenty non-consecutive patients with carotid stenosis (10 symptomatic and 10 asymptomatic). They discovered that symptomatic patients displayed more drastic signal decreases than asymptomatic patients (75% vs. 32%, $p < 0.01$), suggesting the presence of larger inflammatory infiltrates [362]. These results show that Sinerem® may enhance risk assessment of patients with carotid stenosis and improved MR contrast imaging to improve diagnostics and treatment to better assist in establishing the appropriate method of intervention. Despite the initial clinical successes of Sinerem®, the contrast agent faced various shortcomings and limitations. One limitation of Sinerem® was its inability to enhance MR images of various forms of cancer. In one study, Sinerem® displayed no statistically significant sensitivity in MR imaging of pelvic cancer compared with normal MRI. Another limitation was that Sinerem® displayed adverse reactions in patients administered Sinerem®, which led to its temporary discontinuation. Eventually, due to the lack of statistically strong data, Guerbet, LLC took Sinerem® off the market.

3.2.2. Ferumoxytol (Feraheme®)—Ferumoxytol, is a second generation USPIO similar to the discontinued Sinerem, which consists of an iron oxide core coated with carboxymethyl-dextran. It has been primarily used as an iron injection for anemia. It provides an alternative approach for MRI of atherosclerotic plaques. Ferumoxytol can be taken up by macrophages in the atherosclerosis plaque and provide localized signal and imaging. For instance, In 2016, Semple and colleagues applied Ferumoxytol for MR T2-weighted imaging with the potential application towards atherosclerosis [369]. Using Ferumoxytol, they conducted a multicenter cohort study on patients with cardiac inflammation and tested and reported normal MRI T2-weighted values for healthy human hearts and myocardium. This observation established ferumoxytol to be used for potential imaging of atherosclerosis [369].

Expanding upon that, in January 2017, Coolen and colleagues ALSO used Ferumoxytol in a study to determine its ability to image atherosclerosis based on comparisons with ^{18}F-FDG PET/CT imaging. Nine male patients and four controls participated in the study. In this patient group, 15 atherosclerotic plaques were imaged using conventional MRI, USPIO-MRI, and FDG-PET/CT. Changes in signal intensity were measured against baseline values (R2). After the administration of USPIO-MRI, the R2 signal remained increased at 72 h compared with healthy control vessels, which returned to baseline values. USPIO uptake was also higher in the atherosclerotic plaques 72 h post-injection compared with the healthy

vessel wall and the non-plaque vessel wall. These results established the range of normal values in a range of tissues and the feasibility of Ferumoxytol as a contrast agent [292]. In another study in 2019, the same group investigated if the accumulation of the Ferumoxytol in the plaque was associated with the plaque permeability. In particular, 18 patients who previously had claudication and atherosclerotic plaque in their femoral arteries were recruited in the study. In addition, 8 healthy volunteers were also included as controls. The patients were imaged via DCE-MRI before infusion with Ferumoxytol as a baseline and second imaging was applied to the patients 72 h after the infusion. It was found that the change in R2 in plaques in the patients was significantly increased in the plaque compared with the non-plaque vessel wall. Moreover, the accumulation of the Ferumoxytol is strongly correlated with the plaque permeability [387].

Similarly, one recent study conducted by Sadat and coworkers also demonstrated the utility of ferumoxytol to image carotid atheroma using MRI in 20 patients with carotid artery disease. Among the 20 patients, half of them showed symptoms, while the other half were asymptomatic. The MRI was applied to these patients before (baseline) and 24, 48, 72 h after the ferumoxytol administration. The authors found that the optimal imaging time for assessing carotid atheroma is 48 hours post ferumoxytol infusion [390].

4. Summary and Perspective

Atherosclerosis is a chronic inflammatory disease that causes mortality worldwide. This review provides a comprehensive overview of the recent progress in the development of nanomaterials for improving atherosclerosis diagnosis and therapy, particularly in preclinical and clinical phases ranging from 2017 to 2020. Some important studies before 2017 are also included here. Hopefully, this review is an excellent resource for scientific researchers who work in designing nanomaterials for atherosclerosis therapy and diagnosis.

For treating atherosclerosis, nanomaterials play a crucial role in improving the efficacy of therapeutics. According to the review, so far, a wide variety of therapeutics have been loaded in the delivery systems to achieve effective anti-atherosclerotic efficacy. These therapeutics can be from clinically used drugs, anti-atherosclerotic peptides, anti-inflammatory cytokines, growth factors, and nucleic acids. Moreover, the therapeutic mechanism of these agents for treating atherosclerosis include lowering cholesterol amount, enhancing cholesterol efflux, repolarizing macrophage phenotype, enhancing Treg cell differentiation, activating pro-efferocytic effect, inducing autophagy of SMCs, switching SMC phenotype, suppressing attachment, proliferation, and migration of certain types of cells, resolving local inflammation, and reducing MMPs production. Despite all the promising outcomes, future studies might focus on exploring the potential of combining nanomaterials with naturally occurring components possessing anti-inflammatory or antioxidant properties.

Among the nanomaterials discussed as delivery systems, HDL NPs were the most studied for treating atherosclerosis, possibly due to the synergistic effect between HDL NPs and the encapsulated therapeutic molecules. Besides HDL NPs, traditionally studied nanomaterials such as polymeric NPs, dendrimers, micelles, and liposomes were also investigated for improving the efficacy of therapeutics carried by them. However, as demonstrated in the

review, polymer NPs were mainly limited to HA and PLGA NPs, while the mostly studied dendrimers were PMMA dendrimers; thus, future efforts may focus on exploring polymeric NPs and dendrimers of new compositions as effective delivery systems. In addition, new findings suggested that modified carbon nanotubes were able to deliver drugs to enhance atherosclerosis treatment. This finding was interesting, as previous studies showed that the unmodified carbon nanotubes caused an elevation in atherosclerosis; therefore, further research with this particular nanomaterial is needed. In addition to carbon nanotubes, several other new types of nanomaterials such as cyclodextrin NPs, extracellular vesicles, and biomimetic NPs were also presented as feasible candidates for delivering therapeutics to atherosclerotic plaques. Moreover, these NPs demonstrated exceptional ability to suppress atherosclerotic plaque formation *in vivo*. Although some studies discussed the development of inorganic NPs for treating atherosclerosis, this area has not yet to be widely explored. Thus, consistent efforts can be devoted to CD NPs, extracellular vesicles, biomimetic NPs, and inorganic NPs, including how to improve the drug loading process in extracellular vesicles and exploration of new types of extracellular vesicles and biomimetic NPs derived from stem cells for treating atherosclerosis. In addition, the combination of CD NPs with cell membrane coating might also be interesting to investigate in the future. Furthermore, as demonstrated, most of the studies mentioned here were centered on the development of nanomaterials to deliver therapeutics for preventing atherosclerosis progression; only very few studies emphasized the treatment of pre-existing atherosclerosis plaque. Therefore, it is important to make efforts to design novel nanomaterials for developing nanomedicines to treat pre-existing atherosclerotic plaques. Moreover, it would be interesting to compare the therapeutic efficacy of therapeutics delivered by polymeric NPs, liposomes, micelles, and other new types of nanomaterials. As demonstrated in the review, studies have emerged for the development of liposomes and micelles for generating atherosclerosis vaccines. Though this area is new, it is worth making continuous efforts to this area as atherosclerosis prevention is as important as atherosclerosis therapy.

Moreover, in addition to drug delivery systems, nanotechnology recently led to the creation of novel nanomaterials for coating stents, thus improving stent safety and efficacy for treating atherosclerosis. The nanomaterials, such as inorganic nanomaterials, polymeric nanomaterials, carbon-based nanomaterials, biomimetic nanomaterials, and hybrid materials, have been used to design nanofilms, nanotubes, NPs, or nanofibers for stent surface coating. In contrast to early studies that emphasized single drug-eluting, recently, some studies showed an increasing interest in designing nanocoating comprising various types of materials or therapeutics that could show synergistic effects to enhance stent efficacy. Moreover, the development of multifunctional nanocoating, which can promote reendothelization, whereas suppressing SMC proliferation and migration, and reducing platelet adhesion and activation, was the aim of other studies. Despite outcomes of these studies showing improved stent performance by nanocoating, it is worth noting that such promising results were mainly obtained using simple *in vitro* or healthy animal models were commonly used. However, these models have their limitations and cannot provide atherosclerosis environments similar to that in patients. Thus, in future studies, more attention may be devoted to evaluating the efficacy and safety of these stent nanocoating in atherosclerosis models mimicking human patients, thereby moving forward to future clinical

translation. In addition, as recent studies mostly concentrated on improving stent efficacy, the design of nanocoating for minimizing cytotoxicity while improving therapeutic efficacy should bring into focus. Aside from stent modification, nanomaterials—particularly nanofibers—have been widely investigated for improving the properties of vascular grafts. As shown in the review, nanofibers for vascular graft fabrication were primarily composed of PCL and gelatin. The PCL/gelatin nanofibers discussed were mainly used for enhancing mechanical properties, loading therapeutics, and controlled release kinetics of therapeutics to improve the performance of vascular grafts.

The use of nanomaterials was not limited to atherosclerosis therapy. In fact, nanomaterials have been designed and utilized for improving atherosclerosis imaging and diagnosis. Among the inorganic nanomaterials, iron oxide NPs were extensively developed as MRI contrast agents. Iron oxide NPs primarily functioned as T2 MRI contrast agents due to their magnetic properties; however, dual T1/T2 MRI contrast agents were developed by modifying iron oxide NPs with gadolinium, the clinically available T1 MRI contrast agent. Additionally, the use of iron oxide NPs modified with probes for imaging atherosclerosis under dual-imaging modalities (MRI/PET or MRI/CT) were also shown. The surfaces of the NPs were also conjugated with targeting molecules to increase the specificity and localization of the NPs in plaque. This was achieved by modifying the surfaces with targeting ligands, such as antibodies or peptides. In fact, the unique magnetic properties of iron oxide NPs, as well as the ability to specifically modify the surfaces for both dual imaging and targeting, have resulted in iron oxide NPs functioning as a contrast agent for diagnosing atherosclerosis. Additionally, several studies have shown the ability of iron oxide NPs to target early stable lesions, plaque progression, and vulnerable plaques, providing clinicians with improved data for diagnosis and treatment. Similar to iron oxide NPs, Au NPs have also been studied for detecting atherosclerosis. However, unlike iron oxide NPs, Au NPs functioned as optical imaging probes that can be used to image atherosclerosis plaque using CT and NIRF imaging. Gold NPs also functioned as a dual-modality imaging agent by forming gold-gadolinium hybrid NPs for imaging atherosclerosis plaque under MRI. Moreover, organic nanomaterials such as polymeric NPs, liposomes, and micelles were combined with inorganic nanomaterials to function as contrast agents and were also investigated. Particularly, in contrast to inorganic nanomaterials that show specific imaging signals without modification, the signals of organic nanomaterials were obtained by modifying them with iron oxide NPs, Gd, or fluorescent tags. As demonstrated, many recent studies discussed above mainly focused on MRI, fluorescent, and PET imaging; thus, the development of nanomaterials for imaging atherosclerosis using ultrasound would be a fascinating area of research. In addition, recent studies have reported promising results about the development of iron oxide NPs as T1 contrast agents for imaging tumors. Therefore, the design of iron oxide NPs showing T1 contrast can be an alternative strategy that should be explored to improve atherosclerosis imaging while overcoming the cytotoxicity issue of Gd in future studies.

In addition, considerable efforts have been made to a rising field of atherosclerosis diagnosis and therapy, focusing on the design of theranostic agents possessing imaging and therapeutic functions to improve both processes simultaneously. Nanomaterials involved in the development of effective theranostic agents for atherosclerosis were polymeric NPs,

micelles, lipid-based NPs, inorganic NPs, and biomimetic NPs. For achieving therapeutic function, these nanomaterials were loaded with therapeutics such as chemotherapeutics, photothermal agents, photosensitizers, or sonosensitizers; for obtaining diagnostic function, imaging probes were commonly introduced to the nanomaterials. Although appealing outcomes have been achieved *in vitro and in vivo*, the development of theranostic agents for chemo-, photothermal, photodynamic, and sonodynamic therapies for atherosclerosis are still at their incipient preclinical stages and have not been widely researched. Thus, future studies can focus more on these perspectives and emphasize the effective translation of these agents into clinical practice. In addition, designing theranostic agents to improve the atherosclerosis diagnosis and treatment under different therapeutic mechanisms is also a fascinating field of research. Beyond that, another future direction may concentrate on developing theranostic agents by taking advantage of the therapeutic effects of natural products or biotherapeutics. It would also be interesting to design nanomaterials to co-delivery dual therapeutics to the plaque and study the synergistic therapeutic effect of dual therapeutics. Furthermore, as discussed earlier in the review, most reported nanomaterials as theranostic agents were designed to target macrophages or ECs. However, considerable amounts of T cells and B cells and calcification exist in plaque. Therefore, in future studies, the potential of nanomaterials modified with ligands targeting these components should be explored to improve the efficacy of imaging and therapy for atherosclerosis.

Also, it is known that ApoE$^{-/-}$ or Ldlr$^{-/-}$mouse models fed with an HFD were commonly used to evaluate the ability of nanomaterials for atherosclerosis diagnosis, treatment, or both. However, these mouse models do not fully mimic human physiology and atherosclerosis. For instance, the immune systems between humans and mice are largely different, and mouse models do not manifest significant coronary artery lesions. In addition, ApoE deficiency in humans is rare, as ApoE affects inflammation and oxidation processes, as well as plaque development. Furthermore, lipoprotein remnants and VLDL rather than LDL are predominate in the plasma cholesterol of ApoE$^{-/-}$ mouse models. Consequently, it is essential to develop new preclinical atherosclerosis models that better mimic human atherosclerosis for reliable prediction of nanomaterial-based agents' performance in humans to facilitate clinical translation in the future.

Extrapolating the successes in preclinical studies, only some nanomaterials, albeit slowly, have also been applied in clinical therapies and diagnostics for atherosclerosis. The nanomaterials that have been investigated in clinical trials for atherosclerosis treatment and diagnosis are primarily lipid-based and inorganic NPs. For instance, lipid NPs, such as LN-PLPs and PTX-LDEs, acted as drug delivery carriers to treat atherosclerosis by targeting atherosclerotic plaque macrophages in patients. Unfortunately, LN-PLP did not show satisfactory anti-atherosclerotic effects in patients as they did *in vitro* and *in vivo* studies. PTX-LDE demonstrated inconclusive results regarding its efficacy, likely due to the small size study group. Another therapeutic lipid NP is HDL mimetic NP, which mimicked natural pre-beta HDLs that perform reverse cholesterol transport. Among the HDL mimetic NPs, CER-001 at a specific dosage demonstrated the ability to regress atheroma in patients. Above that dosage, the therapeutic effect of CER-001 was reduced. It was also found that patients who were on statins or with low HDL did not receive any therapeutic benefits from CER-001. Other studied HDL mimetic NPs included CSL112, MDCO-216. In addition to

lipid NPs, NANOs were silica-gold NPs used along with plasmonic PTT to reduce total atheroma volume. However, the major concern of using NANOs for large clinical trials is the potential cytotoxicity from the metal NPs. In clinical diagnostics, USPIOs were shown to serve as useful indicators of atherosclerotic plaque in MRI and PET/CT, respectively. Despite the success of some NPs in clinical trials, only a small percentage of experimental NPs ever progress from animal trials to clinical use. One of the largest obstacles from laboratory results to clinical translation is the adherence of NPs to FDA standards. The complexity of nanomaterials can present a challenge in complying with FDA standards due to the conspicuous need for intensive characterization and pharmacological parameterization. In addition, the safety and efficacy of nanomaterials used in human patients need to be carefully assessed before achieving clinical translation, as efficacy needs to be reproduced while also taking patient safety into account. In addition, it is vital to establish good manufacturing practices (GMP) for the fabrication of nanomaterials, as well as to increase the interactions between small laboratories and the pharmaceutical industry. Besides, future studies may also emphasize large-scale manufacture, improvement of stability, and long-term storage of nanomaterial-based therapeutics, contrast agents, and theranostic agents to decrease the risk of future clinical translation failure.

Acknowledgment

This work was supported by the National Institutes of Health (1R01HL125391 to H-W. J.), American Heart Association (18POST34080260 to J. C.; 20PRE35210599 to X. Z.), National Institutes of Health (1R01HL150887 to Y.Y.), and National Research Foundation of Korea (NRF) funded by the Korea government (MSIT) (No. 2020R1A2C3003784; No.2020M3A9I4038454 to Y.Y.)

Abbreviations

ACS	acute coronary syndrome
Ac-β-CD	acetalated β-cyclodextrin
AIM	apoA-I Milano
anti-miR-155	against microRNA-155
anti-miR-712	against microRNA-712
apoA-1	apolipoprotein A1
ApoE$^{-/-}$	apolipoprotein E deficient
AT	atorvastatin
Au	gold
aVD	1,25-dihydroxyvitamin D3
β-CD	β-cyclodextrin
BMS	bare metal stent
B-PAV	baseline percent atheroma volume

CAR	carmustine
CCR2	chemokine receptor type 2
CD44	cluster of differentiation 44
CD36	cluster of differentiation 36
CD68	cluster of differentiation 68
CD	cyclodextrin
CE	esterified cholesterol
CEC	cholesterol efflux capacity
CETP	cholesterol ester transfer protein
CNTs	carbon nanotubes
CT	computed tomography
CS	chitosan
Cur	curcumin
CVDs	cardiovascular diseases
Cy	cyanine
DA	dopamine
DES	drug-eluting stents
Dex	dexamethasone
DTX	docetaxel
DXS	dextran sulfate
ECs	endothelial cells
ECM	extracellular matrix
EGFP	enhanced green fluorescent protein
EGF-1	epdiemral growth factor 1
FC	free cholesterol
Gd	gadolinium
GO	graphene oxide
GP IIb/IIIa	glycoprotein IIb/IIIa
HA	hyaluronic acid

HDL	high density lipoprotein
HFD	high fat diet
HUVECs	human umbilical vein endothelial cells
ICAM-1	intercellular adhesion molecule 1
ICG	indocyanine green
IL-1β	interleukin 1 beta
IL-4	interleukin 4
IL-6	interleukin 6
IL-10	interleukin 10
IVUS	intravascular ultrasound
LDE	lipidic emulsion
LDL	low-density lipoprotein receptor deficient
Ldlr$^{-/-}$	low-density lipoprotein receptor deficient
LOX-1	lectin-like ox-LDL receptor-1
LPS	lipopolysaccharide
LT	lovastatin
LXR	liver X receptor
MACE	major adverse cardiovascular events
MCP-1	monocyte chemoattractant protein-1
miR	microRNA
MMP	matrix metalloproteinase
MRI	magnetic resonance imaging
mRNA	messenger RNA
mTORC	mammalian target of rapamycin complex
MTX	methotrexate
ND	normal diet
NF-κB	nuclear factor kappa-light-chain-enhancer of activated B cell
NIRF	near infrared fluorescence

NO	nitric oxide
NPs	nanoparticles
QD	quantum dots
OPN	osteopontin
ox-LDL	oxidized low-density lipoprotein
Ox-β-CD	oxidative β-cyclodextrin
PA	peptide amphiphile
PAM	peptide amphiphile micelle
PAMAM	polyamidoamine
PAV	percent atheroma volume
PBS	phosphate buffered saline
PCL	polycaprolactone
PDA	polydopamine
PDT	photodynamic therapy
PEI	polyethylenimine
PEG	polyethylene glycol
PET	positron emission tomography
PIO	pioglitazone
PLA	polylactic acid
PLGA	poly (lactic-co-glycolic acid)
PLP	prednisolone phosphate
PPAR	peroxisome proliferator-activated receptor
PT	pitavastatin
PTT	photothermal therapy
PtdSer	phosphatidylserine
PTX	paclitaxel
PzF	Polyzene-F
RAP	rapamycin
rHDL	reconstituted high-density lipoprotein

ROS	reactive oxidative species
scFv	single-chain variable fragment
sHDL	synthetic high-density lipoprotein
siRNA	small interfering ribonucleic acid
SMCs	smooth muscle cells
SPIONs	superparamagnetic iron oxide nanoparticles
SR	scavenger receptor
SR-A	scavenger receptor class A
SR-AI	scavenger receptor type I
SR-BI	scavenger receptor class B type 1
ST	statin
S2P	stabilin-2
SWNTs	single wall carbon nanotubes
TAV	total atheroma volume
TF	tissue factors
TG	triglycerides
Ti	titanium
Ti-O	titanium oxide
TLR	targeted lesion revascularization
TNF-α	tumor necrosis factor alpha
TVF	targeted lesion failure
VCAM-1	vascular cell adhesion protein 1
VEC	vascular endothelial cell
VEGF	vascular endothelial growth factor
VLDL	very low-density lipoprotein
VSMCs	vascular smooth muscle cells

References

[1]. W.H. Organization, Cardiovascular diseases (CVDs) fact sheet, World Health Organization, (2017).

[2]. Frostegård J, Immunity, Atherosclerosis and cardiovascular disease, BMC Med, 11 (2013) 117–117. [PubMed: 23635324]

[3]. Lusis AJ, Atherosclerosis, Nature, 407 (2000) 233–241. [PubMed: 11001066]

[4]. Davies JT, Delfino SF, Feinberg CE, Johnson MF, Nappi VL, Olinger JT, Schwab AP, Swanson HI, Current and emerging uses of statins in clinical therapeutics: a review, Lipid Insights, 9 (2016) 13–29. [PubMed: 27867302]

[5]. d SJ, Giri J, Kobayashi T, Stent-based revascularization for complex lesions in PAD, J Cardiovasc Surg, 58 (2017) 715–721.

[6]. Bentzon Jacob F, Otsuka F, Virmani R, Falk E, Mechanisms of plaque formation and rupture, Circ. Res, 114 (2014) 1852–1866. [PubMed: 24902970]

[7]. Jain RK, Stylianopoulos T, Delivering nanomedicine to solid tumors, Nat Rev Clin Oncol., 7 (2010) 653. [PubMed: 20838415]

[8]. Tiwari JN, Tiwari RN, Kim KS, Zero-dimensional, one-dimensional, two-dimensional and three-dimensional nanostructured materials for advanced electrochemical energy devices, Prog. Mater. Sci, 57 (2012) 724–803.

[9]. Wang X, Li Z, Shi J, Yu Y, One-dimensional titanium dioxide nanomaterials: nanowires, nanorods, and nanobelts, Chem. Rev, 114 (2014) 9346–9384. [PubMed: 24725155]

[10]. Zhang H, Ultrathin two-dimensional nanomaterials, ACS Nano, 9 (2015) 9451–9469. [PubMed: 26407037]

[11]. Wu Z-Y, Liang H-W, Chen L-F, Hu B-C, Yu S-H, Bacterial cellulose: a robust platform for design of three dimensional carbon-based functional nanomaterials, Acc. Chem. Res, 49 (2016) 96–105. [PubMed: 26642085]

[12]. Baimova YA, Murzaev R, Dmitriev S, Mechanical properties of bulk carbon nanomaterials, Phys. Solid State, 56 (2014) 2010–2016.

[13]. Shi J, Kantoff PW, Wooster R, Farokhzad OC, Cancer nanomedicine: progress, challenges and opportunities, Nat. Rev. Cancer, 17 (2017) 20–37. [PubMed: 27834398]

[14]. Brigger I, Dubernet C, Couvreur P, Nanoparticles in cancer therapy and diagnosis, Adv. Drug Deliv. Rev, 64 (2012) 24–36.

[15]. Du B, Yu M, Zheng J, Transport and interactions of nanoparticles in the kidneys, Nat. Rev. Mater, 3 (2018) 358–374.

[16]. Matoba T, Koga J.-i., Nakano K, Egashira K, Tsutsui H, Nanoparticle-mediated drug delivery system for atherosclerotic cardiovascular disease, J. Cardiol, 70 (2017) 206–211. [PubMed: 28416142]

[17]. Ou LC, Zhong S, Ou JS, Tian JW, Application of targeted therapy strategies with nanomedicine delivery for atherosclerosis, Acta Pharmacol. Sin, 0 (2020) 1–8.

[18]. Dai T, He W, Yao C, Ma X, Ren W, Mai Y, Wu A, Applications of inorganic nanoparticles in the diagnosis and therapy of atherosclerosis, Biomater. Sci, 8 (2020) 3784–3799. [PubMed: 32469010]

[19]. DiStasio N, Lehoux S, Khademhosseini A, Tabrizian M, The multifaceted uses and therapeutic advantages of nanoparticles for atherosclerosis research, Materials, 11 (2018) 754.

[20]. Talev J, Kanwar JR, Iron oxide nanoparticles as imaging and therapeutic agents for atherosclerosis, Semin Thromb Hemost, Thieme Medical Publishers, 2020, pp. 553–562.

[21]. Peters EB, Kibbe MR, Nanomaterials to resolve atherosclerosis, ACS Biomater. Sci. Eng, 6 (2020) 3693–3712. [PubMed: 33463318]

[22]. Kiaie N, Gorabi AM, Penson PE, Watts G, Johnston TP, Banach M, Sahebkar A, A new approach to the diagnosis and treatment of atherosclerosis: the era of the liposome, Drug Discov. Today, 25 (2020) 58–72. [PubMed: 31525463]

[23]. Burdick JA, Prestwich GD, Hyaluronic acid hydrogels for biomedical applications, Adv. Mater, 23 (2011) H41–H56. [PubMed: 21394792]

[24]. Necas J, Bartosikova L, Brauner P, Kolar J, Hyaluronic acid (hyaluronan): a review, Vet.Med (Praha), 53 (2008) 397–411.

[25]. Kim JH, Moon MJ, Kim DY, Heo SH, Jeong YY, Hyaluronic acid-based nanomaterials for cancer therapy, Polymers (Basel), 10 (2018) 1133.

[26]. Lin T, Yuan A, Zhao X, Lian H, Zhuang J, Chen W, Zhang Q, Liu G, Zhang S, Cao W, Self-assembled tumor-targeting hyaluronic acid nanoparticles for photothermal ablation in orthotopic bladder cancer, Acta Biomater, 53 (2017) 427–438. [PubMed: 28213097]

[27]. Liu R, Xiao W, Hu C, Xie R, Gao H, Theranostic size-reducible and no donor conjugated gold nanocluster fabricated hyaluronic acid nanoparticle with optimal size for combinational treatment of breast cancer and lung metastasis, J. Control. Release, 278 (2018) 127–139. [PubMed: 29630985]

[28]. Lee GY, Kim JH, Choi KY, Yoon HY, Kim K, Kwon IC, Choi K, Lee BH, Park JH, Kim IS, Hyaluronic acid nanoparticles for active targeting atherosclerosis, Biomaterials, 53 (2015) 341–348. [PubMed: 25890732]

[29]. Beldman TJ, Senders ML, Alaarg A, Pérez-Medina C, Tang J, Zhao Y, Fay F, Deichmöller J, Born B, Desclos E, Hyaluronan nanoparticles selectively target plaque-associated macrophages and improve plaque stability in atherosclerosis, ACS Nano, 11 (2017) 5785–5799. [PubMed: 28463501]

[30]. Beldman TJ, Malinova TS, Desclos E, Grootemaat AE, Misiak ALS, van der Velden S, van Roomen CPAA, Beckers L, van Veen HA, Krawczyk PM, Hoebe RA, Sluimer JC, Neele AE, de Winther MPJ, van der Wei NN, Lutgens E, Mulder WJM, Huveneers S, Kluza E, Nanoparticle-aided characterization of arterial endothelial architecture during atherosclerosis progression and metabolic therapy, ACS Nano, 13 (2019) 13759–13774. [PubMed: 31268670]

[31]. Nasr SH, Rashidijahanabad Z, Ramadan S, Kauffman N, Parameswaran N, Zinn KR, Qian C, Arora R, Agnew D, Huang X, Effective atherosclerotic plaque inflammation inhibition with targeted drug delivery by hyaluronan conjugated atorvastatin nanoparticles, Nanoscale, 12 (2020) 9541–9556. [PubMed: 32314997]

[32]. Shahbazi MA, Sedighi M, Bauleth-Ramos TS, Kant K, Correia A, Poursina N, Sarmento B, Hirvonen J, Santos HIA, Targeted reinforcement of macrophage reprogramming toward M2 polarization by IL-4-loaded hyaluronic acid particles, ACS Omega, 3 (2018) 18444–18455. [PubMed: 31458417]

[33]. Farajzadeh R, Zarghami N, Serati-Nouri H, Momeni-Javid Z, Farajzadeh T, Jalilzadeh-Tabrizi S, Sadeghi-Soureh S, Naseri N, Pilehvar-Soltanahmadi Y, Macrophage repolarization using CD44-targeting hyaluronic acid–polylactide nanoparticles containing curcumin, Artif. Cells Nanomed. Biotechnol, 46 (2018) 2013–2021. [PubMed: 29183161]

[34]. Tran TH, Krishnan S, Amiji MM, MicroRNA-223 induced repolarization of peritoneal macrophages using CD44 targeting hyaluronic acid nanoparticles for anti-inflammatory effects, PLoS One, 11 (2016) e0152024–e0152024. [PubMed: 27148749]

[35]. Tran TH, Rastogi R, Shelke J, Amiji MM, Modulation of macrophage functional polarity towards anti-inflammatory phenotype with plasmid DNA delivery in CD44 targeting hyaluronic acid nanoparticles, Sci. Rep, 5 (2015) 1–15.

[36]. Sadat Tabatabaei Mirakabad F, Nejati-Koshki K, Akbarzadeh A, Yamchi MR, Milani M, Zarghami N, Zeighamian V, Rahimzadeh A, Alimohammadi S, Hanifehpour Y, Joo SW, PLGA-based nanoparticles as cancer drug delivery systems, Asian Pac. J. Cancer Prev, 15 (2014) 517–535. [PubMed: 24568455]

[37]. Rezvantalab S, Drude NI, Moraveji MK, Guvener N, Koons EK, Shi Y, Lammers T, Kiessling F, PLGA-based nanoparticles in cancer treatment, Front. Pharmacol, 9 (2018) 1260. [PubMed: 30450050]

[38]. Upadhyay P, Sarker S, Ghosh A, Gupta P, Das S, Ahir M, Bhattacharya S, Chattopadhyay S, Ghosh S, Adhikary A, Transferrin-decorated thymoquinone-loaded PEG-PLGA nanoparticles exhibit anticarcinogenic effect in non-small cell lung carcinoma via the modulation of miR-34a and miR-16, Biomater. Sci, 7 (2019) 4325–4344. [PubMed: 31411213]

[39]. Arora A, Bhandari RK, Pandey AK, Rather IIG, Malhotra S, Bhatia A, Shafiq N, Effect of atorvastatin nanoparticles compared to free atrovastatin on plaque properties in rabbit model of atherosclerosis, Int. J. Noncommun. Diseases, 4 (2019) 127–131.

[40]. Sun Y, Chen L, Zhao S, Shi L, Li H, Tian W, Qi G, Effects of nanoparticle-mediated delivery of pitavastatin on atherosclerotic plaques in ApoE-knockout mice and THP-1-derived macrophages, Exp. Ther. Med, 19 (2020) 3787–3797. [PubMed: 32346443]

[41]. Zhang XQ, Even-Or O, Xu X, van Rosmalen M, Lim L, Gadde S, Farokhzad OC, Fisher EA, Nanoparticles containing a liver X receptor agonist inhibit inflammation and atherosclerosis, Adv. Healthcare Mater, 4 (2015) 228–236.

[42]. Nakashiro S, Matoba T, Umezu R, Koga JI, Tokutome M, Katsuki S, Nakano K, Sunagawa K, Egashira K, Pioglitazone-incorporated nanoparticles prevent plaque destabilization and rupture by regulating monocyte/macrophage differentiation in ApoE−/− mice, Arterioscler. Thromb. Vase. Biol, 36 (2016) 491–500.

[43]. Esfandyari-Manesh M, Abdi M, Talasaz AH, Ebrahimi SM, Atyabi F, Dinarvand R, S2P peptide-conjugated PLGA-Maleimide-PEG nanoparticles containing Imatinib for targeting drug delivery to atherosclerotic plaques, Daru, 28 (2020) 131–138. [PubMed: 31919789]

[44]. Fredman G, Kamaly N, Spolitu S, Milton J, Ghorpade D, Chiasson R, Kuriakose G, Perretti M, Farokhzad O, Tabas I, Targeted nanoparticles containing the proresolving peptide Ac2-26 protect against advanced atherosclerosis in hypercholesterolemic mice, Sci. Transl. Med, 7 (2015) 275ra220–275ra220.

[45]. Kamaly N, Fredman G, Fojas JJR, Subramanian M, Choi WI, Zepeda K, Vilos C, Yu M, Gadde S, Wu J, Targeted interleukin-10 nanotherapeutics developed with a microfluidic chip enhance resolution of inflammation in advanced atherosclerosis, ACS Nano, 10 (2016) 5280–5292. [PubMed: 27100066]

[46]. Weng Y, Huang Q, Li C, Yang Y, Wang X, Yu J, Huang Y, Liang X-J, Improved Nucleic Acid Therapy with Advanced Nanoscale Biotechnology, Mol. Ther. Nucleic. Acids, 19 (2020) 581–601. [PubMed: 31927331]

[47]. Shen T, Zhang Y, Zhou S, Lin S, Zhang X-B, Zhu G, Nucleic Acid Immunotherapeutics for Cancer, ACS Appl. Bio Mater, 3 (2020) 2838–2849.

[48]. Landmesser U, Poller W, Tsimikas S, Most P, Paneni F, Luscher TF, From traditional pharmacological towards nucleic acid-based therapies for cardiovascular diseases, Eur. Heart J, 41 (2020) 3884–3899. [PubMed: 32350510]

[49]. Xiao Y, Shi K, Qu Y, Chu B, Qian Z, Engineering nanoparticles for targeted delivery of nucleic acid therapeutics in tumor, Mol. Ther. Methods. Clin. Dev, 12 (2019) 1–18. [PubMed: 30364598]

[50]. Zhao Y, He Z, Gao H, Tang H, He J, Guo Q, Zhang W, Liu J, Fine tuning of core–shell structure of hyaluronic acid/cell-penetrating peptides/siRNA nanoparticles for enhanced gene delivery to macrophages in antiatherosclerotic therapy, Biomacromolecules, 19 (2018) 2944–2956. [PubMed: 29641895]

[51]. Tao W, Yurdagul A, Kong N, Li W, Wang X, Doran AC, Feng C, Wang J, Islam MA, Farokhzad OC, SiRNA nanoparticles targeting CaMKIIγ in lesional macrophages improve atherosclerotic plaque stability in mice, Sci. Transl. Med, 12 (2020) eaay1063. [PubMed: 32718990]

[52]. Zhu X, Xie H, Liang X, Li X, Duan J, Chen Y, Yang Z, Liu C, Wang C, Zhang H, Bilayered nanoparticles with sequential release of VEGF gene and paclitaxel for restenosis inhibition in atherosclerosis, ACS Appl. Mater, 9 (2017) 27522–27532.

[53]. Hong Z, Xu Y, Yin JF, Jin J, Jiang Y, Du Q, Improving the effectiveness of (−)-epigallocatechin gallate (EGCG) against rabbit atherosclerosis by EGCG-loaded nanoparticles prepared from chitosan and polyaspartic acid, J. Agric. Food Chem, 62 (2014) 12603–12609. [PubMed: 25483592]

[54]. Mishra S, Bedja D, Amuzie C, Foss C, Pomper MG, Bhattacharya R, Yarema KJ, Chatterjee S, Improved intervention of atherosclerosis and cardiac hypertrophy through biodegradable polymer-encapsulated delivery of glycosphingolipid inhibitor, Biomaterials, 64 (2015) 125–135. [PubMed: 26111596]

[55]. Chmielowski RA, Abdelhamid DS, Faig JJ, Petersen LK, Gardner CR, Uhrich KE, Joseph LB, Moghe PV, Athero-inflammatory nanotherapeutics: Ferulic acid-based poly (anhydride-ester) nanoparticles attenuate foam cell formation by regulating macrophage lipogenesis and reactive oxygen species generation, Acta Biomater, 57 (2017) 85–94. [PubMed: 28522412]

[56]. Meng N, Gong Y, Zhang J, Mu X, Song Z, Feng R, Zhang H, A novel curcumin-loaded nanoparticle restricts atherosclerosis development and promotes plaques stability in apolipoprotein E deficient mice, J. Biomater. Appl, 33 (2019) 946–954. [PubMed: 30541364]

[57]. Yi S, Zhang X, Sangji MH, Liu Y, Allen SD, Xiao B, Bobbala S, Braverman CL, Cai L, Hecker PI, DeBerge M, Thorp EB, Temel RE, Stupp SI, Scott EA, Surface engineered polymersomes for enhanced modulation of dendritic cells during cardiovascular immunotherapy, Adv. Funct. Mater, 29 (2019) 1904399.

[58]. Bozzuto G, Molinari A, Liposomes as nanomedical devices, Int J Nanomedicine, 10 (2015) 975–999. [PubMed: 25678787]

[59]. Filipczak N, Pan J, Yalamarty SSK, Torchilin VP, Recent advancements in liposome technology, Adv. Drug Deliv. Rev , 156 (2020) 4–22. [PubMed: 32593642]

[60]. Kheirolomoom A, Kim CW, Seo JW, Kumar S, Son DJ, Gagnon MKJ, Ingham ES, Ferrara KW, Jo H, Multifunctional nanoparticles facilitate molecular targeting and miRNA delivery to inhibit atherosclerosis in ApoE$^{-/-}$mice, ACS Nano, 9 (2015) 8885–8897. [PubMed: 26308181]

[61]. Calin M, Stan D, Schlesinger M, Simion V, Deleanu M, Constantinescu CA, Gan A-M, Pirvulescu MM, Butoi E, Manduteanu I, VCAM-1 directed target-sensitive liposomes carrying CCR2 antagonists bind to activated endothelium and reduce adhesion and transmigration of monocytes, Eur J Pharm Biopharm, 89 (2015) 18–29. [PubMed: 25438248]

[62]. Pont I, Calatayud-Pascual A, Lopez-Castellano A, Albelda EP, Garcia-Espana E, Martí-Bonmatí L, Frias JC, Albelda MT, Anti-angiogenic drug loaded liposomes: nanotherapy for early atherosclerotic lesions in mice, Plos One, 13 (2018) e0190540. [PubMed: 29338009]

[63]. Jayaraj P, Shavi GV, Srinivasan AK, Raghavendra R, Sivaramakrishna A, Desikan R, A pre-formulation strategy for the liposome encapsulation of new thioctic acid conjugates for enhanced chemical stability and use as an efficient drug carrier for MPO-mediated atherosclerotic CVD treatment, New J Chem, 44 (2020) 2755–2767.

[64]. Kamanna VS, Ganji SH, Kashyap ML, Myeloperoxidase and atherosclerosis, Curr Cardiovasc Risk Rep, 7 (2013) 102–107.

[65]. Li X, Xiao H, Lin C, Sun W, Wu T, Wang J, Chen B, Chen X, Cheng D, Synergistic effects of liposomes encapsulating atorvastatin calcium and curcumin and targeting dysfunctional endothelial cells in reducing atherosclerosis, Int. J. Nanomedicine, 14 (2019) 649–665. [PubMed: 30697048]

[66]. Bartneck M, Peters FM, Warzecha KT, Bienert M, van Bloois L, Trautwein C, Lammers T, Tacke F, Liposomal encapsulation of dexamethasone modulates cytotoxicity, inflammatory cytokine response, and migratory properties of primary human macrophages, Nanomed-Nanotechnol, 10 (2014) 1209–1220.

[67]. Alaarg A, Hamers A, Versloot M, Lobatto M, Mulder W, Stroes ES, Storm G, Metselaar JM, Targeted liposomal drug delivery to inhibit atherosclerotic plaque inflammation, Atherosclerosis, 241 (2015) e87.

[68]. van der Valk FM, van Wijk DF, Lobatto ME, Verberne HJ, Storm G, Willems MC, Legemate DA, Nederveen AJ, Calcagno C, Mani V, Prednisolone-containing liposomes accumulate in human atherosclerotic macrophages upon intravenous administration, Nanomed-Nanotechnol, 11 (2015) 1039–1046.

[69]. Lobatto ME, Fayad ZA, Silvera S, Vucic E, Calcagno C, Mani V, Dickson SD, Nicolay K, Banciu M, Schiffelers RM, Multimodal clinical imaging to longitudinally assess a nanomedical anti-inflammatory treatment in experimental atherosclerosis, Mol. Pharm, 7 (2010) 2020–2029. [PubMed: 21028895]

[70]. van der Valk FM, Schulte DM, Meiler S, Tang J, Zheng KH, Van den Bossche J, Seijkens T, Laudes M, de Winther M, Lutgens E, Alaarg A, Metselaar JM, Dallinga-Thie GM, Mulder WJM, Stroes ESG, Hamers AAJ, Liposomal prednisolone promotes macrophage lipotoxicity in experimental atherosclerosis, Nanomed-Nanotechnol, 12 (2016) 1463–1470.

[71]. Fang D, Jin Q, Jin Z, Wang F, Huang L, Yang Y, He Z, Liu Y, Jiang C, Wu J, Folate-modified liposomes loaded with telmisartan enhance anti-atherosclerotic potency for advanced atherosclerosis in apoE$^{-/-}$mice, J. Biomed. Nanotech, 15 (2019) 42–61.

[72]. Benne N, Martins Cardoso R, Boyle AL, Kros A, Jiskoot W, Kuiper J, Bouwstra J, Van Eck M, Slütter B, Complement receptor targeted liposomes encapsulating the liver X receptor agonist GW3965 accumulate in and stabilize atherosclerotic plaques, Adv. Healthcare. Mater, 9 (2020) 2000043.

[73]. Li J, Ding F, Qian X, Sun J, Ge Z, Yang L, Cheng Z, Anti-inflammatory cytokine IL10 loaded cRGD liposomes for the targeted treatment of atherosclerosis, J. Microencapsul , (2020) 1–19.

[74]. Wu Y, Zhang Y, Dai L, Wang Q, Xue L, Su Z, Zhang C, An apoptotic body-biomimic liposome in situ upregulates anti-inflammatory macrophages for stabilization of atherosclerotic plaques, J. Control. Release, 316 (2019) 236–249. [PubMed: 31672624]

[75]. Kałas W, Wysokińska E, Przybyło M, Langner M, Ulatowska-Jarża A, Biały D, Wawrzyńska M, Zioło E, Gil W, Trzeciak AM, Photoactive liposomal formulation of PVP-conjugated chlorin e6 for photodynamic reduction of atherosclerotic plaque, Int. J. Mol. Sci, 20 (2019) 3852.

[76]. Hansson GK, Nilsson J, Developing a vaccine against atherosclerosis, Nat. Rev. Cardiol, 17 (2020) 451–452. [PubMed: 32587346]

[77]. Wang N, Chen M, Wang T, Liposomes used as a vaccine adjuvant-delivery system: From basics to clinical immunization, J. Control. Release, 303 (2019) 130–150. [PubMed: 31022431]

[78]. Hosseini H, Li Y, Kanellakis P, Tay C, Cao A, Tipping P, Bobik A, Toh B-H, Kyaw T, Phosphatidylserine liposomes mimic apoptotic cells to attenuate atherosclerosis by expanding polyreactive IgM producing B1a lymphocytes, Cardiovasc. Res, 106 (2015) 443–452. [PubMed: 25681396]

[79]. Benne N, van Duijn J, Vigario FL, Leboux RJ, van Veelen P, Kuiper J, Jiskoot W, Slütter B, Anionic 1, 2-distearoyl-sn-glycero-3-phosphoglycerol (DSPG) liposomes induce antigen-specific regulatory T cells and prevent atherosclerosis in mice, J. Control. Release, 291 (2018) 135–146. [PubMed: 30365993]

[80]. Momtazi-Borojeni AA, Jaafari MR, Badiee A, Sahebkar A, Long-term generation of anti PCS K9 antibody using a nanoliposome-based vaccine delivery system, Atherosclerosis, 283 (2019) 69–78. [PubMed: 30797988]

[81]. Momtazi-Borojeni A, Jaafari M, Badiee A, Banach M, Sahebkar A, P6195 nanoliposomal anti-PCSK9 vaccine induces long-term and safe protection against atherosclerosis in C57BL/6 mouse, Eur Heart J, 40 (2019) ehz746. 0800.

[82]. Momtazi-Borojeni A, Jaafari M, Banach M, Sahebkar A, P6194 Therapeutic effect of nanoliposomal anti-PCSK9 vaccine on hypercholesterolemia and atherosclerosis in C57BL/6 mice, Eur Heart J, 40 (2019) ehz746. 0799.

[83]. Aghebati T, Arabsalmani M, Mohammadpour AH, Afshar M, Jaafari MR, Abnous K, Nazemi S, Badiee A, Development of an effective liposomal cholesterol ester transfer protein (CETP) vaccine for protecting against atherosclerosis in rabbit model, Pharm Dev Technol, 25 (2020) 432–439. [PubMed: 31852350]

[84]. Lameijer M, Binderup T, van Leent MMT, Senders ML, Fay F, Malkus J, Sanchez-Gaytan BL, Teunissen AJP, Karakatsanis N, Robson P, Zhou X, Ye Y, Wojtkiewicz G, Tang J, Seijkens TTP, Kroon J, Stroes ESG, Kjaer A, Ochando J, Reiner T, Pérez-Medina C, Calcagno C, Fisher EA, Zhang B, Temel RE, Swirski FK, Nahrendorf M, Fayad ZA, Lutgens E, Mulder WJM, Duivenvoorden R, Efficacy and safety assessment of a TRAF6-targeted nanoimmunotherapy in atherosclerotic mice and non-human primates, Nat Biomed Eng, 2 (2018) 279–292. [PubMed: 30936448]

[85]. Säemann MD, Poglitsch M, Kopecky C, Haidinger M, Hörl WH, Weichhart T, The versatility of HDL: a crucial anti-inflammatory regulator, Eur. J. Clin. Invest, 40 (2010) 1131–1143. [PubMed: 20695882]

[86]. Podrez EA, Anti-oxidant properties of high-density lipoprotein and atherosclerosis, Clin. Exp. Pharmacol. Physiol, 37 (2010) 719–725. [PubMed: 20374263]

[87]. Chen J, Zhang X, Millican R, Creutzmann JE, Martin S, Jun HW, High density lipoprotein mimicking nanoparticles for atherosclerosis, Nano Converg, 7 (2020) 6. [PubMed: 31984429]

[88]. Zhang M, He J, Jiang C, Zhang W, Yang Y, Wang Z, Liu J, Plaque-hyaluronidase-responsive high-density-lipoprotein-mimetic nanoparticles for multistage intimal-macrophage-targeted drug delivery and enhanced anti-atherosclerotic therapy, Int J Nanomedicine, 12 (2017) 533. [PubMed: 28144137]

[89]. Zhao Y, Jiang C, He J, Guo Q, Lu J, Yang Y, Zhang W, Liu J, Multifunctional dextran sulfate-coated reconstituted high density lipoproteins target macrophages and promote beneficial antiatherosclerotic mechanisms, Bioconjugate Chem. , 28 (2017) 438–448.

[90]. Alaarg A, Senders ML, Varela-Moreira A, Pérez-Medina C, Zhao Y, Tang J, Fay F, Reiner T, Fayad ZA, Hennink WE, Metselaar JM, Mulder WJM, Storm G, A systematic comparison of clinically viable nanomedicines targeting HMG-CoA reductase in inflammatory atherosclerosis, J. Control. Release, 262 (2017) 47–57. [PubMed: 28700897]

[91]. Lu J, Zhao Y, Zhou X, He JH, Yang Y, Jiang C, Qi Z, Zhang W, Liu J, Biofunctional polymer–lipid hybrid high-density lipoprotein-mimicking nanoparticles loading anti-miR155 for combined antiatherogenic effects on macrophages, Biomacromolecules, 18 (2017) 2286–2295. [PubMed: 28738148]

[92]. Wang K, Yu C, Liu Y, Zhang W, Sun Y, Chen Y, Enhanced antiatherosclerotic efficacy of statin-loaded reconstituted high-density lipoprotein via ganglioside GM1 modification, ACS Biomater. Sci. Eng, 4 (2018) 952–962. [PubMed: 33418777]

[93]. Zhao Y, Gao H, He J, Jiang C, Lu J, Zhang W, Yang H, Liu J, Co-delivery of LOX-1 siRNA and statin to endothelial cells and macrophages in the atherosclerotic lesions by a dual-targeting core-shell nanoplatform: a dual cell therapy to regress plaques, J. Control. Release, 283 (2018) 241–260. [PubMed: 29885417]

[94]. Jiang C, Qi Z, He W, Li Z, Tang Y, Wang Y, Huang Y, Zang H, Yang H, Liu J, Dynamically enhancing plaque targeting via a positive feedback loop using multifunctional biomimetic nanoparticles for plaque regression, J. Control. Release, 308 (2019) 71–85. [PubMed: 31295543]

[95]. Seijkens TTP, van Tiel CM, Kusters PJH, Atzler D, Soehnlein O, Zarzycka B, Aarts SABM, Lameijer M, Gijbels MJ, Beckers L, den Toom M, Slütter B, Kuiper J, Duchene J, Aslani M, Megens RTA, van 't Veer C, Kooij G, Schrijver R, Hoeksema MA, Boon L, Fay F, Tang J, Baxter S, Jongejan A, Moerland PD, Vriend G, Bleijlevens B, Fisher EA, Duivenvoorden R, Gerdes N, de Winther MPJ, Nicolaes GA, Mulder WJM, Weber C, Lutgens E, Targeting CD40-induced TRAF6 signaling in macrophages reduces atherosclerosis, Am. J. Cardiol, 71 (2018) 527–542.

[96]. Zhong P, Chen M, Kong B, Fu H, Zhang J, Huang H, The therapeutic potential of targeting CD40-TRAF6 pathway in cardiovascular diseases, Int. J. Cardiol, 297 (2019) 118. [PubMed: 31839192]

[97]. He J, Yang Y, Zhou X, Zhang W, Liu J, Shuttle/sink model composed of β-cyclodextrin and simvastatin-loaded discoidal reconstituted high-density lipoprotein for enhanced cholesterol efflux and drug uptake in macrophage/foam cells, J. Mater. Chem. B, 8 (2020) 1496–1506. [PubMed: 31999290]

[98]. Guo Y, Yuan W, Yu B, Kuai R, Hu W, Morin EE, Garcia-Barrio MT, Zhang J, Moon JJ, Schwendeman A, Eugene Chen Y, Synthetic high-density lipoprotein-mediated targeted delivery of Liver X receptors agonist promotes atherosclerosis regression, EBioMedicine, 28 (2018) 225–233. [PubMed: 29361501]

[99]. Parolini C, Adorni MP, Busnelli M, Manzini S, Cipollari E, Favari E, Lorenzon P, Ganzetti GS, Fingerle J, Bernini F, Infusions of large synthetic HDL containing trimeric apoA-I stabilize atherosclerotic plaques in hypercholesterolemic rabbits, Can J Cardiol, 35 (2019) 1400–1408. [PubMed: 31495683]

[100]. White CR, Datta G, Wilson L, Palgunachari MN, Anantharamaiah GM, The apoA-I mimetic peptide 4F protects apolipoprotein A-I from oxidative damage, Chem Phys Lipids, 219 (2019) 28–35. [PubMed: 30707910]

[101]. Parolini C, Adorni MP, Busnelli M, Manzini S, Cipollari E, Favari E, Lorenzon P, Ganzetti GS, Fingerle J, Bernini F, Chiesa G, Infusions of large synthetic HDL containing trimeric apoA-I stabilize atherosclerotic plaques in hypercholesterolemic rabbits, Can J Cardiol, 35 (2019) 1400–1408. [PubMed: 31495683]

[102]. Henrich SE, Hong BJ, Rink JS, Nguyen ST, Thaxton CS, Supramolecular assembly of high-density lipoprotein mimetic nanoparticles using lipid-conjugated core scaffolds, J. Am. Chem. Soc, 141 (2019) 9753–9757. [PubMed: 31177775]

[103]. Yuan W, Yu B, Yu M, Kuai R, Morin EE, Wang H, Hu D, Zhang J, Moon JJ, Chen YE, Guo Y, Schwendeman A, Synthetic high-density lipoproteins delivering liver X receptor agonist prevent atherogenesis by enhancing reverse cholesterol transport, J. Control. Release, (2020) 361–371.

[104]. Tong LT, Ju Z, Qiu J, Wang L, Liu L, Zhou X, Zhou S, Peptide GEQQQQPGM derived from rice α-globulin reduces the risk of atherosclerosis in hamsters by improving vascular endothelial cells injury, RSC Adv, 7 (2017) 49194–49203.

[105]. Wang JL, Gong D, Hu XY, Wu S, Zheng XL, Wu J, Tang XE, Zhang DW, Tang CK, ApoA-1 mimetic peptide ELK-2A2K2E decreases inflammatory factor levels through the ABCA1-JAK2-STAT3-TTP axis in THP-1–derived macrophages, J. Cardiovasc. Pharmacol. Ther, 72 (2018) 60–67.

[106]. Zielińska E, Baraniak B, Karaś M, Identification of antioxidant and anti-inflammatory peptides obtained by simulated gastrointestinal digestion of three edible insects species (Gryllodes sigillatus, Tenebrio molitor, Schistocerca gragaria), Int. J. Food Sci. Technol, 53 (2018) 2542–2551.

[107]. Takahashi Y, Watanabe R, Sato Y, Ozawa N, Kojima M, Watanabe-Kominato K, Shirai R, Sato K, Hirano T, Watanabe T, Novel phytopeptide osmotin mimics preventive effects of adiponectin on vascular inflammation and atherosclerosis, Metabolism, 83 (2018) 128–138. [PubMed: 29410350]

[108]. Yu W, Field CJ, Wu J, Purification and identification of anti-inflammatory peptides from spent hen muscle proteins hydrolysate, Food Chem, 253 (2018) 101–107. [PubMed: 29502808]

[109]. Edmunds SJ, Liébana-García R, Nilsson O, Domingo-Espí;n J, Grönberg C, Stenkula KG, Lagerstedt JO, ApoAI-derived peptide increases glucose tolerance and prevents formation of atherosclerosis in mice, Diabetologia, 62 (2019) 1257–1267. [PubMed: 31069401]

[110]. Tong LT, Ju Z, Wang L, Qiu J, Liu L, Zhou X, Liang T, Geng D, Zhou S, Peptides derived from rice α-globulin reduce atherosclerosis in apolipoprotein E-deficient mice by inhibiting TNF-α-induced vascular endothelial cells injury, J. Funct. Foods, 63 (2019) 103582–103592.

[111]. Canesi F, Mateo V, Couchie D, Karabina S, Nègre-Salvayre A, Rouis M, El Hadri K, A thioredoxin-mimetic peptide exerts potent anti-inflammatory, antioxidant, and atheroprotective effects in ApoE2. Ki mice fed high fat diet, Cardiovasc. Res, 115 (2019) 292–301. [PubMed: 30010817]

[112]. Babinska A, Clement CC, Przygodzki T, Talar M, Li Y, Braun M, Wzorek J, Swiatkowska M, Ehrlich YH, Kornecki E, A peptide antagonist of F11R/JAM-A reduces plaque formation and prolongs survival in an animal model of atherosclerosis, Atherosclerosis, 284 (2019) 92–101. [PubMed: 30877938]

[113]. Suematsu Y, Kawachi E, Idemoto Y, Matsuo Y, Kuwano T, Kitajima K, Imaizumi S, Kawamura A, Saku K, Uehara Y, Anti-atherosclerotic effects of an improved apolipoprotein AI mimetic peptide, Int. J. Cardiol, 297 (2019) 111–117. [PubMed: 31519377]

[114]. Gou S, Wang L, Zhong C, Chen X, Ouyang X, Li B, Bao G, Liu H, Zhang Y, Ni J, A novel apoA-I mimetic peptide suppresses atherosclerosis by promoting physiological HDL function in apoE−/− mice, Br. J. Pharmacol, 177 (2020) 4627–4644. [PubMed: 32726461]

[115]. Hu B, Xu L, Li Y, Bai X, Xing M, Cao Q, Liang H, Song S, Ji A, A peptide inhibitor of macrophage migration in atherosclerosis purified from the leech Whitmania pigra, J. Ethnopharmacol, 254 (2020) 112723. [PubMed: 32119950]

[116]. Rivas-Urbina A, Rull A, Aldana-Ramos J, Santos D, Puig N, Farre-Cabrerizo N, Benitez S, Perez A, de Gonzalo-Calvo D, Julve J, Subcutaneous administration of apolipoprotein J-derived mimetic peptide d-[113–122] apoJ improves LDL and HDL function and prevents atherosclerosis in LDLR-KO mice, Biomolecules, 10 (2020) 829.

[117]. Tavares ER, Freitas FR, Diament J, Maranhão RC, Reduction of atherosclerotic lesions in rabbits treated with etoposide associated with cholesterol-rich nanoemulsions, Int J Nanomedicine, 6 (2011) 2297–2304. [PubMed: 22072867]

[118]. Daminelli EN, Martinelli AE, Bulgarelli A, Freitas FR, Maranhão RC, Reduction of atherosclerotic lesions by the chemotherapeutic agent carmustine associated to lipid nanoparticles, Cardiovasc. Drugs Ther, 30 (2016) 433–443. [PubMed: 27628679]

[119]. Meneghini BC, Tavares ER, Guido MC, Tavoni TM, Stefani HA, Kalil-Filho R, Maranhão RC, Lipid core nanoparticles as vehicle for docetaxel reduces atherosclerotic lesion, inflammation, cell death and proliferation in an atherosclerosis rabbit model, Vase. Pharmacol, 115 (2019) 46–54.

[120]. Gomes FL, Maranhão RC, Tavares ER, Carvalho PO, Higuchi ML, Mattos FR, Pitta FG, Hatab SA, Kalil-Filho R, Serrano CV Jr, Regression of atherosclerotic plaques of cholesterol-fed rabbits by combined chemotherapy with paclitaxel and methotrexate carried in lipid core nanoparticles, J. Cardiovasc. Pharmacol. Ther, 23 (2018) 561–569. [PubMed: 29779420]

[121]. Leite AC, Solano TV, Tavares ER, Maranhão RC, Use of combined chemotherapy with etoposide and methotrexate, both associated to lipid nanoemulsions for atherosclerosis treatment in cholesterol-fed rabbits, Cardiovasc. Drugs Ther, 29 (2015) 15–22. [PubMed: 25672520]

[122]. Owen SC, Chan DP, Shoichet MS, Polymeric micelle stability, Nano Today, 7 (2012) 53–65.

[123]. Biswas S, Kumari P, Lakhani PM, Ghosh B, Recent advances in polymeric micelles for anti-cancer drug delivery, Eur J Pharm Sci, 83 (2016) 184–202. [PubMed: 26747018]

[124]. Lewis DR, Petersen LK, York AW, Zablocki KR, Joseph LB, Kholodovych V, Prud'homme RK, Uhrich KE, Moghe PV, Sugar-based amphiphilic nanoparticles arrest atherosclerosis in vivo, Proc. Natl. Acad. Sci. U.S.A, 112 (2015) 2693–2698. [PubMed: 25691739]

[125]. Zhang Y, Li Q, Welsh WJ, Moghe PV, Uhrich KE, Micellar and structural stability of nanoscale amphiphilic polymers: implications for anti-atherosclerotic bioactivity, Biomaterials, 84 (2016) 230–240. [PubMed: 26828687]

[126]. Wu T, Chen X, Wang Y, Xiao H, Peng Y, Lin L, Xia W, Long M, Tao J, Shuai X, Aortic plaque-targeted andrographolide delivery with oxidation-sensitive micelle effectively treats atherosclerosis via simultaneous ROS capture and anti-inflammation, Nanomed-Nanotechnol, 14 (2018) 2215–2226.

[127]. Allen SD, Liu Y-G, Kim T, Bobbala S, Yi S, Zhang X, Choi J, Scott EA, Celastrol-loaded PEG-b-PPS nanocarriers as an anti-inflammatory treatment for atherosclerosis, Biomater. Sci, 7 (2019) 657–668. [PubMed: 30601470]

[128]. Ma X, Zhang T, Luo Z, Li X, Lin M, Li R, Du P, Yu X, Ma C, Yan P, Su J, Wang L, Li Y, Jiang J, Functional nano-vector boost anti-atherosclerosis efficacy of berberine in Apoe($^{-/-}$) mice, Acta Pharm. Sin. B, 10 (2020) 1769–1783. [PubMed: 33088695]

[129]. Wennink JW, Liu Y, Mäkinen PI, Setaro F, de la Escosura A, Bourajjaj M, Lappalainen JP, Holappa LP, van den Dikkenberg JB, Al Fartousi M, Macrophage selective photodynamic therapy by meta-tetra (hydroxyphenyl) chlorin loaded polymeric micelles: a possible treatment for cardiovascular diseases, Eur J Pharm Sci, 107 (2017) 112–125. [PubMed: 28679107]

[130]. Yi S, Zhang X, Sangji MH, Liu Y, Allen SD, Xiao B, Bobbala S, Braverman CL, Cai L, Hecker PI, Surface engineered polymersomes for enhanced modulation of dendritic cells during cardiovascular immunotherapy, Adv. Funct. Mater, 29 (2019) 1904399.

[131]. Yi S, Karabin NB, Zhu J, Bobbala S, Lyu H, Li S, Liu Y, Frey M, Vincent M, Scott EA, An injectable hydrogel platform for sustained delivery of anti-inflammatory nanocarriers and induction of regulatory T cells in atherosclerosis, Front. Bioeng. Biotechnol, 8 (2020).

[132]. Wei G, Hao L, Li X, Xu W, Liu F, Peng O, Lv S, VCAM-1-targeted and PPARb-agonist-loaded nanomicelles enhanced suppressing effects on apoptosis and migration of oxidized low-density lipoprotein-induced vascular smooth muscle cells, Biosci. Rep, 40 (2020) BSR20200559. [PubMed: 32314783]

[133]. Mlinar LB, Chung EJ, Wonder EA, Tirrell M, Active targeting of early and mid-stage atherosclerotic plaques using self-assembled peptide amphiphile micelles, Biomaterials, 35 (2014) 8678–8686. [PubMed: 25043572]

[134]. Kuo CH, Leon L, Chung EJ, Huang R-T, Sontag TJ, Reardon CA, Getz GS, Tirrell M, Fang Y, Inhibition of atherosclerosis-promoting microRNAs via targeted polyelectrolyte complex micelles, J. Mater. Chem. B, 2 (2014) 8142–8153. [PubMed: 25685357]

[135]. Lee SJ, Sohn YD, Andukuri A, Kim S, Byun J, Han JW, Park IH, Jun HW, Yoon YS, Enhanced therapeutic and long-term dynamic vascularization effects of human pluripotent stem cell-derived endothelial cells encapsulated in a nanomatrix gel, Circulation, 136 (2017) 1939–1954. [PubMed: 28972000]

[136]. Mansukhani NA, Peters EB, So MM, Albaghdadi MS, Wang Z, Karver MR, Clemons TD, Laux JP, Tsihlis ND, Stupp SI, Peptide amphiphile supramolecular nanostructures as a targeted therapy for atherosclerosis, Macromol. Biosci, 19(2019) 1900066.

[137]. So MM, Mansukhani NA, Peters EB, Albaghdadi MS, Wang Z, Rubert Pérez CM, Kibbe MR, Stupp SI, Peptide amphiphile nanostructures for targeting of atherosclerotic plaque and drug delivery, Adv. Biosyst, 2 (2018) 1700123. [PubMed: 30666317]

[138]. García-González V, Delgado-Coello B, Pérez-Torres A, Mas-Oliva J, Reality of a vaccine in the prevention and treatment of atherosclerosis, Arch. Med. Res, 46 (2015) 427–437. [PubMed: 26100340]

[139]. Gutiérrez-Vidal R, Delgado-Coello B, Méndez-Acevedo KM, Calixto-Tlacomulco S, Damián-Zamacona S, Mas-Oliva J, Therapeutic intranasal vaccine HB-ATV-8 prevents atherogenesis and non-alcoholic fatty liver disease in a pig model of atherosclerosis, Arch. Med. Res, 49 (2018) 456–470. [PubMed: 30792163]

[140]. Yao SY, Shen ML, Li SJ, Wu XD, Zhang MM, Ma LN, Li YP, Application of a mechanically responsive, inflammatory macrophage-targeted dual-sensitive hydrogel drug carrier for atherosclerosis, Colloids Surf. B, 186 (2020) 110718.

[141]. Yousefi M, Narmani A, Jafari SM, Dendrimers as efficient nanocarriers for the protection and delivery of bioactive phytochemicals, Adv. Colloid Interface Sci, (2020) 102125. [PubMed: 32109595]

[142]. Kaur D, Jain K, Mehra NK, Kesharwani P, Jain NK, A review on comparative study of PPI and PAMAM dendrimers, J Nanopart Res, 18 (2016) 146.

[143]. Durán-Lara E, Guzmán L, John A, Fuentes E, Alarcón M, Palomo I, Santos LS, PAMAM dendrimer derivatives as a potential drug for antithrombotic therapy, Eur. J. Med. Chem, 69 (2013) 601–608. [PubMed: 24095753]

[144]. Ma Q, Han Y, Chen C, Cao Y, Wang S, Shen W, Zhang H, Li Y, van Dongen MA, He B, Yu M, Xu L, Banaszak Holl MM, Liu G, Zhang Q, Qi R, Oral absorption enhancement of probucol by PEGylated G5 PAMAM dendrimer modified nanoliposomes, Mol. Pharm, 12 (2015) 665–674. [PubMed: 25587935]

[145]. Qi R, Li YZ, Chen C, Cao YN, Yu MM, Xu L, He B, Jie X, Shen WW, Wang YN, van Dongen MA, Liu GQ, Banaszak Holl MM, Zhang Q, Ke X, G5-PEG PAMAM dendrimer incorporating nanostructured lipid carriers enhance oral bioavailability and plasma lipid-lowering effect of probucol, J. Control. Release, 210 (2015) 160–168. [PubMed: 26003044]

[146]. Spyropoulos-Antonakakis N, Sarantopoulou E, Trohopoulos PN, Stefi AL, Kollia Z, Gavriil VE, Bourkoula A, Petrou PS, Kakabakos S, Semashko VV, Selective aggregation of PAMAM dendrimer nanocarriers and PAMAM/ZnPc nanodrugs on human atheromatous carotid tissues: a photodynamic therapy for atherosclerosis, Nanoscale Res. Lett, 10 (2015) 1–19. [PubMed: 25977644]

[147]. Ficker M, Theeuwen MJ, Janaszewska A, Gorzkiewicz M, Svenningsen SW, Klajnert-Maculewicz B, Christensen JB, Complexes of indomethacin with 4-carbomethoxy-pyrrolidone PAMAM dendrimers show improved anti-inflammatory properties and temperature-dependent binding and release profile, Mol. Pharm, 15 (2018) 3573–3582. [PubMed: 30011214]

[148]. Poh S, Putt KS, Low PS, Folate-targeted dendrimers selectively accumulate at sites of inflammation in mouse models of ulcerative colitis and atherosclerosis, Biomacromolecules, 18 (2017) 3082–3088. [PubMed: 28863264]

[149]. He H, Lancina III MG, Wang J, Korzun WJ, Yang H, Ghosh S, Bolstering cholesteryl ester hydrolysis in liver: A hepatocyte-targeting gene delivery strategy for potential alleviation of atherosclerosis, Biomaterials, 130 (2017) 1–13. [PubMed: 28349866]

[150]. Chen Z, Tang M, Huang D, Jiang W, Li M, Ji H, Park J, Xu B, Atchison L, Truskey G, Real-time observation of leukocyte–endothelium interactions in tissue-engineered blood vessel, Lab Chip, 18 (2018) 2047–2054. [PubMed: 29927449]

[151]. He H, Wang J, Yannie PJ, Korzun WJ, Yang H, Ghosh S, Nanoparticle-based “two-pronged” approach to regress atherosclerosis by simultaneous modulation of cholesterol influx and efflux, Biomaterials, 260 (2020) 120333. [PubMed: 32853832]

[152]. Alfei S, Signorello MG, Schito A, Catena S, Turrini F, Reshaped as polyester-based nanoparticles, gallic acid inhibits platelet aggregation, reactive oxygen species production and multi-resistant Gram-positive bacteria with an efficiency never obtained, Nanoscale Adv, 1 (2019) 4148–4157.

[153]. Garzón-Porras AM, Bertuzzi DL, Lucas K, Ornelas C, Anti-inflammatory activity of polyamide dendrimers bearing bile acid termini synthesized via SPAAC, J Nanopart Res, 21 (2019) 227.

[154]. Garzón-Porras AM, Bertuzzi DL, Lucas K, da Silva LC, de Oliveira MG, Ornelas C, Nitric oxide releasing polyamide dendrimer with anti-inflammatory activity, ACS Appl. Polym. Mater, 2 (2020) 2027–2034.

[155]. Zimmer S, Grebe A, Bakke SS, Bode N, Halvorsen B, Ulas T, Skjelland M, De Nardo D, Labzin LI, Kerksiek A, Cyclodextrin promotes atherosclerosis regression via macrophage reprogramming, Sci. Transl. Med, 8 (2016) 333ra350–333ra350.

[156]. Wang H, Zhang X, Yu B, Peng X, Wang A, Zhao D, Pang D, OuYang H, Tang X, Cyclodextrin ameliorates the progression of atherosclerosis via increasing high-density lipoprotein cholesterol plasma levels and anti-inflammatory effects in rabbits, J. Cardiovasc. Pharmacol , 73 (2019) 334–342. [PubMed: 30855405]

[157]. Zhang YM, Liu YH, Liu Y, Cyclodextrin-based multistimuli-responsive supramolecular assemblies and their biological functions, Adv. Mater, 32 (2020) 1806158.

[158]. Shelley H, Babu RJ, Role of cyclodextrins in nanoparticle-based drug delivery systems, J Pharm Pharm Sci 107 (2018) 1741–1753.

[159]. Dou Y, Guo J, Chen Y, Han S, Xu X, Shi Q, Jia Y, Liu Y, Deng Y, Wang R, Sustained delivery by a cyclodextrin material-based nanocarrier potentiates antiatherosclerotic activity of rapamycin via selectively inhibiting mTORC1 in mice, J. Control. Release, 235 (2016) 48–62. [PubMed: 27235978]

[160]. Zhang Q, Zhang F, Chen Y, Dou Y, Tao H, Zhang D, Wang R, Li X, Zhang J, Structure–property correlations of reactive oxygen species-responsive and hydrogen peroxide-eliminating materials with anti-oxidant and anti-inflammatory activities, Chem. Mater, 29 (2017) 8221–8238.

[161]. Dou Y, Chen Y, Zhang X, Xu X, Chen Y, Guo J, Zhang D, Wang R, Li X, Zhang J, Non-proinflammatory and responsive nanoplatforms for targeted treatment of atherosclerosis, Biomaterials, 143 (2017) 93–108. [PubMed: 28778000]

[162]. Wang Y, Li L, Zhao W, Dou Y, An H, Tao H, Xu X, Jia Y, Lu S, Zhang J, Targeted therapy of atherosclerosis by a broad-spectrum reactive oxygen species scavenging nanoparticle with intrinsic anti-inflammatory activity, ACS Nano, 12 (2018) 8943–8960. [PubMed: 30114351]

[163]. Zhu ML, Wang G, Wang H, Guo Y-M, Song P, Xu J, Li P, Wang S, Yang L, Amorphous nano-selenium quantum dots improve endothelial dysfunction in rats and prevent atherosclerosis in mice through Na+/H+ exchanger 1 inhibition, Vase. Pharmacol, 115 (2019) 26–32.

[164]. Keyoumu Y, Huo Q, Cheng L, Ma H, Zhang M, Ma Y, Ma X, The detailed biological investigations about combined effects of novel polyphenolic and photo-plasmonic nanoparticles loaded graphene nanosheets on coronary endothelial cells and isolated rat aortic rings, J Photoch Photobio B, 202 (2020) 111666.

[165]. Li C, Dou Y, Chen Y, Qi Y, Li L, Han S, Jin T, Guo J, Chen J, Zhang J, Site-specific microRNA-33 antagonism by pH-responsive nanotherapies for treatment of atherosclerosis via regulating cholesterol efflux and adaptive immunity, Adv. Funct. Mater, (2020) 2002131.

[166]. Kim H, Kumar S, Kang D-W, Jo H, Park J-H, Affinity-driven design of cargo-switching nanoparticles to leverage a cholesterol-rich microenvironment for atherosclerosis therapy, ACS Nano, 14 (2020) 6519–6531. [PubMed: 32343121]

[167]. Ravishankar S, Lim S, Cyclodextrin conjugated ferritin nanocages reduce intracellular cholesterol level in foam cells, Nano Res, 12 (2019) 2925–2932.

[168]. Zingg JM, Stamatiou C, Daunert S, Modulation of lipid accumulation in monocytes and macrophages by cyclodextrin-based nanocarriers for alpha-tocopheryl phosphate, The FASEB Journal, 33 (2019) 654.614–654.614.

[169]. Xu YY, Yang J, Shen T, Zhou F, Xia Y, Fu JY, Meng J, Zhang J, Zheng YF, Yang J, Xu LH, Zhu X-Q, Intravenous administration of multi-walled carbon nanotubes affects the formation of atherosclerosis in sprague-dawley rats, J. Occup. Health Psychol , 54 (2012) 361–369.

[170]. Suzuki Y, Tada-Oikawa S, Hayashi Y, Izuoka K, Kataoka M, Ichikawa S, Wu W, Zong C, Ichihara G, Ichihara S, Single-and double-walled carbon nanotubes enhance atherosclerogenesis by promoting monocyte adhesion to endothelial cells and endothelial progenitor cell dysfunction, Part. Fibre Toxicol, 13 (2015) 54.

[171]. Kosuge H, Sherlock SP, Kitagawa T, Dash R, Robinson JT, Dai H, McConnell MV, Near infrared imaging and photothermal ablation of vascular inflammation using single-walled carbon nanotubes, J.Am.Heart.Assoc, 1 (2012) e002568. [PubMed: 23316318]

[172]. Han S, Kwon T, Urn JE, Haam S, Kim WJ, Highly selective photothermal therapy by a phenoxylated-dextran-functionalized smart carbon nanotube platform, Adv. Healthcare Mater, 5 (2016) 1147–1156.

[173]. Flores AM, Hosseini-Nassab N, Jarr KU, Ye J, Zhu X, Wirka R, Koh AL, Tsantilas P, Wang Y, Nanda V, Pro-efferocytic nanoparticles are specifically taken up by lesional macrophages and prevent atherosclerosis, Nat. Nanotechnol, 15(2020) 154–161. [PubMed: 31988506]

[174]. Nirala NR, Abraham S, Kumar V, Bansal A, Srivastava A, Saxena PS, Colorimetric detection of cholesterol based on highly efficient peroxidase mimetic activity of graphene quantum dots, Sens. Actuators B Chem, 218 (2015) 42–50.

[175]. Bai J, Jiang X, A facile one-pot synthesis of copper sulfide-decorated reduced graphene oxide composites for enhanced detecting of H202 in biological environments, Anal. Chem, 85 (2013) 8095–8101. [PubMed: 23826825]

[176]. Kailashiya J, Singh N, Singh SK, Agrawal V, Dash D, Graphene oxide-based biosensor for detection of platelet-derived microparticles: a potential tool for thrombus risk identification, Biosens. Bioelectron, 65 (2015) 274–280. [PubMed: 25461169]

[177]. Lee BC, Lee JY, Kim J, Yoo JM, Kang I, Kim JJ, Shin N, Kim DJ, Choi SW, Kim D, Hong BH, Kang KS, Graphene quantum dots as anti-inflammatory therapy for colitis, Sci. Adv, 6 (2020) eaaz2630. [PubMed: 32494673]

[178]. Peng G, Montenegro MF, Ntola CN, Vranic S, Kostarelos K, Vogt C, Toprak MS, Duan T, Leifer K, Bräutigam L, Nitric oxide-dependent biodegradation of graphene oxide reduces inflammation in the gastrointestinal tract, Nanoscale, 12 (2020) 16730–16737. [PubMed: 32785315]

[179]. Oh B, Lee CH, Development of Man-rGO for targeted eradication of macrophage ablation, Mol. Pharm, 12 (2015) 3226–3236. [PubMed: 26161461]

[180]. Han J, Kim YS, Lim MY, Kim HY, Kong S, Kang M, Choo YW, Jun JH, Ryu S, Jeong HY, Dual roles of graphene oxide to attenuate inflammation and elicit timely polarization of macrophage phenotypes for cardiac repair, ACS Nano, 12 (2018) 1959–1977. [PubMed: 29397689]

[181]. Kazemzadeh H, Mozafari M, Fullerene-based delivery systems, Drug Discov. Today, 24 (2019) 898–905. [PubMed: 30703542]

[182]. Minami K, Okamoto K, Doi K, Harano K, Noiri E, Nakamura E, siRNA delivery targeting to the lung via agglutination-induced accumulation and clearance of cationic tetraamino fullerene, Sci. Rep, 4 (2014) 4916. [PubMed: 24814863]

[183]. Zhen M, Shu C, Li J, Zhang G, Wang T, Luo Y, Zou T, Deng R, Fang F, Lei H, Wang C, Bai C, A highly efficient and tumor vascular-targeting therapeutic technique with size-expansible gadofullerene nanocrystals, Sci. China Mater, 58 (2015) 799–810.

[184]. Nitta N, Seko A, Sonoda A, Ohta S, Tanaka T, Takahashi M, Murata K, Takemura S, Sakamoto T, Tabata Y, Is the use of fullerene in photodynamic therapy effective for atherosclerosis?, Cardiovasc Intervent Radiol, 31 (2008) 359–366. [PubMed: 18040738]

[185]. Plotkin JD, Elias MG, Dellinger AL, Kepley CL, NF-κB inhibitors that prevent foam cell formation and atherosclerotic plaque accumulation, Nanomedicine, 13 (2017) 2037–2048. [PubMed: 28457935]

[186]. Li T, Xiao L, Yang J, Ding M, Zhou Z, LaConte L, Jin L, Dorn HC, Li X, Trimetallic nitride endohedral fullerenes carboxyl-Gd3N@C80: a new theranostic agent for combating oxidative stress and resolving inflammation, ACS Appl. Mater, 9 (2017) 17681–17687.

[187]. Jiang L, Wang J, Jiang J, Zhang C, Zhao M, Chen Z, Wang N, Hu D, Liu X, Peng H, Sonodynamic therapy in atherosclerosis by curcumin nanosuspensions: preparation design, efficacy evaluation, and mechanisms analysis, Eur J Pharm Biopharm, 146 (2020) 101–110. [PubMed: 31841689]

[188]. Sun T, Simmons R, Huo D, Pang B, Zhao X, Kim CW, Jo H, Xia Y, Targeted delivery of anti-miR-712 by VCAM1-binding Au nanospheres for atherosclerosis therapy, ChemNanoMat, 2 (2016) 400–406.

[189]. Han X, Kou J, Zheng Y, Liu Z, Jiang Y, Gao Z, Cong L, Yang L, ROS generated by upconversion nanoparticle-mediated photodynamic therapy induces autophagy via PI3K/AKT/mTOR signaling pathway in M1 peritoneal macrophage, Cell Physiol Biochem, 52 (2019) 1325–1338. [PubMed: 31050281]

[190]. Zhang L, Tian XY, Chan CK, Bai Q, Cheng CK, Chen FM, Cheung MS, Yin B, Yang H, Yung WY, Promoting the delivery of nanoparticles to atherosclerotic plaques by DNA coating, ACS Appl. Mater, 11 (2018) 13888–13904.

[191]. Kim M, Sahu A, Hwang Y, Kim GB, Nam GH, Kim IS, Kwon IC, Tae G, Targeted delivery of anti-inflammatory cytokine by nanocarrier reduces atherosclerosis in Apo $E^{-/-}$mice, Biomaterials, 226 (2020) 119550. [PubMed: 31645012]

[192]. Zhang X, Liu J, Yang X, He G, Li B, Qin J, Shearing PR, Brett DJ, Hu J, Lu X, CuCo2S4 nanocrystals as a nanoplatform for photothermal therapy of arterial inflammation, Nanoscale, 11 (2019) 9733–9742. [PubMed: 31066405]

[193]. Gao W, Zhao Y, Li X, Sun Y, Cai M, Cao W, Liu Z, Tong L, Cui G, Tang B, H 2 O 2-responsive and plaque-penetrating nanoplatform for mTOR gene silencing with robust anti-atherosclerosis efficacy, Chem. Sci, 9 (2018) 439–445. [PubMed: 29629115]

[194]. Zhaorigetu S, Prathipati P, Rodriguez-Aguayo C, Walton BL, Sood AK, Berestein-Lopez G, Fatty acid binding protein-4 silencing attenuates atherosclerosis progression by affecting macrophage apoptosis and autophagy, J Biosci Med, 7 (2019) 99.

[195]. Liu F, Ding N, Huo D, Yang G, Wei K, Guan G, Li Y, Yang J, Wang T, Wang Y, Surface-engineered monocyte inhibits atherosclerotic plaque destabilization via graphene quantum dot-mediated microRNA delivery, Adv. Healthcare Mater, 8 (2019) 1900386.

[196]. Yang L, Zang G, Li J, Li X, Li Y, Zhao Y, Cell-derived biomimetic nanoparticles as a novel drug delivery system for atherosclerosis: predecessors and perspectives, Regen. Biomater, 7 (2020) 349–358. [PubMed: 32793380]

[197]. Song Y, Huang Z, Liu X, Pang Z, Chen J, Yang H, Zhang N, Cao Z, Liu M, Cao J, Platelet membrane-coated nanoparticle-mediated targeting delivery of Rapamycin blocks atherosclerotic plaque development and stabilizes plaque in apolipoprotein E-deficient ($ApoE^{-/-}$) mice, Nanomed-Nanotechnol, 15 (2019) 13–24.

[198]. Lee CH, Hsieh MJ, Chang SH, Hung KC, Wang CJ, Hsu MY, Juang JH, Hsieh IC, Wen MS, Liu SJ, Nanofibrous vildagliptin-eluting stents enhance re-endothelialization and reduce neointimal formation in diabetes: in vitro and in vivo, Int J Nanomedicine, 14 (2019) 7503–7513. [PubMed: 31686818]

[199]. Boada C, Zinger A, Tsao C, Zhao P, Martinez JO, Hartman K, Naoi T, Sukhoveshin R, Sushnitha M, Molinaro R, Trachtenberg B, Cooke JP, Tasciotti E, Rapamycin-loaded biomimetic nanoparticles reverse vascular inflammation, Circ. Res, 126 (2020) 25–37. [PubMed: 31647755]

[200]. Gao W, Yang H, Liu X, Liu Z, Tong L, Sun Y, Cao W, Cao Y, Tang B, Reductively dissociable biomimetic nanoparticles for control of integrin-coupled inflammatory signaling to retard atherogenesis, ChemComm, 55 (2019) 11535–11538.

[201]. Gao C, Huang Q, Liu C, Kwong CH, Yue L, Wan J-B, Lee SM, Wang R, Treatment of atherosclerosis by macrophage-biomimetic nanoparticles via targeted pharmacotherapy and sequestration of proinflammatory cytokines, Nat. Commun, 11 (2020) 1–14. [PubMed: 31911652]

[202]. Ain QU, Chung H, Chung JY, Choi JH, Kim YH, Amelioration of atherosclerotic inflammation and plaques via endothelial adrenoceptor-targeted eNOS gene delivery using redox-sensitive polymer bearing l-arginine, J. Control. Release, 262 (2017) 72–86. [PubMed: 28710003]

[203]. Wu T, Xiao H, Lu L, Chen Y, Wang Y, Xia W, Long M, Tao J, Shen J, Shuai X, Polymeric vector-mediated targeted delivery of Anti-PAK1 siRNA to macrophages for efficient atherosclerosis treatment, ACS Biomater. Sci. Eng, 5 (2019) 4455–4462. [PubMed: 33438411]

[204]. Pan H, Palekar RU, Hou KK, Bacon J, Yan H, Springer LE, Akk A, Yang L, Miller MJ, Pham CT, Anti-JNK2 peptide-siRNA nanostructures improve plaque endothelium and reduce

thrombotic risk in atherosclerotic mice, Int J Nanomedicine, 13 (2018) 5187. [PubMed: 30233180]

[205]. Briguori C, Sarais C, Pagnotta P, Liistro F, Montorfano M, Chieffo A, Sgura F, Corvaja N, Albiero R, Stankovic G, In-stent restenosis in small coronary arteries: impact of strut thickness, Am. J. Cardiol, 40 (2002) 403–409.

[206]. Shuchman M, Debating the risks of drug-eluting stents, N. Engl. J. Med, 356 (2007) 325–328. [PubMed: 17251527]

[207]. Mao L, Shen L, Chen J, Wu Y, Kwak M, Lu Y, Xue Q, Pei J, Zhang L, Yuan G, Enhanced bioactivity of Mg–Nd–Zn–Zr alloy achieved with nanoscale MgF2 surface for vascular stent application, ACS Appl. Mater, 7 (2015) 5320–5330.

[208]. Junkar I, Kulkarni M, Benčina M, Kovač J, Mrak-Poljšak K, Lakota K, Sodin-Šemrl S, Mozetič M, Iglič A, Titanium dioxide nanotube arrays for cardiovascular stent applications, ACS Omega, 5 (2020) 7280–7289. [PubMed: 32280869]

[209]. Yang F, Chang R, Webster TJ, Atomic layer deposition coating of TiO(2) nano-thin films on magnesium-zinc alloys to enhance cytocompatibility for bioresorbable vascular stents, Int. J. Nanomedicine, 14 (2019) 9955–9970. [PubMed: 31908452]

[210]. Mori H, Jinnouchi H, Diljon C, Torii S, Sakamoto A, Kolodgie FD, Virmani R, Finn AV, A new category stent with novel polyphosphazene surface modification, Future Cardiol, 14 (2018) 225–235. [PubMed: 29582698]

[211]. Maillard L, Corseaux D, Altie A, Ung A, Courageot J, Barakat M, Teiger E, Van Belle E, Time course of reendothelialization with Polyzene-F nanocoated Cobra PzF™ coronary stent on rabbit iliac arteries, Cardiovasc Revasc Med, 21 (2020) 195–199. [PubMed: 31727585]

[212]. Lee SJ, Jo HH, Lim KS, Lim D, Lee S, Lee JH, Kim WD, Jeong MH, Lim JY, Kwon IK, Heparin coating on 3D printed poly (l-lactic acid) biodegradable cardiovascular stent via mild surface modification approach for coronary artery implantation, Chem. Eng. J, 378 (2019) 122116.

[213]. Liu S, Hu Y, Tao R, Huo Q, Wang L, Tang C, Pan C, Gong T, Xu N, Liu T, Immobilization of Fibronectin-Loaded Polyelectrolyte Nanoparticles on Cardiovascular Material Surface to Improve the Biocompatibility, Biomed Res. Int, 2019 (2019).

[214]. Xue W, Nasr SH, Guan G, Gao L, Zhao F, Gao J, Wang F, Qian C, Wang L, An efficient surface modification strategy improving endothelialization with polydopamine nanoparticles and REDV peptides for stent-grafts, ACS Appl. Bio Mater, 2 (2019) 3820–3827.

[215]. Bricout N, Chai F, Sobocinski J, Hertault A, Laure W, Ung A, Woisel P, Lyskawa J, Blanchemain N, Immobilisation of an anti-platelet adhesion and anti-thrombotic drug (EP224283) on polydopamine coated vascular stent promoting anti-thrombogenic properties, Mater. Sci. Eng. C, (2020) 110967.

[216]. Li JA, Chen L, Zhang XQ, Guan SK, Enhancing biocompatibility and corrosion resistance of biodegradable Mg-Zn-Y-Nd alloy by preparing PDA/HA coating for potential application of cardiovascular biomaterials, Mater. Sci. Eng. C, 109 (2020) 110607.

[217]. Ye W, Chen Y, Tang W, Zhang N, Li Z, Liu Z, Yu B, Xu F-J, Reduction-responsive nucleic acid delivery systems to prevent in-stent restenosis in rabbits, ACS Appl. Mater, 11 (2019) 28307–28316.

[218]. Lee CH, Hsieh MJ, Liu KS, Cheng CW, Chang SH, Liu SJ, Wang CJ, Hsu MY, Hung KC, Yeh YH, Chen WJ, Hsieh IC, Juang JH, Wen MS, Promoting vascular healing using nanofibrous ticagrelor-eluting stents, Int J Nanomedicine, 13 (2018) 6039–6048. [PubMed: 30323591]

[219]. Du R, Wang Y, Huang Y, Zhao Y, Zhang D, Du D, Zhang Y, Li Z, McGinty S, Pontrelli G, Design and testing of hydrophobic core/hydrophilic shell nano/micro particles for drug-eluting stent coating, NPG Asia Mater, 10 (2018) 642–658.

[220]. Lee CH, Hsieh MJ, Liu SC, Chen JK, Liu SJ, Hsieh IC, Wen MS, Hung KC, Novel bifurcation stents coated with bioabsorbable nanofibers with extended and controlled release of rosuvastatin and paclitaxel, Mater. Sci. Eng C, 88 (2018) 61–69.

[221]. Janjic M, Pappa F, Karagkiozaki V, Gitas C, Ktenidis K, Logothetidis S, Surface modification of endovascular stents with rosuvastatin and heparin-loaded biodegradable nanofibers by electrospinning, Int J Nanomedicine, 12 (2017) 6343. [PubMed: 28919738]

[222]. Ponce A, Ramos-Peréz V, Borrós S, Controlled release on cardiovascular stents using plasma-enhanced adhesion of biodegradable nanoparticles, Med One, 4 (2019) e190014.

[223]. Kersani D, Mougin J, Lopez M, Degoutin S, Tabary N, Cazaux F, Janus L, Maton M, Chai F, Sobocinski J, Stent coating by electrospinning with chitosan/poly-cyclodextrin based nanofibers loaded with simvastatin for restenosis prevention, Eur J Pharm Biopharm, 150 (2020) 156–167. [PubMed: 32179100]

[224]. Zhi B, Mao Y, Vapor-deposited nanocoatings for sustained zero-order release of antiproliferative drugs, ACS Appl. Bio Mater, 3 (2020) 1088–1096.

[225]. Obiweluozor FO, Maharjan B, Gladys Emechebe A, Park CH, Kim CS, Mussel-inspired elastic interpenetrated network hydrogel as an alternative for anti-thrombotic stent coating membrane, Chem Eng J, 347 (2018) 932–943.

[226]. Belibel R, Sali S, Marinval N, Garcia-Sanchez A, Barbaud C, Hlawaty H, PDMMLA derivatives as a promising cardiovascular metallic stent coating: Physicochemical and biological evaluation, Mater. Sci. Eng. C, 117 (2020) 111284.

[227]. Mo H, Fu C, Wu Z, Liu P, Wen Z, Hong Q, Cai Y, Li G, IL-6-targeted ultrasmall superparamagnetic iron oxide nanoparticles for optimized MRI detection of atherosclerotic vulnerable plaques in rabbits, RSC Adv, 10 (2020) 15346–15353.

[228]. Ye SH, Chen Y, Mao Z, Gu X, Shankarraman V, Hong Y, Shanov V, Wagner WR, Biodegradable zwitterionic polymer coatings for magnesium alloy stents, Langmuir, 35 (2019) 1421–1429. [PubMed: 30056712]

[229]. Rivera L, Betancur A, Zarate D, Torres DT, Hoyos L, Garcia A, Reduction and simultaneous doping of graphene oxide to repel LDL in treatment of atherosclerosis disease, arXiv preprint arXiv:1902.01850 (2019).

[230]. Alexander GC, Hwang P, Chen J, Kim J.-a., Brott BC, Yoon Y, Jun HW, Nanomatrix coated stent enhances endothelialization but reduces platelet, smooth muscle cell, and monocyte adhesion under physiologic conditions, ACS Biomater. Sci. Eng, 4 (2018) 107–115. [PubMed: 31538110]

[231]. Jang TS, Cheon KH, Ahn JH, Song EH, Kim HE, Jung HD, In-vitro blood and vascular compatibility of sirolimus-eluting organic/inorganic hybrid stent coatings, Colloids Surf. B, 179 (2019) 405–413.

[232]. Fan Y, Zhang Y, Zhao Q, Xie Y, Luo R, Yang P, Weng Y, Immobilization of nano Cu-MOFs with polydopamine coating for adaptable gasotransmitter generation and copper ion delivery on cardiovascular stents, Biomaterials, 204 (2019) 36–45. [PubMed: 30875517]

[233]. Ge S, Xi Y, Du R, Ren Y, Xu Z, Tan Y, Wang Y, Yin T, Wang G, Inhibition of in-stent restenosis after graphene oxide double-layer drug coating with good biocompatibility, Regen. Biomater, 6 (2019) 299–309. [PubMed: 31616567]

[234]. Yang MC, Tsou HM, Hsiao YS, Cheng YW, Liu CC, Huang LY, Peng XY, Liu TY, Yung MC, Hsu CC, Electrochemical polymerization of PEDOT-graphene oxide-heparin composite coating for anti-fouling and anti-clotting of cardiovascular stents, Polymers (Basel), 11 (2019) 1520.

[235]. ElSawy AM, Attia NF, Mohamed HI, Mohsen M, Talaat M, Innovative coating based on graphene and their decorated nanoparticles for medical stent applications, Mater. Sci. Eng. C, 96 (2019) 708–715.

[236]. Misra SK, Ostadhossein F, Babu R, Kus J, Tankasala D, Sutrisno A, Walsh KA, Bromfield CR, Pan D, 3D-printed multidrug-eluting stent from graphene-nanoplatelet-doped biodegradable polymer composite, Adv. Healthcare Mater, 6 (2017) 1700008.

[237]. Jeong DW, Park W, Bedair TM, Kang EY, Kim IH, Park DS, Sim DS, Hong YJ, Koh WG, Jeong MH, Augmented re-endothelialization and anti-inflammation of coronary drug-eluting stent by abluminal coating with magnesium hydroxide, Biomater. Sci , 7 (2019) 2499–2510. [PubMed: 30957801]

[238]. Hou R, Wu L, Zhu Y, Wang J, Yang Z, Tu Q, Huang N, Study of functional drug-eluting stent in promoting endothelialization and antiproliferation, J. Biomater. Sci. Polym. Ed, 31 (2020) 244–260. [PubMed: 31626738]

[239]. Llopis-Grimalt MA, Forteza-Genestra MA, Alcolea-Rodriguez V, Ramis JM, Monjo M, Nanostructured titanium for improved endothelial biocompatibility and reduced platelet adhesion in stent applications, Coatings, 10 (2020) 907.

[240]. Wang Y, Lan H, Yin T, Zhang X, Huang J, Fu H, Huang J, McGinty S, Gao H, Wang G, Covalent immobilization of biomolecules on stent materials through mussel adhesive protein coating to form biofunctional films, Mater. Sci. Eng. C, 106 (2020) 110187.

[241]. Yang Z, Zhao X, Hao R, Tu Q, Tian X, Xiao Y, Xiong K, Wang M, Feng Y, Huang N, Pan G, Bioclickable and mussel adhesive peptide mimics for engineering vascular stent surfaces, Proc. Natl. Acad. Sci. U.S.A, 117 (2020) 16127–16137. [PubMed: 32601214]

[242]. Yu M, Niu Y, Zhou D, Jiang R, Zhang L, Ju H, Gong A, Zou S, Zhang M, Du F, Hyaluronic acid-functionalized gadolinium doped iron oxide nanoparticles for atherosclerosis-targeted Mr imaging, J Biomed Nanotechnol, 15 (2019) 127–137. [PubMed: 30480520]

[243]. Yang Z, Yang Y, Zhang L, Xiong K, Li X, Zhang F, Wang J, Zhao X, Huang N, Mussel-inspired catalytic selenocystamine-dopamine coatings for long-term generation of therapeutic gas on cardiovascular stents, Biomaterials, 178 (2018) 1–10. [PubMed: 29902532]

[244]. Yang Y, Gao P, Wang J, Tu Q, Bai L, Xiong K, Qiu H, Zhao X, Maitz MF, Wang H, Endothelium-mimicking multifunctional coating modified cardiovascular stents via a stepwise metal-catechol-(amine) surface engineering strategy, Research, 2020 (2020) 9203906. [PubMed: 32405627]

[245]. Tu Q, Zhao X, Liu S, Li X, Zhang Q, Yu H, Xiong K, Huang N, Yang Z, Spatiotemporal dual-delivery of therapeutic gas and growth factor for prevention of vascular stent thrombosis and restenosis, Appl. Mater. Today 19 (2020) 100546.

[246]. Qiu H, Qi P, Liu J, Yang Y, Tan X, Xiao Y, Maitz MF, Huang N, Yang Z, Biomimetic engineering endothelium-like coating on cardiovascular stent through heparin and nitric oxide-generating compound synergistic modification strategy, Biomaterials, 207 (2019) 10–22. [PubMed: 30947118]

[247]. Torsney E, Mayr U, Zou Y, Thompson WD, Hu Y, Xu Q, Thrombosis and neointima formation in vein grafts are inhibited by locally applied aspirin through endothelial protection, Circ. Res, 94 (2004) 1466–1473. [PubMed: 15117816]

[248]. Tang D, Chen S, Hou D, Gao J, Jiang L, Shi J, Liang Q, Kong D, Wang S, Regulation of macrophage polarization and promotion of endothelialization by NO generating and PEG-YIGSR modified vascular graft, Mater. Sci. Eng. C, 84 (2018) 1–11.

[249]. Gui L, Dash BC, Luo J, Qin L, Zhao L, Yamamoto K, Hashimoto T, Wu H, Dardik A, Tellides G, Implantable tissue-engineered blood vessels from human induced pluripotent stem cells, Biomaterials, 102 (2016) 120–129. [PubMed: 27336184]

[250]. Karimi F, McKenzie TG, O'Connor AJ, Qiao GG, Heath DE, Nano-scale clustering of integrin-binding ligands regulates endothelial cell adhesion, migration, and endothelialization rate: novel materials for small diameter vascular graft applications, J. Mater. Chem. B, 5 (2017) 5942–5953. [PubMed: 32264351]

[251]. Park C, Park S, Kim J, Han A, Ahn S, Min S-K, Jae HJ, Chung JW, Lee J-H, Jung H-D, Enhanced endothelial cell activity induced by incorporation of nano-thick tantalum layer in artificial vascular grafts, Appl. Surf. Sci, 508 (2020) 144801.

[252]. Wang D, Wang X, Zhang Z, Wang L, Li X, Xu Y, Ren C, Li Q, Turng LS, Programmed release of multimodal, cross-linked vascular endothelial growth factor and heparin layers on electrospun polycaprolactone vascular grafts, ACS Appl. Mater, 11 (2019) 32533–32542.

[253]. Augustine R, Dan P, Sosnik A, Kalarikkal N, Tran N, Vincent B, Thomas S, Menu P, Rouxel D, Electrospun poly(vinylidene fluoride-trifluoroethylene)/zinc oxide nanocomposite tissue engineering scaffolds with enhanced cell adhesion and blood vessel formation, Nano Res, 10 (2017) 3358–3376.

[254]. Cafarelli A, Losi P, Salgarella AR, Barsotti MC, Di Cioccio IB, Foffa I, Vannozzi L, Pingue P, Soldani G, Ricotti L, Small-caliber vascular grafts based on a piezoelectric nanocomposite elastomer: mechanical properties and biocompatibility, J Mech Behav Biomed, 97 (2019) 138–148.

[255]. Mi HY, Jiang Y, Jing X, Enriquez E, Li H, Li Q, Turng LS, Fabrication of triple-layered vascular grafts composed of silk fibers, polyacrylamide hydrogel, and polyurethane nanofibers with biomimetic mechanical properties, Mater. Sci. Eng C, 98 (2019) 241–249.

[256]. Park S, Kim J, Lee MK, Park C, Jung HD, Kim H-E, Jang T-S, Fabrication of strong, bioactive vascular grafts with PCL/collagen and PCL/silica bilayers for small-diameter vascular applications, Mater. Des, 181 (2019) 108079.

[257]. Ma K, Rozet S, Tamada Y, Yao J, Ni QQ, Multi-layer nanofibrous tubes with dual drug-release profiles for vascular graft engineering, J Drug Deliv Sci Technol, 53 (2019) 100900.

[258]. Johnson R, Ding Y, Nagiah N, Monnet E, Tan W, Coaxially-structured fibres with tailored material properties for vascular graft implant, Mater. Sci. Eng. C, 97 (2019) 1–11.

[259]. Norouzi SK, Shamloo A, Bilayered heparinized vascular graft fabricated by combining electrospinning and freeze drying methods, Mater. Sci. Eng. C, 94 (2019) 1067–1076.

[260]. Li N, Xue F, Zhang H, Sanyour HJ, Rickel AP, Uttecht A, Fanta B, Hu J, Hong Z, Fabrication and characterization of pectin hydrogel nanofiber scaffolds for differentiation of mesenchymal stem cells into vascular cells, ACS Biomater. Sci. Eng, 5 (2019) 6511–6519. [PubMed: 33417803]

[261]. Yang Y, Lei D, Zou H, Huang S, Yang Q, Li S, Qing F-L, Ye X, You Z, Zhao Q, Hybrid electrospun rapamycin-loaded small-diameter decellularized vascular grafts effectively inhibit intimal hyperplasia, Acta Biomater, 97 (2019) 321–332. [PubMed: 31523025]

[262]. Zhao J, Bai L, Ren X.-k., Guo J, Xia S, Zhang W, Feng Y, Co-immobilization of ACH11 antithrombotic peptide and CAG cell-adhesive peptide onto vascular grafts for improved hemocompatibility and endothelialization, Acta Biomater, 97 (2019) 344–359. [PubMed: 31377424]

[263]. Wen M, Zhi D, Wang L, Cui C, Huang Z, Zhao Y, Wang K, Kong D, Yuan X, Local delivery of dual microRNAs in trilayered electrospun grafts for vascular regeneration, ACS Appl. Mater, 12 (2020) 6863–6875.

[264]. Mankoff DA, A definition of molecular imaging, J Nucl Med, 48 (2007) 18N–21N.

[265]. Peterson TE, Manning HC, Molecular imaging: 18F-FDG PET and a whole lot more, J Nucl Med Technol, 37 (2009) 151–161. [PubMed: 19692452]

[266]. Owen DR, Lindsay AC, Choudhury RP, Fayad ZA, Imaging of atherosclerosis, Annu Rev Med, 62 (2011) 25–40. [PubMed: 21226610]

[267]. Tarkin JM, Dweck MR, Evans NR, Takx RA, Brown AJ, Tawakol A, Fayad ZA, Rudd JH, Imaging atherosclerosis, Circ. Res, 118 (2016) 750–769. [PubMed: 26892971]

[268]. Syed MB, Fletcher AJ, Forsythe RO, Kaczynski J, Newby DE, Dweck MR, van Beek EJ, Emerging techniques in atherosclerosis imaging, Br J Radiol, 92 (2019) 20180309. [PubMed: 31502858]

[269]. Evans NR, Tarkin JM, Chowdhury MM, Warburton EA, Rudd JH, PET imaging of atherosclerotic disease: advancing plaque assessment from anatomy to pathophysiology, Curr Atheroscler Rep, 18 (2016) 30. [PubMed: 27108163]

[270]. Douma K, Prinzen L, Slaaf DW, Reutelingsperger CP, Biessen EA, Hackeng TM, Post MJ, van Zandvoort MA, Nanoparticles for optical molecular imaging of atherosclerosis, Small, 5 (2009) 544–557. [PubMed: 19226595]

[271]. Wickline SA, Neubauer AM, Winter PM, Caruthers SD, Lanza GM, Molecular imaging and therapy of atherosclerosis with targeted nanoparticles, J Magn Reson Imaging, 25 (2007) 667–680. [PubMed: 17347992]

[272]. Chung EJ, Tirrell M, Recent advances in targeted, self-assembling nanoparticles to address vascular damage due to atherosclerosis, Adv. Healthcare Mater, 4 (2015) 2408–2422.

[273]. Saravanakumar G, Kim K, Park JH, Rhee K, Kwon IC, Current status of nanoparticle-based imaging agents for early diagnosis of cancer and atherosclerosis, J Biomed Nanotechnol, 5 (2009) 20–35. [PubMed: 20055103]

[274]. Bejarano J, Navarro-Marquez M, Morales-Zavala F, Morales JO, Garcia-Carvajal I, Araya-Fuentes E, Flores Y, Verdejo HE, Castro PF, Lavandero S, Kogan MJ, Nanoparticles for diagnosis and therapy of atherosclerosis and myocardial infarction: evolution toward prospective theranostic approaches, Theranostics, 8 (2018) 4710–4732. [PubMed: 30279733]

[275]. Wang X, Hu Y, Wang R, Zhao P, Gu W, Ye L, Albumin-mediated synthesis of fluoroperovskite KMnF3 nanocrystals for T1-T2 dual-modal magnetic resonance imaging of brain gliomas with improved sensitivity, Chem. Eng. J, 395 (2020) 125066.

[276]. Xiao YD, Paudel R, Liu J, Ma C, Zhang ZS, Zhou SK, MRI contrast agents: classification and application, Int J Mol Med, 38 (2016) 1319–1326. [PubMed: 27666161]

[277]. Jeon M, Halbert MV, Stephen ZR, Zhang M, Iron oxide nanoparticles as T1 contrast agents for magnetic resonance imaging: fundamentals, challenges, applications, and prospectives, Adv. Mater, (2020) 1906539.

[278]. Hossaini Nasr S, Tonson A, El-Dakdouki MH, Zhu DC, Agnew D, Wiseman R, Qian C, Huang X, Effects of nanoprobe morphology on cellular binding and inflammatory responses: hyaluronan-conjugated magnetic nanoworms for magnetic resonance imaging of atherosclerotic plaques, ACS Appl. Mater, 10 (2018) 11495–11507.

[279]. Xu W, Zhang S, Zhou Q, Chen W, VHPKQHR peptide modified magnetic mesoporous nanoparticles for MRI detection of atherosclerosis lesions, Artif. Cells Nanomed. Biotechnol, 47 (2019) 2440–2448. [PubMed: 31190559]

[280]. Wei Q, Wang J, Shi W, Zhang B, Jiang H, Du M, Mei H, Hu Y, Improved in vivo detection of atherosclerotic plaques with a tissue factor-targeting magnetic nanoprobe, Acta Biomater, 90 (2019) 324–336. [PubMed: 30954623]

[281]. Ta HT, Li Z, Hagemeyer CE, Cowin G, Zhang S, Palasubramaniam J, Alt K, Wang X, Peter K, Whittaker AK, Molecular imaging of activated platelets via antibody-targeted ultra-small iron oxide nanoparticles displaying unique dual MRI contrast, Biomaterials, 134 (2017) 31–42. [PubMed: 28453956]

[282]. Ta HT, Arndt N, Wu Y, Lim HJ, Landeen S, Zhang R, Kamato D, Little PJ, Whittaker AK, Xu ZP, Activatable magnetic resonance nanosensor as a potential imaging agent for detecting and discriminating thrombosis, Nanoscale, 10 (2018) 15103–15115. [PubMed: 30059122]

[283]. Qiao H, Wang Y, Zhang R, Gao Q, Liang X, Gao L, Jiang Z, Qiao R, Han D, Zhang Y, Qiu Y, Tian J, Gao M, Cao F, MRI/optical dual-modality imaging of vulnerable atherosclerotic plaque with an osteopontin-targeted probe based on Fe3O4 nanoparticles, Biomaterials, 112 (2017) 336–345. [PubMed: 27788352]

[284]. Su T, Wang YB, Han D, Wang J, Qi S, Gao L, Shao YH, Qiao HY, Chen JW, Liang SH, Nie YZ, Li JY, Cao F, Multimodality imaging of angiogenesis in a rabbit atherosclerotic model by GEBP11 peptide targeted nanoparticles, Theranostics, 7 (2017) 4791–4804. [PubMed: 29187904]

[285]. Lariviere M, Lorenzato CS, Adumeau L, Bonnet S, Hemadou A, Jacobin-Valat MJ, Noubhani A, Santarelli X, Minder L, Di Primo C, Sanchez S, Mornet S, Laroche-Traineau J, Clofent-Sanchez G, Multimodal molecular imaging of atherosclerosis: Nanoparticles functionalized with scFv fragments of an anti-alphaIIbbeta3 antibody, Nanomedicine, 22 (2019) 102082. [PubMed: 31404651]

[286]. Stein-Merlob AF, Hara T, McCarthy JR, Mauskapf A, Hamilton JA, Ntziachristos V, Libby P, Jaffer FA, Atheroma susceptible to thrombosis exhibit impaired endothelial permeability in vivo as assessed by nanoparticle-based fluorescence molecular imaging, Circ Cardiovasc Imaging, 10 (2017) e005813. [PubMed: 28487316]

[287]. Liu Y, Wu Y, Zhang R, Lam J, Ng JC, Xu ZP, Li L, Ta HT, Investigating the use of layered double hydroxide nanoparticles as carriers of metal oxides for theranostics of ROS-related diseases, ACS Appl. Bio Mater, 2 (2019) 5930–5940.

[288]. Reimann C, Brangsch J, Kaufmann JO, Adams LC, Onthank DC, Thone-Reineke C, Robinson SP, Hamm B, Botnar RM, Makowski MR, Dual-probe molecular MRI for the in vivo characterization of atherosclerosis in a mouse model: simultaneous assessment of plaque inflammation and extracellular-matrix remodeling, Sci. Rep, 9 (2019) 13827. [PubMed: 31554825]

[289]. Hucker WJ, Jaffer FA, F-FDG PET imaging of atherosclerosis-a new approach to detect inflamed, high-risk coronary plaques?, Curr Cardiovasc Imaging Rep, 4 (2011) 1–3. [PubMed: 21297872]

[290]. Liang M, Tan H, Zhou J, Wang T, Duan D, Fan K, He J, Cheng D, Shi H, Choi HS, Yan X, Bioengineered H-ferritin nanocages for quantitative imaging of vulnerable plaques in atherosclerosis, ACS Nano, 12 (2018) 9300–9308. [PubMed: 30165015]

[291]. Wang T, He J, Duan D, Jiang B, Wang P, Fan K, Liang M, Yan X, Bioengineered magnetoferritin nanozymes for pathological identification of high-risk and ruptured atherosclerotic plaques in humans, Nano Res, 12 (2019) 863–868.

[292]. Smits LP, Tiessens F, Zheng KH, Stroes ES, Nederveen AJ, Coolen BF, Evaluation of ultrasmall superparamagnetic iron-oxide (USPIO) enhanced MRI with ferumoxytol to quantify arterial wall inflammation, Atherosclerosis, 263 (2017) 211–218. [PubMed: 28662398]

[293]. Stirrat CG, Alam SR, MacGillivray TJ, Gray CD, Forsythe R, Dweck MR, Payne JR, Prasad SK, Petrie MC, Gardner RS, Mirsadraee S, Henriksen PA, Newby DE, Semple SI, Ferumoxytol-enhanced magnetic resonance imaging methodology and normal values at 1.5 and 3T, J Cardiovasc Magn Reson, 18 (2016) 46. [PubMed: 27465647]

[294]. Poon C, Gallo J, Joo J, Chang T, Banobre-Lopez M, Chung EJ, Hybrid, metal oxide-peptide amphiphile micelles for molecular magnetic resonance imaging of atherosclerosis, J Nanobiotechnology, 16 (2018) 92. [PubMed: 30442135]

[295]. Kao CW, Wu PT, Liao MY, Chung IJ, Yang KC, Tseng WI, Yu J, Magnetic nanoparticles conjugated with peptides derived from monocyte chemoattractant protein-1 as a tool for targeting atherosclerosis, Pharmaceutics, 10 (2018) p.62.

[296]. Tarin C, Carril M, Martin-Ventura JL, Markuerkiaga I, Padro D, Llamas-Granda P, Moreno JA, Garcia I, Genicio N, Plaza-Garcia S, Blanco-Colio LM, Penades S, Egido J, Targeted gold-coated iron oxide nanoparticles for CD163 detection in atherosclerosis by MRI, Sci. Rep, 5 (2015) 17135. [PubMed: 26616677]

[297]. Hedgire S, Krebill C, Wojtkiewicz GR, Oliveira I, Ghoshhajra BB, Hoffmann U, Harisinghani MG, Ultrasmall superparamagnetic iron oxide nanoparticle uptake as noninvasive marker of aortic wall inflammation on MRI: proof of concept study, Br J Radiol, 91 (2018) 20180461. [PubMed: 30160173]

[298]. Chhour P, Naha PC, O'Neill SM, Litt HI, Reilly MP, Ferrari VA, Cormode DP, Labeling monocytes with gold nanoparticles to track their recruitment in atherosclerosis with computed tomography, Biomaterials, 87 (2016) 93–103. [PubMed: 26914700]

[299]. Kwon SP, Jeon S, Lee SH, Yoon HY, Ryu JH, Choi D, Kim JY, Kim J, Park JH, Kim DE, Kwon IC, Kim K, Ahn CH, Thrombin-activatable fluorescent peptide incorporated gold nanoparticles for dual optical/computed tomography thrombus imaging, Biomaterials, 150 (2018) 125–136. [PubMed: 29035738]

[300]. Li L, Wang J, Wu M, He Y, Zhang H, Xu G, Chen L, Jia X, Guo Q, Zhang X, Macrophage-targeted and clearable glutathione-based MRI nanoprobes for atherosclerosis molecular imaging, J Nanopart Res, 21 (2019) 231.

[301]. Wang J, Wu M, Chang J, Li L, Guo Q, Hao J, Peng Q, Zhang B, Zhang X, Li X, Scavenger receptor-AI-targeted ultrasmall gold nanoclusters facilitate in vivo MR and ex vivo fluorescence dual-modality visualization of vulnerable atherosclerotic plaques, Nanomedicine, 19 (2019) 81–94. [PubMed: 31028886]

[302]. Chen H, Chen L, Liang R, Wei J, Ultrasound and magnetic resonance molecular imaging of atherosclerotic neovasculature with perfluorocarbon magnetic nanocapsules targeted against vascular endothelial growth factor receptor 2 in rats, Mol. Med. Rep, 16 (2017) 5986–5996. [PubMed: 28849045]

[303]. Liu Y, Luehmann HP, Detering L, Pressly ED, McGrath AJ, Sultan D, Nguyen A, Grathwohl S, Shokeen M, Zayed M, Gropler RJ, Abendschein D, Hawker CJ, Woodard PK, Assessment of targeted nanoparticle assemblies for atherosclerosis imaging with positron emission tomography and potential for clinical translation, ACS Appl. Mater, 11 (2019) 15316–15321.

[304]. Chen JA, Guo W, Wang Z, Sun N, Pan H, Tan J, Ouyang Z, Fu W, Wang Y, Hu W, Gu X, In Vivo Imaging of Senescent Vascular Cells in Atherosclerotic Mice Using a β-Galactosidase-Activatable Nanoprobe, Anal. Chem, 92 (2020) 12613–12621. [PubMed: 32786453]

[305]. Woodside DG, Tanifum EA, Ghaghada KB, Biediger RJ, Caivano AR, Starosolski ZA, Khounlo S, Bhayana S, Abbasi S, Craft JW Jr., Maxwell DS, Patel C, Stupin IV, Bakthavatsalam D, Market RV, Willerson JT, Dixon RAF, Vanderslice P, Annapragada AV, Magnetic resonance

imaging of atherosclerotic plaque at clinically relevant field strengths (1T) by targeting the integrin alpha4beta1, Sci. Rep, 8 (2018) 3733. [PubMed: 29487319]

[306]. Narita Y, Shimizu K, Ikemoto K, Uchino R, Kosugi M, Maess MB, Magata Y, Oku N, Ogawa M, Macrophage-targeted, enzyme-triggered fluorescence switch-on system for detection of embolism-vulnerable atherosclerotic plaques, J. Control. Release, 302 (2019) 105–115. [PubMed: 30936020]

[307]. Lobatto ME, Binderup T, Robson PM, Giesen LFP, Calcagno C, Witjes J, Fay F, Baxter S, Wessel CH, Eldib M, Bini J, Carlin SD, Stroes ESG, Storm G, Kjaer A, Lewis JS, Reiner T, Fayad ZA, Mulder WJM, Perez-Medina C, Multimodal positron emission tomography imaging to quantify uptake of (89)Zr-Labeled liposomes in the atherosclerotic vessel wall, Bioconjugate Chem, 31 (2020) 360–368.

[308]. Ye S, Liu Y, Lu Y, Ji Y, Mei L, Yang M, Gong X, Gu Q, Li D, Yang F, Li CJ, Cyclic RGD functionalized liposomes targeted to activated platelets for thrombosis dual-mode magnetic resonance imaging, J. Mater. Chem. B, 8 (2020) 447–453. [PubMed: 31833530]

[309]. Poon C, Sarkar M, Chung EJ, Synthesis of monocyte-targeting peptide amphiphile micelles for imaging of atherosclerosis, J Vis Exp, (2017) e56625.

[310]. Chin DD, Wang J, Mel de Fontenay M, Plotkin A, Magee GA, Chung EJ, Hydroxyapatite-binding micelles for the detection of vascular calcification in atherosclerosis, J. Mater. Chem. B, 7 (2019) 6449–6457. [PubMed: 31553027]

[311]. Qiao R, Qiao H, Zhang Y, Wang Y, Chi C, Tian J, Zhang L, Cao F, Gao M, Molecular imaging of vulnerable atherosclerotic plaques in vivo with osteopontin-specific upconversion nanoprobes, ACS Nano, 11 (2017) 1816–1825. [PubMed: 28121134]

[312]. Wang Y, Zhang Y, Wang Z, Zhang J, Qiao RR, Xu M, Yang N, Gao L, Qiao H, Gao M, Cao F, Optical/MRI dual-modality imaging of M1 macrophage polarization in atherosclerotic plaque with MARCO-targeted upconversion luminescence probe, Biomaterials, 219 (2019) 119378. [PubMed: 31382209]

[313]. Sun X, Li W, Zhang X, Qi M, Zhang Z, Zhang XE, Cui Z, In vivo targeting and imaging of atherosclerosis using multifunctional virus-like particles of simian virus 40, Nano Lett, 16 (2016) 6164–6171. [PubMed: 27622963]

[314]. Aanei IL, Huynh T, Seo Y, Francis MB, Vascular cell adhesion molecule-targeted MS2 viral capsids for the detection of early-stage atherosclerotic plaques, Bioconjugate Chem, 29 (2018) 2526–2530.

[315]. Bonnard T, Jayapadman A, Putri JA, Cui J, Ju Y, Carmichael C, Angelovich TA, Cody SH, French S, Pascaud K, Pearce HA, Jagdale S, Caruso F, Hagemeyer CE, Low-fouling and biodegradable protein-based particles for thrombus imaging, ACS Nano, 12 (2018) 6988–6996. [PubMed: 29874911]

[316]. Gao W, Li X, Liu Z, Fu W, Sun Y, Cao W, Tong L, Tang B, A Redox-responsive self-assembled nanoprobe for photoacoustic inflammation imaging to assess atherosclerotic plaque vulnerability, Anal. Chem, 91 (2019) 1150–1156. [PubMed: 30497260]

[317]. Kim HJ, Capacitance imaging for the discrimination of lipid region in atherosclerotic plaque ex vivo using polypyrrole-coated multi-walled carbon nanotube multi-electrode array, Curr. Appl. Phys, 19 (2019) 1238–1244.

[318]. Park J, Gao H, Wang Y, Hu H, Simon DI, Steinmetz NF, S100A9-targeted tobacco mosaic virus nanoparticles exhibit high specificity toward atherosclerotic lesions in ApoE(−/−) mice, Vase. Pharmacol, 7 (2019) 1842–1846.

[319]. Xue Y, Wu Y, Wang Q, Xue L, Su Z, Zhang C, Cellular vehicles based on neutrophils enable targeting of atherosclerosis, Mol. Pharm, 16 (2019) 3109–3120. [PubMed: 31082253]

[320]. Wu Z, Chen C, Zhang B, Tang L, Shi W, Liao D, Di G, Davis JR, Wang H, EGFP-EGF1-conjugated poly(lactic-co-glycolic acid) nanoparticles, a new diagnostic tool and drug carrier for atherosclerosis, Int. J. Nanomedicine, 14 (2019) 2609–2618. [PubMed: 31043777]

[321]. Brusini R, Dormont F, Cailleau C, Nicolas V, Peramo A, Varna M, Couvreur P, Squalene-based nanoparticles for the targeting of atherosclerotic lesions, Int. J. Pharm, 581 (2020) 119282. [PubMed: 32259640]

[322]. Darwitan A, Tan YF, Wong YS, Nedumaran AM, Czarny B, Venkatraman S, Targeting efficiency of nanoliposomes on atherosclerotic foam cells: polyethylene glycol-to-ligand ratio effects, Expert Opin. Drug Deliv, 17 (2020) 1165–1176. [PubMed: 32484723]

[323]. Li X, Kim J, Yoon J, Chen X, Cancer-associated, stimuli-driven, turn on theranostics for multimodality imaging and therapy, Adv. Mater, 29 (2017) 1606857.

[324]. Huang X, El-Sayed MA, Plasmonic photo-thermal therapy (PPTT), Alexandria J. Med, 47 (2011) 1–9.

[325]. Zhi D, Yang T, O'Hagan J, Zhang S, Donnelly RF, Photothermal therapy, J. Control. Release, 325 (2020) 52–71. [PubMed: 32619742]

[326]. Dos Santos AIF, De Almeida DRQ, Terra LF, Baptista M.c.S., Labriola L, Photodynamic therapy in cancer treatment-an update review, J. Cancer Metastasis Treat, 5 (2019) 10.20517.

[327]. Yan K, Zhang Y, Mu C, Xu Q, Jing X, Wang D, Dang D, Meng L, Ma J, Versatile nanoplatforms with enhanced photodynamic therapy: designs and applications, Theranostics, 10 (2020) 7287–7318. [PubMed: 32641993]

[328]. Kim H, Kim Y, Kim IH, Kim K, Choi Y, ROS-responsive activatable photosensitizing agent for imaging and photodynamic therapy of activated macrophages, Theranostics, 4 (2013) 1–11. [PubMed: 24396511]

[329]. Park D, Cho Y, Goh SH, Choi Y, Hyaluronic acid–polypyrrole nanoparticles as pH-responsive theranostics, ChemComm, 50 (2014) 15014–15017.

[330]. Wang TY, Kendrick-Williams LL, Choy MY, Gilmore KA, Bonnard T, Pearce HA, Law LS, Carmichael I, Cody SH, Alt K, Hagemeyer CE, Harth E, Collagen-targeted theranostic nanosponges for delivery of the matrix metalloproteinase 14 inhibitor naphthofluorescein, Chem. Mater, 32 (2020) 3707–3714.

[331]. Stigliano C, Ramirez MR, Singh JV, Aryal S, Key J, Blanco E, Decuzzi P, Methotraxate-loaded hybrid nanoconstructs target vascular lesions and inhibit atherosclerosis progression in apoE−/− mice, Adv. Healthcare Mater, 6 (2017) 1601286.

[332]. Majmudar MD, Keliher EJ, Heidt T, Leuschner F, Truelove J, Sena BF, Gorbatov R, Iwamoto Y, Dutta P, Wojtkiewicz G, Monocyte-directed RNAi targeting CCR2 improves infarct healing in atherosclerosis-prone mice, Circulation, 127 (2013) 2038–2046. [PubMed: 23616627]

[333]. Lobatto ME, Fayad ZA, Silvera S, Vucic E, Calcagno C, Mani V, Dickson SD, Nicolay K, Banciu M, Schiffelers RM, Multimodal clinical imaging to longitudinally assess a nanomedical anti-inflammatory treatment in experimental atherosclerosis, Mol Pharm, 7 (2010) 2020–2029. [PubMed: 21028895]

[334]. Bagalkot V, Badgeley MA, Kampfrath T, Deiuliis JA, Rajagopalan S, Maiseyeu A, Hybrid nanoparticles improve targeting to inflammatory macrophages through phagocytic signals, J. Control. Release, 217 (2015) 243–255. [PubMed: 26386437]

[335]. Mog B, Asase C, Chaplin A, Gao H, Rajagopalan S, Maiseyeu A, Nano-antagonist alleviates inflammation and allows for MRI of atherosclerosis, Nanotheranostics, 3 (2019) 342–355. [PubMed: 31723548]

[336]. Dong Y, Chen H, Chen C, Zhang X, Tian X, Zhang Y, Shi Z, Liu Q, Polymer-lipid hybrid theranostic nanoparticles co-delivering ultrasmall superparamagnetic iron oxide and paclitaxel for targeted magnetic resonance imaging and therapy in atherosclerotic plaque, J Biomed Nanotechnol, 12 (2016) 1245–1257. [PubMed: 27319218]

[337]. Ma B, Xu H, Zhuang W, Wang Y, Li G, Wang Y, Reactive oxygen species responsive theranostic nanoplatform for two-photon aggregation-induced emission imaging and therapy of acute and chronic inflammation, ACS Nano, 14 (2020) 5862–5873. [PubMed: 32379416]

[338]. Chin DD, Poon C, Trac N, Wang J, Cook J, Joo J, Jiang Z, Sta Maria NS, Jacobs RE, Chung EJ, Collagenase-cleavable peptide amphiphile micelles as a novel theranostic strategy in atherosclerosis, Adv. Ther, 3 (2020) 1900196.

[339]. Qin J, Peng Z, Li B, Ye K, Zhang Y, Yuan F, Yang X, Huang L, Hu J, Lu X, Gold nanorods as a theranostic platform for in vitro and in vivo imaging and photothermal therapy of inflammatory macrophages, Nanoscale, 7 (2015) 13991–14001. [PubMed: 26228112]

[340]. Gongalves DPVKO, Courrol LC,, Synthesis and characterization of aminolevulinic acid gold nanoparticles: photo and sonosensitizer agent for atherosclerosis, J. Lumin, 197 (2018) 317–323.

[341]. Yeager D, Chen Y-S, Litovsky S, Emelianov S, Intravascular photoacoustics for image-guidance and temperature monitoring during plasmonic photothermal therapy of atherosclerotic plaques: a feasibility study, Theranostics, 4 (2014) 36.

[342]. Jaffer FA, Nahrendorf M, Sosnovik D, Kelly KA, Aikawa E, Weissleder R, Cellular imaging of inflammation in atherosclerosis using magnetofluorescent nanomaterials, Mol. Imaging, 5 (2006) 85–92. [PubMed: 16954022]

[343]. McCarthy JR, Korngold E, Weissleder R, Jaffer FA, A light-activated theranostic nanoagent for targeted macrophage ablation in inflammatory atherosclerosis, Small 6(2010) 2041–2049. [PubMed: 20721949]

[344]. Zhang S, Xu W, Gao P, Chen W, Zhou Q, Construction of dual nanomedicines for the imaging and alleviation of atherosclerosis, Artif. Cells Nanomed. Biotechnol, 48 (2020) 169–179. [PubMed: 31852323]

[345]. Yao Y, Li B, Fu C, Teng G, Ma G, Liu N, Anti-connective tissue growth factor detects and reduces plaque inflammation in early-stage carotid atherosclerotic lesions, Nanomed-Nanotechnol, 13 (2017) 2385–2394.

[346]. Ma LL, Feldman MD, Tam JM, Paranjape AS, Cheruku KK, Larson TA, Tam JO, Ingram DR, Paramita V, Villard JW, Jenkins JT, Wang T, Clarke GD, Asmis R, Sokolov K, Chandrasekar B, Milner TE, Johnston KP, Small multifunctional nanoclusters (nanoroses) for targeted cellular imaging and therapy, ACS Nano, 3 (2009) 2686–2696. [PubMed: 19711944]

[347]. Ye M, Zhou J, Zhong Y, Xu J, Hou J, Wang X, Wang Z, Guo D, SR-A-targeted phase-transition nanoparticles for the detection and treatment of atherosclerotic vulnerable plaques, ACS Appl. Mater, 11 (2019) 9702–9715.

[348]. Liu J, Guo X, Zhao Z, Li B, Qin J, Peng Z, He G, Brett DJ, Wang R, Lu X, Fe3S4 nanoparticles for arterial inflammation therapy: Integration of magnetic hyperthermia and photothermal treatment, Appl. Mater. Today 18 (2020) 100457.

[349]. Gao W, Sun Y, Cai M, Zhao Y, Cao W, Liu Z, Cui G, Tang B, Copper sulfide nanoparticles as a photothermal switch for TRPV1 signaling to attenuate atherosclerosis, Nat. Commun, 9 (2018) 231. [PubMed: 29335450]

[350]. Khurana A, Tekula S, Saifi MA, Venkatesh P, Godugu C, Therapeutic applications of selenium nanoparticles, Biomed. Pharmacother, 111 (2019) 802–812. [PubMed: 30616079]

[351]. Lu KY, Lin PY, Chuang EY, Shih CM, Cheng TM, Lin TY, Sung HW, Mi FL, H2O2-depleting and O2-generating selenium nanoparticles for fluorescence imaging and photodynamic treatment of proinflammatory-activated macrophages, ACS Appl. Mater, 9 (2017) 5158–5172.

[352]. Ma S, Motevalli SM, Chen J, Xu MQ, Wang Y, Feng J, Qiu Y, Han D, Fan M, Ding M, Fan L, Guo W, Liang XJ, Cao F, Precise theranostic nanomedicines for inhibiting vulnerable atherosclerotic plaque progression through regulation of vascular smooth muscle cell phenotype switching, Theranostics, 8 (2018) 3693–3706. [PubMed: 30026877]

[353]. Wu G, Wei W, Zhang J, Nie W, Yuan L, Huang Y, Zuo L, Huang L, Xi X, Xie HY, A self-driven bioinspired nanovehicle by leukocyte membrane-hitchhiking for early detection and treatment of atherosclerosis, Biomaterials, 250 (2020) 119963. [PubMed: 32334199]

[354]. Martinez JO, Molinaro R, Hartman KA, Boada C, Sukhovershin R, De Rosa E, Kirui D, Zhang S, Evangelopoulos M, Carter AM, Bibb JA, Cooke JP, Tasciotti E, Biomimetic nanoparticles with enhanced affinity towards activated endothelium as versatile tools for theranostic drug delivery, Theranostics, 8 (2018) 1131–1145. [PubMed: 29464004]

[355]. Wu G, Zhang J, Zhao Q, Zhuang W, Ding J, Zhang C, Gao H, Pang DW, Pu K, Xie HY, Molecularly engineered macrophage-derived exosomes with inflammation tropism and intrinsic heme biosynthesis for atherosclerosis treatment, Angew. Chem. Int. Ed, 59 (2020) 4068–4074.

[356]. Schmitz SA, Taupitz M, Wagner S, Wolf KJ, Beyersdorff D, Hamm B, Magnetic resonance imaging of atherosclerotic plaques using superparamagnetic iron oxide particles, J Magn Reson Imaging, 14 (2001) 355–361. [PubMed: 11599058]

[357]. Nissen SE, Tsunoda T, Tuzcu EM, Schoenhagen P, Cooper CJ, Yasin M, Eaton GM, Lauer MA, Sheldon WS, Grines CL, Halpern S, Crowe T, Blankenship JC, Kerensky R, Effect of recombinant ApoA-I Milano on coronary atherosclerosis in patients with acute coronary syndromes: a randomized controlled trial, Jama, 290 (2003) 2292–2300. [PubMed: 14600188]

[358]. Kooi ME, Cappendijk VC, Cleutjens KB, Kessels AG, Kitslaar PJ, Borgers M, Frederik PM, Daemen MJ, van Engelshoven JM, Accumulation of ultrasmall superparamagnetic particles of iron oxide in human atherosclerotic plaques can be detected by in vivo magnetic resonance imaging, Circulation, 107 (2003) 2453–2458. [PubMed: 12719280]

[359]. Tang TY, Howarth SP, Miller SR, Graves MJ, JM UK-I, Li ZY, Walsh SR, Hayes PD, Varty K, Gillard JH, Comparison of the inflammatory burden of truly asymptomatic carotid atheroma with atherosclerotic plaques in patients with asymptomatic carotid stenosis undergoing coronary artery bypass grafting: an ultrasmall superparamagnetic iron oxide enhanced magnetic resonance study, Eur J Vase Endovasc Surg, 35 (2008) 392–398.

[360]. Tang TY, Howarth SP, Li ZY, Miller SR, Graves MJ, JM UK-I, Trivedi RA, Walsh SR, Brown AP, Kirkpatrick PJ, Gaunt ME, Gillard JH, Correlation of carotid atheromatous plaque inflammation with biomechanical stress: utility of USPIO enhanced MR imaging and finite element analysis, Atherosclerosis, 196 (2008) 879–887. [PubMed: 17350023]

[361]. Tang TY, Howarth SP, Miller SR, Graves MJ, Patterson AJ, JM UK-I, Li ZY, Walsh SR, Brown AP, Kirkpatrick PJ, Warburton EA, Hayes PD, Varty K, Boyle JR, Gaunt ME, Zalewski A, Gillard JH, The ATHEROMA (atorvastatin therapy: effects on reduction of macrophage activity) study, evaluation using ultrasmall superparamagnetic iron oxide-enhanced magnetic resonance imaging in carotid disease, J. Am. Coll. Cardiol, 53 (2009) 2039–2050. [PubMed: 19477353]

[362]. Howarth SP, Tang TY, Trivedi R, Weerakkody R, J UK-I, Gaunt ME, Boyle JR, Li ZY, Miller SR, Graves MJ, Gillard JH, Utility of USPIO-enhanced MR imaging to identify inflammation and the fibrous cap: a comparison of symptomatic and asymptomatic individuals, Eur J Radiol, 70 (2009) 555–560. [PubMed: 18356000]

[363]. Tardif JC, Ballantyne CM, Barter P, Dasseux JL, Fayad ZA, Guertin MC, Kastelein JJ, Keyserling C, Klepp H, Koenig W, L'Allier PL, Lespérance J, Lüscher JF, Paolini JF, Tawakol A, Waters DD, Effects of the high-density lipoprotein mimetic agent CER-001 on coronary atherosclerosis in patients with acute coronary syndromes: a randomized trial, Eur Heart J, 35 (2014) 3277–3286. [PubMed: 24780501]

[364]. van der Valk FM, van Wijk DF, Lobatto ME, Verberne HJ, Storm G, Willems MC, Legemate DA, Nederveen AJ, Calcagno C, Mani V, Ramachandran S, Paridaans MP, Otten MJ, Dallinga-Thie GM, Fayad ZA, Nieuwdorp M, Schulte DM, Metselaar JM, Mulder WJ, Stroes ES, Prednisolone-containing liposomes accumulate in human atherosclerotic macrophages upon intravenous administration, Nanomedicine, 11 (2015) 1039–1046. [PubMed: 25791806]

[365]. Tricoci P, D'Andrea DM, Gurbel PA, Yao Z, Cuchel M, Winston B, Schott R, Weiss R, Blazing MA, Cannon L, Bailey A, Angiolillo DJ, Gille A, Shear CL, Wright SD, Alexander JH, Infusion of reconstituted high-density lipoprotein, CSL112, in patients with atherosclerosis: safety and pharmacokinetic results from a phase 2a randomized clinical trial, J. Am. Heart. Assoc, 4 (2015) e002171. [PubMed: 26307570]

[366]. Kharlamov AN, Tyurnina AE, Veselova VS, Kovtun OP, Shur VY, Gabinsky JL, Silica-gold nanoparticles for atheroprotective management of plaques: results of the NANOM-FIM trial, Nanoscale, 7 (2015) 8003–8015. [PubMed: 25864858]

[367]. Kharlamov A, CRT-800.01 glagovian window of external elastic membrane enlargement as cornerstone phenomenon of artery remodeling in natural history of atherosclerosis: subanalysis of NANOM-FIM trial, JACC Cardiovasc. Interv , 9 (2016) S61.

[368]. Shiozaki AA, Senra T, Morikawa AT, Deus DF, Paladino-Filho AT, Pinto IMF, Maranhão RC, Treatment of patients with aortic atherosclerotic disease with paclitaxel-associated lipid nanoparticles, Clinics (Sao Paulo), 71 (2016) 435–439. [PubMed: 27626473]

[369]. Stirrat CG, Alam SR, MacGillivray TJ, Gray CD, Forsythe R, Dweck MR, Payne JR, Prasad SK, Petrie MC, Gardner RS, Mirsadraee S, Henriksen PA, Newby DE, Semple SIK, Ferumoxytol-enhanced magnetic resonance imaging methodology and normal values at 1.5 and 3T, J Cardiovasc Magn Reson, 18 (2016) 46. [PubMed: 27465647]

[370]. Zheng KH, van der Valk FM, Smits LP, Sandberg M, Dasseux J-L, Baron R, Barbaras R, Keyserling C, Coolen BF, Nederveen AJ, Verberne HJ, Nell TE, Vugts DJ, Duivenvoorden R, Fayad ZA, Mulder WJM, van Dongen GAMS, Stroes ESG, HDL mimetic CER-001 targets atherosclerotic plaques in patients, Atherosclerosis, 251 (2016) 381–388. [PubMed: 27263077]

[371]. Styllou P, Silber S, A case report of the new Polyzene™-F COBRA PzF™ Nanocoated Coronary Stent System (NCS): Addressing an unmet clinical need, Cardiovasc Revasc Med , 17 (2016) 209–211. [PubMed: 26944851]

[372]. Kallend DG, Reijers JAA, Bellibas SE, Bobillier A, Kempen H, Burggraaf J, Moerland M, Wijngaard PLJ, A single infusion of MDCO-216 (ApoA-1 Milano/POPC) increases ABCA1-mediated cholesterol efflux and pre-beta 1 HDL in healthy volunteers and patients with stable coronary artery disease, Eur Heart J, 2 (2016) 23–29.

[373]. Kempen HJ, Gomaraschi M, Simonelli S, Calabresi L, Moerland M, Otvos J, Jeyarajah E, Kallend D, Wijngaard PLJ, Persistent changes in lipoprotein lipids after a single infusion of ascending doses of MDCO-216 (apoA-IMilano/POPC) in healthy volunteers and stable coronary artery disease patients, Atherosclerosis, 255 (2016) 17–24. [PubMed: 27816804]

[374]. Kempen Herman J, Asztalos Bela F, Moerland M, Jeyarajah E, Otvos J, Kallend David G, Bellibas SE, Wijngaard Peter LJ, High-density lipoprotein subfractions and cholesterol efflux capacities after infusion of MDCO-216 (Apolipoprotein A-IMilano/Palmitoyl-Oleoyl-Phosphatidylcholine) in Healthy Volunteers and Stable Coronary Artery Disease Patients, Arterioscler. Thromb. Vase. Biol, 36 (2016) 736–742.

[375]. Maillard L, Tavildari A, Barra N, Bille J, Joly P, Peycher P, Silvestri M, Vochelet F, Immediate and 1-year follow-up with the novel nanosurface modified COBRA PzF stent, Arch. Cardiovasc. Dis , 110 (2017) 682–688. [PubMed: 29102364]

[376]. Cutlip DE, Garratt KN, Novack V, Barakat M, Meraj P, Maillard L, Erglis A, Jauhar R, Popma JJ, Stoler R, Silber S, Cutlip D, Allaqaband S, Caputo R, Beohar N, Brown D, Garratt K, Jauhar R, George J, Varghese V, Huth M, Larrain G, Lee T, Malik A, Martin S, McGarry T, Phillips C, Shah A, Stoler R, Ball M, Price RJ, Rossi J, Taylor C, Tolleson T, Nicholson W, Kesanakurthy S, Shoukfeh M, Finn A, Devireddy C, Shoultz C, Robbins M, Kiesz R, Menon P, Weilenmann D, Sievert H, Erglis A, Stankovic G, Berland J, Delarche N, Hirsch JL, Maillard L, Shayne J, Serra A, Fernandez-Ortiz A, Monassier JP, Silber S, 9-Month clinical and angiographic outcomes of the COBRA polyzene-F nanocoated coronary stent system, JACC Cardiovasc. Interv , 10 (2017) 160–167. [PubMed: 28104210]

[377]. Kataoka Y, Andrews J, Duong M, Nguyen T, Schwarz N, Fendler J, Puri R, Butters J, Keyserling C, Paolini JF, Dasseux JL, Nicholls SJ, Regression of coronary atherosclerosis with infusions of the high-density lipoprotein mimetic CER-001 in patients with more extensive plaque burden, Cardiovasc Diagn Ther, 7 (2017) 252–263. [PubMed: 28567351]

[378]. Andrews J, Janssan A, Nguyen T, Pisaniello AD, Scherer DJ, Kastelein JJP, Merkely B, Nissen SE, Ray K, Schwartz GG, Worthley SG, Keyserling C, Dasseux J-L, Butters J, Girardi J, Miller R, Nicholls SJ, Effect of serial infusions of reconstituted high-density lipoprotein (CER-001) on coronary atherosclerosis: rationale and design of the CARAT study, Cardiovasc Diagn Ther, 7 (2017) 45–51. [PubMed: 28164012]

[379]. Keyserling CH, Barbaras R, Benghozi R, Dasseux J-L, Development of CER-001: preclinical dose selection through to phase I clinical findings, Clin. Drug Investig, 37 (2017) 483–491.

[380]. Kharlamov AN, Feinstein JA, Cramer JA, Boothroyd JA, Shishkina EV, Shur V, Plasmonic photothermal therapy of atherosclerosis with nanoparticles: long-term outcomes and safety in NANOM-FIM trial, Future Cardiol, 13 (2017) 345–363. [PubMed: 28644056]

[381]. Kharlamov A, Plasmonic photothermal therapy of atherosclerosis proves atheroprotective effectiveness for real clinical practice: long-term subanalysis from NANOM-FIM, XVIII International Symposium on AtherosclerosisToronto, Canada, 2018.

[382]. Nicholls SJ, Puri R, Ballantyne CM, Jukema JW, Kastelein JJP, Koenig W, Wright RS, Kallend D, Wijngaard P, Borgman M, Wolski K, Nissen SE, Effect of infusion of high-density lipoprotein mimetic containing recombinant apolipoprotein A-I milano on coronary disease in patients with an acute cornary syndrome in the MILANO-PILOT trial: a randomized clinical trial, JAMA cardiology, 3 (2018) 806–814. [PubMed: 30046837]

[383]. Gille A, D'Andrea D, Tortorici MA, Hartel G, Wright SD, CSL112 (Apolipoprotein A-I [Human]) enhances cholesterol efflux similarly in healthy individuals and stable atherosclerotic disease patients, Arterioscler. Thromb. Vase. Biol, 38 (2018) 953–963.

[384]. Gurbel PA, Tantry US, D'Andrea D, Chung T, Alexander JH, Bliden KP, Wright SD, Tricoci P, Evaluation of potential antiplatelet effects of CSL112 (Apolipoprotein A-l [Human]) in patients

with atherosclerosis: results from a phase 2a study, J. Thromb. Thrombolysis, 45 (2018) 469–476. [PubMed: 29582212]

[385]. Kharlamov A, Plasmonic photothermal therapy o atherosclerosis and preparation of target lesion in patients with arterial remodeling: subanalysis of nanom-fim trial, Atherosclerosis, 287 (2019) e34.

[386]. Maillard L, Vochelet F, Peycher P, Ayari A, Barra N, Billé J, Joly P, Silvestri M, Sévilla J, Tavildari A, MAPT (mono antiplatelet therapy) as regular regimen after COBRA PzF™ nanocoated coronary stent (NCS) implantation, Cardiovasc Revasc Med. , 21 (2020) 785–789. [PubMed: 31780418]

[387]. Zheng KH, Schoormans J, Stiekema LCA, Calcagno C, Cicha I, Alexiou C, Strijkers GJ, Nederveen AJ, Stroes ESG, Coolen BF, Plaque permeability assessed With DCE-MRI associates with USPIO uptake in patients with peripheral artery disease, JACC Cardiovasc. Imaging, 12 (2019) 2081–2083. [PubMed: 31202746]

[388]. Zheng KH, Kaiser Y, van Olden CC, Santos RD, Dasseux J-L, Genest J, Gaudet D, Westerink J, Keyserling C, Verberne HJ, No benefit of HDL mimetic CER-001 on carotid atherosclerosis in patients with genetically determined very low HDL levels, Atherosclerosis, 311 (2020) 13–19. [PubMed: 32919280]

[389]. Maillard L, de Labriolle A, Brasselet C, Faurie B, Durel N, de Poli F, Bosle S, Madiot H, Berland J, Belle L, Evaluation of the safety and efficacy of the Cobra PzF NanoCoated coronary stent in routine, consecutive, prospective, and high-risk patients: The e-Cobra study, Catheter. Cardiovasc. Interv, 29065 (2020) 1–10.

[390]. Usman A, Patterson AJ, Yuan J, Cluroe A, Patterson I, Graves MJ, Gillard JH, Sadat U, Ferumoxytol-enhanced three-dimensional magnetic resonance imaging of carotid atheroma- a feasibility and temporal dependence study, Sci. Rep, 10 (2020) 1808. [PubMed: 32020031]

[391]. van der Valk FM, Schulte DM, Meiler S, Tang J, Zheng KH, Van den Bossche J, Seijkens T, Laudes M, de Winther M, Lutgens E, Alaarg A, Metselaar JM, Dallinga-Thie GM, Mulder WJ, Stroes ES, Hamers AA, Liposomal prednisolone promotes macrophage lipotoxicity in experimental atherosclerosis, Nanomedicine, 12 (2016) 1463–1470. [PubMed: 27015770]

[392]. Kempen HJ, Gomaraschi M, Bellibas SE, Plassmann S, Zerler B, Collins HL, Adelman SJ, Calabresi L, Wijngaard PL, Effect of repeated apoA-IMilano/POPC infusion on lipids, (apo)lipoproteins, and serum cholesterol efflux capacity in cynomolgus monkeys, J. Lipid Res, 54 (2013) 2341–2353. [PubMed: 23828780]

[393]. Kharlamov AN, Gabinsky JL, Plasmonic photothermic and stem cell therapy of atherosclerotic plaque as a novel nanotool for angioplasty and artery remodeling, Rejuvenation Res, 15 (2012) 222–230. [PubMed: 22533437]

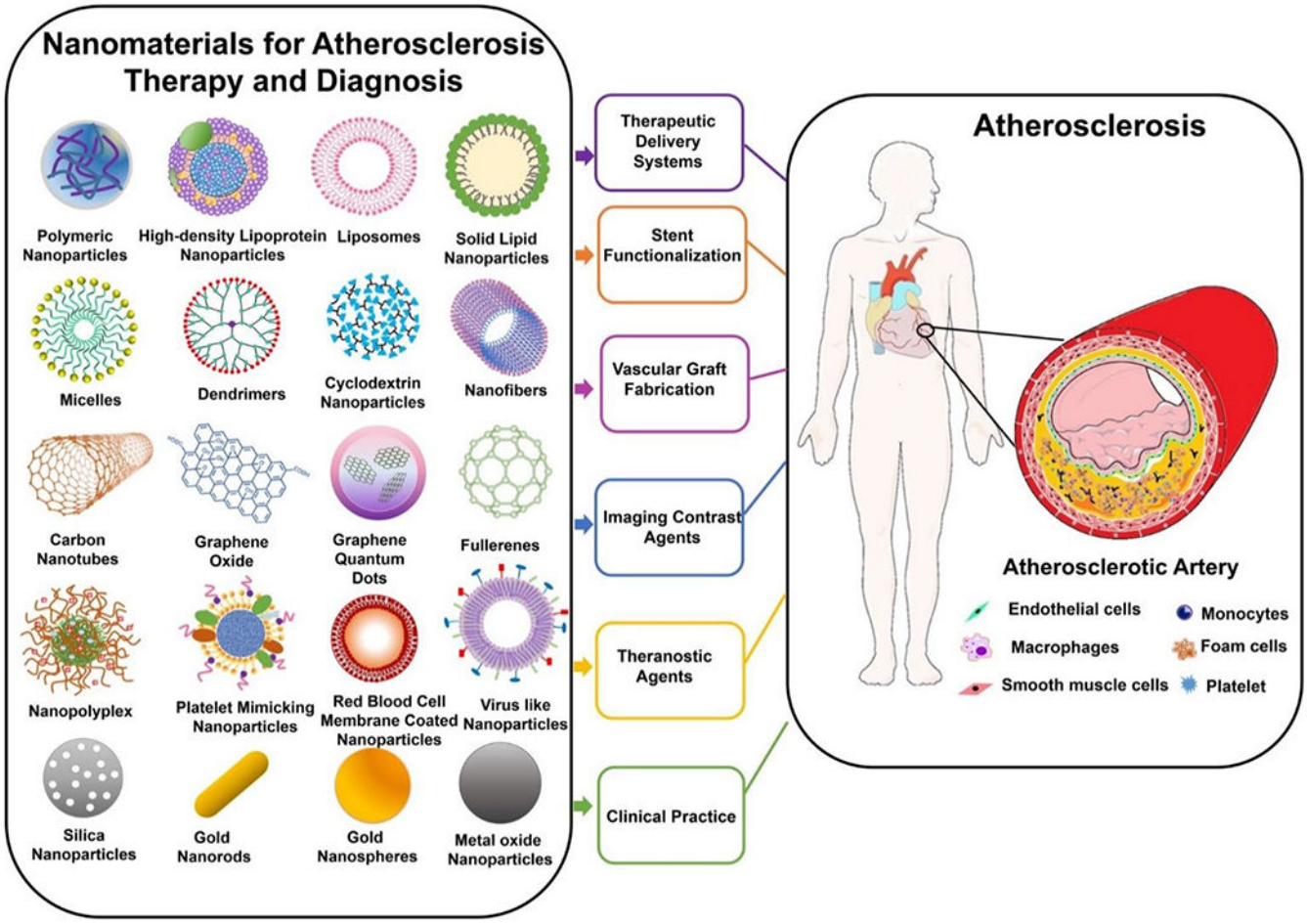

Fig.1.

Schematics of nanomaterials and associated applications discussed in the review for atherosclerosis therapy and diagnosis.

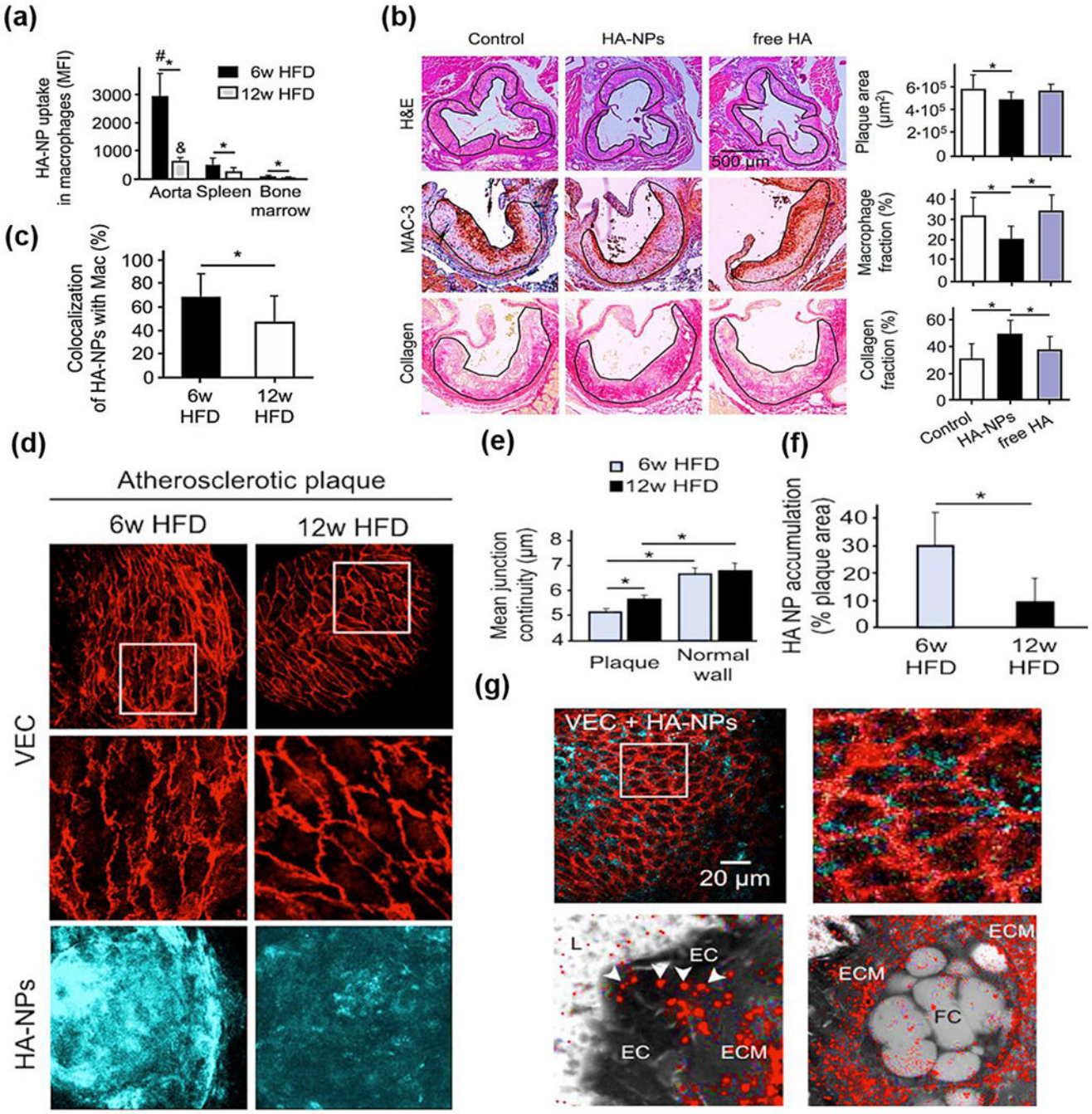

Fig.2.

(a) Uptake efficacy of cyanine (Cy)7-HA-NPs in aortic, splenic, and bone marrow macrophages measured by flow cytometry. (b) Representative images of aortic roots from mice that received either buffer (control), HA-NPs, or free HA during a 12-week high-fat feeding period. (c) Selectivity of HA-NPs toward plaque-associated macrophages expressed as the percentage of HANP-positive area that colocalizes with CD68-positive macrophage area. (d) Comparison of the endothelial adherens junction architecture and HA-NP uptake efficacy in atherosclerotic lesions of mice under 6 weeks and 12 weeks of HFD: the upper

chart displays low and high resolution of the mean VEC continuity determined in the plaque, and the lower chart shows the HA-NP uptake efficacy expressed as the fraction of HA-NP-positive plaque area and (e-f) associated quantification of mean junction continuity (e) and HA NP accumulation (f). (g) Confocal microscopy images of VEC-stained endothelial junctions (red) and HA-NPs (cyan blue) at the surface of an atherosclerotic plaque. Reproduced with permission from Ref. [29, 30]. Copyright 2017 and 2020, American Chemical Society.

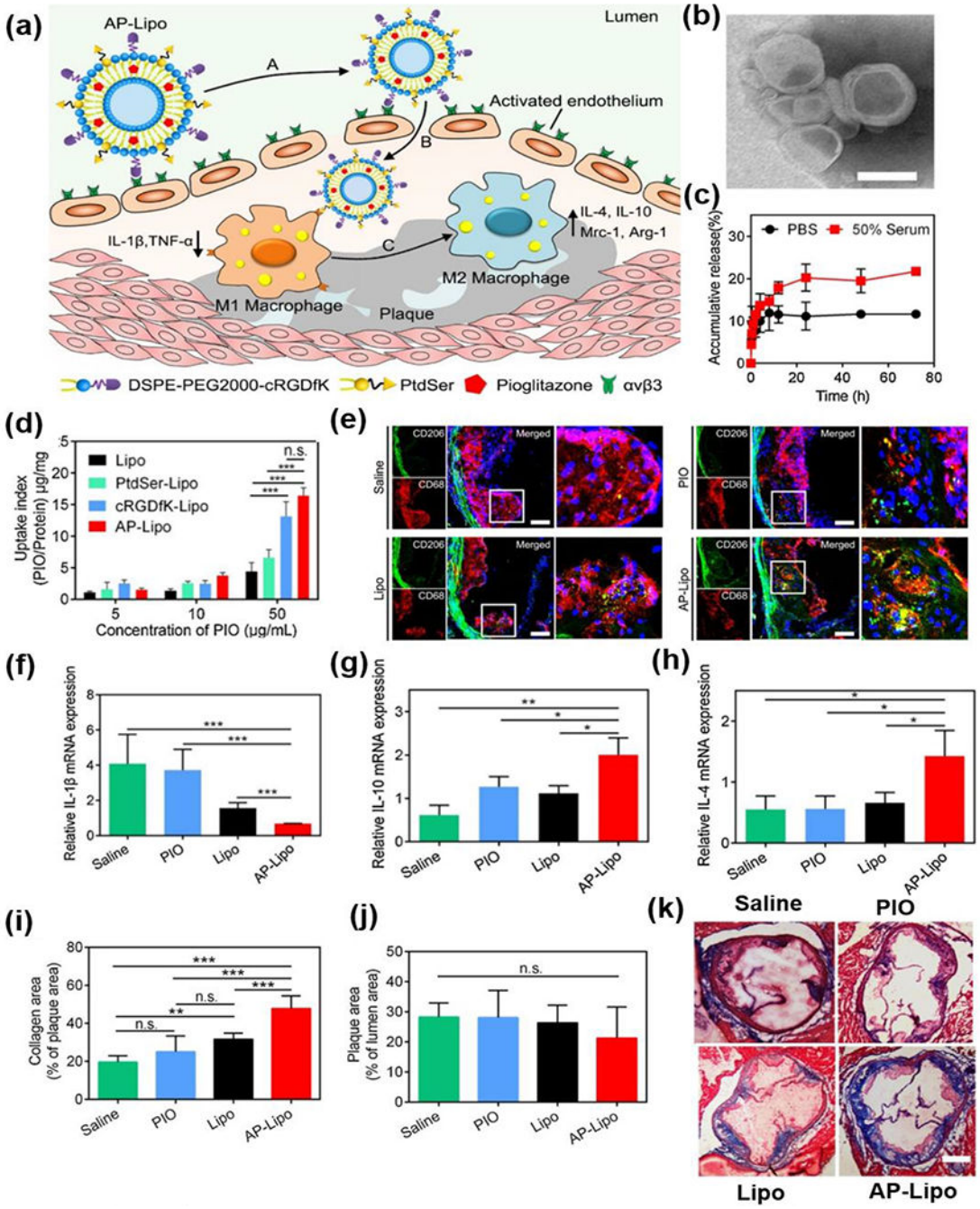

Fig.3.

(a) Schematic of AP-Lipo *in situ* upregulates anti-inflammatory macrophages for atherosclerosis regression. (b) TEM image of AP-Lipo. (c) *In vitro* release of PIO from liposomes after treating with PBS or serum. (d) The influence of PIO concentration on cellular uptake when incubated Lipo, PtdSer-Lipo, cRGDfK-Lipo and AP-Lipo with activated HUVECs. (e) Confocal microscopy images of the aortic root for M2 macrophages with CD68 (red) and CD206 (green) immunostaining. (f-h) The relative mRNA expression of macrophages secreted cytokines for (f) IL-1β, (g) IL-10 and (h) IL-4 in plaques after

treating with saline, PIO, Lipo and AP-Lipo, respectively. (i) Quantitative analysis of collagen area in plaque area. (j) Quantitative analysis of plaque area. (k) Masson trichrome staining of the aortic root sections after received with different treatments. Reproduced with permission from Ref. [74]. Copyright 2019, American Chemical Society.

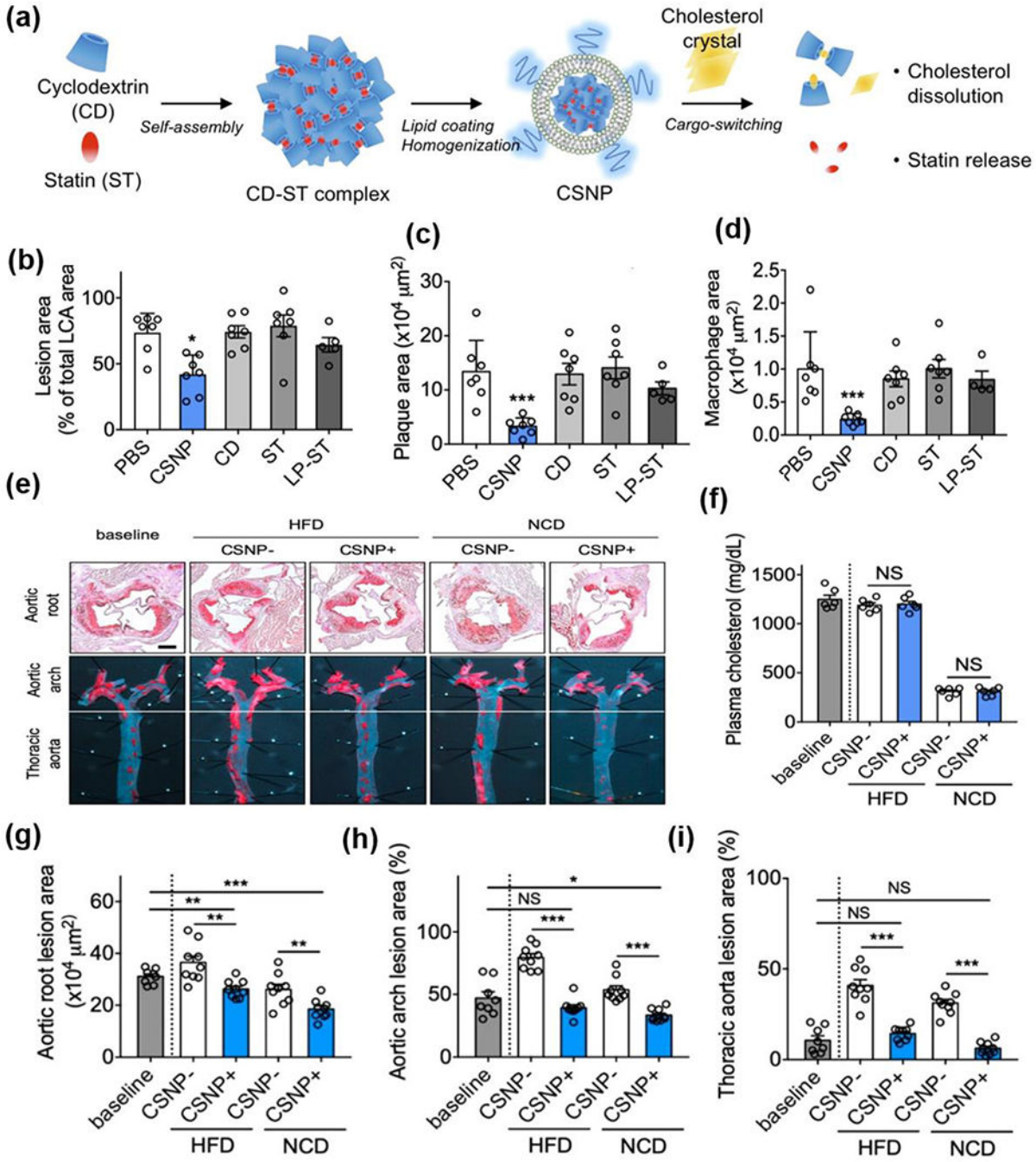

Fig.4.

(a) Schematic of CSNP preparation and cargo-switching. (b) Quantification of lesion areas. (c) Quantification of plaque area. (d) Quantification of macrophage area. (e) representative images of aortic root sections and en face aortic arch and thoracic aorta after Oil-Red-O staining. (f) plasma cholesterol concentrations. (g-i) Quantification of plaque area in (g) aortic root and lesion areas, (h) aortic arch, and (i) thoracic aorta after CSNP treatment. Reproduced with permission from Ref. [166]. Copyright 2020, American Chemical Society.

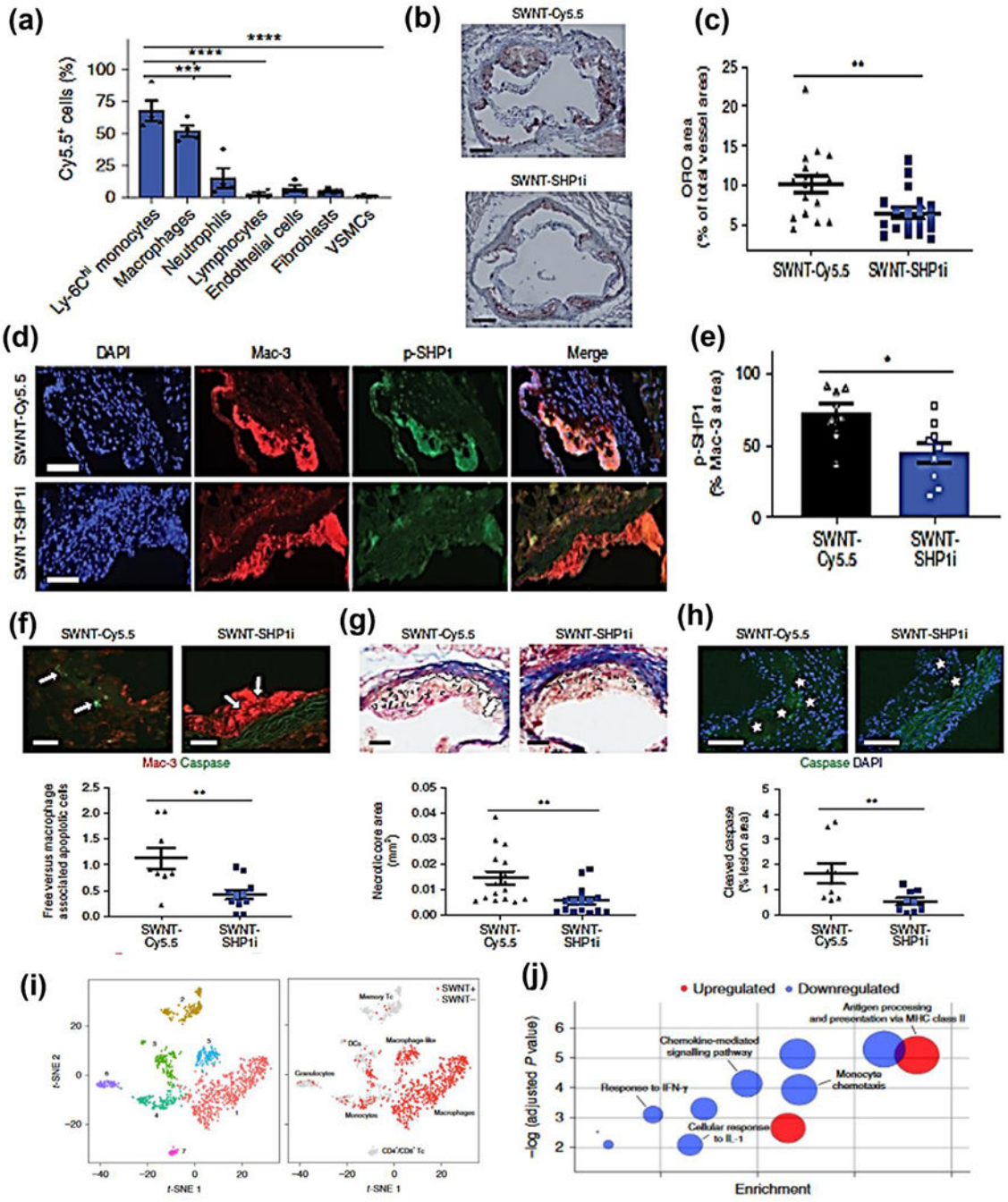

Fig.5.

(a) SWNTs specifically accumulate within Ly-6C^{hi} monocytes and macrophages in the atherosclerotic aorta, whereas SWNT detection is low in other vascular cells. (b-c) Mice treated with SWNT-SHP1i develop significantly reduced plaque content in the aortic sinus relative to SWNT-Cy5.5 controls. (d-e) Compared to the control, SWNT-SHP1i decreases the phosphorylation of SHP-1, which indicates silencing of the antiphagocytic CD47-SIRPα signal. (f-h) Lesion from mice treated with pro-efferocytic SWNTs are more likely to have (f) apoptotic cells that have been ingested by lesional macrophages; (g) develop smaller

necrotic cores; (h) accumulate less apoptotic debris. (i) Unsupervised dimensionality reduction identifies seven major cell types with a similar gene expression from the combine SWNT-Cy5.5 control and SWNTI-SHP1i datasets. (j) Heat map showing the gene expression of ten cluster-defining genes and leukocyte markers. Reproduced with permission from Ref. [173]. Copyright 2020, Nature publishing group.

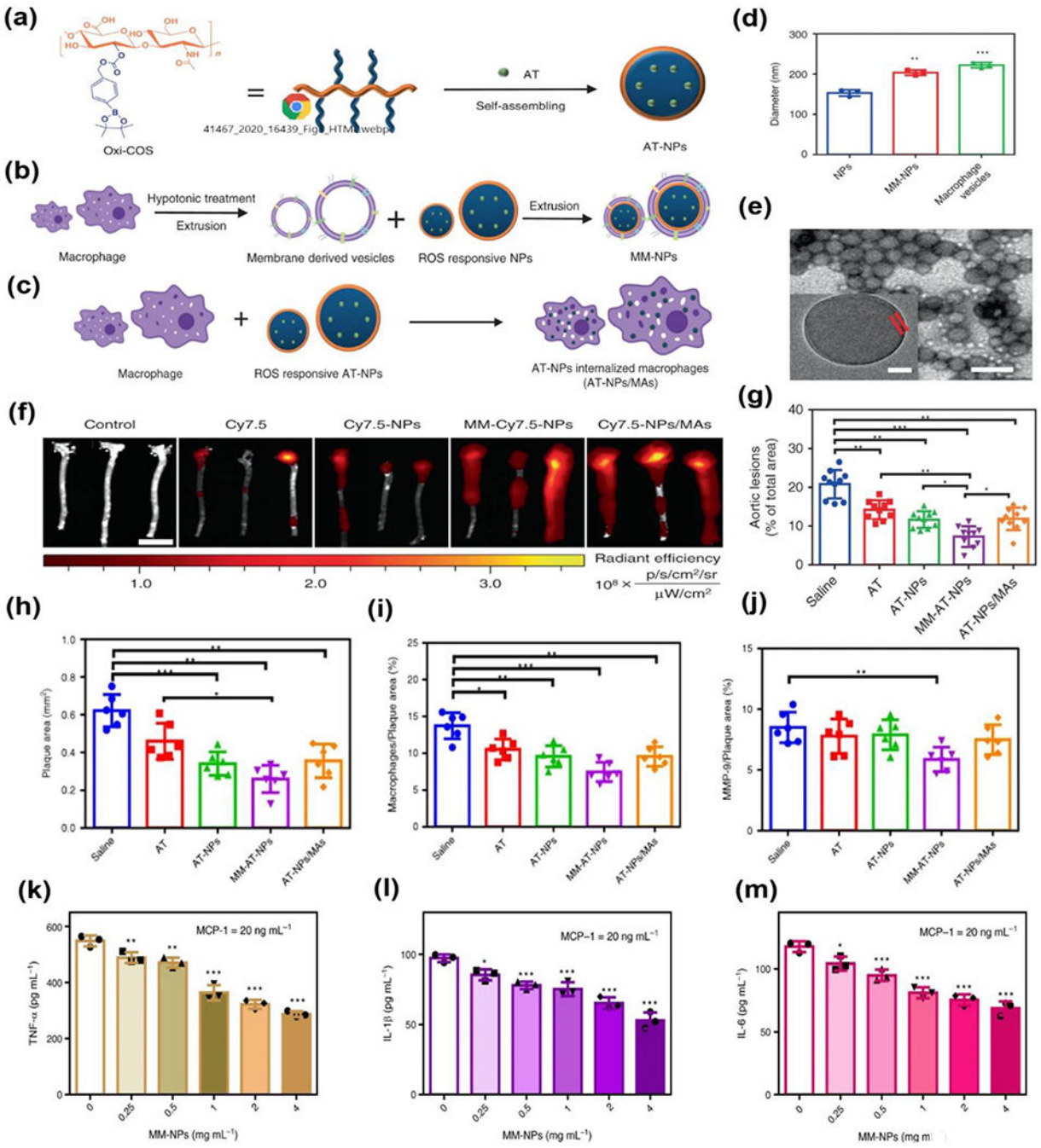

Fig.6.

(a) Schematic illustration of the preparation of AT-NPs. (b) Schematic illustration of preparation of MM-NPs through an extrusion method. (c) Schematic illustration of preparation of AT-NPs/MAs. (d) size measurement of NPs, MM-NPs and macrophage vesicle. (e) Representative TEM image of MM-NPs. (f) *Ex vivo* fluorescence bio-imaging and quantitative analysis of Cy7.5 fluorescent signal in aorta tissues from different types of treatments. (g) Quantitative analysis of lesion area in aorta tissues. (h-j) Quantitative analysis of (h) plaque area, (j) percentage of macrophage area, and (j) percentage of MMP-9 positive

area. (k-m) MM-NP's dose-dependent inhibition of macrophage inflammation induced by MCP-1, respectively, with MM-NP varied from 0 to 4 mg mL^{-1}. Reproduced with permission from Ref. [201]. Copyright 2020, Nature publishing group.

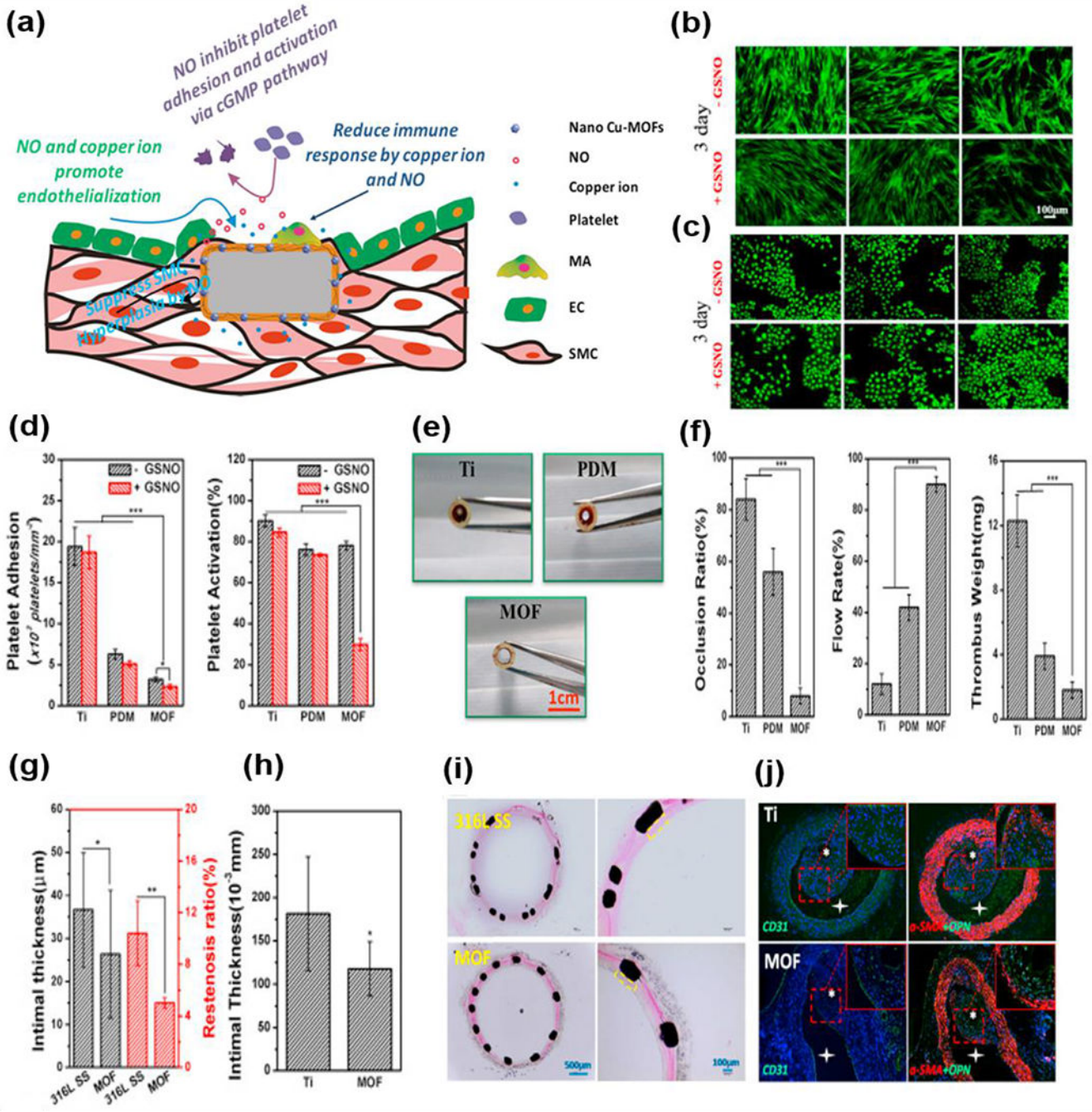

Fig.7.

(a) Schematic of nano Cu-MOFs-immobilized coating function. The NO release and copper ion delivery of the nano Cu-MOFs-immobilized coating exhibited a synergistic effect on inhibiting platelet adhesion and activation, promoting endothelialization, regulating immune response, and suppressing SMCs hyperplasia. (b-c) Rhodamine staining of ECs (b) and SMCs (c) on samples for 3 days. (d) Platelet adhesion and activation level after 45 min incubation with or without a NO donor. (e) Cross-sectional observation of the sample containing catheters after 30 min circulation. (f) Occlusion ratio of a sample containing

catheters by measuring the cross-section diameter of the circulating tube. (g) Statistical analysis of the neointimal thickness and restenosis rate. (h) Intimal thickness of Ti and nano Cu-MOFs-immobilized Ti wire after implantation into the abdominal aorta of rats for four weeks. (i) Effect of the bare stents and nano Cu-MOFs-immobilized stents on in-stent restenosis assessed by histomorphometric analysis. (j) Immunofluorescence staining of the abdominal aorta after implantation for four weeks for CD31 (green), α-SMA (red), OPN (osteopontin) (green). Reproduced with permission from Ref. [232]. Copyright 2019, Elsevier.

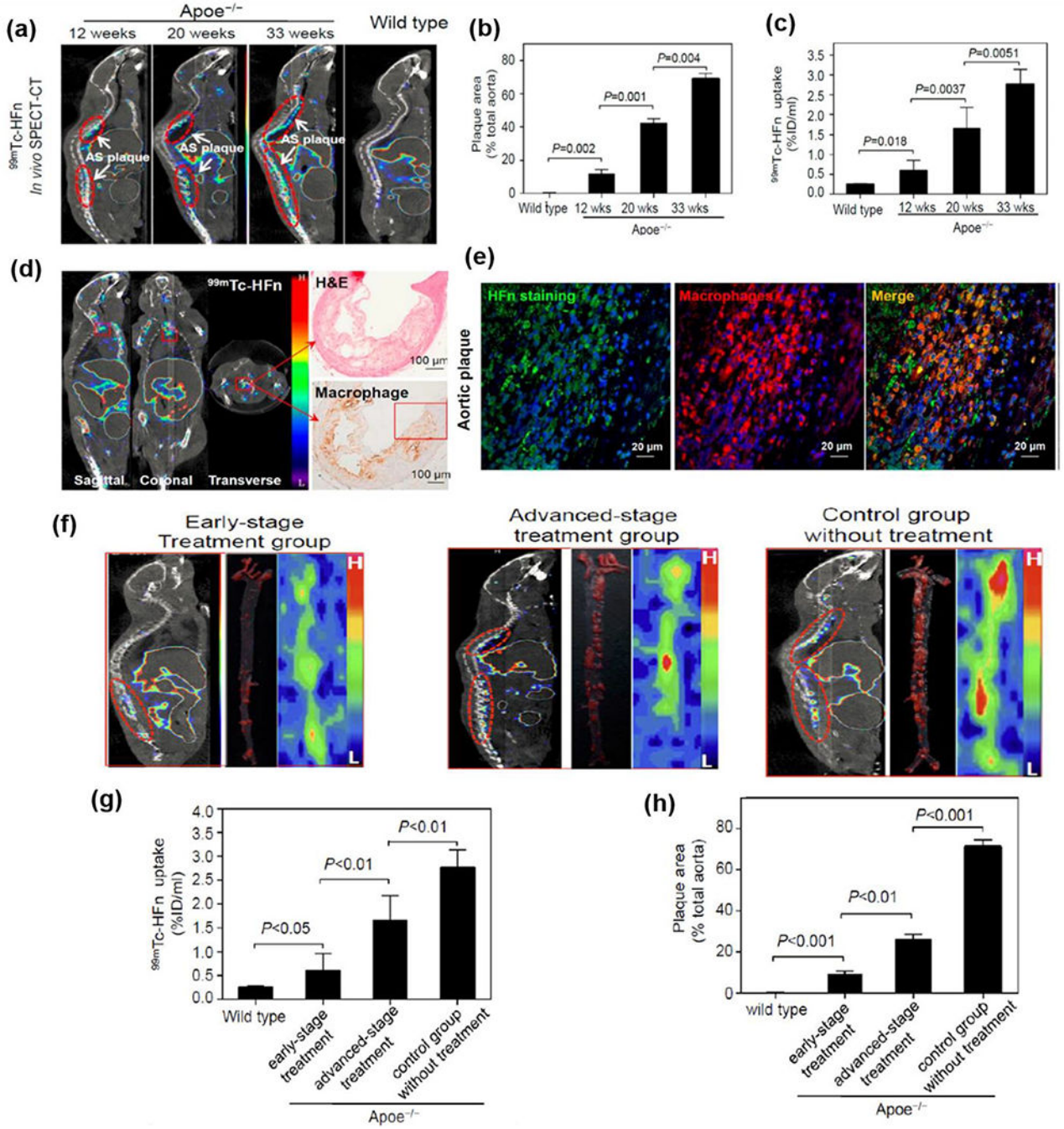

Fig.8.

(a) Images of ^{99m}Tc-HFn SPECT-CT imaging in atherosclerotic and control mice. Red circles indicate atherosclerotic plaques. (b-c) Quantitative image analysis showing a high correlation between ^{99m}Tc-HFn uptake in aortas and the plaque area measured by Oil Red O staining. (d) Histology of the 99mTc-HFn-positive plaque region from the excised aorta showed intense macrophage infiltration (Mac-3 staining) and quantitative analysis showed high correlation between ^{99m}Tc-HFn uptake and the extent of macrophage infiltration within plaques. (e) Immunofluorescent staining of ^{99m}Tc-HFn-positive plaque region demonstrated

colocalization of HFn staining with macrophages (Mac-3 staining) within plaques. (f) Images of ^{99m}Tc-HFn SPECT-CT imaging (left panels) in different treatment mice and the corresponding *ex vivo* planar imaging (right panels) and Oil Red O-stained aortas (middle panels) excised from mice after imaging with ^{99m}Tc-HFn. (g-h) Quantitative analysis of ^{99m}Tc-HFn uptake in aortas and plaque areas measured by Oil Red O staining of the aortas from different treatment groups. Reproduced with permission from Ref. [290]. Copyright 2018, American Chemistry Society.

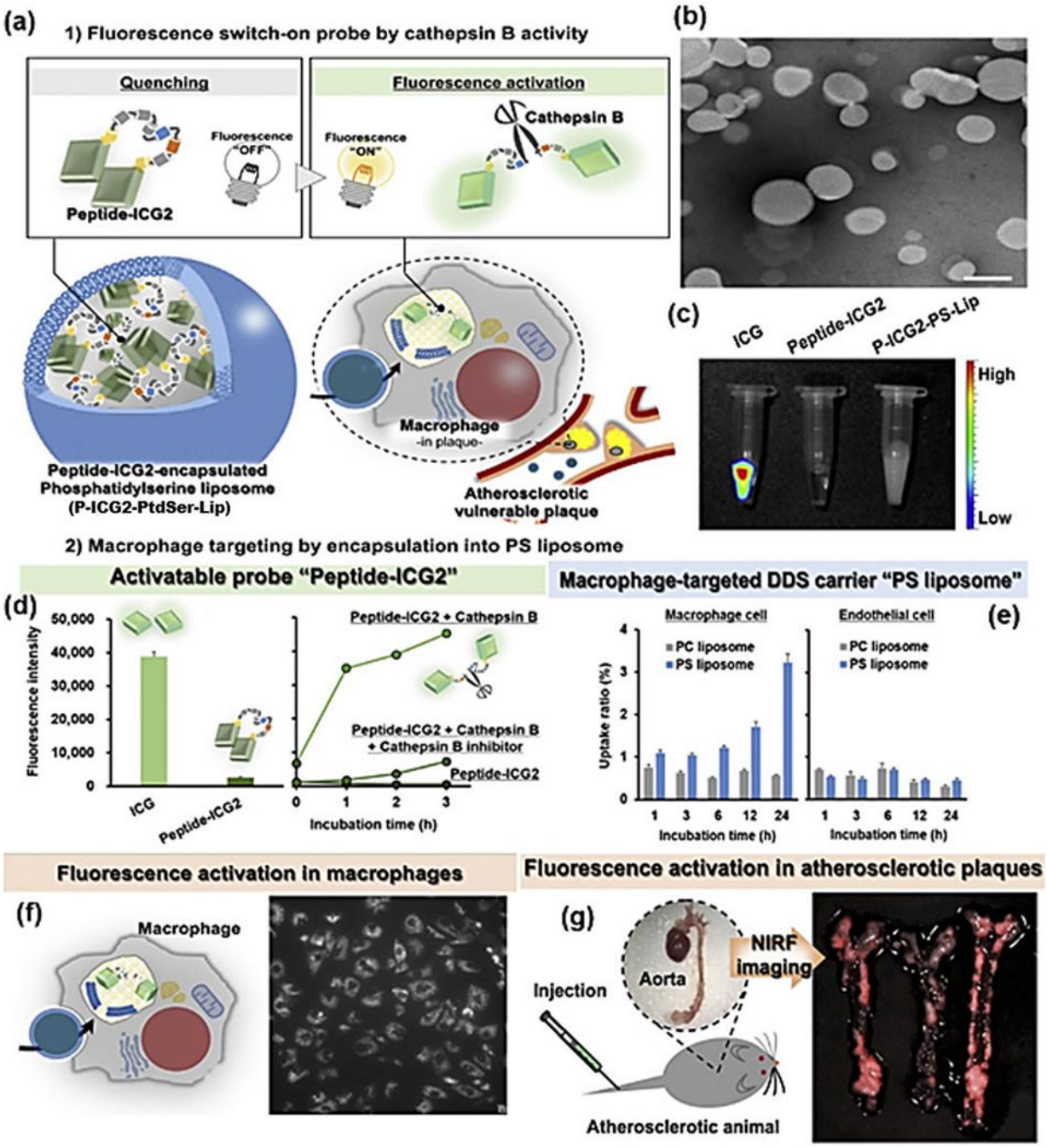

Fig.9.

(a) Strategy of atherosclerosis imaging using P-ICG2-PtdSer -Lip and a scheme represents the fluorescence imaging system of P-ICG2-PtdSer-Lip for diagnosis of atherosclerosis. (b) TEM image of P-ICG2-PtdSer-Lip. (c) Fluorescence images of ICG, Peptide-ICG2 and P-ICG2-PtdSer-Lip. (d) Comparison of fluorescence intensity of Peptide-ICG2 with that of ICG (left) and fluorescence intensity of Peptide-ICG2 was plotted by measuring the fluorescence intensity at the indicated times during incubation with cathepsin B in the presence or absence of leupeptin (left). (e) Quantitative analysis of liposome uptake into

macrophage cells (left) and endothelial cells (right). (f) Observation of fluorescence activation of P-ICG2-PtdSer-Lip in macrophage cells after 6h incubation of P-ICG2-PtdSer-Lip with RAW264 cells. (g) NIRF imaging of atherosclerotic plaques in ApoE$^{-/-}$ mice. The aortae were dissected at 24 h after the injection of the P-ICG2-PtdSer -Lip. The images were obtained by using a Maestro fluorescence imaging system. Reproduced with permission from Ref. [306] Copyright 2019, Elsevier.

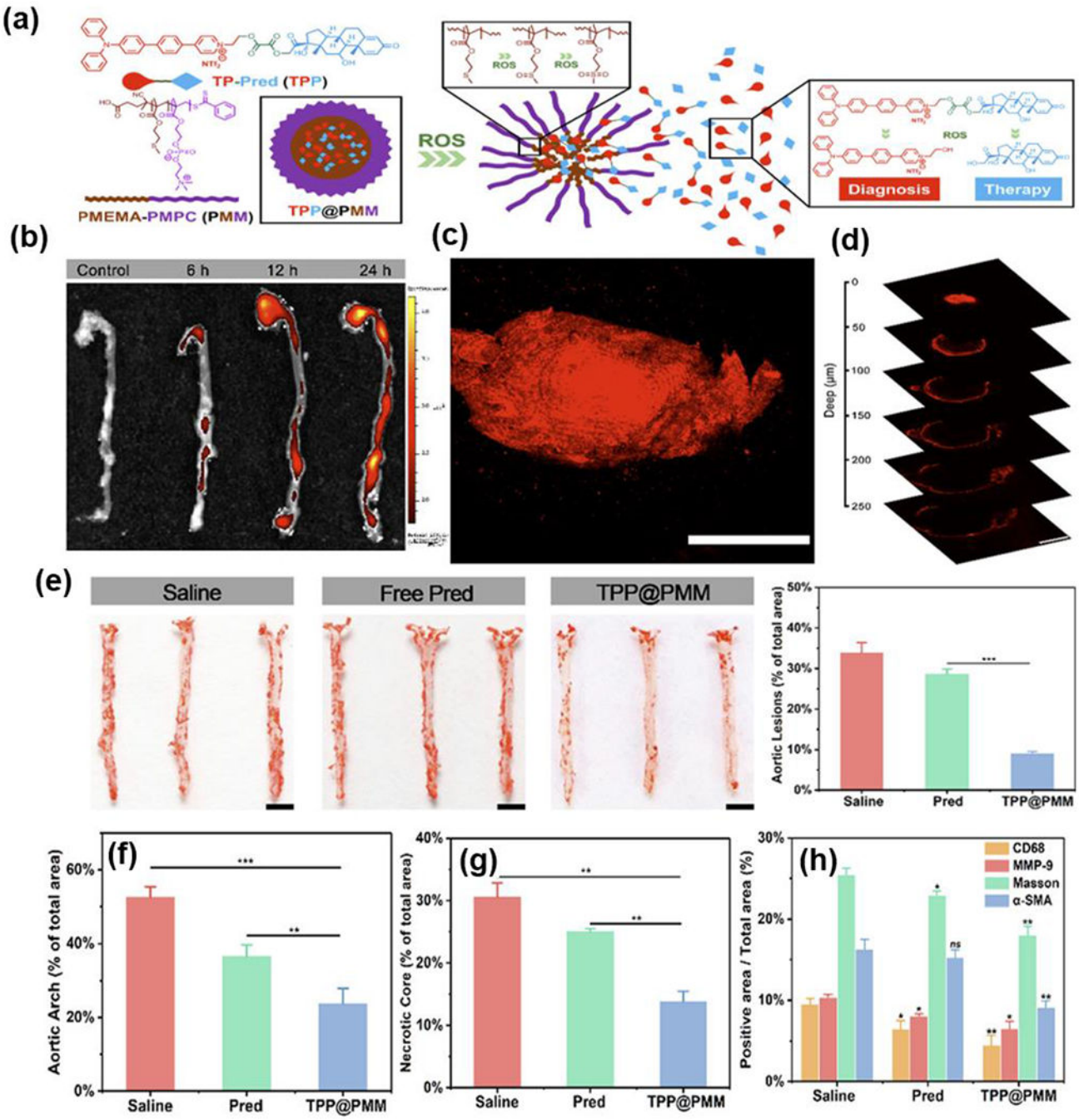

Fig.10.

(a) Illustration of developing a nanoplatform with two-photon imaging. (b) *Ex* vivo fluorescence images and quantitative result of TPP@PMM accumulation in aortas. (c) Two-photon confocal image of the atherosclerotic plaques. (d) Two-photon CLSM images of the plaques at various imaging depths. (e) Photographs of *en face* Oil red O-stained aortas and quantitative result of the Oil red O positive areas from the mice treated with different formulations. (f) Quantitative analysis of the plaque area, (g) necrotic core area and (h)

positive area in different histochemistry analyses. Reproduced with permission from Ref. [337]. Copyright 2020, American Chemistry Society.

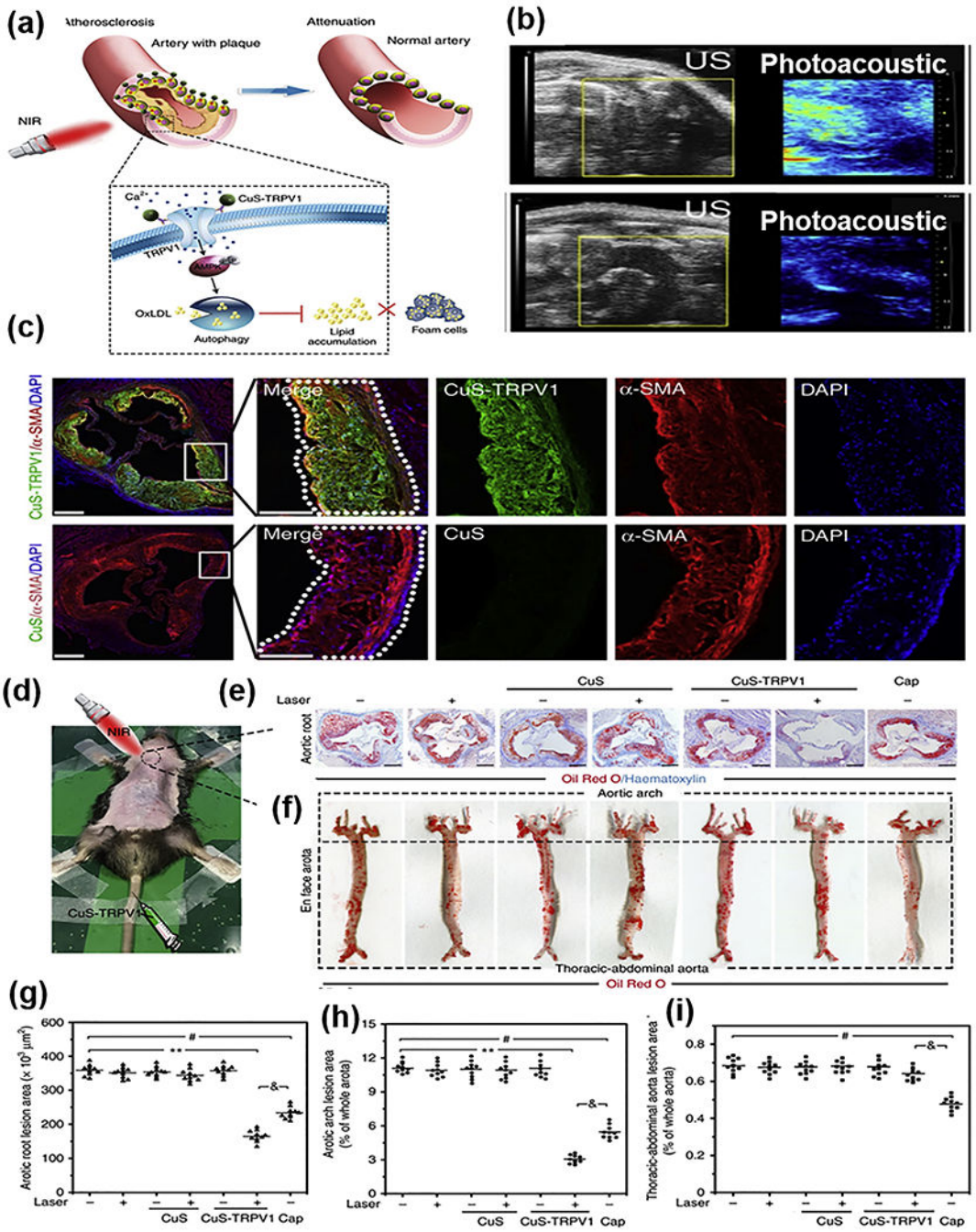

Figure 11.

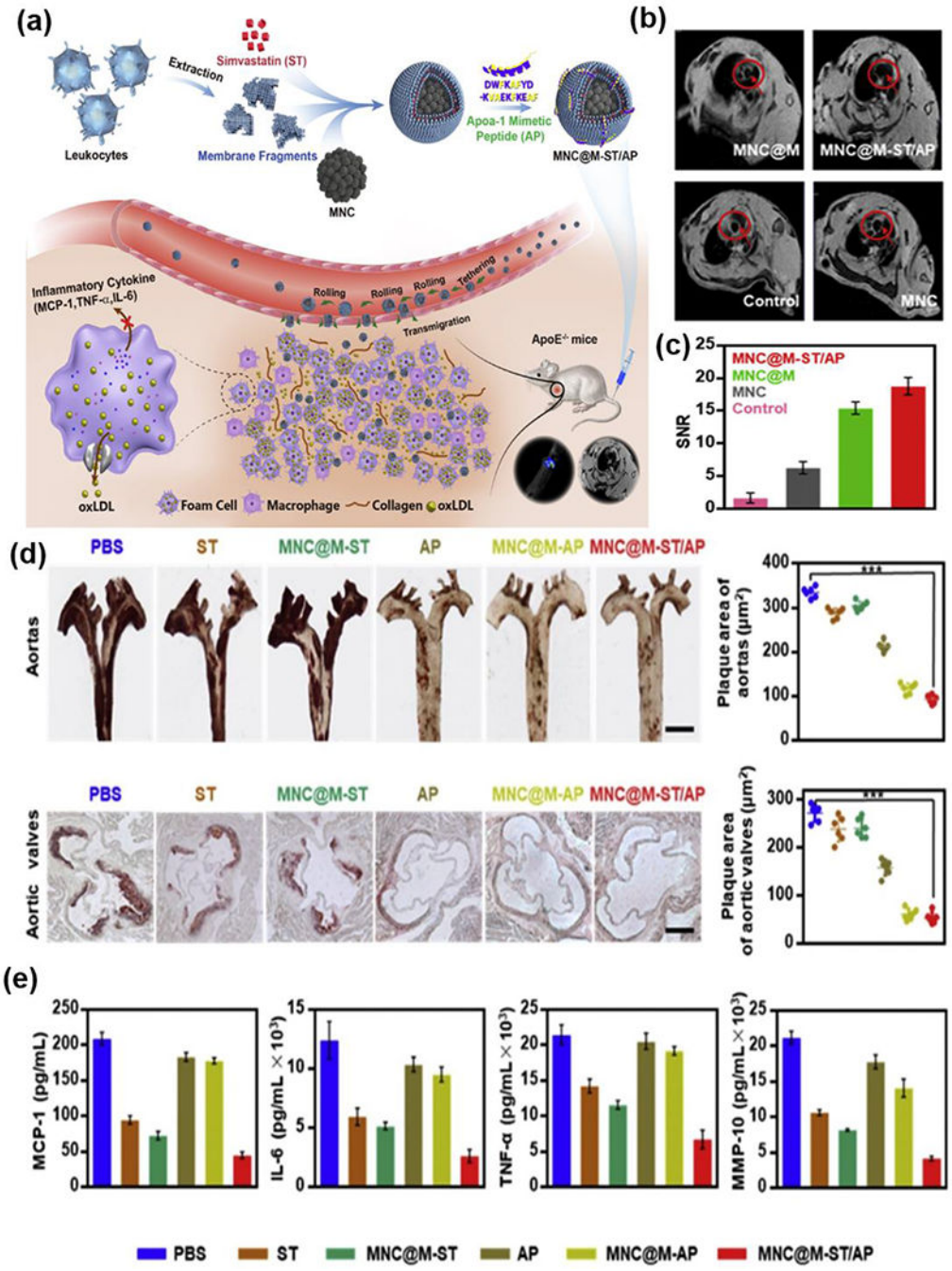

Fig.12.

(a) Schematic illustration of the bioinspired MNC@M-ST/AP fabrication and its application for anti-atherosclerosis by integrating multiple-targeting. (b) *In vivo* T_2-weighted MRI images of the aorta areas, PBS injected mice were used as control. (c) The signal to notice ratio (SNR) values of different MNC-based nanoparticles in aorta areas determined by cine flash MR imaging system. (d) Photographs of excised Oil red O-stained aortas at the time of sacrifice and the corresponding quantitative analyses of plaque areas (top); photographs of Oil red O-stained cryosections of the aortic valves and the corresponding quantitative

analyses of plaque areas (bottom). (e) ELISA assays for the expression levels of MCP-1, IL-6, TNF-α, and MMP-10 in the plaque areas of mice with different treatments. Reproduced with permission from Ref. [349]. Copyright 2019, Elsevier.

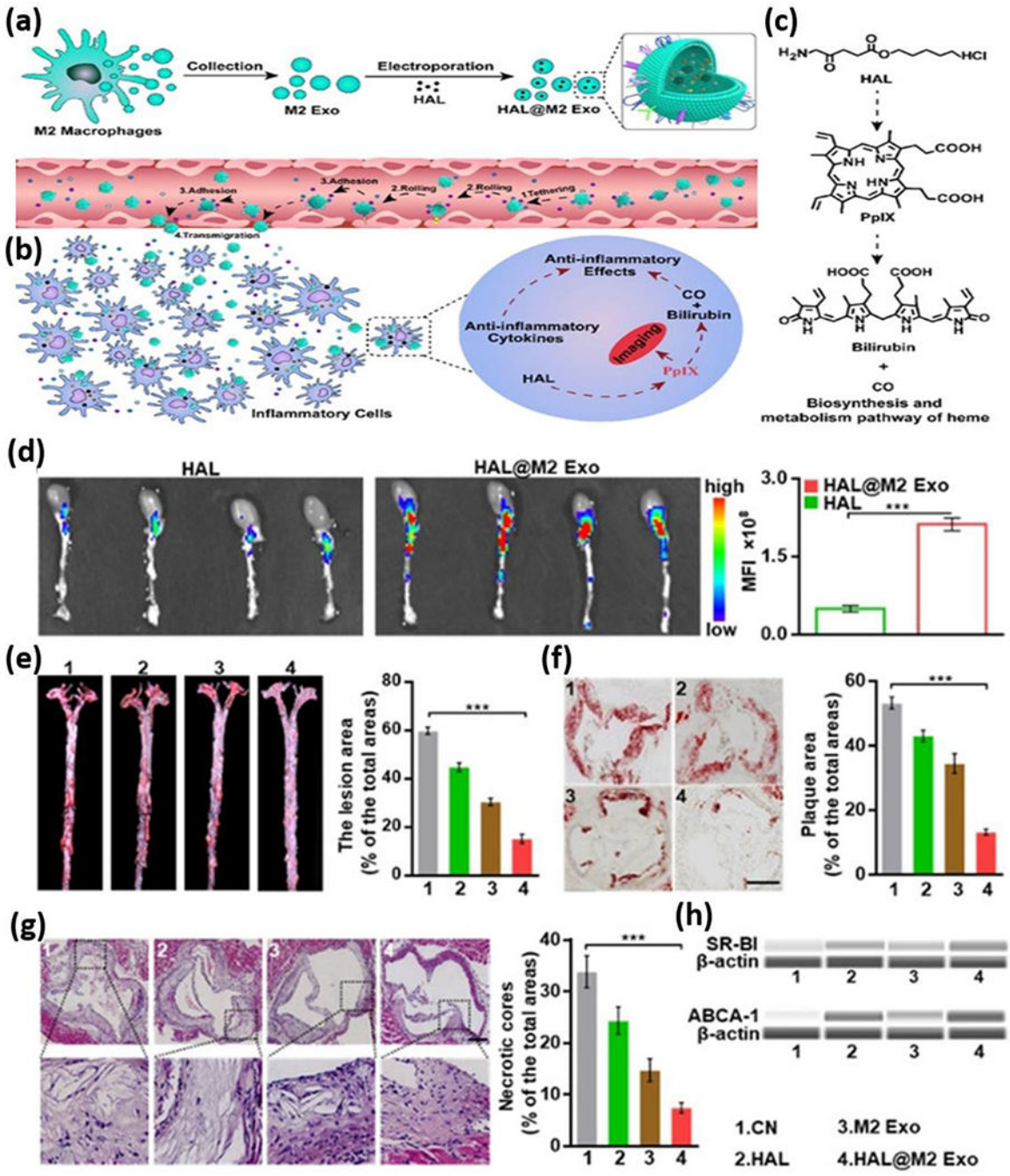

Fig.13.

(a) Schematic illustration of the anti-atherosclerosis treatment by preparing HAL@M2 Exo. (b) The inflammation-tropism and anti-inflammation effect of HAL@M2 Exo. (c) The simplified biosynthesis and metabolism pathway of heme induced by HAL. (d) Fluorescence imaging of the aortas excised from mice. (e) Photographs of the excised aortas stained by Oil red O and the corresponding quantitative analyses of plaque areas. (f) Cryosection photographs of the aortic valves stained by Oil red O and the corresponding quantitative analyses of plaque areas. (g) H&E staining images and the necrosis area statistics of aortic

valves after different treatments. (h) Western blotting analyses of ABCA-1 and SR-BI. Reproduced with permission from Ref. [353]. Copyright 2020, Wiley-VCH.

Table 1.

Novel rHDL NPs developed for atherosclerosis treatment.

Year	Group	HDL	Animal model	Key Findings	Ref.
2017	Liu	HA-PLGA-ST-rHDL	NZW rabbits	1) Avoided liver clearance and increased the accumulation of NPs at the leaky endothelium compared to HA unmodified NPs; 2) showed better cholesterol efflux and accumulation in atherosclerotic aortic root *in vivo*.	[88]
2017	Liu	DXS-AT-rHDL	N/A	1) Demonstrated better macrophage targeting than PLGA-rHDL NPs without modification; 2) exhibited better efficacy in preventing foam cell formation and inflammation.	[89]
2017	Mulder	ST-rHDL	$ApoE^{-/-}$ mice	1) Demonstrated similar accumulation within macrophages in plaque as ST-polymer micelles, which was better than that of ST-liposomes; 2) showed less accumulation in monocytes and efficacy in reducing macrophage burden than ST-polymer micelles.	[90]
2017	Liu	rHDL-anti-miR-155	N/A	1) Escaped from endolysosomes via clathrin-mediated endocytosis; 2) showed high transfection efficiency; 3) induced cholesterol efflux and antioxidation.	[91]
2018	Chen	LT-GM1-rHDL	$ApoE^{-/-}$ mice	1) Showed an extended circulation time, better accumulation in plaque, and stronger anti-atherogenic ability *in vivo* compared to unmodified LT-rHDL NPs; 2) demonstrated better inhibition of foam cell formation *in vitro*.	[92]
2018	Liu	HA-PLGA-rHDL NPs loaded with LOX-1 siRNA and AT	$ApoE^{-/-}$ mice	Targeted ECs and macrophages; efficacy for atherosclerosis increased as HA molecular weight increased; 3) LOX-1 siRNA and AT demonstrated synergistic therapeutic efficacy.	[93]
2019	Liu	ATP-rHDL NPs, loaded with SR-A siRNA and oxygen-evolving catalase, PtdSer, and PT	$ApoE^{-/-}$ mice	1) Demonstrated the effectiveness of apoA-I and PtdSer for targeting SR-BI and CD36 receptors; 2) showed excellent targeting ability; 3) induced 65.8% plaque reduction *in vivo*.	[94]
2018	Lutgens	TRAF6-rHDL NPs: rHDL NPs loaded with inhibitor (687702), targeting the interaction between CD40 and TRAF6 while leaving CD40 mediated immunity intact	$ApoE^{-/-}$ mice and non-human primates	1) Reduced monocyte recruitment and suppressed the initiation of atherosclerosis in mice by decreasing CD40 and integrin expression in monocytes; 2) stabilized plaque and suppressed the progression of plaque in mice; 3) lowered macrophage and T cell contents in mice aorta; 4) downregulated genes controlling monocyte migration and upregulated genes affecting lymphocyte homing in mice; 5) exhibited non-toxicity to mice and non-human primates.	[84, 95, 96]
2020	Liu	β-cyclodextrin and ST-loaded discoidal rHDL	shuttle/sink model	1) Demonstrated better ability to remove cholesterol than ST-rHDL without β-cyclodextrin; 2) the concentration of β-cyclodextrin has a positive effect on the rHDL cholesterol removal capability for foam cells.	[97]

Notes and Abbreviations: rHDL: reconstituted high-density lipoprotein; NP: nanoparticle; HA: hyaluronic acid; PLGA: poly (lactic-co-glycolic acid); ST: statin; NZW: New Zealand white; DXS: dextran sulfate; AT: atorvastatin; $ApoE^{-/-}$: Apolipoprotein E-deficient; anti-miR-155: against microRNA-155; LT: lovastatin; GM1: monosialoganglioside; LOX-1: lectin-like oxidized low-density lipoprotein receptor-1; siRNA: small interfering ribonucleic acid; EC: endothelial cells; MCP-1: monocyte chemoattractant protein-1; ATP: adenosine triphosphate; SR-A: scavenger receptor class A; PtdSer: phosphatidylserine; PT: pitavastatin; apoA-I: Apolipoprotein A1; SR-BI: scavenger receptor class B type 1; TRAF6: tumor necrosis factor receptor-associated factor 6; CD40 and CD36: cluster of differentiation 40,and 36.

Table 2.

Novel HDL mimetic NPs developed by using apoA-I mimetic peptides, constructs multivalent apoA-I mimetics, and apoA-I generated by bacteria.

Year	Group	HDL	Animal model	Key finding	Ref.
2018	Chen	sHDL mimetic-T1317: composed of a 22-amino acid apoA-I-mimetic, DMPC and POPC	ApoE$^{-/-}$ mice	1) Significantly promoted cholesterol efflux in macrophages compared to T1317 and sHDL NPs alone; 2) did not increase serum TG levels as sHDL NPs did; 3) reduced side effects in the liver; 4) significantly reduced plaque size compared to T1317 and sHDL NP treatment alone.	[98]
2019	Chiesa	TN-sHDL mimetic: composed of a trimeric form of human apoA-I expressed from *Escherichia coli*, POPC and DPPC	NZW	1) Induced plaque stabilization and showed lower macrophage content in plaque compared to groups treated with placebo.	[99]
2019	White	4F-POPC HDL mimetic: composed of apoA-I mimetic (4F) and POPC	N/A	1) Showed better ability to ameliorate lipid-related disorders than nanodiscs composed of apoA-I and POPC; 2) demonstrated resistance to oxidative processes.	[100]
2019	Chiesa	TN-sHDL NPs: composed of trimeric apoA-I, POPC, and DPPC	NZW	1) Stabilization and regression of atheroma were observed in the treatment group.	[101]
2019	Thaxton	LC HDL NPs: composed of apoA-I, DPPC, and PL_4 or DNA-PL_4core	N/A	1) Closely mimic the human HDLs 2) Reduced NF-κB activity in LPS stimulated human monocytes.	[102]
2020	Schwendeman	T1317-SHDL NPs: composed of POPC, DMPC, DPPC, apoA-I mimetic peptide 22A and T1317,	ApoE$^{-/-}$ mice	1) Better inhibition of plaque formation compared to sHDL or T1317 in plaque existing mice.	[103]

Notes and Abbreviations: HDL: high-density lipoprotein; NP: nanoparticle; apoA-I: Apolipoprotein A1; sHDL: synthetic high-density lipoprotein; T1317: liver X receptor agonist; DMPC: dipalmitoylphosphatidylcholine; POPC: 1-palmitoyl-2-oleoyl-sn-glycero-3-phosphocholine; ApoE$^{-/-}$: Apolipoprotein E-deficient; TG: triglycerides; TN: trimeric form; DPPC: dipalmitoylphosphatidylcholine; 4F: apoA-I mimetic peptide named 4F; LC: lipid conjugated; PL_4: small molecule-phospholipid cores; DNA-PL_4: phospholipid conjugate cores linked with DNA. LPS: lipopolysaccharide; NF-κB: nuclear factor kappa-light-chain-enhancer of the activated B cell.

Table 3.

Recent novel peptides showing anti-atherosclerotic or anti-inflammatory effects

Year	Group	Peptide	Sequence or Component	Ref.
2017	Zhou	Rice α-globulin peptide	GEQQQQPGM	[104]
2018	Tang	apoA-I mimetic peptide	ELK-2A2K2E	[105]
2018	Karas	Schistocerca gragaria peptide	FDPFPK	[106]
2018	Watanabe	Nicotiana tabacum peptide	Osmotin	[107]
2018	Wu	Spent hen muscle proteins	FLWGKSY	[108]
2019	Lagerstedt	apoA-I mimetic peptide	RG54, 54 amino acid sequence	[109]
2019	Zhou	Rice α-globulin peptides	YYGGEGSSSEQG; SESEM	[110]
2019	Hadri	Thioredoxin-mimetic peptide	Ac-CPC-amide	[111]
2019	Salifu	F11 receptor derived peptide	2HN-(dK)-SVT-(dR)-EDTGTYTC-CONH2	[112]
2019	Miura	apoA-I mimetic peptide	ALEHLFTLYEKALKALEDLLKKLLD-A	[113]
2020	Ni	apoA-I mimetic peptide	FLEKLKELLEHLKELLTKLL	[114]
2020	Ji	Leech peptide	EAGSAKELEGDPVAG	[115]
2020	Sanchez-Quesada	apoJ mimetic peptide	Ac-LVGRQLEEFL-NH2	[116]

Notes and Abbreviations: apoA-I: apolipoprotein A1; F11 receptor: Junctional adhesion molecule A encoded by the F11R gene; apoJ: apolipoprotein J.

Table 4.

Recent studies reqardina the fabrication of vascular araft usina nanofibers

Year	Group	Vascular Composition	Key Findings	Ref.
2019	Turng	Silk fiber, PAM hydrogel, and TPU-nanofiber as the inner, middle, and outer layers, respectively.	1) The modulus around 1.44 MPa is similar to that of human arteries; 2) Enhanced elasticity; 3) Higher burst pressure than that of the saphenous vein (3600 mmHg) due to the high burst pressure of PAM	[255]
2019	Jang	Aligned thin PCL/collagen NF layer as the inner layer and thick PCL/silica nanofiber layer as the outer layer	1) The ultimate TS is 3 MPa and Young's modulus is around 4 MPa; 2) The inner aligned layer allowed for more cell attachment than that of the randomly oriented layer (control); 3) The outer layer enhanced fibroblast attachment and enhanced cell viability compared with pure PCL.	[256]
2019	Ni	PCL/OPC nanofiber multilayer	1) The TS and Young's modulus decreased as the layers of PCL increased; 2) PCL/OPC two-layered NF tube showed the highest tensile strength (5.51 MPa) and Young's modulus (16.42 MPa); 3) Dual release kinetics: Burst release of drug from inner layer but a slow release of drug from outer NF; 4) Allowed HUVEC attachment	[257]
2019	Tan)	Coaxially nanofiber PCL/gelatin	1) PCL/gelatin nanofiber graft possessed a burst pressure of around 800 mmHg; 2) PCL/gelatin nanofiber graft with a thin PCL cap possessed a burst pressure of around 1000 mmHg; 3) Enhanced activity for inhibiting platelet adhesion by decreasing 75% of the number of platelet attachment compared with pure PLC graft; 4) Improved patency *in vivo*.	[258]
2019	Shamloo	PCL/freeze-dried gelatin/heparin nanofiber	1) Heparin-modified PCL nanofiber graft demonstrated a more sustained and release of Heparin compared with Heparin-loaded gelatin graft; 2) PCL/freeze-dried gelatin/Hep exhibited the best hydrophilicity for EC attachment compared with single-component graft; 3) PCL-Heparin prevented platelet adhesion; 4) PCL/freeze-dried gelatin/Heparin showed similar Young's modulus (1.1±0.12 Mpa) to coronary arteries (1.41±0.72 Mpa).	[259]
2019	Hong	Pectin nanofiber with 25% and 50% oxidation	1) The MSC-derived VSMC phenotype marker was more expressed on pectin-nanofiber with 50% oxidation, whereas the MSC-derived EC expressed a higher degree of phenotype marker expression on pectin-nanofiber with 50% oxidation.	[260]
2019	Zhao	PCL nanofiber/RAP/DRA	1) Burst release of RAP at the initial 7 days but sustained release for 8 weeks; 2) Young's modulus (0.81 MPa) and tensile strength (4.95 MPa) of PCL-nanofiber/RAP/DRA are higher than that of DRA; 3) Significantly decreased intimal hyperplasia *in vivo*	[261]
2019	Feng	CAG/ACH_{11} PLCL/ coated blend gelatin nanofiber	1) Exhibited good hydrophilicity and the lowest plasma protein absorption compared with other controls; 2) Promoted better EC but not SMC proliferation compared with other controls; 3) Completely covered with ECs of normal morphology after it was implanted in rabbits for 10 weeks and kept patency	[262]
2020	Yuan	PELCL/PELCL-REDV NFs with TPR/miR-126, PELCL NF with TPV/miR-145, and PCL NFs as inner, middle, and outer layer, respectively.	1) Demonstrated fast release of miR-126 but a slow release of miR-145; 2) Enhanced EC proliferation; 3) Regulated SMC phenotype transition from synthetic to contractile type; 4) Polarized macrophages towards M2 phenotype; 5) Demonstrated the ability of the grafts to promote EC proliferation and NO oroduction and reduce calcification *in vivo*.	[263]

Notes and Abbreviations; PAM: peptide amphiphile micelle; TPU: thermoplastic urethane; PCL: polycaprolactone; TS: tensile strength; OPC: oligomeric proanthocyanidin; HUVEC: human umbilical vascular endothelial cells; EC: endothelial cells; MSC: mesenchymal stem cells; VSMC: vascular smooth muscle cells; RAP: rapamycin; DRA: decellularized rat aortas; CAG: cell adhesive peptide; ACHu: antithrombotic peptide with sequence LTFPRIVFVLG; PLCL: poly(lactic acid-co-caprolactone); SMC: smooth muscle cells; PELCL: poly(ethylene glycol)-b-poly(L-lactide-co-ε-caprolactone; REDV: peptide with the sequence of Arg-Glu-Asp-Val; TPR: thermoplastic rubber; miRNA-126: miR-126; TPV: peptide with the sequence of Val-Ala-Pro-Gly; miR-145: microRNA-145; M2: alternatively activated phenotype; EC: endothelial cells; NO: nitric oxide.

Table 5.

Summary of nanomaterials used for atherosclerosis diagnosis and therapy in the clinical setting

Year	Group	Name	Nanomaterial	Function	Ref.
2001	Hamma	Sinerem®	Iron oxide NPs	Diagnosis	[356]
2003	Nissen	ETC-216	HDL mimetic NPs	Therapy	[357]
2003	Engelshoven	Sinerem®	Iron oxide NPs	Diagnosis	[358]
2008	Gillard	Sinerem®	Iron oxide NPs	Diagnosis	[359] [360]
2009	Gillard	Sinerem®	Iron oxide NPs	Diagnosis	[361] [362]
2014	Waters	CER-001	HDL mimetic NPs	Therapy	[363]
2015	Stroes	LN-PNP	Lipid NPs	Therapy	[364]
2015	Alexander	CSL112	HDL mimetic NPs	Therapy	[365]
2015	Ganbinsky	NaNO	Silica-gold NPs	Therapy	[366] [367]
2016	Maranhao	PTX-LDE	Lipid NPs	Therapy	[368]
2016	Semple	Feraheme®	Iron oxide NPs	Diagnosis	[369]
2016	Zheng	CER-001	HDL mimetic NPs	Therapy	[370]
2016	Siber	COBRA PzF	PzF nanocoating	Therapy	[371]
2016	Wijngaard	MDCO-216	HDL mimetic NPs	Therapy	[372] [373] [374]
2017	Vochelet	COBRA PzF	PzF nanocoating	Therapy	[375]
2017	Siber	COBRA PzF	PzF nanocoating	Therapy	[376]
2017	Nicholls	CER-001	HDL mimetic NPs	Therapy	[377] [378]
2017	Dasseux	CER-001	HDL mimetic NPs	Therapy	[379]
2017	Ganbinsky	NaNO	Silica-gold NPs	Therapy	[380]
2017	Coolen	Feraheme®	Iron oxide NPs	Diagnosis	[292]
2018	Ganbinsky	NaNO	Silica-gold NPs	Therapy	[381]
2018	Butters	CER-001	HDL mimetic NPs	Therapy	[382]
2018	Wright	CSL112	HDL mimetic NPs	Therapy	[383]
2018	Tricoci	CSL112	HDL mimetic NPs	Therapy	[384]
2018	Nissen	MDCO-216	HDL mimetic NPs	Therapy	[382]
2019	Kharlamov	NaNO	Silica-gold NPs	Therapy	[385]
2019	Tavildari	COBRA PzF	PzF nanocoating	Therapy	[386]
2019	Coolen	Feraheme®	Iron oxide NPs	Diagnosis	[387]
2020	Stroes	CER-001	HDL mimetic NPs	Therapy	[388]
2020	Belle	COBRA PzF	PzF nanocoating	Therapy	[389]
2020	Sadat	Feraheme®	Iron oxide NPs	Diagnosis	[390]
2020	CSL Behring	CSL112	HDL mimetic NPs	Therapy	NCT03473223
2020	Maranhão	PTX-LDE	Lipid NPs	Therapy	NCT04148833
2020	Maranhão	MTX-LDE	Lipid NPs	Therapy	NCT04616872
2020	CeloNova BioSciences, Inc.	COBRA PzF	PzF nanocoating	Therapy	NCT02594501

Note and abbreviations: NPs: nanoparticles; HDL: high-density lipoprotein; PzF: Polyzene-F